NASA CR-120875

N72-24492

HYBRID THERMOCOUPLE DEVELOPMENT PROGRAM (U)

FINAL REPORT

by

L. P. Garvey, T. R. Krebs, and E. Lee

RCA Electronic Components

prepared for

NATIONAL AERONAUTICS AND SPACE ADMINISTRATION

NASA Lewis Research Center
Contract NAS 3-11843
William J. Bifano, Project Manager

Requests for copies of this report should be referred to

National Aeronautics and Space Administration
Scientific and Technical Information Facility
P.O. Box 33
College Park, Md. 20740

1. Report No. NASA CR-120875	2. Government Accession No. -	3. Recipient's Catalog No. -
4. Title and Subtitle Final Report. Hybrid Thermocouple Development Program		5. Report Date October 1971
		6. Performing Organization Code -
7. Author(s) L. P. Garvey, T. R. Krebs and E. Lee		8. Performing Organization Report No. -
9. Performing Organization Name and Address RCA Electronic Components Harrison, New Jersey 07029		10. Work Unit No. -
		11. Contract or Grant No. NAS 3-11843
		13. Type of Report and Period Covered Contractor Report
12. Sponsoring Agency Name and Address National Aeronautics and Space Administration Lewis Research Center 21000 Brookpark Road Cleveland, Ohio 44135		14. Sponsoring Agency Code -
15. Supplementary Notes William J. Bifano, Project Manager Direct Energy Conversion Division NASA Lewis Research Center Cleveland, Ohio 44135		

16. Abstract

The design and development of a Hybrid thermocouple, having a segmented SiGe-PbTe n-leg encapsulated within a hollow cylindrical p-SiGe leg, is described. Hybrid couple efficiency is calculated to be 10% to 15% better than that of an all-SiGe couple. A preliminary design of a planar RTG, employing Hybrid couples and a water heat pipe radiator, is described as an example of a possible system application.

Hybrid couples, fabricated initially, were characterized by higher than predicted resistance and, in some cases, bond separations. Couples made later in the program, using improved fabrication techniques, exhibited normal resistances, both as-fabricated and after 700 hours of testing.

Two flat-plate sections of the Reference Design Thermoelectric Converter were fabricated and delivered to NASA Lewis for testing and evaluation.

17. Key Words (Suggested by Author(s))		18. Distribution Statement	
Thermoelectric Converter Segmented Silicon-Germanium and Lead Telluride		Unclassified - Unlimited	
19. Security Classif. (of this report) Unclassified	20. Security Classif. (of this page) Unclassified	21. No. of Pages 191	22. Price* $3.00

* For sale by the National Technical Information Service, Springfield, Virginia 22151

NASA-C-168 (Rev. 6-71)

FORWORD

The work described herein was done at the Thermoelectric Products Engineering Department, RCA Corporation, under NASA Contract NAS 3-11843 with Mr. William J. Bifano, Direct Energy Conversion Division, NASA-Lewis Research Center, as Project Manager.

TABLE OF CONTENTS

Section		Page
I	SUMMARY	1
II	INTRODUCTION	4
III	DESIGN AND ANALYSIS	8
	A. Design Requirements	8
	B. Hybrid Thermocouple Design	9
	1. Performance of the Hybrid Thermocouple	9
	2. Stress Analysis of Hybrid Thermocouple Components	27
	C. Generator Design	32
	1. Hybrid Planar Converter Designs	32
	2. Analysis of Light-Weight Heat Rejection Systems	38
	3. Selection of Converter Reference Designs	44
	4. Projected Improvements in Hybrid Planar Converter Designs	44
	D. Module Reference Design	46
	1. Module Design	46
	2. Test Panels	52
IV	THERMOCOUPLE DEVELOPMENT AND TESTING	54
	A. Subcomponent Development	54
	1. p-SiGe Element	54
	2. n-SiGe Element	64
	3. n-PbTe Element	67
	4. Cold Stack	75
	5. Intermediate Bond System	82

TABLE OF CONTENTS (contd.)

Section		Page
IV	B. Thermocouple Development	87
	1. Heat Receptor Subassembly	97
	2. SiGe Subassembly	99
	3. n-Type PbTe Subassembly	99
	4. Thermocouple Subassembly	99
	5. Cold Stack Subassembly	99
	6. Final Assembly	99
	C. Thermocouple Testing	100
V	FABRICATION OF MODULE PANELS	123
	A. Hybrid Couple and Panel Assembly Processes	137
	1. Heat Receptor Assembly - HTS-1A1A	137
	2. SiGe Assembly - HTS-2A1A	139
	3. n-Type PbTe Assembly - HTS-3A1A	141
	4. Thermocouple Assembly - HTS-4A1A	142
	5. Cold Stack Assembly - HTS-5A1A	144
	6. Final Assembly - HTS-6A1A	145
	7. Module Panel Assembly - HTS-7A1A	146
VI	SUMMARY OF RESULTS	148
	APPENDIX I	149
	APPENDIX II	160

LIST OF ILLUSTRATIONS

Figure Number	Title	Page
1	Hybrid Thermocouple Prototype Design	5
2	Hybrid Thermocouple Assembly	6
3	Physical Model of Hybrid Couple for Cases 1B to 1E	11
4	Couple Efficiency vs. p-Type Element Length for Various Heat Flux Densities	13
5	Couple Efficiency vs. Heat Receptor Area for Various Heat Flux Densities and Radii of n-PbTe Element	14
6	Couple Efficiency vs. Radius n-Type PbTe Element for Various ANP Ratios	15
7	Couple Efficiency vs. Heat Flux Density for Various ANP Ratios	16
8	Couple Efficiency vs. Ratio of n-Type SiGe to n-Type PbTe Area (ANR) for Various AN to AP Ratios (ANP)	17
9	Couple Efficiency vs. p-Type Element Length for Various n-Type SiGe to PbTe Area Ratios (ANR) and n-Type PbTe Area to p-Type SiGe Area Ratios (ANP)	19
10	Efficiency vs. Ratio of n-Type SiGe Area n-Type PbTe Area (ANR) for Various AN/AP Ratios (ANP)	20
11	p-Type Element Wall Thickness vs. Radius of n-Type PbTe Element for Various n-Type PbTe Area to p-Type SiGe Area Ratios (ANP)	21
12	Length of n-Type SiGe and n-Type PbTe Segments vs. n-Type SiGe to n-Type PbTe Area Ratio (ANR) for Various p-Type Element Lengths	22
13	Room Temperature Stresses in Bond Area p-Type SiGe Cylinder to p-Type SiMo Heat Receptor	29
14	Load Distribution in Direction of Radius	31
15	Planar Converter Recessed into Flight Vehicle	33
16	Environmental Parameter (PE) vs. Radiating Heat Pipe Fin Temperature	39

LIST OF ILLUSTRATIONS (contd.)

Figure Number	Title	Page
17	Heat Pipe Weight vs. Total Pipe Length for Several Environmental Parameter Ratios	41
18	Typical Heat Pipe Radiator for Converter Design, B-III	42
19	Weight vs. Evaporator Gas Temperature °C for Three Heat Pipe Sizes	43
20	Module for Hybrid Converter Design, B-III	49
21	Module Strip Insulation	50
22	"Plug-Thru" Air-Vac Thermocouple	51
23	Hybrid Structure Module Panel Assembly	53
24	Subcomponent Assemblies	55
25	Diamond Core Drilled p-SiGe Cylinder	58
26	p-SiGe Cylinder Bonded to p-SiMo Heat Receptor	61
27	p-Type SiGe Cylinder Assembly, Accelerated 2000°F Thermal Cycle	62
28	Coefficient of Thermal Expansion as Function of Temperature for SiGe and SiMo Alloys	63
29	p-SiGe (80.0 at.% Si) Bonded to Tungsten Cold Shoe	65
30a	Hot Shoe Bond n-SiGe Leg to n-SiMo Hot Shoe	66
30b	Cold Shoe Bond n-SiGe Leg to Tungsten Cold Shoe	66
31	Thickness Limits of Chemical Vapor Plated Tungsten on 303 Stainless Steel Shoes	68
32	Tungsten Vapor Plated 303 SS Shoes One Run of Five Shoes .375D x .040	69
33	PbTe Element in Shoe Bonding Die	71
34	n-Type PbTe Element - Bond Overflow	72
35	PbTe 3N Element Bond Structure	73
36	PbTe 3N Element Bond Structure	74

LIST OF ILLUSTRATIONS (contd.)

Figure Number	Title	Page
37	3N PbTe Element Shoe Bond Structure	77
38	3N PbTe Element Shoe Bond Structure	78
39	Experimental Cold Stack Designs	79
40	Two Piece T-Mount Stud - Cold Stack Design (Copper T-Steel Screw)	80
41a	One Piece Copper T-Mount Stud - Cold Stack Design - Aluminum Plate	81
41b	Cold Stack Design (Copper T-Steel Screw) Aluminum Plate	81
42	Tensile Test. Cold Stack Design. Two Piece T-Mount Stud	83
43	Tensile Tested at 320 lbs (6400 psi)	84
44	Shear Test. Cold Stack Design. Two Piece T-Mount Stud	85
45	Intermediate Bond System Coupon	86
46	Intermediate Bond Coupon, Tungsten-Gold Bond Structure	88
47	Intermediate Bond Coupon, 303 Stainless Steel-Gold Bond Structure	89
48	Hybrid Thermocouple Assembly Sequence - A	92
49	Hybrid Thermocouple Assembly Sequence - B	93
50	Hybrid Thermocouple Assembly Sequence - C	94
51	Hybrid Thermocouple Assembly Sequence - D	95
52	Heat Receptor Bond - p-SiMo--n-SiMo	98
53	Hybrid Couple Resistance Plotted Against Test Time	104
54	Couple B-12, 6284 Hours - T_S 938°C - T_C 216°C	106
55	Couple B-12, 6284 Hours - T_S 938°C - T_C 216°C	107
56	Thermocouple Attachments Couple No. B-18	108

LIST OF ILLUSTRATIONS (contd.)

Figure Number	Title	Page
57	Hybrid Thermocouple Assembly - Design BX-1	111
58	Hybrid Thermocouple Assembly - Design BX-2	112
59	Hybrid Thermocouple Assembly - Design BX-3	113
60	Hybrid Thermocouple Assembly - Design BX-4	114
61	Special Test Samples	116
62	Test Coupon Bond Systems	118
63	Test Coupon Bond Systems	119
64	Wiring Arrangement - Special Test Samples	120
65	Hybrid Thermocouple Components	126
66	Reference Design Hybrid Couple	127
67	Hybrid Module Panel	128
68	Hybrid Structure Module Panel Assembly	129
69	Hybrid Module Panel Strips	130
70	Hybrid Module Strips Instrumented - Cold Shoe Thermocouples	131
71	Completed Hybrid Flat Plate Panel Section	132
72	Heat Receptor Thermocouple Locations and Power Leads Locations (W3Re/W25Re Thermocouples Used)	133
73	C/A Cold Junction T/C, Voltage Taps and Current Lead Location	134
74	No. 1 Panel Resistance Data	135
75	No. 2 Panel Resistance Data	136

LIST OF ILLUSTRATIONS (contd.)

APPENDICES

Figure Number	Title	Page
76	Carrier Concentrations (Atoms per Cubic Centimeter x 10^{19})	151
77	63.5 At.% SiGe, Thermoelectric Properties Seebeck Coefficient and Electrical Resistivity vs. Temperature	152
78	63.5 At.% SiGe, Thermoelectric Properties Thermal Conductivity and Figure of Merit vs. Temperature	153
79	80.0 At.% SiGe, Thermoelectric Properties Seebeck Coefficient and Electrical Resistivity vs. Temperature	154
80	80.0 At.% SiGe, Thermoelectric Properties Thermal Conductivity and Figure of Merit vs. Temperature	155
81	70.0 At.% SiGe, Thermoelectric Properties Seebeck Coefficient and Electrical Resistivity vs. Temperature	156
82	70.0 At.% SiGe, Thermoelectric Properties Thermal Conductivity and Figure of Merit vs. Temperature	157
83	Electrical Resistivity n-Type and p-Type SiMo Alloy	158
84	Thermal Resistivity of Silicon Molybdenum Alloy	159

LIST OF TABLES

Table Number	Title	Page
I	Proposed Hybrid Couple Designs	23
II	Proposed Hybrid Couple Designs	25
III	Hybrid Couple Designs Selected for Subcomponent Development Program	26
IV	Preliminary Hybrid Converter Designs	36
V	Preliminary Hybrid Couple Designs	37
VI	Selected Generator Designs	44
VII	Projected Hybrid Couple and Converter Efficiencies 63.5 At.% SiGe and 3M PbTe Compared to RCA 80 At.% SiGe and n-PbTe Thermoelectric Materials	45
VIII	Comparison of Present and Projected B-III Converter Design	47
IX	Projected Test Panel Performance	52
X	Results of p-Type SiGe Cylinder Fabrication	57
XI	Tensile and Shear Strength of n-SiGe Elements	67
XII	Tensile and Shear Strength of n-PbTe Elements	70
XIII	Resistance of PbTe Elements Subjected to Isothermal Life Testing in Argon	76
XIV	Tensile Strength of Intermediate Bond Coupons	87
XV	Summary of Fabrication Methods - Hybrid Thermocouple	91
XVI	Chronological Fabrication Modifications - Hybrid Thermocouple	96
XVII	Summary of Hybrid Couples Fabricated	101
XVIII	Hybrid Couple Performance Summary	102
XIX	Specially Instrumented Thermocouple B-18	109
XX	Bond Resistances of Special Test Samples	117

LIST OF TABLES (contd.)

Table Number	Title	Page
XXI	Bond Resistances of Special Test Samples on Life Test	122
XXII	Hybrid Thermocouple Material and Part Specifications	124
XXIII	Hybrid Thermocouple Assembly Specifications	125

APPENDICES

XXIV	Physical Properties - Thermoelectric Materials	150

Section I.

SUMMARY

The objectives of the Hybrid Thermocouple Development Program, as defined by Contract NAS 3-11843, are: (1) the design and development of a Hybrid thermocouple consisting of a segmented silicon-germanium/lead-telluride n-type leg encapsulated within a hollow cylindrical p-type silicon-germanium leg; (2) a preliminary design of a 250-watt (EOL) planar RTG employing Hybrid thermocouples; and (3) the fabrication of two representative module sections of the generator (nine couples in a three-by-three array) for testing at NASA Lewis Research Center. The program, initiated in January, 1969, was divided into five major tasks as follows:

Task I. Thermocouple Parametric Design Analysis
II. Thermocouple Fabrication and Testing
III. Preliminary Converter Design
IV. Detail Thermoelectric Module Design
V. Fabrication of Modules

The design phase of the program (Tasks I, III and IV) is presented in Section III, Design and Analysis. Task II and Task V, dealing with fabrication and testing, are presented, respectively, in Sections IV and V.

A computer program was formulated to perform the detailed parametric analyses required to optimize the Hybrid couple efficiency for the design operating conditions selected. These operating conditions were as follows:

Hot Junction Temperature	1700°F (926°C)
Intermediate Temperature (PbTe Hot Junction)	1000°F (538°C)
Cold Junction Temperature	450°F (232°C)
Incident Heat Flux	2.0 watts/cm^2

The study indicated that the efficiency of the Hybrid couple would be 10 to 15 percent better than an all-SiGe (63 at.% Si) couple. As a result of the detailed parametric analyses performed and the couple development effort conducted, a Hybrid thermocouple reference design was established with the following characteristics:

Performance	Couple Design B
Power per thermocouple*	0.84 watts
Voltage*	0.185 volts
Current*	4.54 amperes
Internal Resistance*	0.033 ohm
Thermocouple Efficiency*	7.35 %

* Based on analyses which included 5% extraneous resistance and 7% thermal (shunt) loss. Subsequent programs have indicated that 20% extraneous resistance is more realistic. This would reduce couple design B power, for example, from 0.84 to 0.77 watts per couple.

Geometrics	Couple Design B
Area ratio: A_n(n-PbTe)/A_p(p-SiGe)	1.6
Area ratio: A_n(SiGe)/A_n(PbTe)	0.7
Radius of n-type PbTe	0.476 cm (0.1875 inch)
Wall thickness of p-SiGe	0.117 cm (0.046 inch)
Gap between n-PbTe and p-SiGe legs	0.076 cm (0.030 inch)
Length of p-type SiGe	2.86 cm (1.125 inch)
Length of n-type SiGe	1.81 cm (0.714 inch)
Length of n-type PbTe	0.797 cm (0.314 inch)
Heat receptor area	5.9 cm^2 (0.914 $inch^2$)
Heat receptor size	2.44 x 2.44 cm (0.96 x 0.96 inch)
Thermocouple - OD	1.34 cm (0.527 inch)
Thermocouple - ID	1.1 cm (0.435 inch)
n-type SiGe - OD	0.796 cm (0.314 inch)
n-type PbTe - OD	0.953 cm (0.375 inch)

In the development of the thermocouple structure, a number of thermal stress problems were encountered initially in testing of Hybrid thermocouples. Typically, mechanical separation occurred in the cold junction bond of the p-SiGe and the hot junction bond of the n-PbTe segments. Although these same bonds maintained integrity during subcomponent testing, apparently somewhat higher stress levels were encountered in testing of the complete couple assemblies. This problem was corrected by insertion of a gold ring, formed from 0.127 cm (0.050 inch) OD gold tubing, between the p-SiGe tungsten cold shoe and the cold stack prior to the final braze operation to add compliance to the structure.

A total of four couples completed the specified test time of 5000 hours at reference design temperature conditions. Thermal cycling was also performed during these tests.

A preliminary design of a 250-watt (EOL) planar RTG using the reference design Hybrid thermocouples and a water heat pipe radiator was prepared, and its performance is summarized below.

Converter Parameter	Converter B III
Power Output (BOL)	273 watts
Efficiency	6.4 %
Hot Junction Temperature	926°C (1700°F)
Cold Junction Temperature	232°C (450°F)
Converter Weight	33.8 kg (76 lbs)
Heat Pipe Radiator Weight	10.2 kg (23 lbs)
Fuel Source Weight	32.5 kg (73 lbs)
Total Generator Weight	78.2 kg (172 lbs)
Specific Power (BOL)	3.5 w/kg (1.59 w/lb)

The reference Hybrid converter design is based on the predicted performance of couple design B, above. Although preliminary test results to date are encouraging, much more testing and evaluation of Hybrid couples are required to establish this concept. Further improvements in Hybrid couple performance might be achieved with additional development effort. Some of the possible design modifications and their corresponding predicted performance are presented below.

	Couple Efficiency	Converter Efficiency	Converter Specific Power (BOL)
Reference Design B-III	7.4%	6.4%	3.5 w/kg (1.59 w/lb)
(1) Thermoelectric Materials 80% n-SiGe - RCA ternary n-PbTe	8.5%	7.5%	4.1 w/kg (1.86 w/lb)
(2) Hot Shoe Temperature - 1000°C and Thermoelectric Materials	9.4%	8.4%	4.58 w/kg (2.08 w/lb)

Hybrid couples, fabricated initially, were characterized by higher than predicted resistance and, in some cases, bond separations. Couples made later in the program, using improved fabrication techniques, exhibited normal resistances both as-fabricated and after 700 hours of testing.

At the conclusion of the program, two module sections of the reference design Hybrid module were fabricated and delivered to NASA Lewis for testing.

Section II.

INTRODUCTION

The thermoelectric materials most often considered for purposes of energy conversion in space are alloys of silicon and germanium and alloys of lead and tellurium. Silicon-germanium alloys are attractive in terms of mechanical strength, machineability and their unprotected operation in either air or vacuum environments at temperatures up to 1000°C (1832°F). The n-type SiGe alloys exhibit a slight change in electrical resistivity and Seebeck coefficient with time because of a temperature dependence of the solid solubility of dopant (see Figure 76, Appendix I). While these effects are self-cancelling to some extent, the electrical resistivity change is considerably greater than the increase in Seebeck coefficient, thus resulting in a slight decrease in thermoelectric performance with time. The largest change occurs at the intermediate temperatures, i.e., 200°C to 600°C, due to a combination of a highly supersaturated dopant-SiGe solid solution and a reasonable rate of dopant diffusion. Metallurgical bonds are employed for both hot and cold contacts in the SiGe thermocouples.

Lead telluride (PbTe) alloys can be operated from room temperature to about 600°C (1100°F); however, they must be protected from the environment in most applications. The main attractiveness of tellurides is their excellent ability to convert heat to electricity, reflected by the so-called "figure-of-merit". Up to temperatures of about 550°C (1022°F), the tellurides have a higher figure-of-merit than the SiGe alloys. Although some problems have been encountered with metallurgically bonded PbTe couples, indications are that the n-type PbTe bonds are reliable.

A careful review of the operating characteristics of both alloys and results of preliminary development of a low temperature "Hybrid" thermocouple conducted by RCA, suggested a high temperature, 926°C (1700°F), Hybrid thermocouple design having a segmented SiGe--PbTe n-leg and a SiGe p-leg. The low temperature, 538°C (1000°F), Hybrid couple, built and tested in 1968, consisted of a n-PbTe leg encapsulated within a p-SiGe cylindrical leg as shown in Figure 1. The high temperature Hybrid thermocouple, described herein, employs SiGe air-vac technology and has a segmented n-leg. The n-type PbTe is used up to temperatures of about 538°C (1000°F), and n-type SiGe at higher temperatures. This arrangement takes advantage of the high figure-of-merit of PbTe below 538°C (1000°F) and stable performance of n-type SiGe above 538°C (1000°F). The p-leg is fabricated in the form of a hollow cylinder and used to encapsulate the segmented n-leg, thereby protecting the PbTe. This high temperature Hybrid thermocouple configuration should provide a high performance device with stable electrical characteristics. Details of the proposed Hybrid couple design are shown schematically in Figure 2. Both ends of the p-type SiGe cylinder are metallurgically bonded, one to the silicon-molybdenum hot shoe and the other to the cold-stack assembly. The cold-stack assembly is attached to a mounting stud. Two electrical insulators in the cold-stack assembly provide electrical isolation of the two thermocouple legs from each other and from the stud. Each leg is contacted to an electrical connector. The n-type PbTe thermo-

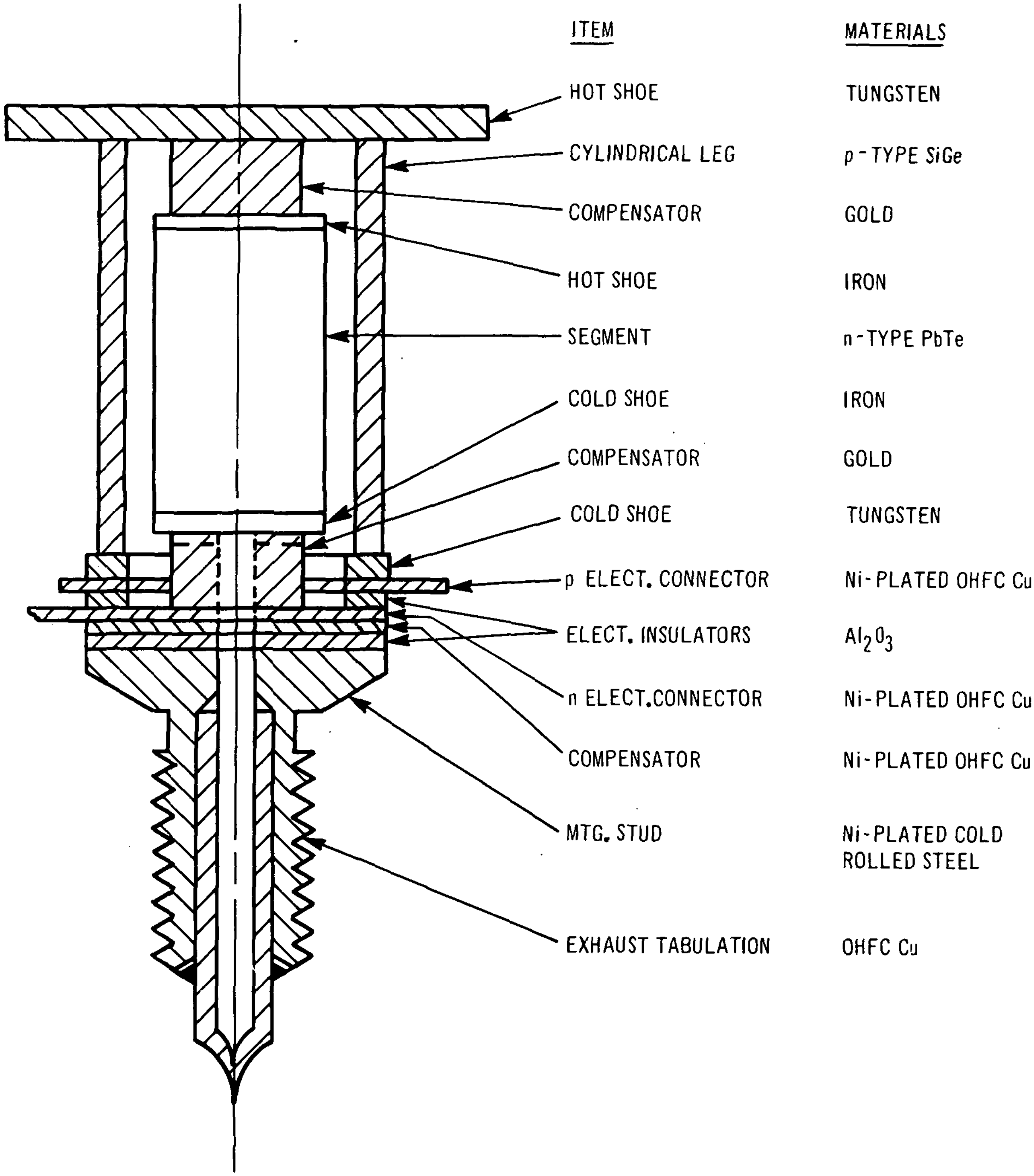

Figure 1. Hybrid Thermocouple Prototype Design

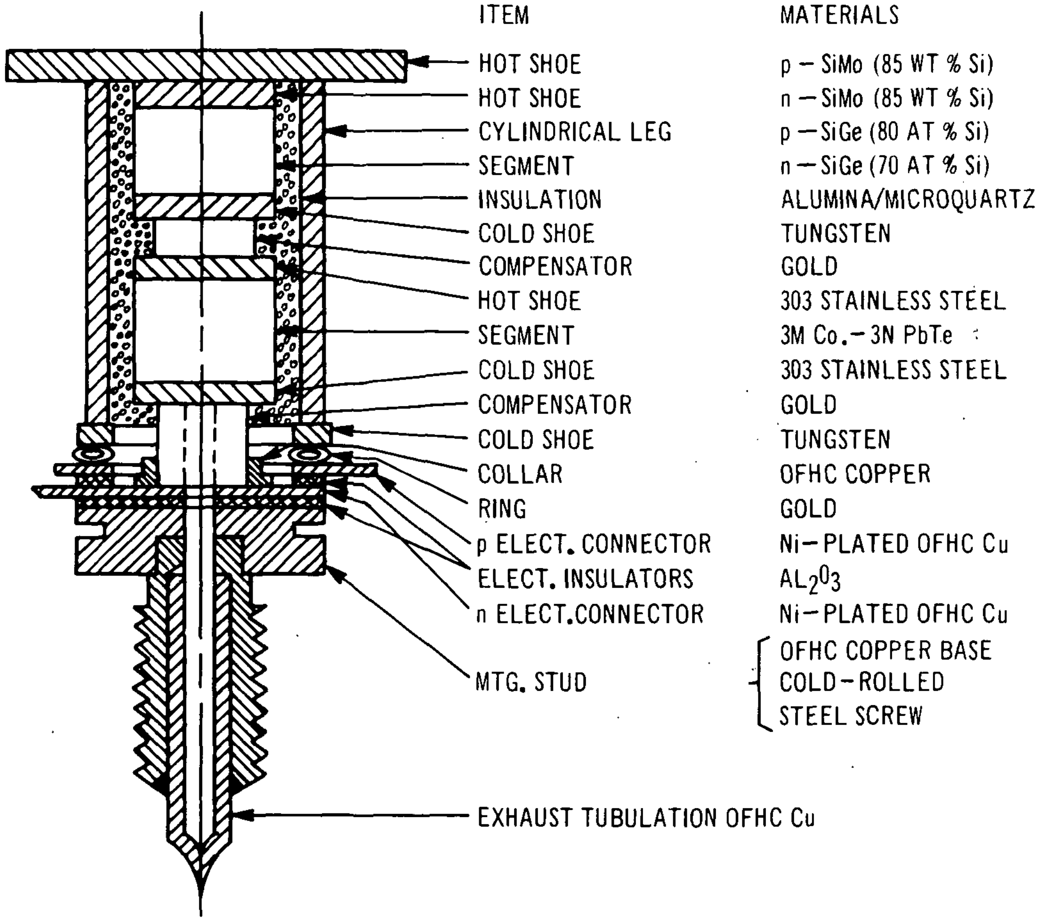

Figure 2. Hybrid Thermocouple Assembly

element is contacted to metal shoes. The n-type PbTe cold shoe is bonded through a stress compensator to the cold-stack assembly. The n-type PbTe hot shoe is bonded through a stress compensator to the cold shoe of the n-type SiGe. The hot end of the SiGe element is bonded to the SiMo hot shoe. The space between the p-type and n-type thermoelements is filled with thermal insulation. Finally, the couple is sealed in an inert-gas atmosphere to inhibit sublimation of the PbTe.

The Hybrid thermocouple efficiency is predicted to exceed that of an all-silicon-germanium thermocouple by approximately 10-15% depending upon the operating temperatures.

On January 23, 1969, a contract was awarded RCA Electronic Components, Harrison, N.J., by NASA Lewis Research Center to design and develop the Hybrid thermocouple concept. The overall objectives were:

1. The design and development of a Hybrid thermocouple consisting of a segmented silicon-germanium/lead-telluride n-type leg encapsulated within a SiGe p-type concentric leg.

2. The fabrication and delivery to NASA Lewis Research Center of two flat plate module sections of a thermoelectric converter employing Hybrid thermocouples. Each module section was to have a projected area of between 9 and 16 square inches.

To accomplish these objectives, the program was divided into five major tasks as follows:

Task I. Thermocouple Parametric Design Analysis
II. Thermocouple Fabrication and Testing
III. Preliminary Converter Design
IV. Detail Thermoelectric Module Design
V. Fabrication of Modules

The results of Tasks I, III and IV are presented in total in Section II, Design and Analysis; Task II and Task V are presented, respectively, in Sections IV and V.

Section III.

DESIGN AND ANALYSIS

A. Design Requirements

The primary design objective of this program is to develop a flat plate thermoelectric module using Hybrid thermocouples, capable of integration into a 250-watt thermoelectric planar converter. A heat pipe radiator is to be considered analytically (no hardware development) for the heat sink. The performance objectives are given below.

1. Converter Power - 250 watts (EOL)

2. Converter Life

   Modules shall produce the design power at the end of five years.

3. Operating Temperatures

   Hot Junction - 926°C (1700°F) maximum
   Interface (PbTe Hot Junction) - 538°C (1000°F) maximum
   Cold Junction - 316°C (600°F) maximum

4. Incident Heat Flux - 2 watts/cm^2

5. Thermoelectric Material Properties

	SiGe	PbTe
Temperature	900°C (1674°F)	500°C (954°F)
Seebeck Coefficient (μV/°C, max)	270	230
Electrical Resistivity (ohms-cm, max)	0.003	0.003
Thermal Conductivity (watts/cm-°C, max)	0.045	0.017

6. Performance Degradation

Thermoelectric Material	10% maximum
Electrical Insulation	5% maximum
Extraneous Resistance (joints, bonds, etc.)	5% maximum

7. Environmental Conditions

   The module shall be designed to meet the following requirements, but no environmental testing of the module is required under this contract.

   a. Acoustic Noise: The module shall be capable of withstanding for five minutes a total integrated sound pressure level of 152 decibels referred to 0.0002 dyne per square centimeter.

b. Vibration: The module shall be capable of withstanding sinusoidal input applied at the mounting points for a period of 15 minutes along each of three mutually perpendicular axes as follows:

5-33 cps at 0.14 inch D.A. displacement
33-140 cps at 8.0 G's peak
140-240 cps at 0.003 inch D.A. displacement
240-2000 cps at 15.0 G's peak

c. Acceleration: The module shall be capable of withstanding 6 G's acceleration for five minutes in both directions along three mutually perpendicular axes.

d. Shock: The module shall be capable of withstanding a 20-G shock along each of three mutually perpendicular axes. The waveshape shall be a half-sine pulse of 10-millisecond duration.

e. Thermal Transient: The module shall be capable of withstanding the following thermal transient test. It shall be heated to an absorber surface temperature of 1700°F as rapidly as possible when subjected to the thermal flux required to achieve this hot junction temperature. Immediately after temperature equilibrium has been established, heating shall cease. The module shall be allowed to cool to an equilibrium temperature by radiating to the surrounding walls of a water-cooled chamber. When a steady temperature has been obtained, the absorber surface shall again be heated to a temperature of 1700°F and allowed to cool to a steady temperature in the water-cooled chamber.

B. Hybrid Thermocouple Design

1. Performance of the Hybrid Thermocouple

The design of the Hybrid thermocouple was undertaken with the object of optimizing its conversion efficiency, consistent with physical and manufacturing constraints. A computer program was established in order to perform the detailed parametric analyses required to optimize the Hybrid couple efficiency for the design operating conditions selected. The thermoelectric materials used in the initial Hybrid couple design analyses are listed below.

n-type PbTe segment - 3M Co.'s 3N alloy
n-type SiGe segment - RCA 63.5 At.% Si-SiGe alloy
p-type SiGe cylinder - RCA 63.5 At.% Si-SiGe alloy

The Hybrid couple computer design program and the thermoelectric material properties are presented in detail in Appendix II, Sections A and C-1, respectively.

Figure 3 shows the physical model on which the analytical program was based. The thickness dimensions, materials, and geometrical configuration are based on the earlier RCA development effort but do not represent a specific design. Because the design of the cold stack of both the n- and p-type element legs depends on fabrication constraints, availability of materials, and cost, it is not represented as it would be fabricated, but rather as a representative cold stack for analytical purposes. The couple efficiency is not highly sensitive to small variations in cold-stack temperature drop because these variations are small compared to the total temperature difference, ΔT, that appears across the total length of the thermoelectric element. When selecting the final design configuration, every effort was made to minimize the temperature drop across the cold stack.

In addition to the thermoelectric materials, the important input parameters which affect the Hybrid thermocouple efficiency are the incident heat flux density, the hot and cold junction operating temperatures, and the geometry. To permute the many values and variables associated with each of these parameters would result in design data too cumbersome to analyze. Therefore, some of the parameters and their values were fixed in order to limit the number of cases generated.

The values of input parameters used initially are as follows:

a. Operating Conditions

1) Heat receptor temperature (THP): 926°C (1700°F)
2) Interface temperature of PbTe hot junction (THN2C): 538°C (1000°F)
3) Cold junction temperature of p-type element (THP): 232°C (450°F)
4) Incident heat flux densities considered (PHI): 1, 3, 5, watt/cm^2

b. Couple Geometrics

1) P-type element length (FLP): 2.54 cm (1.00 in.), 3.17 cm (1.25 in.), 3.81 cm (1.50 in.)
2) Ratio of n-type PbTe area to p-type element area (ANP): 1.0, 1.4, 1.8, 2.2
3) Ratio of n-type SiGe area to n-type PbTe area (ANR): 0.4, 0.7, 1.0
4) Radius of n-type PbTe element (RRN): 0.406 cm (0.16 in.), 0.508 cm (0.20 in.), 0.61 cm (0.24 in.)

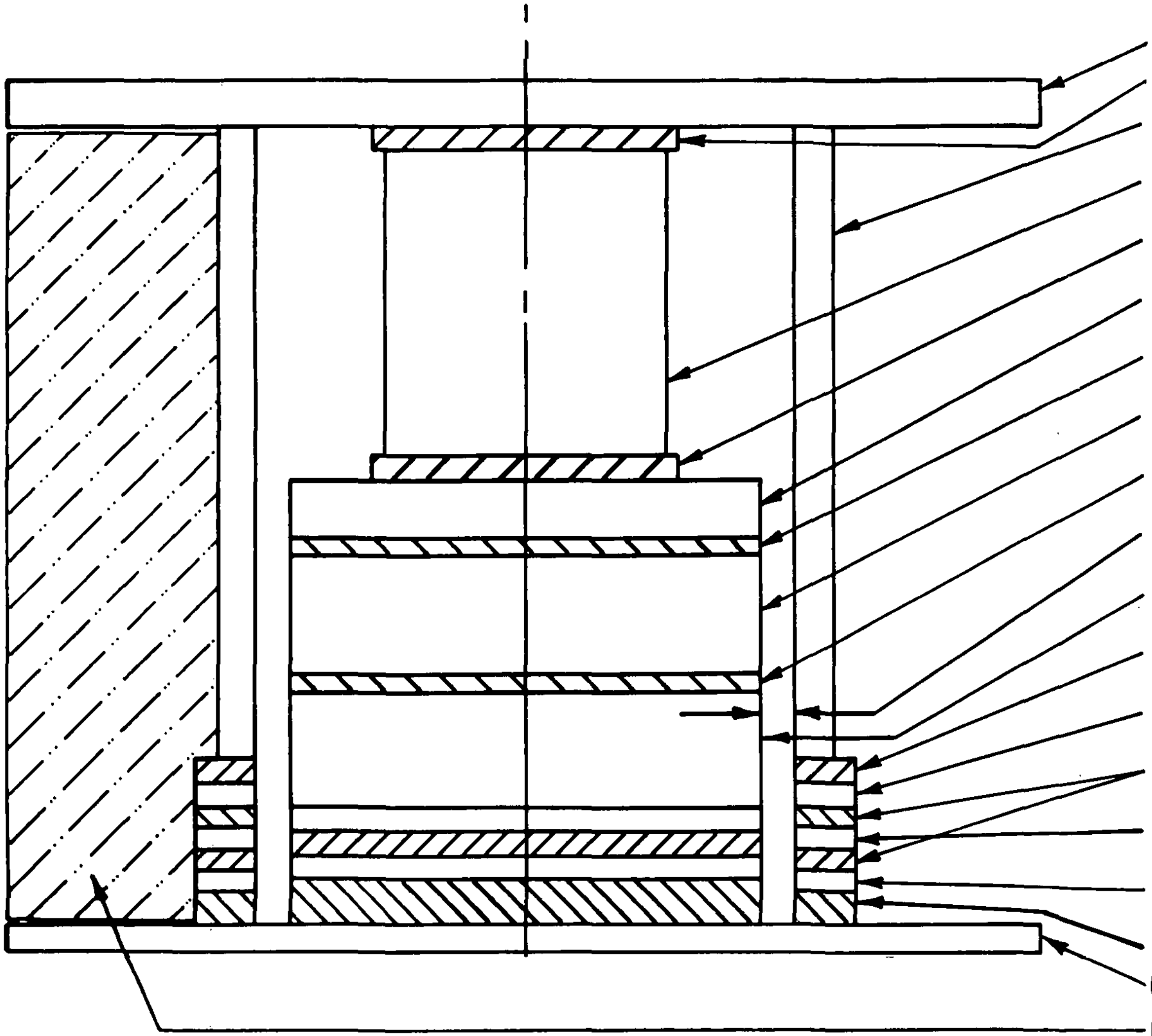

COMPONENT	MATERIALS	THICKNESS (MILS)
HEAT RECEPTOR	p-TYPE	75
HOT SHOE	n-TYPE	20
CYLINDRICAL	p-TYPE SiGe	xx
SEGMENT 1	n-TYPE SiGe	xx
COLD SHOE	W	40
COMPENSATOR	Au	40
HOT SHOE	Fe	40
SEGMENT 2	n-PbTe (3N)	xx
COLD SHOE	Fe	40
GAP	—	30
COMPENSATOR	Au	90
COLD SHOE	W	40
p-TYPE ELECTRICAL CONN	Cu (Ni PLATE)	20
INSULATOR	Al_2O_3	20
n-TYPE ELECTRICAL CONN.	Cu (Ni PLATE)	20
COMPENSATOR	Cu (Ni PLATE)	20
MTG STUD	304 SS	50
HEAT REJ. PLATE	Al	125
INSULATION	MIN-K 2020	xx

xx – DIMENSIONS GIVEN AS OUTPUT DATA IN THE ANALYSIS.

Figure 3. Physical Model of Hybrid Couple for Cases 1B to 1E

The capital letters in parentheses are the code names of the input variables used in the computer program. A complete list of computer symbols is given in Appendix II, Section D-1. Briefly, the program, through an iterative process, successively approximates a consistent set of values for the heat flowing through the element legs and for the proportionate lengths of the n-type segments. Having converged these values to 0.1 percent, the program continues to determine the proper heat receptor size (p-type SiMo hot shoe size) for the desired incident heat flux density. The various input parameters are sequentially permuted to obtain the couple design yielding optimum efficiency. The effects of these input variables on the Hybrid couple design and the resultant output data are presented in Figures 4 through 12.

The following discussion primarily involves couple materials, geometrics, and operating conditions. (Constrains such as part availability, costs, and mechanical limitations will be considered later.)

Figure 4 shows the relationship of incident heat flux density and p-type element length to couple efficiency. In general, it is desirable to make the couple as long as possible and to design for the highest possible heat flux density. Note that as the incident heat flux density is increased (from 1 to 3 watts/cm^2, for example), the relative gain in efficiency as a result of increasing element length is reduced.

Figure 5 shows the effect of varying heat receptor area on couple efficiency for various values of incident heat flux density and n-type PbTe radius for a p-type element length of 1.25 inches. At the time of the analysis, fabrication considerations limited the SiMo heat receptor size to an area of 14.5 cm^2 (1.5 in. x 1.5 in. square hot shoe). Subsequent development of hot pressing procedures has essentially removed this constraint.

Figure 6 shows that varying the diameter of the n-type PbTe element has minimum effect on efficiency, whereas the n-PbTe/p-SiGe area ratio, ANP, more significantly affects the efficiency.

Figure 7 shows the effect of varying the incident heat flux density and the ANP ratio on couple efficiency. Generally, as the flux density decreases, so does the effect of ANP on efficiency. In this case, as will be seen later, a lower ANP ratio is desirable in order to maintain adequate p-type SiGe element wall thickness.

Figure 8 shows couple efficiency plotted against the ratio of n-type SiGe area to n-type PbTe area (ANR). The need to consider ANR values less than one becomes apparent when analyzing the relative n-type segment lengths of SiGe and PbTe. (See Figure 12.) Reducing the value of ANR below 1.0 has the effect of lengthening the PbTe segment with an attendant decrease in the n-SiGe segment length, assuming fixed

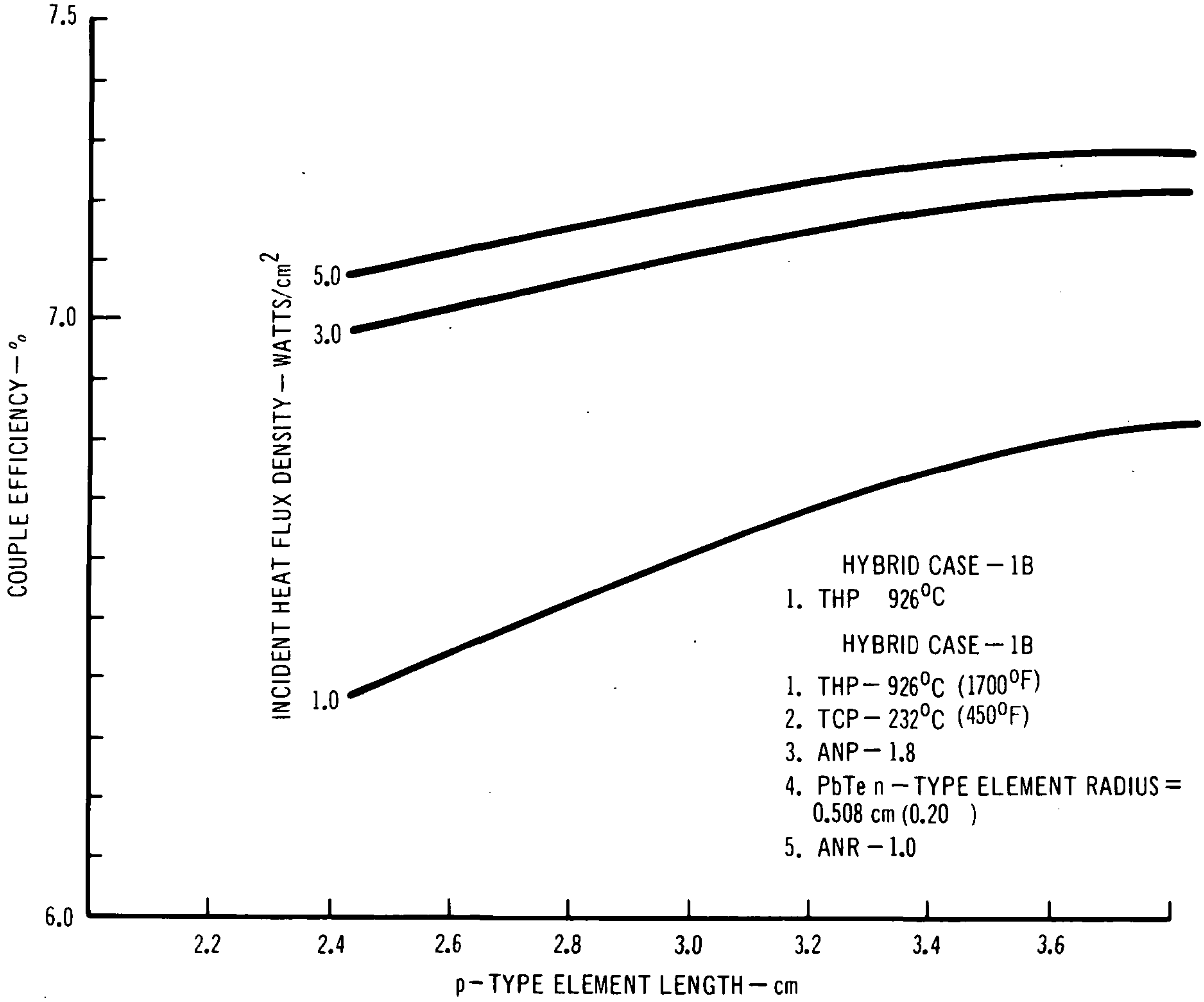

Figure 4. Couple Efficiency Vs p – Type Element Length for Various Heat Flux Densities

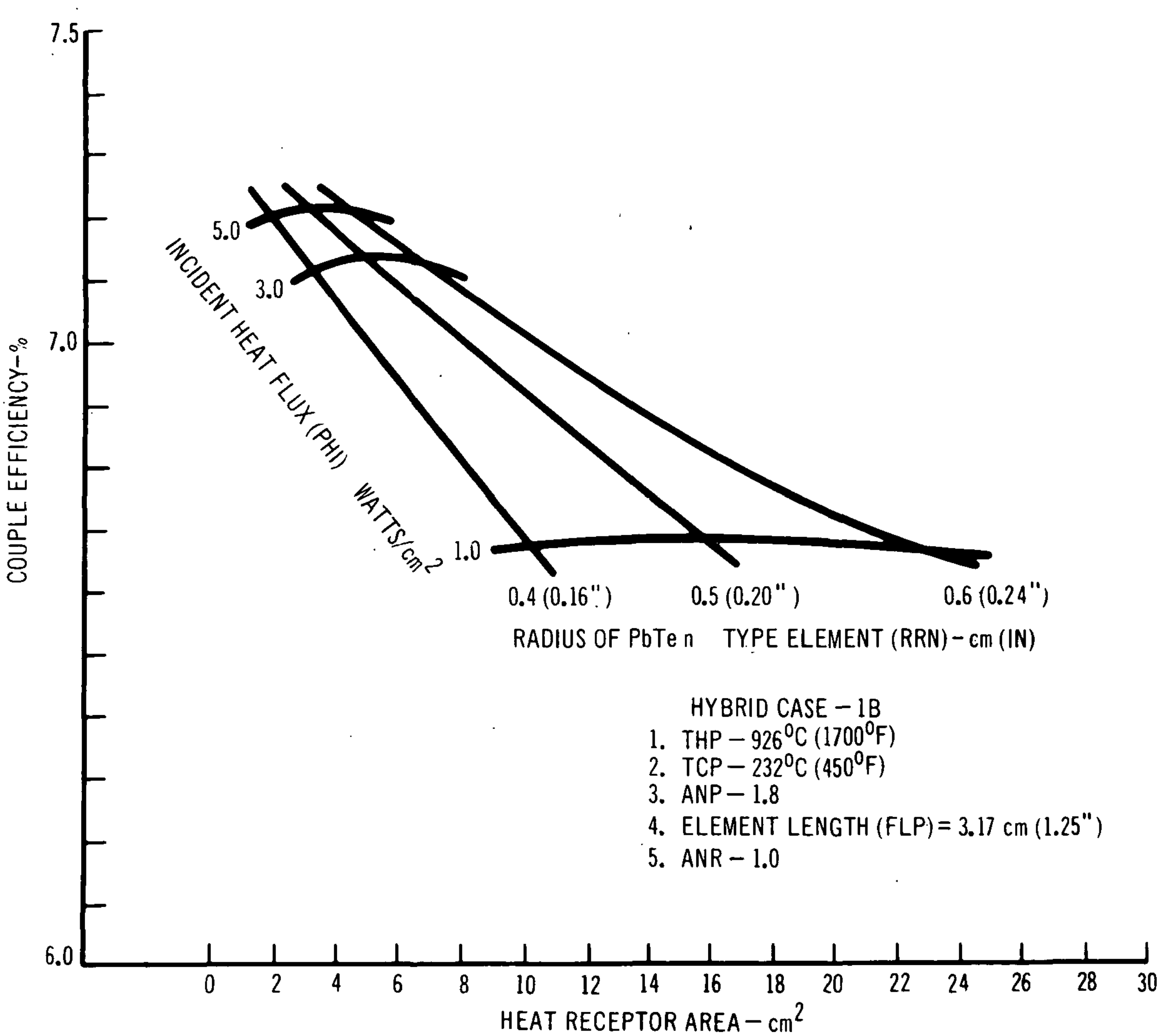

Figure 5. Couple Efficiency Vs Heat Receptor Area For Various Heat Flux Densities and Radii of n PbTe Element

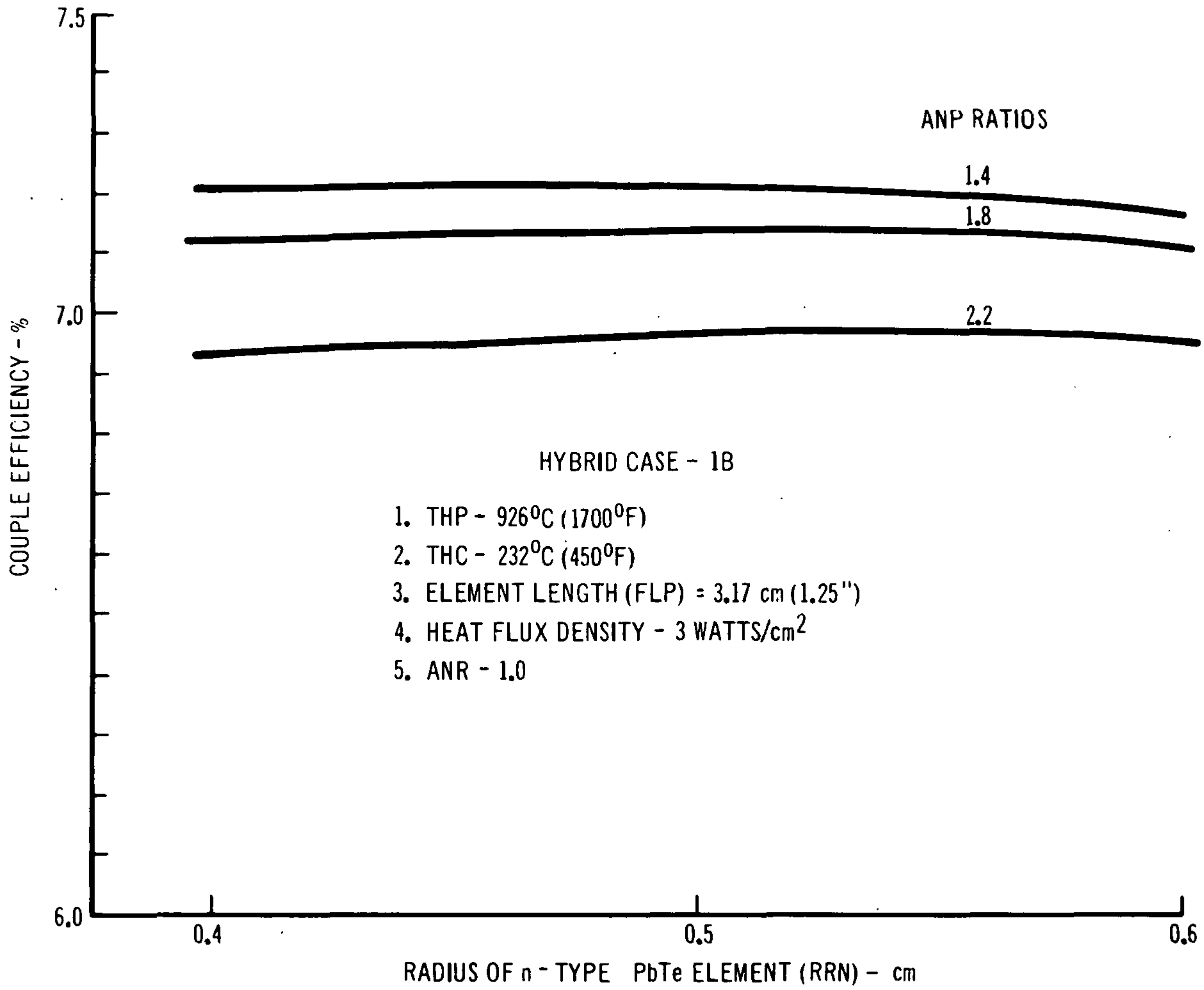

Figure 6. Couple Efficiency Vs. Radius n Type PbTe Element for Various ANP Ratios

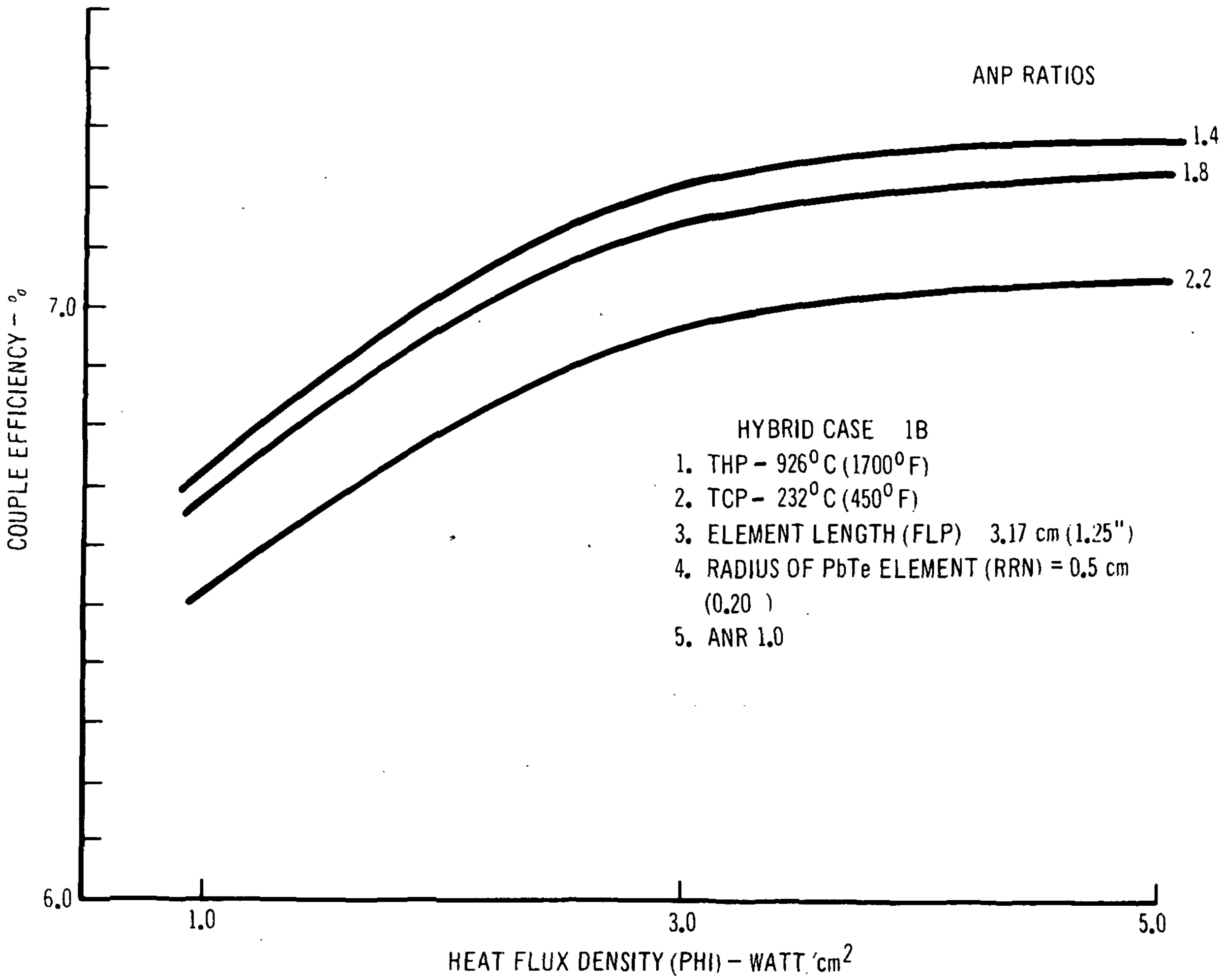

Figure 7. Couple Efficiency Vs. Heat Flux Density For Various ANP Ratios

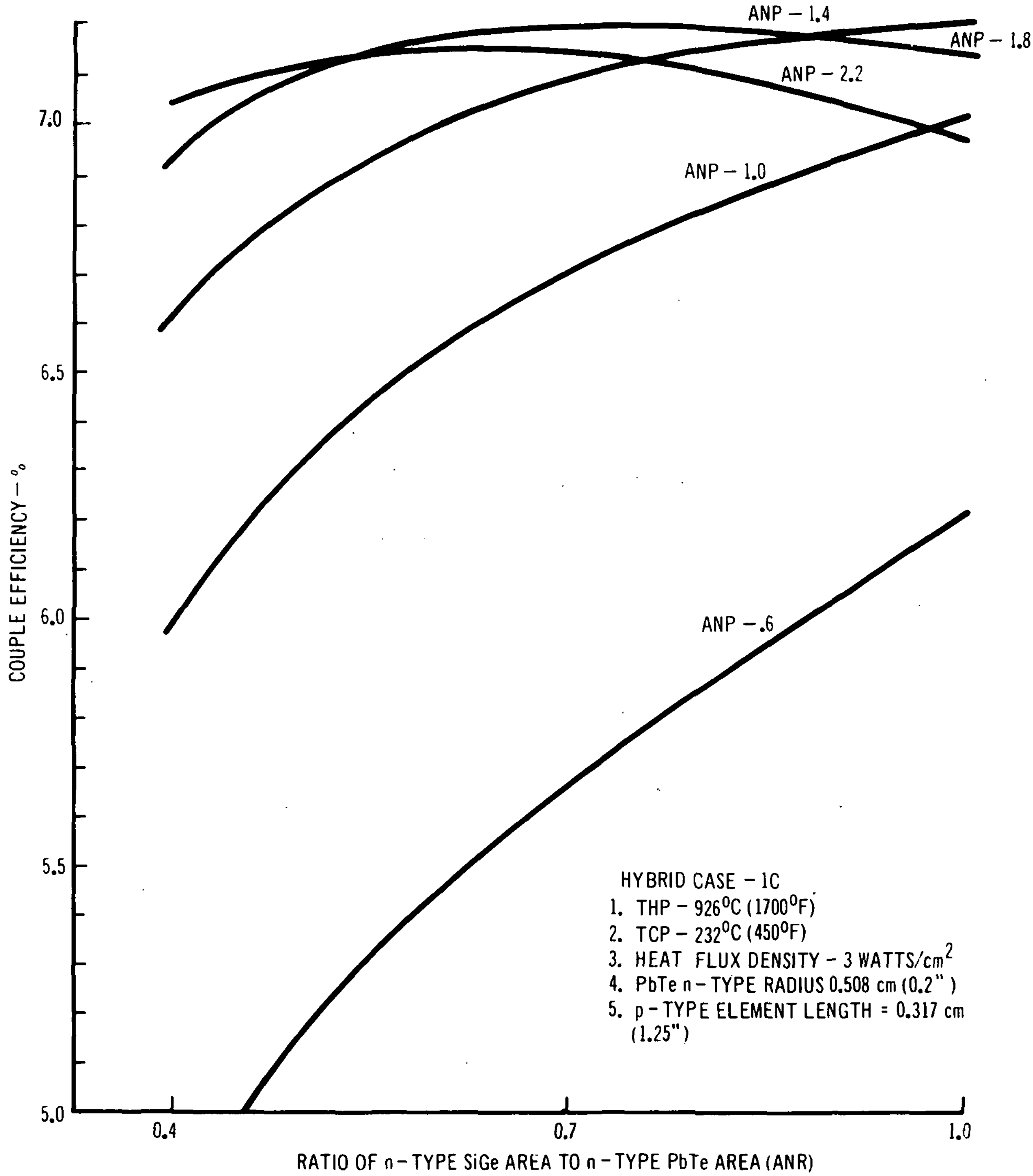

Figure 8. Couple Efficiency Vs. Ratio of n – Type SiGe To n – Type PbTe Area (ANR) For Various AN TO AP Ratios (ANP)

junction temperatures. With an ANR near 1.0 and an overall couple length of approximately one inch, the PbTe segment assumes the geometric proportions of a tablet. From a thermal stress point of view and in order to minimize the effect of contact resistance, it is desirable to lengthen the PbTe element. Figure 8 was constructed to illustrate the extent to which the n-PbTe length could be increased without compromising couple efficiency.

Figure 9 illustrates the effect of input variables of FLP (p-type element length), ANP, and ANR on couple efficiency. A couple length of 3.17 cm (1.25 inches), an ANP of 1.8 and an ANR of 0.7 represent a reasonable compromise for lengthening the n-type PbTe segment while maintaining a relatively high efficiency.

Figure 10 again shows the effect of ANR and ANP on couple efficiency to give a better definition of where the optimums occur relative to efficiency. For the expanded efficiency scale drawn, ANP values between 1.6 and 1.8 would affect efficiency less than 0.1% for an ANR equal to 0.7. Also, lower ANP ratios would result in an increase in the wall thickness of the p-type element cylinder.

Figures 11 and 12 illustrate the important geometrical relationships involved in fabricating a Hybrid couple. The most important of these curves is Figure 11, relating wall thickness of the p-type element cylinder to ANP and the radius of the n-PbTe segment. The constraining factors here involve fabrication costs and hermeticity; both problems diminish as the wall thickness increases. The lower practical limit of wall thickness is about 40 mils (0.106 cm).

Based on the parametric analyses of the Hybrid couple, three couple designs (see Table I) were proposed as the design basis for initiation of Task II, Thermocouple Development and Testing. The data presented in Table I indicate the operational characteristics of these designs as well as the associated geometrical factors. The intent of these couple designs was to determine the capability of fabricating couples with varying geometries to meet expected requirements of operating conditions while maintaining optimum efficiency.

These designs covered a broad range of geometrical sizes and shapes for couples intended for operation with heat sources providing 1.0, 3.0, and 5.0 watts per cm^2 incident heat flux densities. Although a range of couple geometries was covered, the operating incident heat flux densities did not appear wholly consistent with heat sources that would be available for use with thermoelectrics in the foreseeable future. Consequently, the Hybrid couple design was reoriented for use with a heat source having a heat flux density of 2.0 watts per cm^2. This change was proposed by NASA-LeRC as being more representative of future heat source capability. Furthermore, investigation was recommended of various couple diameters as well as of the previously proposed variations in heat receptor sizes and element length. Varying the diameter of the couples, in effect, varies

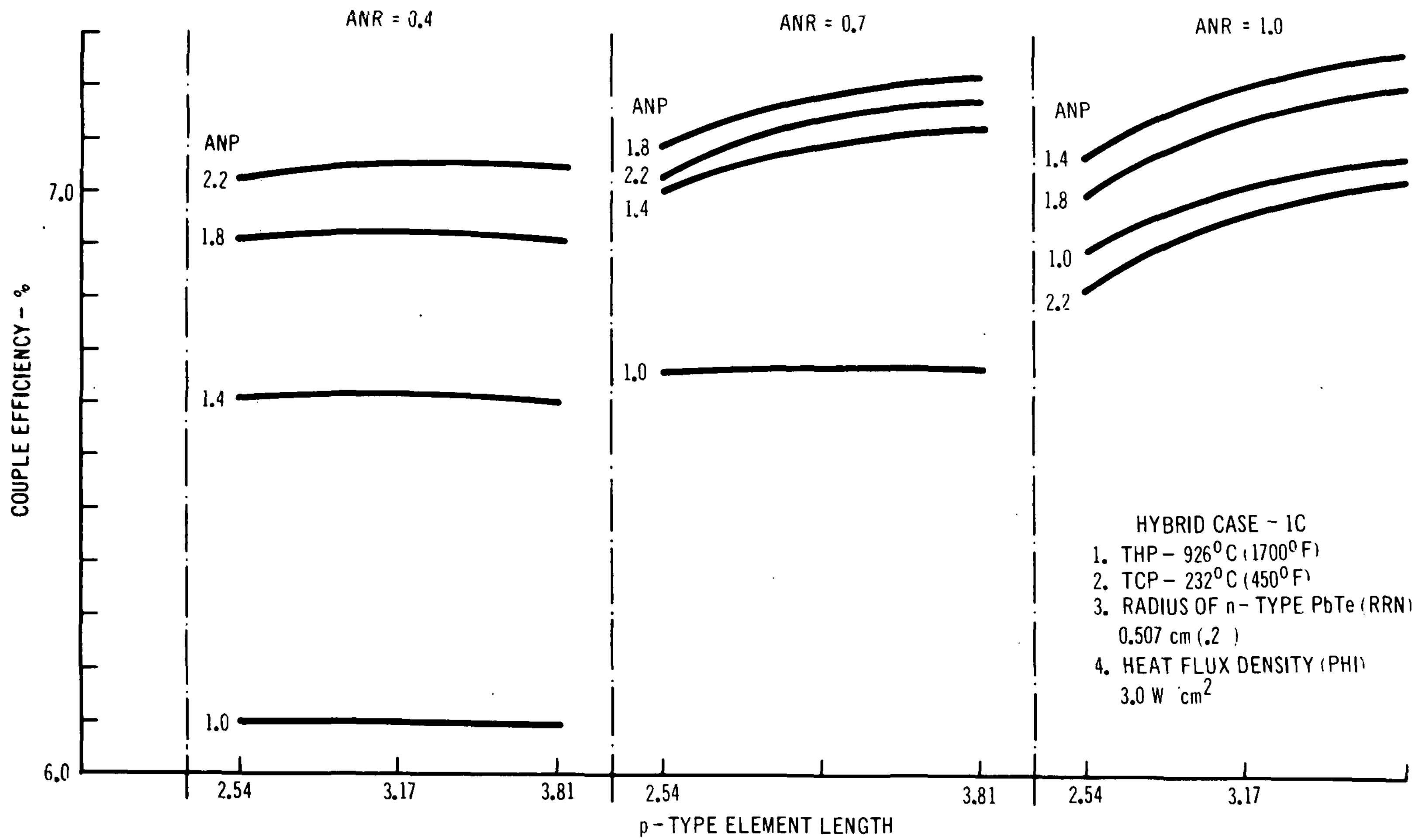

Figure 9. Couple Efficiency Vs. p – Type Element Length for Various n – Type SiGe to PbTe Area Ratios (ANR) and n – Type PbTe Area to p – Type SiGe Area Ratios (ANP)

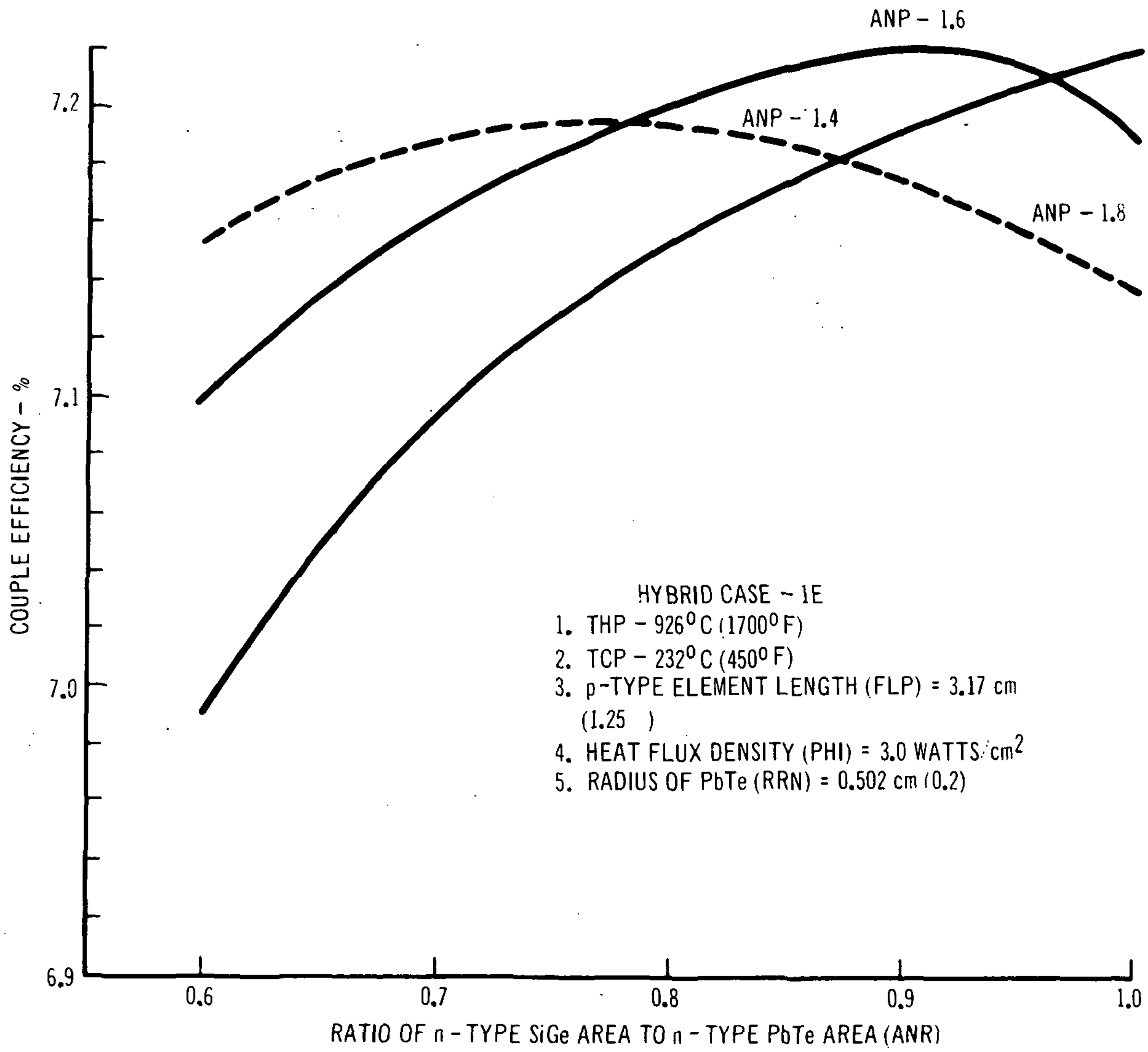

Figure 10. Efficiency Vs. Ratio of n - Type SiGe Area n - Type PbTe Area (ANR) for Various AN/AP Ratios (ANP)

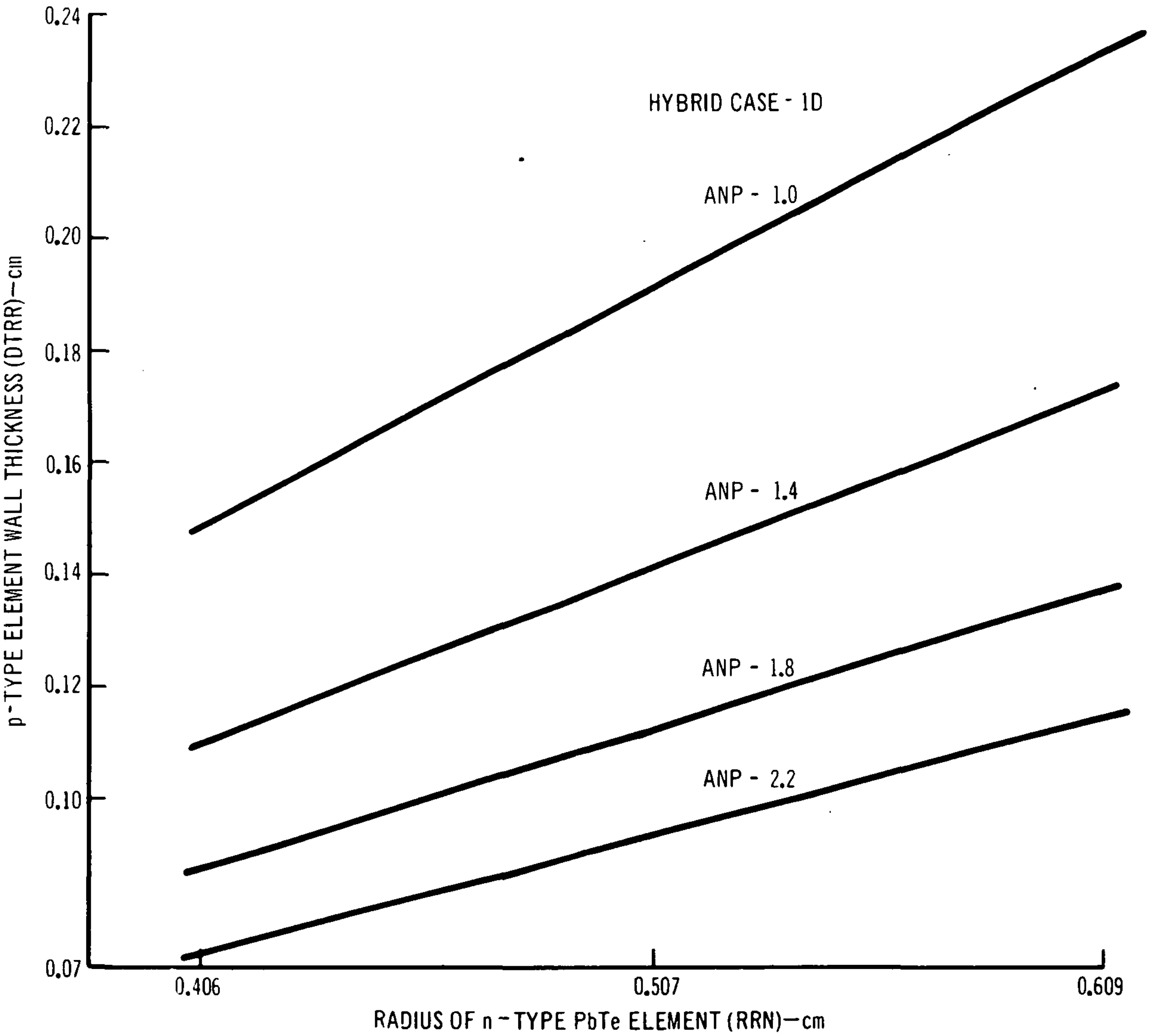

Figure 11. p- Type Element Wall Thickness Vs. Radius of n - Type PbTe Element for Various n- Type PbTe Area to p- Type SiGe Area Ratios (ANP)

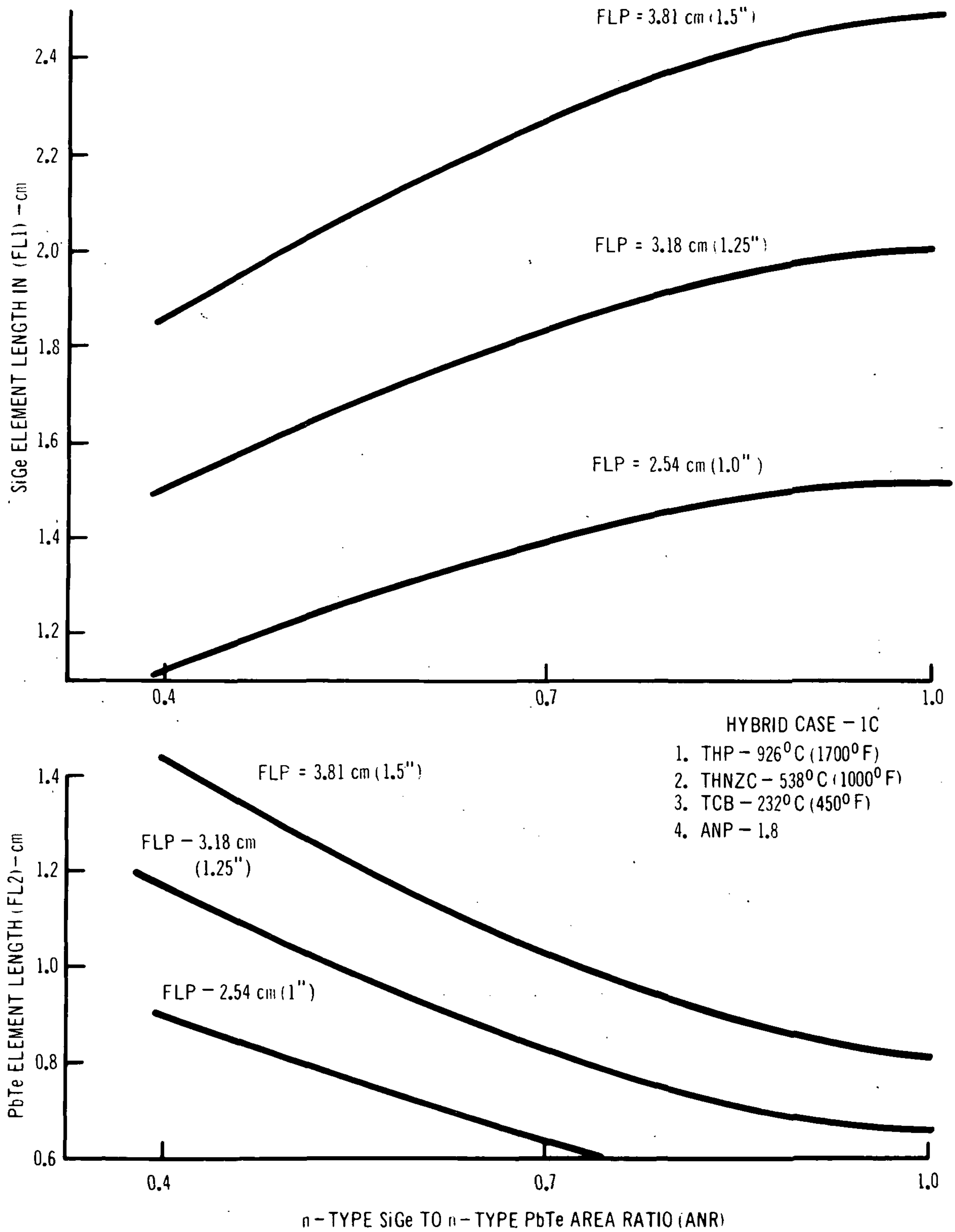

Figure 12. Length of n-Type SiGe and n-Type PbTe Segments Vs. n-Type SiGe to n-Type PbTe Area Ratio (ANR) for Various p-Type Element Lengths

TABLE I

PROPOSED HYBRID COUPLE DESIGNS

DESIGN PARAMETERS	Units	A	B	C
Operational				
1) Couple Efficiency	%	7.7	7.7	7.6
2) Power per Couple	watts	0.737	0.886	1.11
3) Voltage	volt	0.186	0.186	0.186
4) Current	Amps	3.962	4.763	5.968
5) Internal Resistance	ohms	0.0393	0.0326	0.026
6) Hot Junction Temp.	°C/°F	926/1700	926/1700	926/1700
7) Cold Junction Temp.	°C/°F	232/450	232/450	232/450
8) Interface Temp.	°C/°F	538/1000	538/1000	538/1000
9) Incident Heat Flux	$watt/cm^2$	1.0	3.0	5.0
Geometrics				
1) RRN - Radius of n-type PbTe (in.)		0.1875	0.1875	0.1875
2) ANP - A_n/A_p		1.6	1.6	1.6
3) ANR - A_n(SiGe)/A_n(PbTe)		0.7	0.7	0.7
4) DTRR - Wall Thickness (in.)		0.046	0.046	0.046
5) GAP - Gap between n-p legs (in.)		0.030	0.030	0.030
6) FLP - Length of p-type SiGe (in.)		1.500	1.250	1.000
7) FL1 - Length of n-type SiGe (in.)		0.910	0.720	0.550
8) FL2 - Length of n-type PbTe (in.)		0.390	0.330	0.250
9) AH - Heat Receptor Area ($in.^2$)		1.500	0.590	0.460
10) FH - Heat Receptor Dimension (in.)		1.225 x 1.225	0.77 x 0.77	0.68 x 0.68
11) Thermocouple OD (in.)		0.531	0.531	0.531

the wall thickness of the p-element cylinder, assuming a constant A_n/A_p ratio. The wall thickness depends upon fabrication limitations which, in turn, becomes a design constraint.

As a result of a design review meeting, a consistent set of Hybrid couple design conditions were again developed. The incident heat flux density was fixed at 2.0 watts per cm^2, for a hot junction temperature of 926°C (1700°F), a cold junction of 232°C (450°F), and an interface temperature of 538°C (1000°F). In addition, three couple diameters and element lengths were permuted. The design variations for the above operating conditions and geometric inputs are covered in the nine cases of Table II.

Analyses of these designs indicated that the greatest spread of geometrics existed in designs A-3, B-2, and C-1. Based on the current state-of-the-art fabrication techniques, design B-2 comes closest to representing current capability. Cases A-3 and C-1, however, typify designs which expand current technology in terms of element length, wall thickness, and couple diameter. Hence, these three designs were selected as offering the desired variation in couple geometrics.

Closer inspection of designs A-3 and C-1 in Table II revealed that minor changes in dimensions could be made based on certain practical considerations. With reference to the A-3 design, for example, the 0.150-inch radius of the n-type PbTe segment is a non-standard size. Modifying this radius, however, to 0.125 inch would permit purchase of standard material with the attendant benefits of cost and immediate availability. Consequently, design A of Table III was adopted as a practical version of design A-3 of Table II. Moreover, design A enhances the spread of couple geometrics to be investigated.

Design C-1 of Table II requires a p-type element cylinder of a diameter which exceeds current "state-of-the-art" ingot sizes, the maximum being 0.600 inch in diameter. Thus, in design C of Table III, the radial dimensions have been accordingly reduced to meet the fabrication constraint placed on the O.D. of the p-type cylinder.

The three designs of Table III, therefore, represent a compromise in terms of operating conditions, couple geometrics, and practical material considerations, while maintaining near-optimum operating efficiencies for the designs cited. The indicated Hybrid couple efficiencies of 7.1 to 7.5 percent represent a beginning-of-life improvement of 10 to 15 percent over an all-SiGe thermocouple (63 at.% Si alloy) operating at the same junction temperature. These couple designs formed the basis for the subcomponent and thermocouple development performed in Task II-A, 1 and 2.

TABLE II

PROPOSED HYBRID COUPLE DESIGNS

DESIGN PARAMETERS		A			B			C		
Operational	Units	1	2	3	1	2	3	1	2	3
1) Couple efficiency*	%	7.2	7.4	7.5	7.2	7.4	7.5	7.1	7.3	7.4
2) Power per couple*	watt	0.719	0.573	0.476	1.110	0.886	0.737	1.570	1.260	1.050
3) Voltage*	volt	0.186								
4) Current*	amperes	3.866	3.081	2.559	5.968	4.763	3.962	8.441	6.774	5.645
5) Internal resistance*	ohms	0.040	0.050	0.061	0.026	0.033	0.039	0.018	0.023	0.028
6) Hot junction temperature	°C/°F	926/1700								
7) Cold junction temperature	°C/°F	232/450								
8) Interface temperature	°C/°F	538/1000								
9) Incident heat flux	watt/cm^2	2.0	2.0	2.0	2.0	2.0	2.0	2.0	2.0	2.0
Geometrics										
1) ANP - A_n/A_p		1.6	1.6	1.6	1.6	1.6	1.6	1.6	1.6	1.6
2) ANR - A_n(SiGe)/A_n(PbTe)		0.7	0.7	0.7	0.7	0.7	0.7	0.7	0.7	0.7
3) RRN - Radius of n-type PbTe	inch	0.150	0.150	0.150	0.1875	0.1875	0.1875	0.225	0.225	0.225
4) DTRR - Wall thickness	inch	0.036	0.036	0.036	0.046	0.046	0.046	0.056	0.056	0.056
5) GAP - Gap between n-p legs	inch	0.030	0.030	0.030	0.030	0.030	0.030	0.030	0.030	0.030
6) FLP - Length of p-type SiGe	inch	1.000	1.250	1.500	1.000	1.250	1.500	1.000	1.250	1.500
7) FL1 - Length of n-type SiGe	inch	0.560	0.737	0.915	0.559	0.736	0.914	0.558	0.735	0.913
8) FL2 - Length of n-type PbTe	inch	0.240	0.313	0.387	0.241	0.314	0.387	0.241	0.315	0.388
9) AH - Heat receptor area	inch^2	0.734	0.575	0.473	1.140	0.882	0.736	1.780	1.280	1.060
10) FH - Heat receptor dimension	inch	0.086 x 0.086	0.76 x 0.76	0.69 x 0.69	0.94 x 0.94	0.94 x 0.94	0.86 x 0.86	1.33 x 1.33	1.13 x 1.13	1.03 x 1.03
11) Thermocouple OD	inch	0.432	0.432	0.432	0.527	0.527	0.527	0.622	0.622	0.622

* See explanation at bottom of Table III

TABLE III

HYBRID COUPLE DESIGNS SELECTED FOR SUBCOMPONENT DEVELOPMENT PROGRAM

DESIGN PARAMETERS

Geometrics	Units	A	B	C
n-leg to p-leg area ratio, A_n/A_p		1.6	1.6	1.6
n-SiGe to n-PbTe area ratio, A_{n1}/A_{n2}		0.7	0.7	0.7
PbTe element, r_n	cm(in.)	0.381(0.150)	0.476(0.1875)	0.571(0.225)
p-leg wall thickness, t	"	0.091(0.036)	0.117(0.046)	0.142(0.056)
Gap between n-leg and p-leg	"	0.076(0.030)	0.076(0.030)	0.076(0.030)
Length of p-type SiGe, L	"	3.81(1.50)	3.17(1.25)	2.54(1.00)
Length of n-type SiGe, ℓ_1	"	2.32(0.915)	1.87(0.736)	1.42(0.558)
Length of n-type PbTe, ℓ_2	"	0.983(0.387)	0.798(0.314)	0.613(0.241)
Heat receptor area	cm^2($in.^2$)	3.05(0.473)	5.69(0.882)	11.5(1.78)
p-SiGe cylinder OD	cm(in.)	1.10(0.432)	1.34(0.527)	1.58(0.622)

Operational	Units	A	B	C
Couple efficiency*	%	7.5	7.35	7.1
Power per couple*	watts	0.476	0.886	1.570
Voltage*	volts	0.186	0.186	0.186
Current*	amps	2.56	4.76	8.45
Internal resistance*	ohms	0.061	0.033	0.018
Hot junction temperature, T_{HJ}	°C(°F)	926(1700)	926(1700)	926(1700)
Interface temperature, T_I	"	533(1000)	538(1000)	538(1000)
Cold junction temperature, T_{CJ}	"	232(450)	232(450)	232(450)
Incident heat flux	watts/cm^2	2.0	2.0	2.0

* Based on analysis which included 5% extraneous resistance and 7% thermal (shunt) loss. Subsequent programs have indicated that 20% extraneous resistance is more realistic. This would reduce design B power, for example, from 0.886 to 0.77 watts per couple.

2. Stress Analysis of Hybrid Thermocouple Components

Two significant areas that are related to the effect of thermal stress on the Hybrid couple are discussed below.

(1) First, stresses are induced in the thermoelements as a result of differential expansion between the couple legs. The stresses induced axially by the differential expansion were relaxed by the use of gold, a highly ductile material. How gold yields in this particular situation is not known quantitatively; however, the percentage of elongation through which the gold must move can be calculated and compared to acceptable limits. Moreover, previous RCA development efforts in the Hybrid program demonstrated the ability of gold to sufficiently relax the axially-directed stresses caused by thermal expansions. An early-design low-temperature Hybrid couple which contained gold withstood more than 3000 hours of stable operational life after enduring several thermal cycles to room temperature.

The differential expansion between both couple legs was calculated to determine the percentage of elongation or of contraction through which the gold would have to move. The calculation was based on the differential expansion that occurs between 400°C, the final bonding temperature where axial stresses are minimal, and room temperature where the stresses are more severe. Another situation exists in which the couple is operating at typical temperatures of 926°C and 232°C, and producing thermally-induced stresses, but they are less severe than those in the isothermal case at room temperature; consequently, this case was not pursued.

For the case in which the couple temperature was isothermally lowered from 400°C to 25°C, a differential expansion of 0.00278 inch between couple legs would result if the legs were not constrained. At room temperature, the differential expansion is such that the stress on the inner n-type leg is tension while the stress on the p-type cylinder is compression. If the gold yields completely, the compression or the elongation, relative to its axial length, would produce an elongation of gold by about two percent. This result is within the limits of the 4 to 30 percent elongation cited for gold.[1]

However, if the gold were replaced with a material which was not ductile and would not yield to the thermally-induced stresses, an axial stress of 33,360 psi could result. This stress was calculated from the equation

---

1. Metals Reference Book, 3rd Ed., Vol. 2, 1962, Smithells, Colin J., p.893.

$$\sigma = \frac{\Delta L \, E_p}{L}$$

where σ is the axial stress in psi, ΔL is the differential expansion (0.00278 inch), L is the length of the p-type leg (1.500 inches) and E_p is the modulus of elasticity of p-type SiGe (1.8×10^6 psi). Such a stress would cause fracture and separation in the weakest couple component which is the n-type telluride segment in tension. (Tensile strength of the tellurides is typically 1500 psi.) Therefore, inasmuch as the initial Hybrid couples have shown successful application of gold as a leg component, it is assumed that the gold sufficiently relaxes the induced stress caused by differential expansion between the couple legs.

(2) The second area of potential mechanical weakness is that region in the p-type SiGe cylinder near the bond with the SiMo hot shoe. Because this bond is normally made at a temperature in excess of the hot shoe temperature, the induced stresses that result from the interaction of both materials increase as the couple temperature is reduced. As a limiting case for maximum stress, the isothermal situation of the couple at room temperature has been investigated.

The nature of these stresses at room temperature would place the SiMo hot shoe in compression along radial and tangential vectors lying in the plane of the hot shoe and emanating from a point on axis with the cylinder (see Figure 13). Conversely, the p-SiGe cylinder contracts more than the SiMo upon cooling to room temperature and therefore results in a hoop stress tension (tangential component) and a shear stress (radial component) directed normal to the cylinder wall. Of the two stress cases, the radially-directed shear stress is of greatest significance and interest, and is discussed further.

Assumptions made for this case include a SiGe cylinder with a mean radius of 0.241 inch and a wall thickness of 0.046 inch bonded to a SiMo heat receptor. The differential radial component due to thermal expansion between the SiMo and cylinder at room temperature was calculated to be 1.30×10^{-4} inches. This value was then used in the stress equation

$$\sigma = \frac{\Delta R G}{R}$$

where σ is the shear stress, R is the radius of the SiMo heat receptor inscribed by the cylinder at 25°C, and G is the value for shear modulus. Substituting R = 0.241 inch and G = 7.8×10^6 psi in the equation yields the radial shear stress of 424 psi. In the absence of test data on the shear strength of SiGe material, the calculated

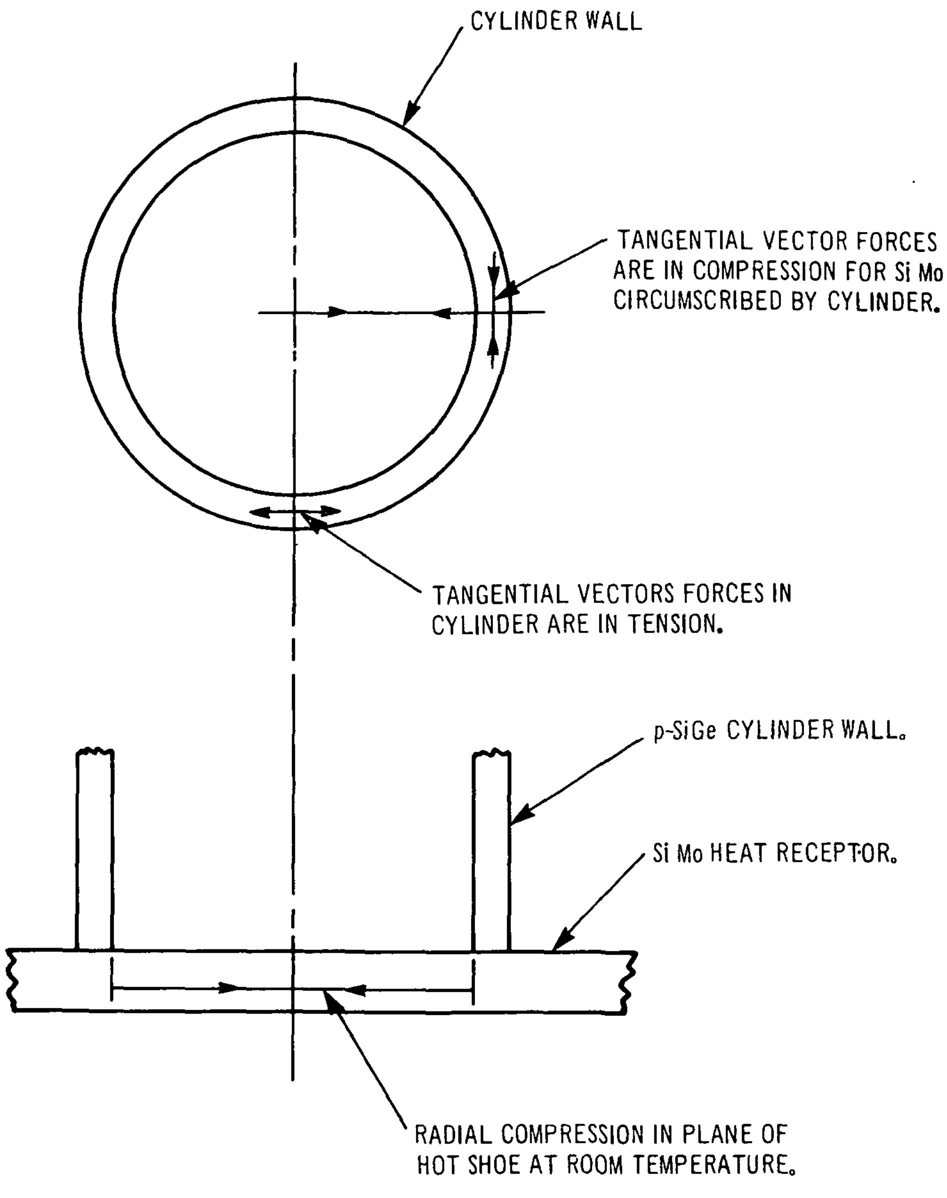

Figure 13. Room Temperature Stresses in Bond Area p-Type SiGe Cylinder to p-Type Si Mo Heat Receptor.

value of 424 psi was compared to tensile test data of p-type SiGe which yields at 3900 psi.

Because the shear modulus is approximately 0.4 times the modulus of elasticity, it was assumed that the shear strength would be 0.4 times the ultimate tensile strength; i.e., the shear yield point would be approximately 1600 psi. Comparison of the calculated shear stress of 424 psi to the ultimate shear strength derived from the tensile test data demonstrated that the calculated shear stress was sufficiently below the shear stress limit and would not fracture the cylinder wall. This conclusion is further strengthened by the fact that couples previously fabricated by RCA of similar materials and geometries have not shown fractures at this bond joint.

In addition to the aforementioned thermal stress cases, a third one which analyzes the capability of the Hybrid couple to withstand lateral acceleration of 6 g's has been considered.

Figure 14 shows the direction of forces, pivot point P, and point Q for which the extreme fiber stress has been calculated. The plane in which points P and Q lie is in the plane of the SiGe-to-tungsten cold shoe bond. From a lateral acceleration point of view, this bond is considered the most likely place for failure to occur since the combination of factors of induced stress to material strength would be least favorable at this point.

Initially the stress (σ) in the extreme fiber at point Q was computed from the equation shown below which gives the stress for the Hybrid couple viewed as a solid cylinder.

$$\sigma = \frac{3a \rho_t \ell^2}{8R} + \frac{6a\, V_{hr}\, \rho_{hr} \left(\ell + \frac{T_{hr}}{2}\right)}{8\pi R^3}$$

where R is the radius of the cylinder, ρ_t is the density of SiGe, a is the acceleration, ℓ is the element length, V_{hr} is the volume of the heat receptor, ρ_{hr} is the density of the heat receptor. The values used were:

$R = 1.52$ cm	$\rho_{hr} = 2.6$ g/cm^3
$\rho_t = 3.53$ g/cm^3	$T_{hr} = 1.91 \times 10^{-1}$ cm
$a = 5.78\ 10^3$ cm/sec^2	$\sigma = 84.6\ 10^2$ dynes/cm^2
$\ell = 3.81$ cm	$= 1.23$ psi
$V_{hr} = 2.76$ cm^3	

However, the Hybrid couple is a thin-walled cylinder and provides a reduced bonding area to the tungsten cold shoe. This reduced area has the effect of increasing the value of the unit fiber stress at a point, Q, relative to the stress for the solid cylinder. An approximation of stress increase could be obtained by applying the ratio of bonding area

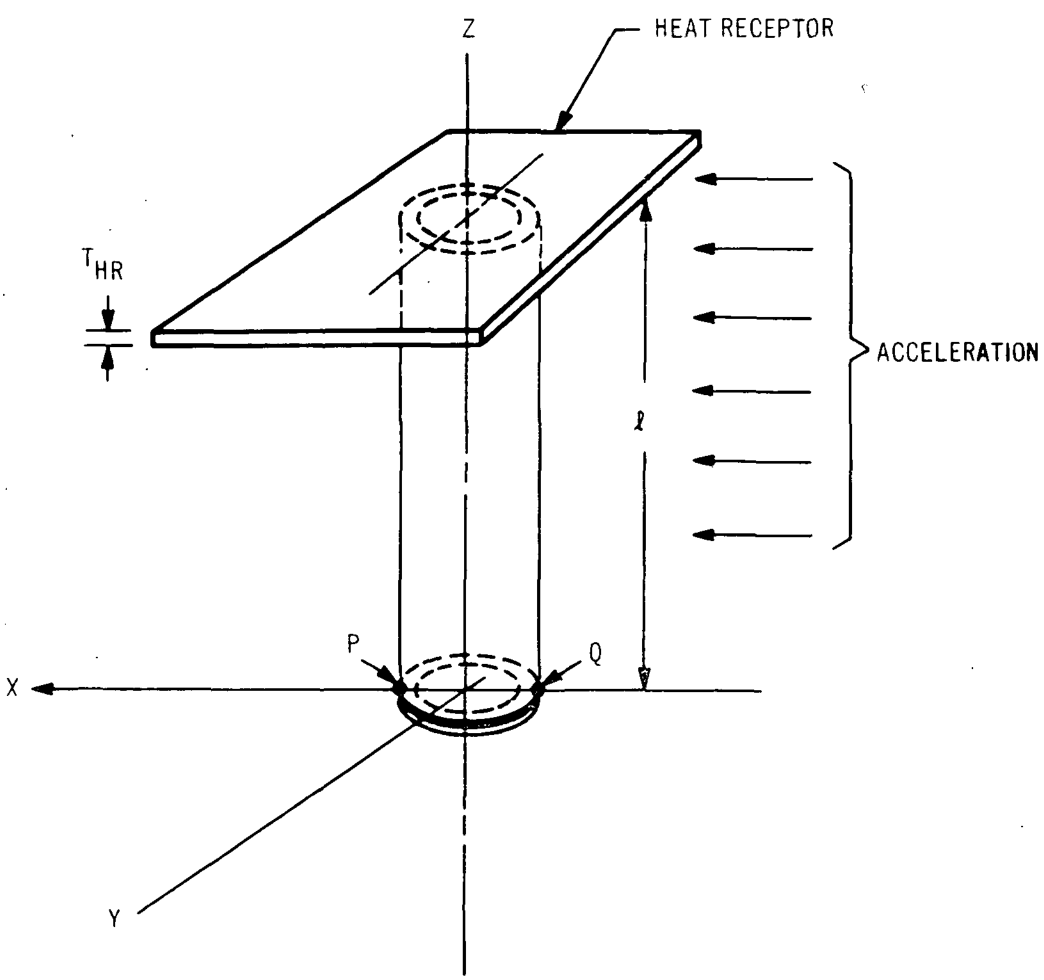

Figure 14. Load Distribution in Direction of Radius

of the solid cylinder to that of the thin-walled cylinder, and to increase the unit fiber stress of the solid cylinder by this factor. This calculation, considering a wall thickness of 0.050 inch, yielded the unit fiber stress of 4 psi at Q.

From a comparison of this stress level to the tensile strength of SiGe (typically 3900 psi for p-type SiGe) which is considered the weakest material in tension in the p-type cylinder leg, the conclusion was drawn that this form of mechanical testing would not cause fractures or separations in the p-type SiGe near this bond.

C. Generator Design

1. Hybrid Planar Converter Designs

A parametric analysis of a 250-watt, 28-volt planar converter employing the Hybrid thermocouple was performed using a computer program. The objective of the program was to define a specific thermocouple geometry and a thermocouple layout configuration that would maximize efficiency for given operating temperatures. In addition to efficiency, specific power also is computed. Other outputs of the program include operating conditions of various converter segments, thermocouple and converter geometries, and converter performance.

The analytical concept of the Hybrid converter and the assumptions made in developing the model can be made clearer by referring to Figure 15. (A converter is defined as the power generating system without the isotope heat source, and a generator as a converter plus the isotope heat source.)

The converter consists of a planar array of Hybrid thermocouples (arranged as nearly square as possible) which are attached to a radiating, finned heat sink with fuel capsules distributed above the hot shoes. Insulation of the multifoil type surrounds the thermocouples and the entire converter. For weight consideration as well as cost, the foil insulation is assumed to be a composite of molybdenum, nickel, and aluminum foils with an opacified paper separator between foils. Initially an effective thermal conductivity of 6.6×10^{-5} watts/°C-cm was used for the Hybrid thermocouple analysis and for other thermoelectric programs. More recent test data from other programs conducted at RCA, however, suggest that the effective foil insulation thermal conductivity is the same or somewhat higher than the predicted value. Current design programs, therefore, were modified to use the more conservative foil thermal-conductivity value of 1.6×10^{-4} watt/°C-cm.

The heat balance equations, as in previous analytical models, take into account the thermocouple conduction, Peltier, and Thompson heats. Temperature gradients that normally occur in the hot shoe and radiating fin also have been taken into account. In the case of the fin, it was assumed that all heat to be rejected radiates directly to space. This

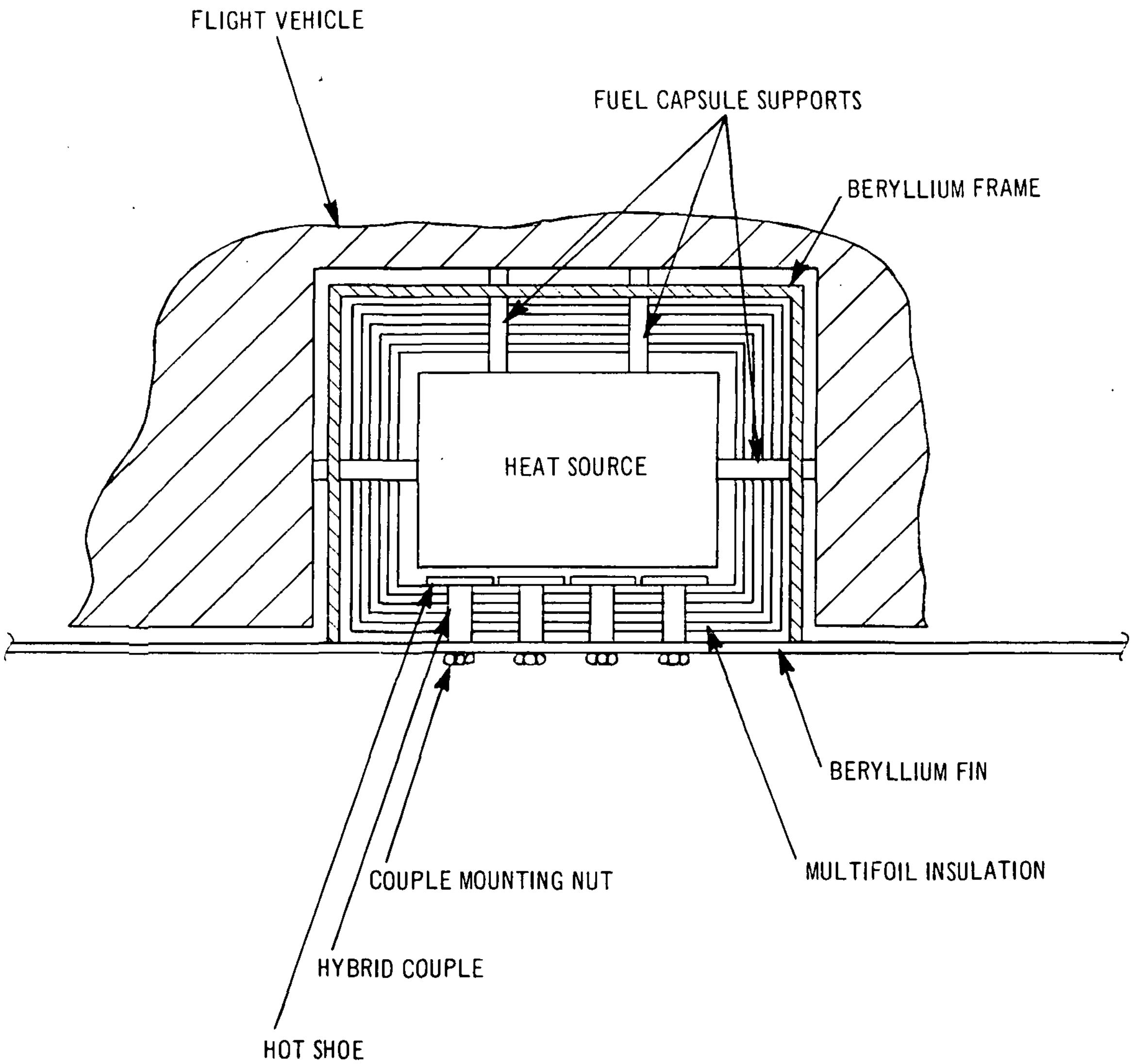

Figure 15. Planar Converter Recessed into Flight Vehicle

assumption has the effect of requiring a slightly larger fin area than actually may be required, because some heat is lost from fin radiation and body conduction to the flight vehicle into which the converter is recessed. Vehicle and deep-space temperatures were taken as 298°K and 73°K, respectively.

Materials comprising the Hybrid couple are those discussed previously for the thermocouple design phase. The use of 63.5 at.% SiGe material data in this analysis, which is consistent with the prior thermocouple analysis, gives a conservative view of converter performance. The thermoelectric SiGe materials used to fabricate the Reference Design Hybrid Couples, as described in Section IV, have a higher silicon content, 80.0 at.% silicon for the p-type cylinder leg and 70.0 at.% for the n-type leg. This value of silicon content enhances mechanical stability at bond interfaces between SiMo hot shoes and element legs. Measurements of material properties on alloys containing 80.0 at.% silicon showed a slight increase in the figure-of-merit relative to the lower silicon content material for the phosphorus-doped n-type materials. (The solubility of phosphorus in the n-type SiGe material increases proportionately with the silicon content of the alloy.) The figure-of-merit of the p-type material, on the other hand, remains essentially unaffected because the boron-doping level is not limited by solubility in the matrix. Although the final Hybrid thermocouple design used thermoelectric materials with higher per cent silicon alloys, the resultant changes in thermoelectric properties are small, and the performance predicted by the original analytical model (assuming lower silicon content alloys) is still valid.

Other significant assumptions include the use of beryllium for the fin and protecting converter cover to keep weight to a minimum. The additional weight of mounting hardware and fuel capsule support was compensated by increasing the computed converter weight by 10 per cent. The specific power includes the weight of the capsule or the fuel to be used with the converter, based on 60 thermal watts per pound. The total computed heat required for the converter was increased by 5 per cent to account for the heat-shunt loss through the capsule supports to the flight vehicle.

In summary, the planar converter computer-aided design program, known as HYGEN (see Appendix II, Sections B, C, and D), establishes converter geometries for various inputs of thermocouple geometries and operating temperatures. The more significant outputs of the program, in addition to converter geometries, are the power output, efficiency, number of thermocouples, voltage, specific power, and temperature profiles of various components of the converter.

As in other thermoelectric programs, the weight and specifics of heat-source design were not included in the converter design model. Only tentative assumptions can be made until a heat source can be specified, i.e., allowing sufficient volume space to accommodate the fuel capsule(s). It generally appears feasible to have heat source designs approximately 3.5 inches in diameter and 6 to 12 inches in length. Safety usually is the limiting consideration in defining heat source designs. In the present Hybrid converter design, 3.5 inches plus clearances were allowed normal to the plane of the thermopile hot shoes to accommodate the heat sources. The volume space allowed would be adequate for a fuel loading of about 4000 watts. The required radiant-heat flux from one side of the capsule would be on the order of 2 to 3 watts/cm^2, which is within the reasonable capability of fuel capsules currently being developed.

Three converter designs were established based on variation of the cold junction temperatures, 122°C(250°F), 177°C(350°F), and 232°C (450°F), respectively, for each of two Hybrid couple designs selected initially in Task II. The preliminary Hybrid Converter Designs are presented in Table IV and the Hybrid Couple Designs in Table V. The agreement between both computer programs, the Hybrid Couple Program (HYBRID) and the Hybrid Converter Program (HYGEN) is very close. This is evidenced by comparing Couple Design B of Table V with Converter Case III-B of Table IV, and Couple Design B-1 of Table V with Converter Case VI of Table IV. In addition to describing the couple, the HYGEN program arranges the appropriate number of couples in a square array and computes converter parameters such as specific weight, efficiency, component weights, geometries, electrical performance, etc.

The HYGEN computer program treats the converter model as a square array of Hybrid couples arranged with two series strings of couples electrically connected in parallel for greater reliability. When the couple strings are electrically paralleled, the output voltage and power requirement at end of the specified five-year design life should be 28 volts and 250 watts, respectively. To achieve this, the beginning of life (BOL) power requirement has been increased 10 per cent to 275 watts. This assumes a fuel source power decay of 6 per cent and 4 per cent for the converter. A beryllium fin was used to reject waste heat to deep space (from one side of the converter only). To reject several thousand watts of waste heat, as in the case of this converter, a large fin having an area of about 8500 in.^{2} (fin effectiveness 0.2) is required. This size fin becomes too heavy and large for a practical generator. The high calculated fin weights (WFIN) and low specific powers (WGPO) indicated for the cases presented in Table IV confirm the assumption made at the beginning of the program that a solid finned radiator might not be suitable for application to this converter.

In general, all cases shown meet or exceed within a per cent the BOL power requirement of 275 watts. It is desirable to minimize the fuel loading in order to reduce fuel cost and fuel source weight. Case B-II of Table IV appears attractive in this respect but the load voltage would be too marginal for BOL consideration. Case B-I is the same couple but operates at a lower cold side temperature. This design results in a voltage of 29.2 volts which is marginal since 30 volts is assumed necessary at BOL. Although Case B-1-IV exceeds 30 volts,

TABLE IV

PRELIMINARY HYBRID CONVERTER DESIGNS

Solid Fin Beryllium Radiator - 0.25" Thick

CONVERTER PARAMETERS	Program Symbol*	Units	B I	B II	B III	B-1 IV	B-1 V	B-1 VI
1) Efficiency**	GETA	%	7.15	6.79	6.38	6.93	6.57	6.20
2) Power Output** (BOL)	GPO	watts	312	277	273	335	298	293
3) Fuel Loading	GQT	watts	4274	4091	4363	4835	4531	4730
4) Heat Loss through Case	GQ Case	watts	312	312	337	333	333	360
5) Heat Rejected by Fin	-	watts	3526	3308	3462	3937	3684	3853
6) Number of Couples	GCPL	-	289	289	324	289	289	324
7) Load Voltage**	GEL	volts	29.2	28.0	29.9	29.6	28.3	30.3
8) Weight of Case	W Case	lb	13.6	13.6	14.7	14.5	14.5	15.7
9) Weight of Fin	W Fin	lb	470	230	85	542	265	160
10) Weight of Foil	W Foil	lb	26.9	26.9	29.2	28.9	28.9	31.4
11) Weight of Couples	WGCPL	lb	29.1	28.6	32.0	29.8	29.5	32.8
12) Specific Power**,xx	WGPO	watts/lb	.511	.755	1.17	.481	.719	.918
13) Fuel Capsule Temperature	TFCC	°C	1034	1028	1023	1026	1020	1014

xx Fuel Source Weight based on 60 thermal watts per pound

COUPLE PARAMETERS	Program Symbol*	Units	B I	B II	B III	B-1 IV	B-1 V	B-1 VI
1) Hot Junction Temperature	THP	°C	926	926	926	926	926	926
2) PbTe Hot Junction Temperature	THN2C	°C	538	538	538	500	500	500
3) Cold Junction Temperature	TCP	°C	122	177	232	122	177	232
4) Couple Efficiency**	ETA	%	8.1	7.7	7.3	7.9	7.5	7.0
5) Closed Circuit Voltage**	EL	volts	.202	.194	.185	.205	.196	.187
6) Resistance**	R	ohms	.0316	.0327	.0337	.0301	.0311	.0322
7) A_n/A_p	ANP	-	1.6	1.6	1.6	1.3	1.3	1.3
8) Wall Thickness	DTRR	inch	.046	.046	.046	.055	.055	.055
9) Length of p-type SiGe	FLP	inch	1.25	1.25	1.25	1.25	1.25	1.25
10) Length of n-type SiGe	FL1	inch	.658	.696	.734	.706	.746	.784
11) Length of n-type PbTe	FL2	inch	.393	.354	.315	.343	.304	.264
12) Heat Receptor Dimension	FH	inch	.960	.960	.960	1.01	1.01	1.01
13) Radius of n-PbTe Element	RRN	inch	.1875	.1875	.1875	.1875	.1875	.1875

* See Appendix II, Section D-2
** See explanation at bottom of Table III

TABLE V

PRELIMINARY HYBRID COUPLE DESIGNS

DESIGN PARAMETERS

Operational	Unit	Design B	Design B-1
Thermocouple efficiency*	%	7.35	7.11
Power per thermocouple*	watt	0.867	0.934
Voltage*	volt	0.185	0.187
Current*	amperes	4.69	4.99
Internal resistance*	ohm	0.033	0.031
Hot junction temperature	°C/°F	926/1700	926/1700
Cold junction temperature	°C/°F	232/450	232/450
Interface temperature	°C/°F	538/1000	500/932
Incident heat flux	$watts/cm^2$	2.0	2.0
Geometrics			
A_n/A_p (ANP)	-	1.6	1.3
A_n(SiGe/A_n(PbTe) (ANR)	-	0.7	0.7
Radius of n-type PbTe (RRN)	inch	0.1875	0.1875
Wall thickness (DTRR)	inch	0.046	0.055
Gap between n-p legs (GAP)	inch	0.030	0.030
Length of p-type SiGe (FLP)	inch	1.250	1.250
Length of n-type SiGe (FL1)	inch	0.736	0.788
Length of n-type PbTe (FL2)	inch	0.314	0.262
Heat receptor area (AH)	$inch^2$	0.914	1.019
Heat receptor dimension (FH)	inch	0.96 x 0.96	1.01 x 1.01
Thermocouple OD	inch	0.527	0.545
Thermocouple ID	inch	0.435	0.435
n-type SiGe OD	inch	0.314	0.314
n-type PbTe OD	inch	0.375	0.375

* See explanation at bottom of Table III

the excess power and lower efficiency indicate that this case is far from being optimum. Improved converter performance, however, can be obtained through better matching of converter performance to the required power and voltage at BOL.

From the foregoing converter analyses, it is evident that the solid 0.25-inch-thick beryllium accounts for the majority of the converter weight which results in low specific powers. The converter specific power for the six cases cited ranges from 0.48 to 1.17 watts per pound. To improve the specific power, alternate heat light-weight heat rejection systems were considered.

2. Analysis of Light-Weight Heat Rejection Systems

A preliminary study of a honeycomb-heat pipe radiator was conducted. RCA's Defense Electronics Division made available an existing analytical computer program for determining the minimum weight configuration. In all, 756 cases were treated. The analytical program considered the following variables: skin materials of beryllium and aluminum; white-coated surface and second-surface mirrors; water heat pipe diameters of .25 inch (.64 cm), .37 inch (.94 cm), and .50 inch (1.27 cm); and nine evaporator gas temperatures ranging from 68°C (155°F) to 200°C (392°F). In addition, the effect of external energy impinging on the radiator surface is treated by means of an environmental parameter, which is varied over a range from 0 through 0.6. See Figure 16 for the definition of environmental parameter. Radiator weight, radiator area, spacing between adjacent heat pipes, skin thickness, and total length of heat pipe required were outputs of the program. Other assumptions were that the heat pipe was a straight, stainless steel tube, having a .010-inch wall thickness, and operating isothermally along its entire length. The total radiator size and weight were calculated assuming heat rejection from one side of the radiator only.

Results of this analysis indicated that an aluminum honeycomb radiator was, in general, slightly lighter than its beryllium counterpart. Hence, aluminum was chosen as the radiator material. Mechanical and structural constraints, however, might alter this conclusion.

The choice between a white-coated radiating surface or a surface of second-surface mirrors, having a lower absorptance, depends greatly on the radiator heat rejection temperature and the external energy impinging on the radiator surface. These quantities of external energy and radiator surface temperature are related by the environmental parameter (PE) and significantly affect the size and weight of the radiator required to reject the converter waste heat. The environmental parameter is defined as the ratio of the external energy absorbed by the radiator to the total heat which would be radiated by an isothermal radiator at the heat pipe temperature. Figure 16 shows the increase in the environmental parameter as the radiator temperature decreases as a function of several levels of heat flux absorbed by the radiator. In essence, the external impinging heat flux on the radiator should be made as low as possible through orientation of the radiating surface to the flight vehicle and celestial bodies and/or using low absorptance radiating surfaces. Although second-surface mirrors have lower absorptance characteristics than the white-coated surfaces, they do weigh more on a per unit area basis. Hence, a tradeoff exists in selecting a surface finish to obtain minimum weight at a given radiating temperature. For a typical mission with the radiator at 200°C and using second-surface mirrors (absorptance, $\alpha = 0.1$), the environmental parameter value would be on the order of 0.1 or less. Using a white-surfaced radiator under similar conditions, the environmental parameter would increase typically to a value of 0.3

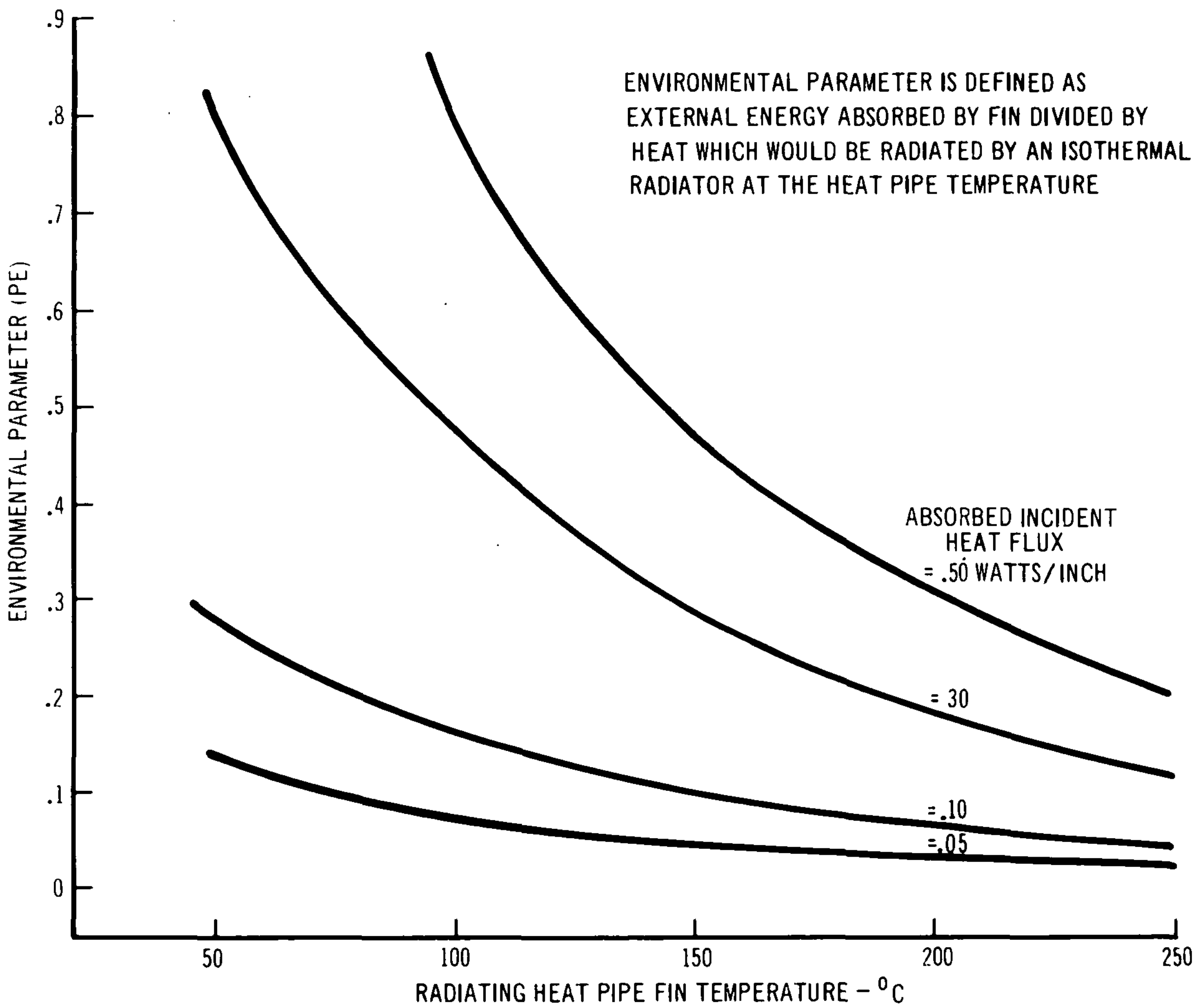

Figure 16. Environmental Parameter (PE) Vs Radiating Heat Pipe Fin Temperature

due to the higher solar absorptance. In these cases the external energy impinging on either surface has been assumed constant. Although the environmental parameter numbers are different, the weights of both type radiators are nearly the same at this temperature, indicating the area of the second-surface mirror radiator is less than the white-coated surface radiator. Further study would be required in this area to assess the effects of mission, radiator orientation, surface finish, and heat rejection temperature on weight.

As an example of the importance of the environmental parameter on radiator weight, a typical case for a 0.37-inch OD heat pipe-honeycomb radiator is presented in Figure 17. This figure indicates the minimum weight condition for the proper combination of adjacent heat pipe spacing (CCS) and skin thickness (T). The total length of a single heat pipe is calculated based on the total heat rejection area required. In actual practice the total heat pipe length would be subdivided into a number of smaller practical size lengths. This would yield a number of pipes which would be spaced adjacent to each other to form a practical, minimum-weight honeycomb heat pipe radiator assembly (see Figure 18).

Another significant variable affecting weight is the size heat pipe used. Figure 19 shows the advantage of using the smallest practical heat pipe diameter to keep radiator weight low. Constraints to using very small heat pipes would involve the practical fabrication limitation of such pipes and the radial heat transfer capability, i.e., temperature drop from evaporator surface of heat pipe to vapor inside. The dashed line in Figure 19 indicates for one case the penalty paid in weight due to the increased temperature drop as the input heat flux increases inversely to pipe diameter. For the assumptions cited, even the small 0.25-inch heat pipe seems acceptable as heat flux or temperature drop is not a constraint. From practical considerations, the size and material for the heat pipe needs further study for optimum heat pipe operation. At present, water is the best working fluid for this temperature range; however, its compatibility with stainless steel is questionable. Consequently, pipes of copper or copper-lined stainless should be studied further for determination of reliability and minimum weight. Copper heat pipes using water have been operated by RCA at 150°C (302°F) and have shown good performance after 15,000 hours of life with negligible degradation. Extending equivalent performance to 200°C (392°F) using copper in contact with water appears quite feasible.

Based on the above analysis, a typical honeycomb-heat pipe radiator can now be nominally characterized in terms of weight and interfaced with one of the present converter designs. Figure 18 shows a typical radiator that would be used with converter design B-III. To keep the temperature drop as low as possible, an arrangement of 16 0.37-inch diameter stainless steel heat pipes joined by a honeycomb structure and aluminum skin has been used. The tubes have been fanned out to meet the spacing requirements between pipes for minimum weight.

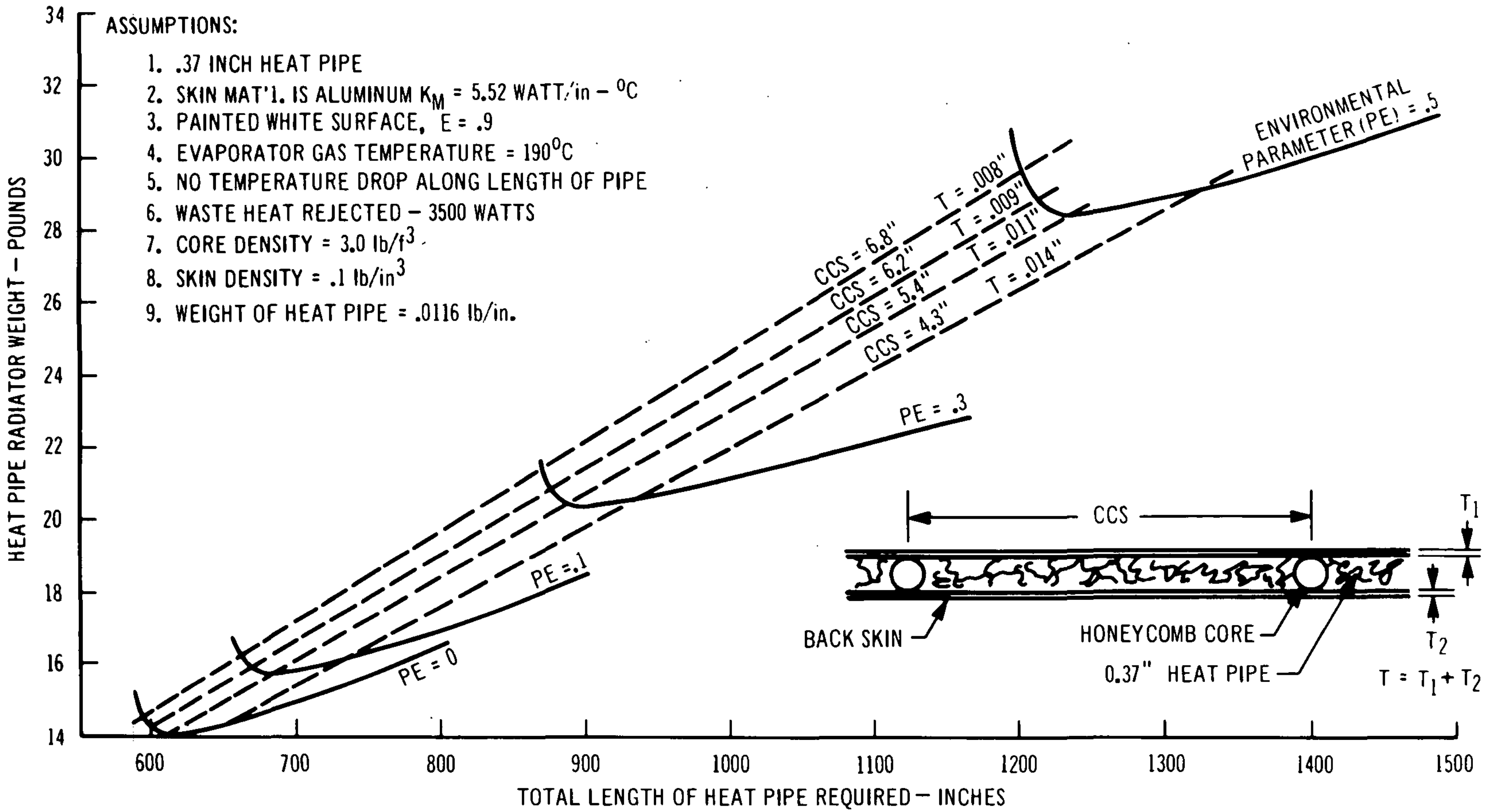

Figure 17. Heat Pipe Weight Vs Total Pipe Length for Several Environmental Parameter Ratios

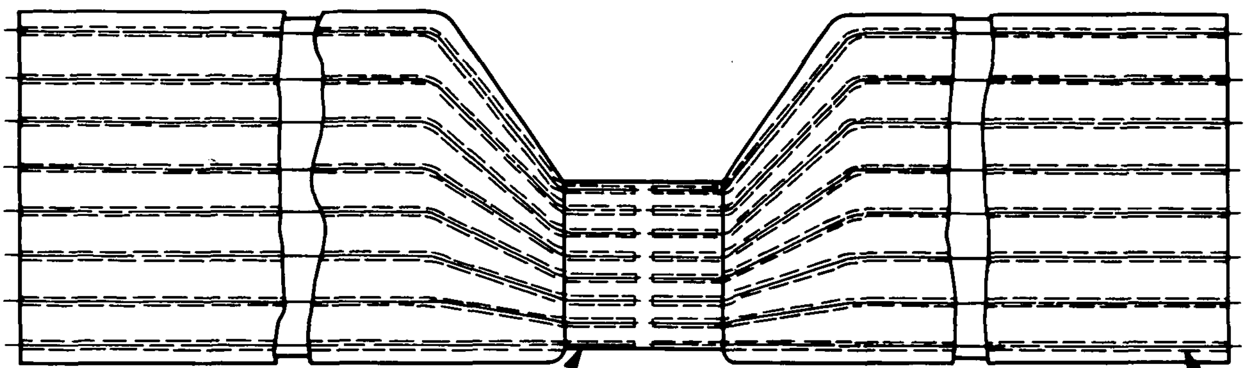

18" x 18" SQUARE CONVERTER HEAT REJECTION PLATE, WEIGHT≈2 LBS.

TOTAL OF 16 - .37" DIAMETER HEAT PIPES 56" LONG SPACED ON 5" CENTERS. WEIGHT≈21 LBS.

ASSUMPTIONS.

1. WHITE SURFACE RADIATOR
2. ALUMINUM SKIN≈.012"THICK
3. ENVIRONMENTAL PARAMETER = .3
4. WASTE HEAT REJECTED FROM ONE SIDE OF RADIATOR ONLY = 3500 WATTS
5. EVAPORATOR GAS TEMPERATURE = 190°C
6. UNIFORM TEMPERATURE MAINTAINED ALONG PIPE LENGTH

Figure 18. Typical Heat Pipe Radiator for Converter Design, B - III

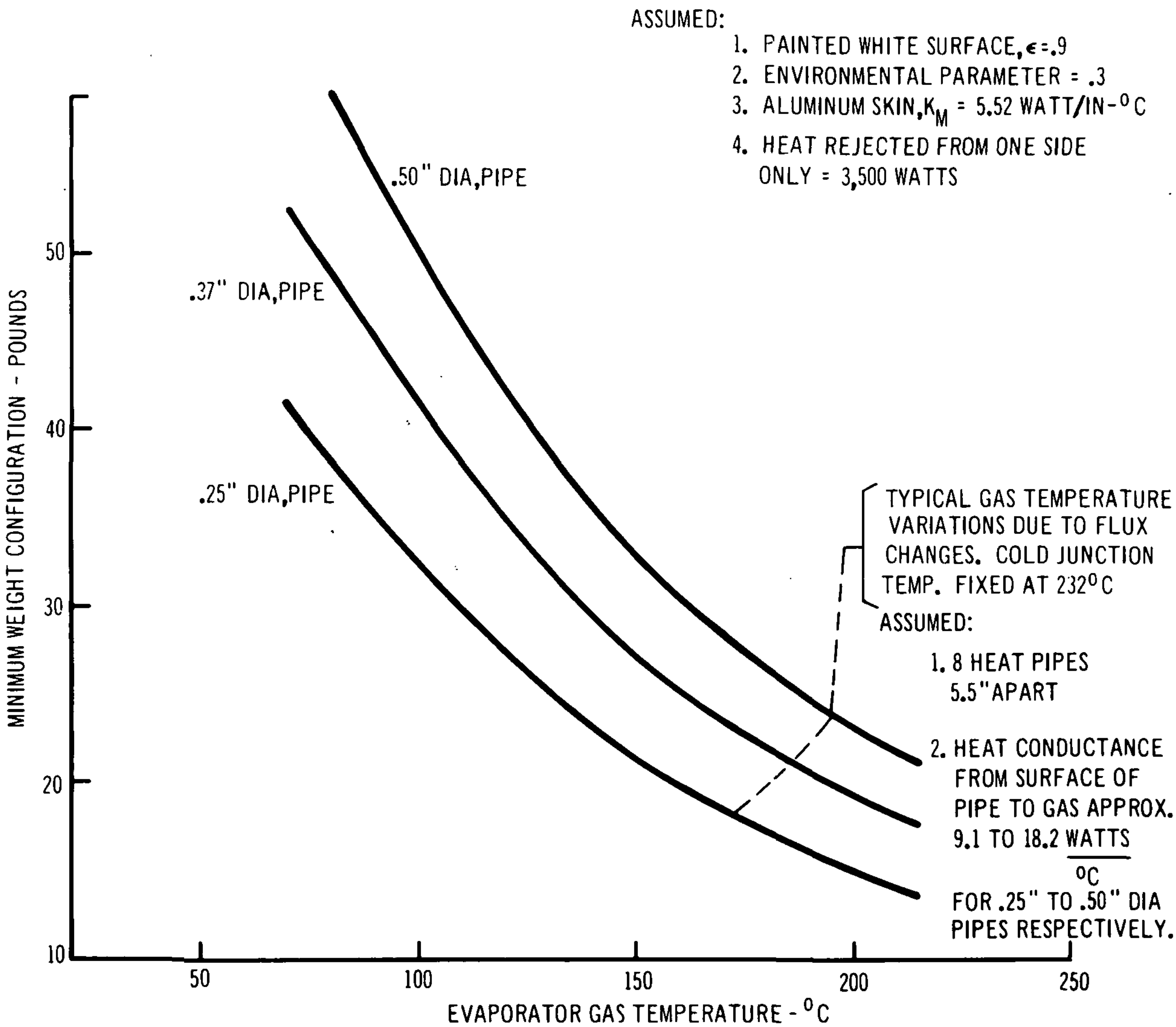

Figure 19. Weight Vs. Evaporator Gas Temperature-°C for Three Heat Pipe Sizes

Approximately 896 inches of total length of heat pipe was indicated from the computer analysis. Subdividing this by 16 permits a reasonable individual heat pipe length of 56 inches. This is considered practical for heat pipe design and fabrication. (RCA has fabricated and operated 0.25 OD inch pipes, 48 inches long, and 0.50 OD inch pipes, 96 inches long.) In practice, however, temperature drops along the length of the pipe, while small, plus some performance degradation due to bending of the heat pipes, have not been taken into account in the present analysis. These effects are real and their significance should be investigated further.

3. Selection of Converter Reference Designs

As a result of the development concluded in Task II, Thermocouple Development and Testing, Design B (see Table V) was selected as the Reference Design Hybrid Couple. Therefore, the three preliminary converter designs selected were based on the Hybrid Reference Design Couple (Design B) and the use of the honeycomb-heat pipe radiator system (see Table VI).

TABLE VI

SELECTED GENERATOR DESIGNS

		B-I	B-II	B-III
Power output (BOL)	watts	312	277	273
Efficiency	%	7.2	6.8	6.4
Hot junction temperature	°C	926	126	926
Cold junction temperature	°C	122	177	232
Converter weight	lbs	70	69	76
Heat pipe radiator weight	lbs	53	34	23
Fuel source weight*	lbs	71	68	73
Total generator weight	lbs	194	171	172
Specific power	watts/lb	1.60	1.62	1.59

* Fuel source weight based on 60 thermal watts per pound

The above generator designs indicate that the specific power remains essentially constant for the specified range of cold junction temperatures when using the heat pipe radiator; therefore, the lower cold side temperatures become attractive only in terms of efficiency.

4. Projected Improvements in Hybrid Planar Converter Designs

Further improvement in the performance of both the Hybrid couple and the Reference Generator Design could possibly be obtained by several modifications as noted in the following:

a. Substituting improved thermoelectric materials:
   (1) 80 at.% SiGe for 63.5 at.% SiGe.
   (2) RCA n-PbTe--GeTe Alloy* for 3M Co. 3N Alloy.
b. Increasing T_c to 1000°C.
c. Further optimization of converter weight.

The potential improvement in converter performance, based on the use of the improved thermoelectric alloys, is presented in Table VII for the three selected generator designs. The material properties of the 80 at.% SiGe and RCA n-type lead telluride alloy have been listed in a new data table, HDATA1 (see Appendix II, Section C-2).

TABLE VII

PROJECTED HYBRID COUPLE AND CONVERTER EFFICIENCIES
63.5 At.% SiGe AND 3M PbTe COMPARED TO
RCA 80 At.% SiGe AND n-PbTe THERMOELECTRIC MATERIALS

		Thermoelectric Materials	
	Converter Design B	63.5 at.% SiGe/ 3M PbTe	80 at.% SiGe/ RCA n-PbTe
I.	Couple Efficiency, %	8.1	9.6
	Converter Efficiency, %	7.2	8.5
II.	Couple Efficiency, %	7.7	9.1
	Converter Efficiency, %	6.8	8.0
III.	Couple Efficiency, %	7.4	8.5
	Converter Efficiency, %	6.4	7.5

Increasing the hot junction temperature to 1000°C results in an increase of converter efficiency of 10%. The effect on the three selected generator designs is given as follows.

* "Improved Compatible Material for Thermoelectric Power," Final Report, August 1969; J.P. Dismukes, I. Kudman, and H.I. Moss. TID-4500, Category UC-33; Contract AT(30-1)-3886.

	Converter Design B	Hot Shoe Temperature* 926°C	1000°C
I.	Couple Efficiency, %	8.1	8.9
	Converter Efficiency, %	7.2	7.9
II.	Couple Efficiency, %	7.7	8.5
	Converter Efficiency, %	6.8	7.6
III.	Couple Efficiency, %	7.3	8.1
	Converter Efficiency, %	6.4	7.1

*T_c = 232°C

A review of the converter weight has indicated that by (1) simplifying the cold stack, (2) optimizing the multi-foil insulation structure, and (3) improving fuel capsule supports, the present estimate of 76 pounds might be reduced to 56 pounds. This would increase the specific power for Converter Design B-III from 1.59 to 1.80 watts/pound. Moreover, by increasing the hot junction temperature to 1000°C, the specific power could be increased to 2.1 watts/pound and, by substituting the improved thermoelectric alloys, the specific power is increased to 2.4 watts/pound.

A summary of the effect of these improvements on Converter Design B-III is presented in Table VIII. These improvements represent the possible growth potential of the Hybrid Couple concept.

D. Module Reference Design

1. Module Design

The B-III Generator Design requires that 324 Hybrid couples in an 18-inch by 18-inch planar array be electrically connected in a series-parallel circuit. This requirement could be met in two different ways. First, each series string could consist of 162 couples with paralleling electrical connections between both series strings made at the terminals for series-parallel operation. The second is similar to the first except that electrical connections are provided between equal potential points of each couple string. With this method, should a couple degrade during life, there exists an alternate current path which permits continued generator performance with a decrease of only 0.5 per cent in total power. In the first method, should the couple degradation go to the limit of being an open, the generator power would be halved. Although the second method of paralleling is more complex and causes greater generator weight due to the many interconnections than the first, it is recommended because of its greater reliability over the first.

TABLE VIII

COMPARISON OF PRESENT AND PROJECTED
B-III CONVERTER DESIGN

Converter Modification					Converter	
SiGe Alloy	PbTe Alloy	T_h °C (°F)	T_c °C (°F)	Weight lbs (kg)	Specific Power W/lb (W/kg)	Efficiency %
63.5 at.% Si	3M - 3N	926 (1700)	232 (450)	172 (78)	1.59 (3.50)	6.4
63.5 at.% Si	3M - 3N	926 (1700)	232 (450)	154 (70)	1.80 (3.96)	6.4
63.5 at.% Si	3M - 3N	1000 (1832)	232 (450)	154 (70)	2.10 (4.64)	7.2
80.0 at.% Si	RCA - PbTe-GeTe	1000 (1832)	232 (450)	154 (70)	2.40 (5.28)	8.4

A 6 x 18 array of Hybrid couples was assumed for the module, as shown in Figure 20. It requires three module sections of 108 couples each to meet the requirements of the generator. Using more modules of fewer couples each would require more mounting hardware and cause greater difficulty in integrating the numerous modules into a converter. Total gap area between adjacent modules would also increase, thus creating greater heat shunt losses. In the other extreme, the converter could be built as a single unit; however, should replacement of a couple be desired after converter assembly, this would necessitate rebuilding and handling of the entire converter, which would detract from its initial reliability. The module size shown in Figure 20 is seen as the best compromise of the above considerations and was selected as the Module Reference Design.

Other important considerations regarding module design are the processes used to insert the thermal insulation and the technique used to join the electrical interconnections. With regard to the fibrous-type insulation, this would be machined as shown in Figure 21. The insulation would be dovetailed to the adjacent piece in order to decrease any line of sight radiation through any voids that might occur at the interface of adjacent strips of insulation. Alternately, a line of 18 couples and strips of insulation would be affixed to a mounting fixture. The mounting fixture would be similar to the mounting plate but have additional holes in it to permit a special crimping tool to cold-weld the copper electrical interconnectors together. No significant difficulties are seen in this area but development is required since the standard connection technique relies on the compression of adjacent connectors using a nut and screw.

Figure 23 also shows this type electrical connector. Typical of past connector designs used on previous programs at RCA, the linking electrical connector relieves the stresses between adjacent couples through the use of a small bend or "omega" in the connector. In addition to the geometry of the connector, relieving stress build-up within the module or converter, the connector itself, being copper, has low inherent stress because the final processing step of the couple anneals the copper and leaves it soft. Consequently, the stress developed between adjacent couples is not considered significant in view of the geometry and softness of the copper connector and the cantilevered air-vac couple construction.

Ultimate construction of the module panel could be simplified by development of a "plug through" Hybrid couple similar to the present air-vac construction (see Figure 22) which would permit a solid piece of insulation with appropriate holes to receive the couples. The electrical interconnection would then be crimped as previously described. With this approach, either fibrous-type insulation or multifoil insulation could be used.

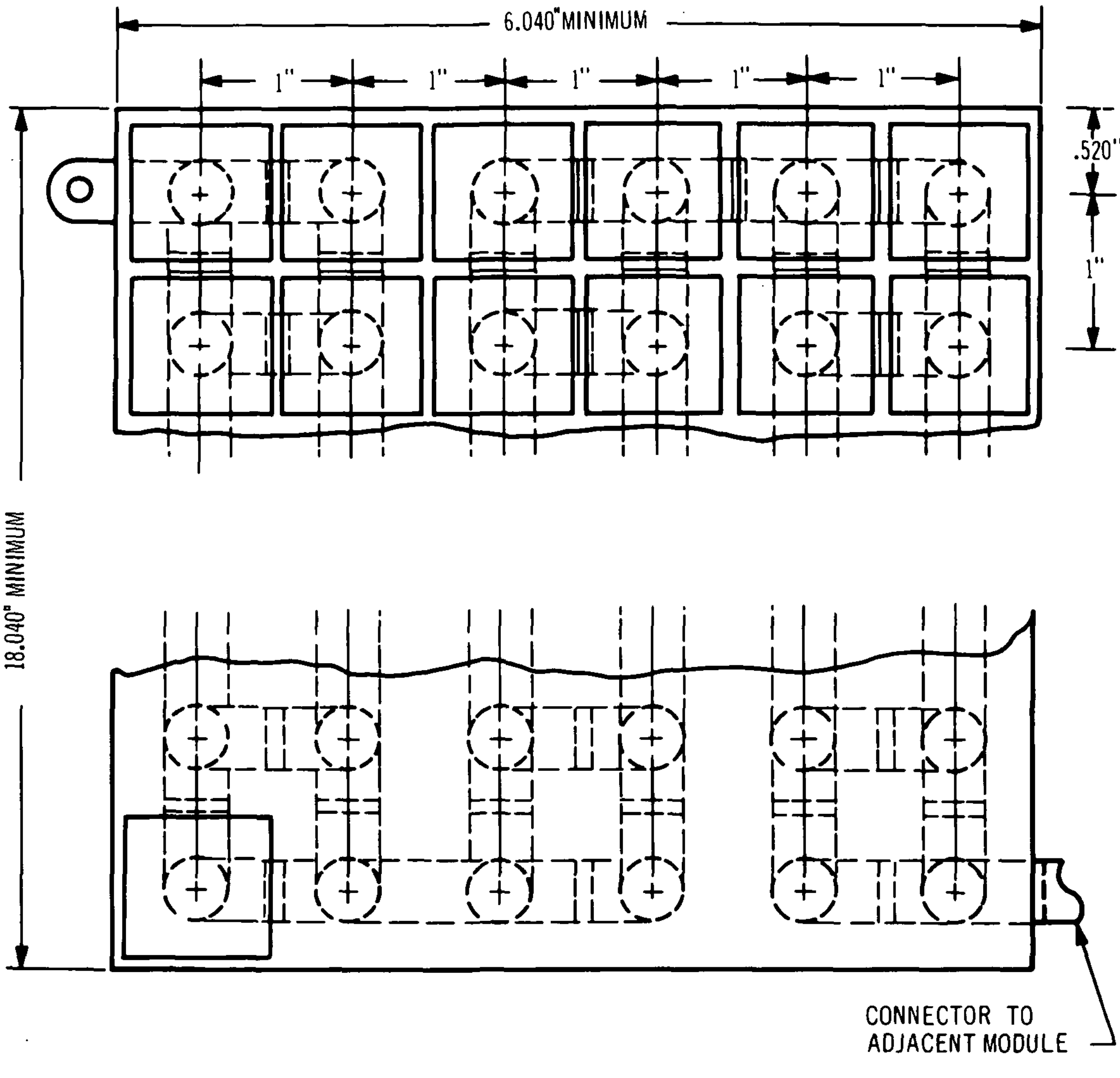

NOTES:

1. THIS SHOWS A 6x18 COUPLE ARRAY WHICH IS ONE OF 3 MODULES USED IN THE CONVERTER B - III DESIGN REQUIRING 324 COUPLES.

2. COUPLE INTERCONNECTIONS PROVIDE A SERIES - PARALLEL ELECTRICAL CIRCUIT.

3. COUPLES ARE ARRANGED AS COUPLETS PROVIDING MAXIMUM RELIABILITY FOR SERIES - PARALLEL ELECTRICAL CIRCUIT.

Figure 20. Module for Hybrid Converter Design, B - III

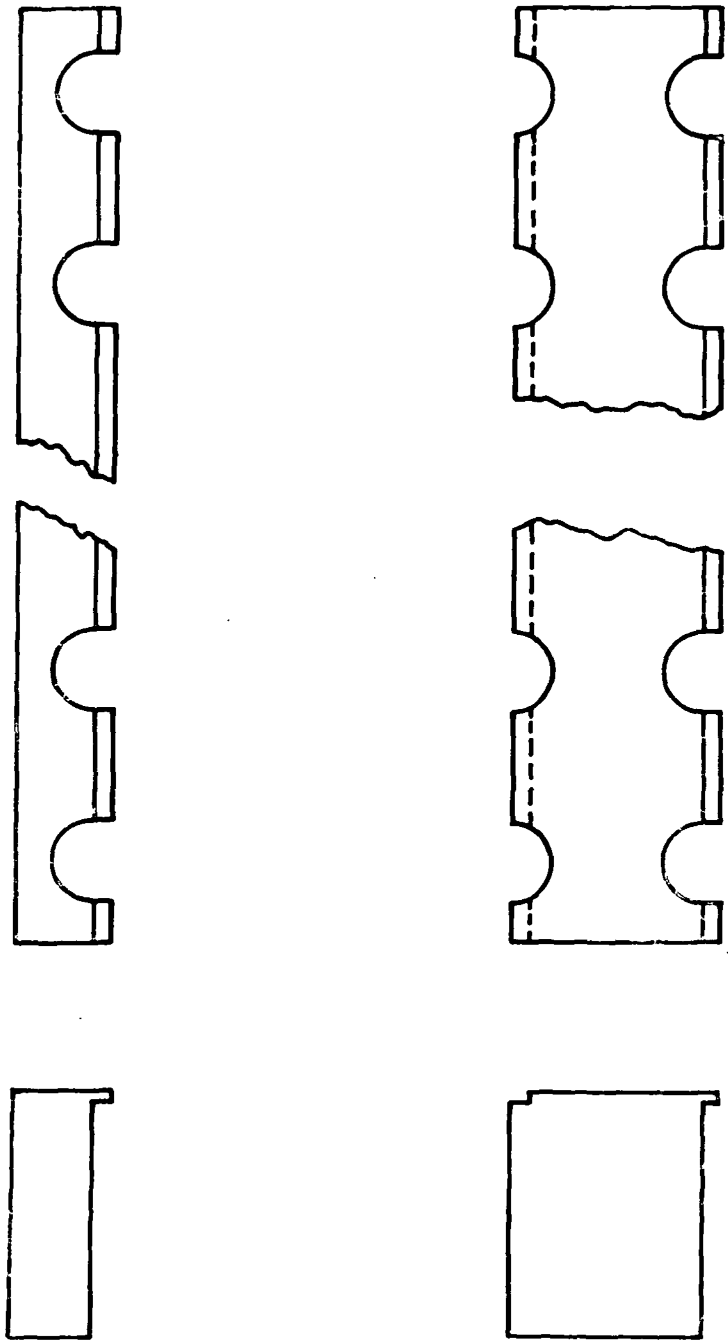

Figure 21. Module Strip Insulation

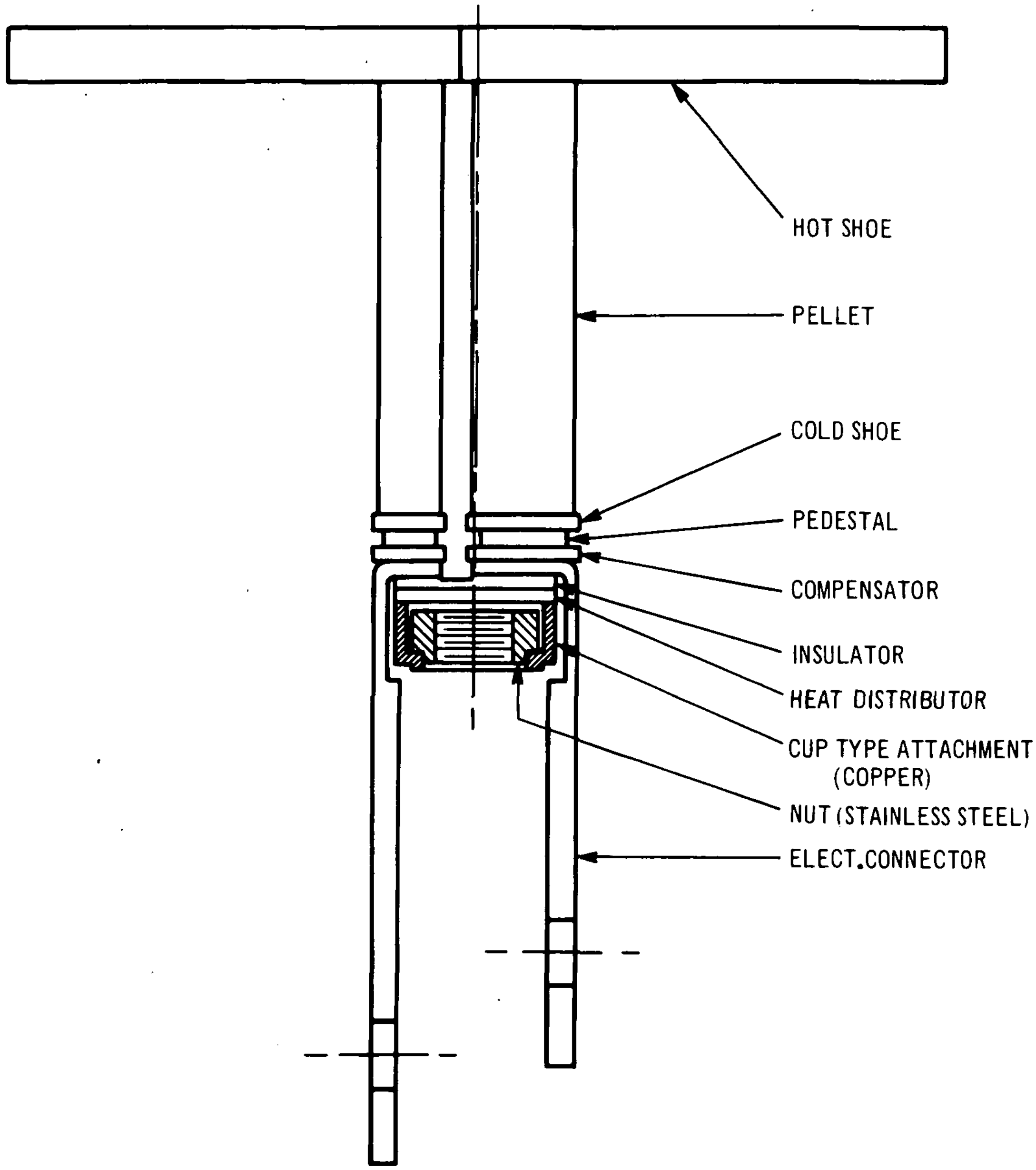

Figure 22. "Plug-Thru" Air-Vac Thermocouple

2. Test Panels

Of the two types of radiator panels considered for the Hybrid couple panel sections, it was decided to use the mounting and cooling plate assembly Design No. 2 (Figure 23). Nine thermocouples would be attached to the mounting plate to form the module section and a water-cooled or finned auxiliary heat exchanger would be subsequently bolted onto the mounting plate during testing for control of the cold junction temperature. This approach provides more flexibility as the water cooling or fin are first attached to the "cooling plate" and the cooling plate is then bolted onto the module section. The expected test panel operating conditions and projected performance are given in Table IX.

TABLE IX

PROJECTED TEST PANEL PERFORMANCE

Operation Temperature Conditions		°C	°F
(THRC)	p-SiMo hot shoe edge temperature	941	1725
(THPC)	p-SiGe leg hot junction temperature	926	1700
(THNC)	n-SiGe leg hot junction temperature	923.5	1694
(TCNC)	n-SiGe leg cold junction temperature	541	1006
(THN2C)	n-PbTe leg cold junction temperature	538	1000
(TCPC)	p-SiGe leg cold junction temperature	232	450
(TCN2C)	n-PbTe leg cold junction temperature	233.85	452
(TCBC)	Heat rejection base plate temperature	223.3	434

Thermoelectric Performance Characteristics

		Units	Couple	Panel
(ETA)	Thermocouple Efficiency	%	7.35	7.35
(PO)	Power per Thermocouple	watt	.77	6.93
(EL)	Closed Circuit Voltage	volt	.166	1.5
(R)	Internal Resistance	ohm	.030	0.30
(CUR)	Current	amperes	4.64	4.64

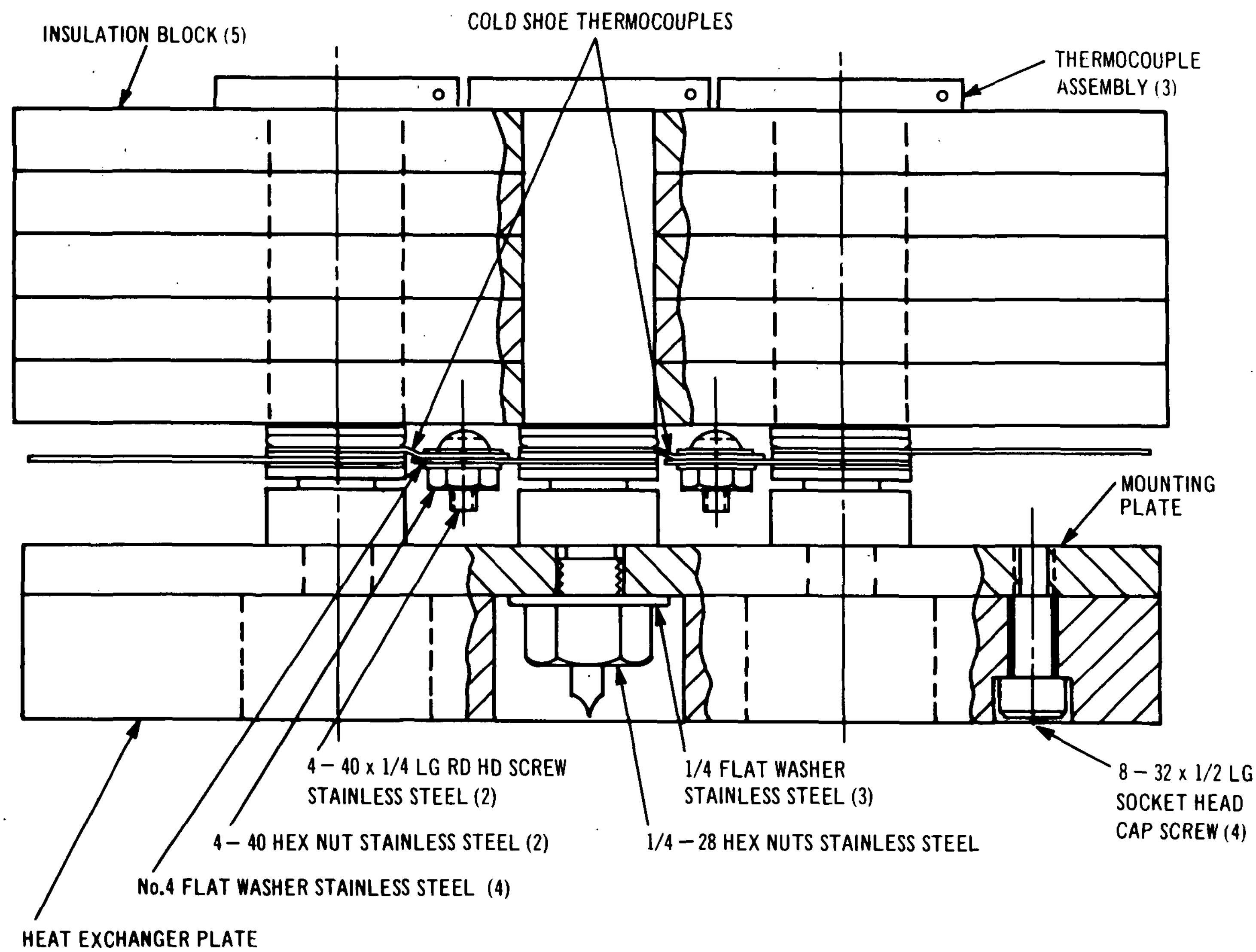

Figure 23. Hybrid Structure Module Panel Assembly

Section IV

THERMOCOUPLE DEVELOPMENT AND TESTING

A. Subcomponent Development

The objective of this phase of the program was to evaluate bond systems and further define fabrication constraints for the subcomponents to be used in the construction of the three Hybrid couple designs (Table III). The following subcomponents were evaluated (see Figure 24):

(a) p-SiGe element metallurgically bonded to a p-SiMo heat receptor plate and a tungsten cold shoe.

(b) n-SiGe element metallurgically bonded to a n-SiMo heat receptor plate and a tungsten cold shoe.

(c) n-PbTe element (3N PbTe) metallurgically bonded to hot and cold stainless steel shoes.

(d) Cold stack; electrical connectors, insulators, compensators, mount stud and a copper exhaust tubulation brazed together.

(e) Intermediate bond system; consists of a gold disc bonded between a stainless steel PbTe hot shoe and a SiGe tungsten cold shoe.

1. p-SiGe Element

a. p-SiGe Cylinder Fabrication

With the initiation of this program, studies were made to determine the practical range of cylinder lengths and wall thickness that could be fabricated by the Elox (spark dischrage) method, and to consider other possible alternate methods if required.

SiGe pellets ranging in alloy composition from 63.5 at.% Si to 80.0 at.% and lengths from 1.42 cm (0.560"), 1.9 cm (0.750") and 2.54 cm (1.0") were drilled by the Elox technique; in each case, mechanically strong, leak-tight cylinders resulted when machined at the slower drilling rates. At faster drilling rates, failures occurred in the form of microcracks and/or complete fracture of the cylinder wall. The leak checks were made using (1) a Veeco Model MS-9 mass spectrometer with helium and (2) a penetrating dye placed inside the cylinder which was temporarily sealed at one end. The outside of the cylinder was coated with a carbonate (white) material. The exact location of leaks could then be determined by direct observation of dye marks.

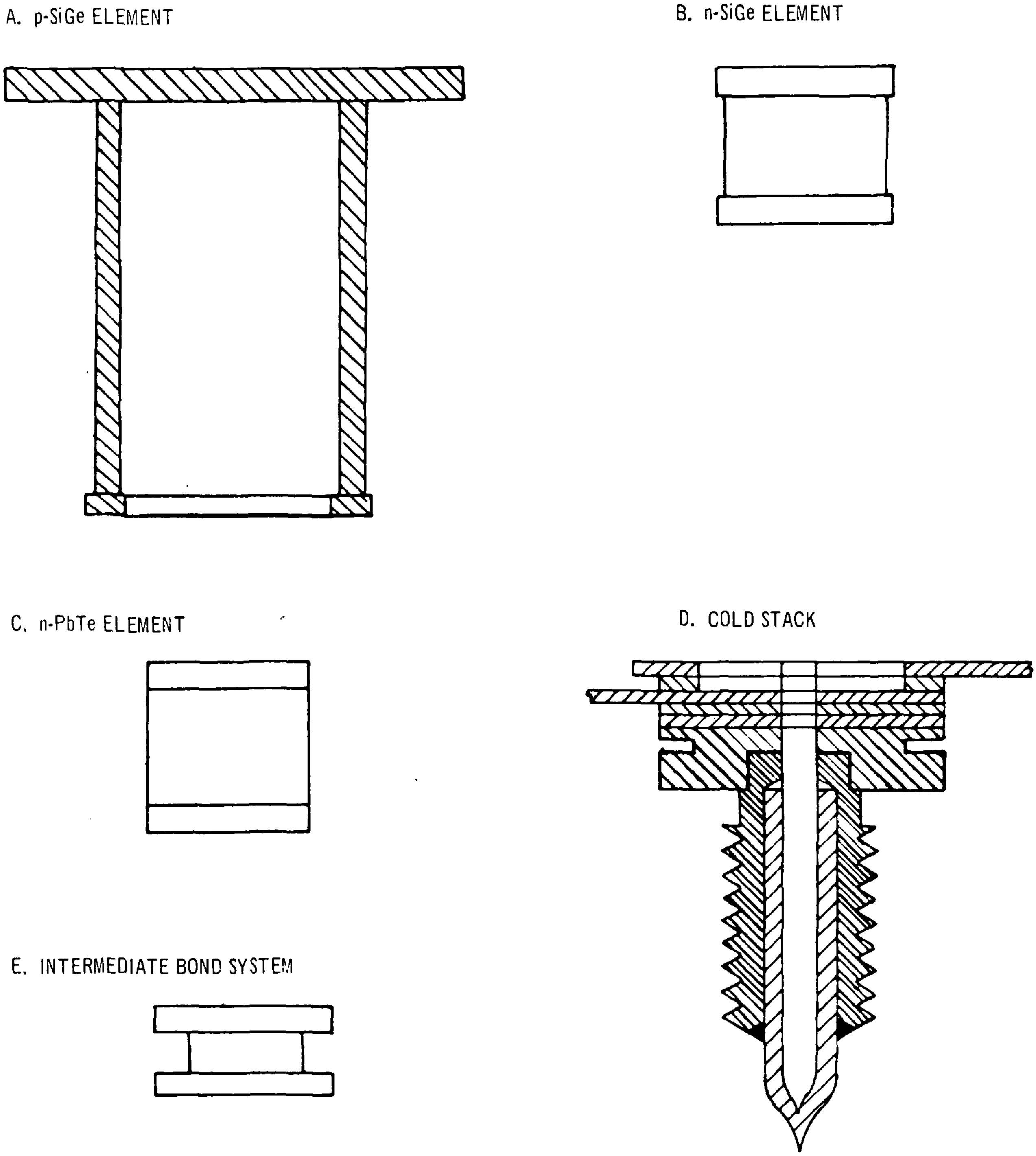

Figure 24. Subcomponent Assemblies

With the definition of the developmental Hybrid couple geometries (Table III), cylinder lengths and diameters indicated were, in some cases, larger than any of the cylinders fabricated to date. Many problems were encountered in attempting to fabricate the larger cylinders by Elox drilling in one operation with lengths up to 3.81 cm (1.5"); namely, cracking and non-uniform wall thickness. Because of the long cylinder length, the machining was done in two stages; first, the blank was drilled half-way though; then the blank was reversed and the remaining half drilled. Although some of the problems were relieved through the redesign of the holding fixtures, they were not fully eliminated.

As a result of the difficulty in obtaining the longer length cylinders, several alternate methods were investigated, including ultrasonic machining, hot pressing, isostatic pressing and sintering, and diamond core drilling. The ultrasonic drilling technique was not feasible, as a non-uniform wall thickness was obtained and excessive cracking of the SiGe wall occurred. Several attempts were made at hot pressing the cylinders. A special graphite die was fabricated and several runs were made, all of which were only partially successful because of equipment problems. The pressure could not be maintained at temperature, and resulted in porous cylinders of non-uniform density. Initial attempts to fabricate cylinders by isostatic cold pressing and sintering also resulted in cylinders with high porosity, 30-40%. Because of the difficulties encountered in the above three alternate approaches, they were discontinued.

The machining of the cylinders was then attempted by an outside vendor using a special diamond core drilling technique. The first cylinders fabricated were 2.54 cm (1.0") in length and 1.13 cm (0.444") in diameter with a 0.101 cm (0.040") wall thickness. Leak checks with the Veeco MS-9 leak detector and dye penetrant showed no leaks, with the exception of where defects (micro cracks) in the starting material were present. Visual inspection of these parts showed a smoother surface than obtained by the Elox technique. The dimensional tolerances were also found to be better. The initial success with the diamond core drilling prompted a more intensified study comparing the two techniques. The evaluation of the two techniques showed the diamond core drilling technique produced higher quality cylinders with better yields than the Elox electrical discharge machining process. It also was capable of producing good cylinders with lengths of 3.81 cm (1.5"). It was for these reasons the diamond core drilling technique was chosen for the fabrication of the cylinders. A summary of fabrication cylinder results is given in Table X. The cylinder produced by diamond core drilling is shown in Figure 25.

TABLE X

RESULTS OF p-TYPE SiGe CYLINDER FABRICATION

Batch	Batch Size	Length (inch)	OD (inch)	Max. Wall Thickness (mils)	Fabrication Method	Appearance	Leak Test Veeco(1)	Leak Test Dye(2)	Disposition
1	8	0.5	0.444	50	Elox	Good	All passed	All passed	Used for bonding tests
2	6	0.75	0.444	50	Elox	One broken circumferential	1 leak	1 leak	Remaining 4 used for bond tests
3	3	0.75	0.444	40	Elox	Good	All passed	All passed	Remaining used for bond tests
	3	1.0	0.444	50	Elox	Good	1 leak	1 leak	
	3	1.0	0.444	40	Elox	Good	All passed	All passed	
4	3	0.5	0.384	50	Elox	Hot-pressed pellets - good	All passed	All passed	1 Met Lab; 2 bond test
5	8	1.5	0.384	45	Elox	3 broken	All leak	All leak	Pinhole leaks
6	8	1.25	0.527	45	Elox	Good	All leak	All leak	Circumferential cracks
Subtotal							17 leak		
7	10	1.5	0.500	50	Diamond-core drilling	Good	2 leak	2 leak	8 bonded
8	8	1.25	0.500	50	Diamond-core drilling	Good	All passed	All passed	All bonded
9	11	1.25	0.527(3)	50	Diamond-core drilling	Good	All passed	All passed	To be bonded
10(4)	6	1.25	0.500	50	Diamond-core drilling	Good	All passed	All passed	1 bonded
11(4)	168	1.25	0.527(3)	50	Diamond-core drilling	Good	All passed	All passed	Couple bonding

NOTES:
1. Veeco leak detector, Model MS-9
2. RCA dye penetrant test
3. Machined from large-size ingot (0.600-inch OD)
4. 80 at.% SiGe alloy

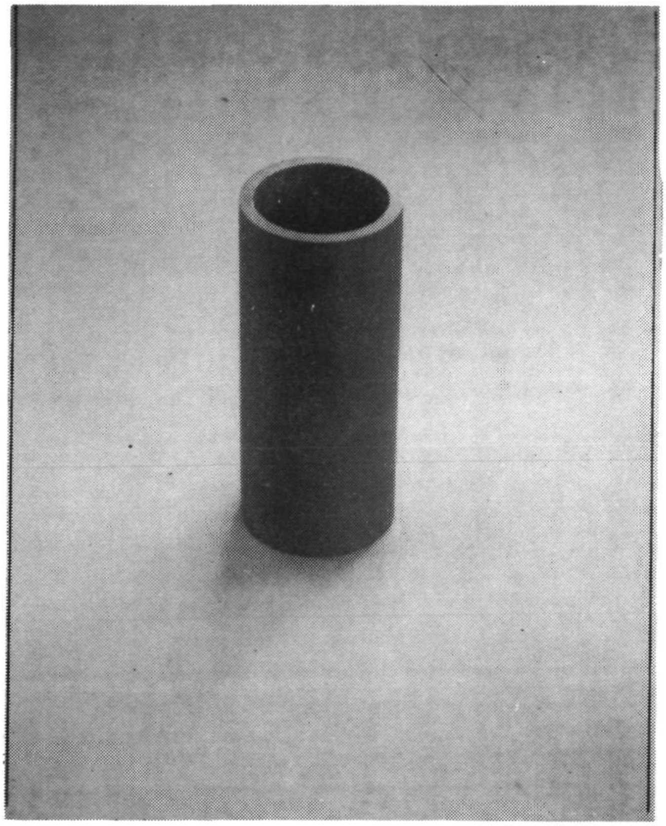

Figure 25. Diamond Core Drilled p-SiGe Cylinder

The cylinders had all been machined from the standard size SiGe zone-leveled "loaf-shaped" ingot which has a maximum diameter of 1.35 cm (0.530 in.) (see sketch below).

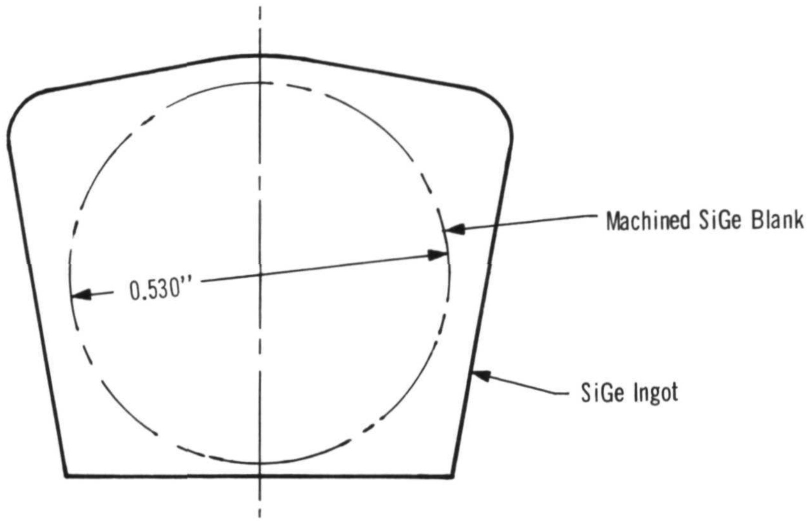

In order to provide a larger size SiGe blank for the cylinders, the SiGe zone leveling process was modified. The largest size ingot that could be fabricated on the available equipment had an OD of 1.52 cm (0.600 in.).

Attempts to fabricate cylinders of couple design A (Table III), 3.81-cm (1.5-in.) length and 0.091-cm (0.036-in.) wall thickness, were unsuccessful due principally to radial cracking. Cylinders of couple design C (Table III), 2.54-cm (1.0-in.) length and 1.58-cm (0.622-in.) OD, were not possible to fabricate since there was insufficient material in the largest size ingot, 1.52-cm (0.600-in.) OD, that could be fabricated in presently available equipment. As a result, all testing of p-SiGe element subcomponents was conducted with couple design B cylinders (Table III), i.e., 3.17-cm (1.25-in.) length, 1.34-cm (0.527-in.) OD, and 0.117-cm (0.046-in.) wall thickness.

b. <u>p-SiGe Cylinder--p-SiMo Heat Receptor</u>

The p-SiGe cylinder must be joined to the p-SiMo heat receptor so as to achieve a sound metallurgical bond with a hermetic seal. Two designs were initially considered; the first employed a conventional butt joint in which the p-SiGe cylinder is bonded directly to the flat surface of the p-SiMo heat receptor; while the second employed a compression joint, in which a shallow cut (5 to 25 mils deep) was made into the SiMo heat receptor to accept the SiGe cylinder, thus putting the bond in compression. Leak-tight cylinders of 63.5 at.% Si composition were bonded to SiMo (85 wt.% Si) heat receptors, using the standard "butt-type" joint technique. Cylinder lengths ranged from 1.42 cm (0.560 in.) to 3.18 cm (1.250 in.) with a wall thickness of 0.127 cm (0.050 in.). Similar results were obtained with cylinders of 80 at.% Si composition. Figures 26a and 26b show these to be metallurgically sound. Bonds made with the compression joint were all unsuccessful. Depression cuts of 5 to 10 and 25 mils were made in the p-SiMo with cylinders inserted into the depression and bonded per the normal practice. In each case, the p-SiGe cylinders cracked in an area 10 to 50 mils above the top lip of the depression cut. The butt-type bond was therefore selected for the bonding of the p-element subcomponent.

Normal bonding practice calls for close matches in thermal expansion among materials bonded at high temperatures unless the seal area is very small. Experimental evidence accumulated during the initial stages of this program showed that consistent leak-tight seals were obtained in the bonding of 63.5 at.% SiGe cylinders to the 85 wt.% SiMo heat receptors at temperatures in excess of 1093°C (2000°F). Based upon these results it was expected that the thermal expansion match would be close enough to permit operation of the device at design temperature. Life testing of the p-SiGe element was conducted at accelerated test conditions, 982°C (1800°F) for 300 hours and at 1090°C (2000°F) for four hours, and thermal cycling tests from 982°C (1800°F) to 150°C (300°F) to assess the mechanical and thermal capability of the p-SiGe to p-SiMo bond. Due to equipment limitations, the accelerated thermal cycle test was more severe than the test defined in the Hybrid Thermocouple Development Program Plan. A comparison of both thermal cycles is shown in Figure 27. No changes in electrical resistance or microstructure were noted in the life-tested samples; however, microcracks developed in the bond region resulting in loss of hermeticity in those specimens subjected to both high temperature soaking and thermal cycling. It was evident that a closer thermal expansion match was required. Figure 28 is a plot of the thermal expansions of various SiGe and SiMo alloys as a function of temperature. These data indicate that the SiGe alloy composition required to match SiMo is in the range of 80 at.% Si. Because the thermoelectric properties of the two p-type SiGe alloys (i.e., 63 and 80 at.%) are essentially the same, one alloy can be substituted for the other without requiring a change in design calculations. This new alloy-bond combination was successfully subjected to ten accelerated (see Figure 27) thermal cycles from 982°C (1800°F) to 150°C (300°F). The bonds were leak-tight as evidenced by helium leak check and the dye penetrant tests. The tensile strength of as-fabricated and life-tested specimens (982°C (1800°F) for 300 hours and 1090°C (2000°F) for four hours) averaged 3300 psi and 2550 psi, respectively. These values are typical for SiGe alloys with the fractures occurring in the bulk SiGe.

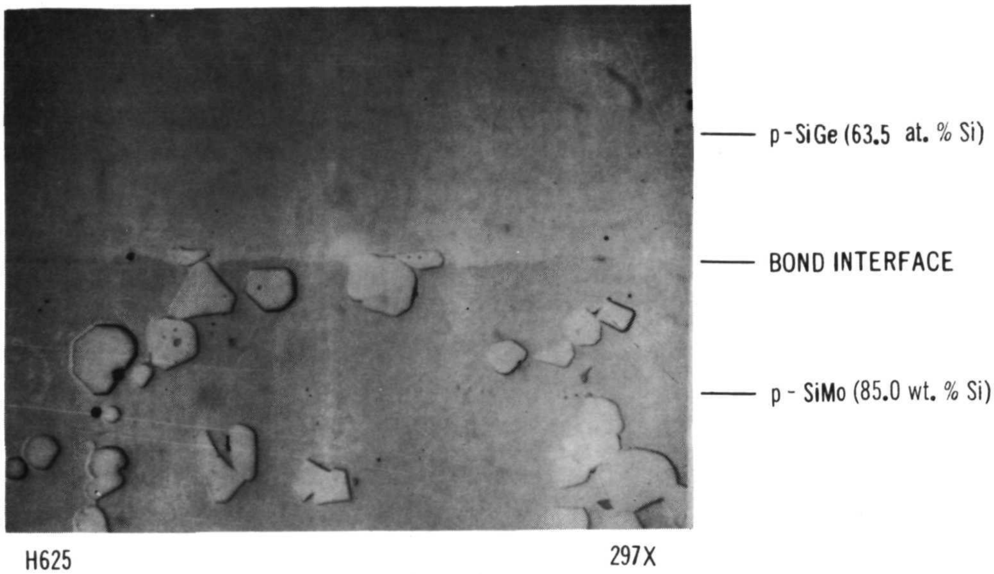

a. p-SiGe (63.5 at.% Si) Bonded to p-SiMo

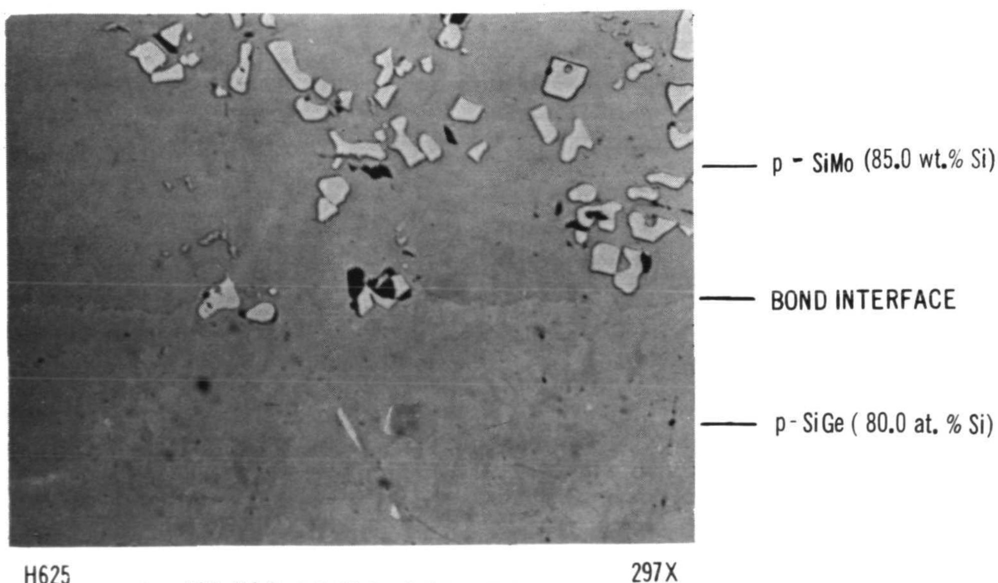

b. p-SiGe(80.0 at.% Si) Bonded to p-SiMo

Figure 26

p-SiGe Cylinder Bonded to p-SiMo Heat Receptor

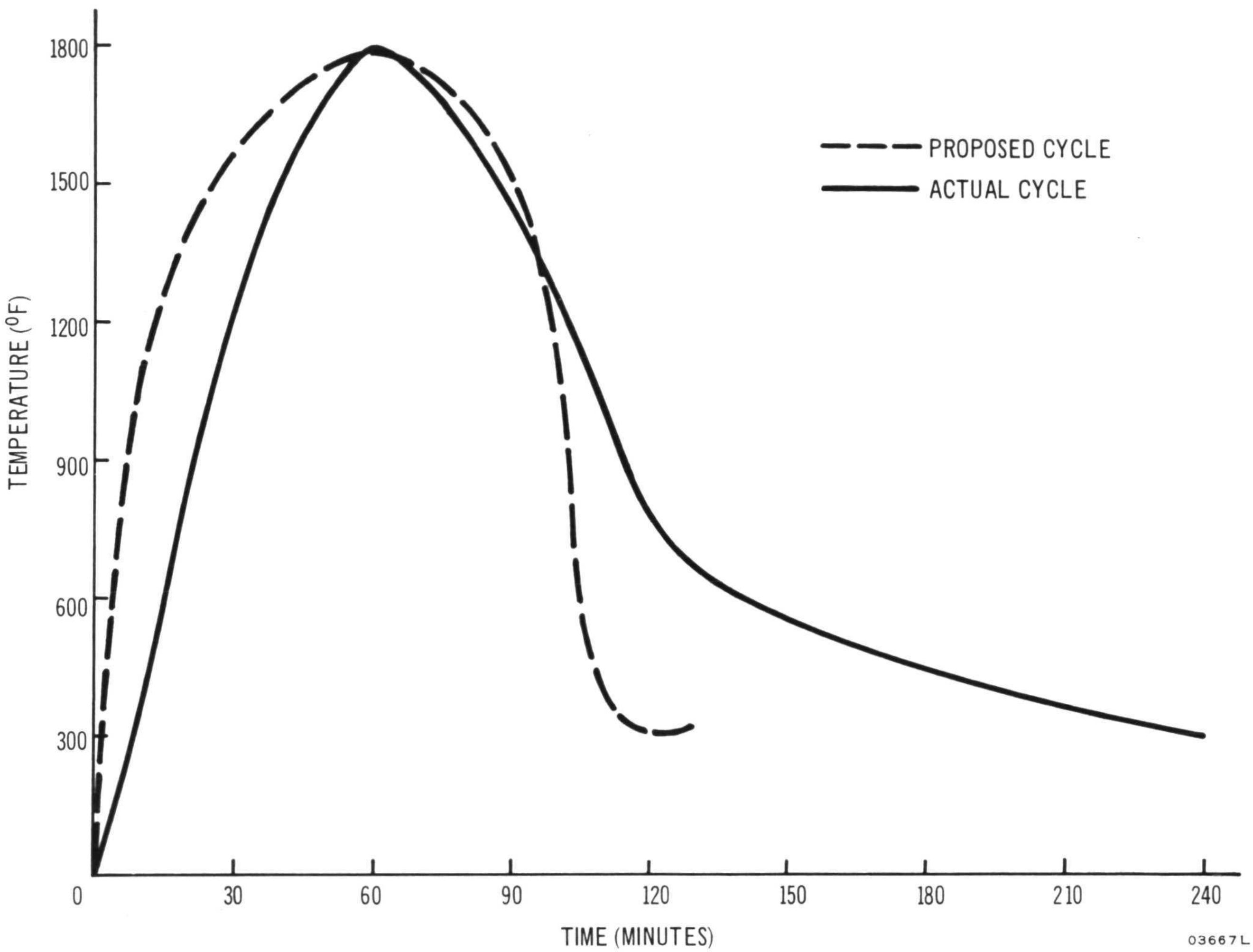

Figure 27. p-Type SiGe Cylinder Assembly, Accelerated 2000°F Thermal Cycle

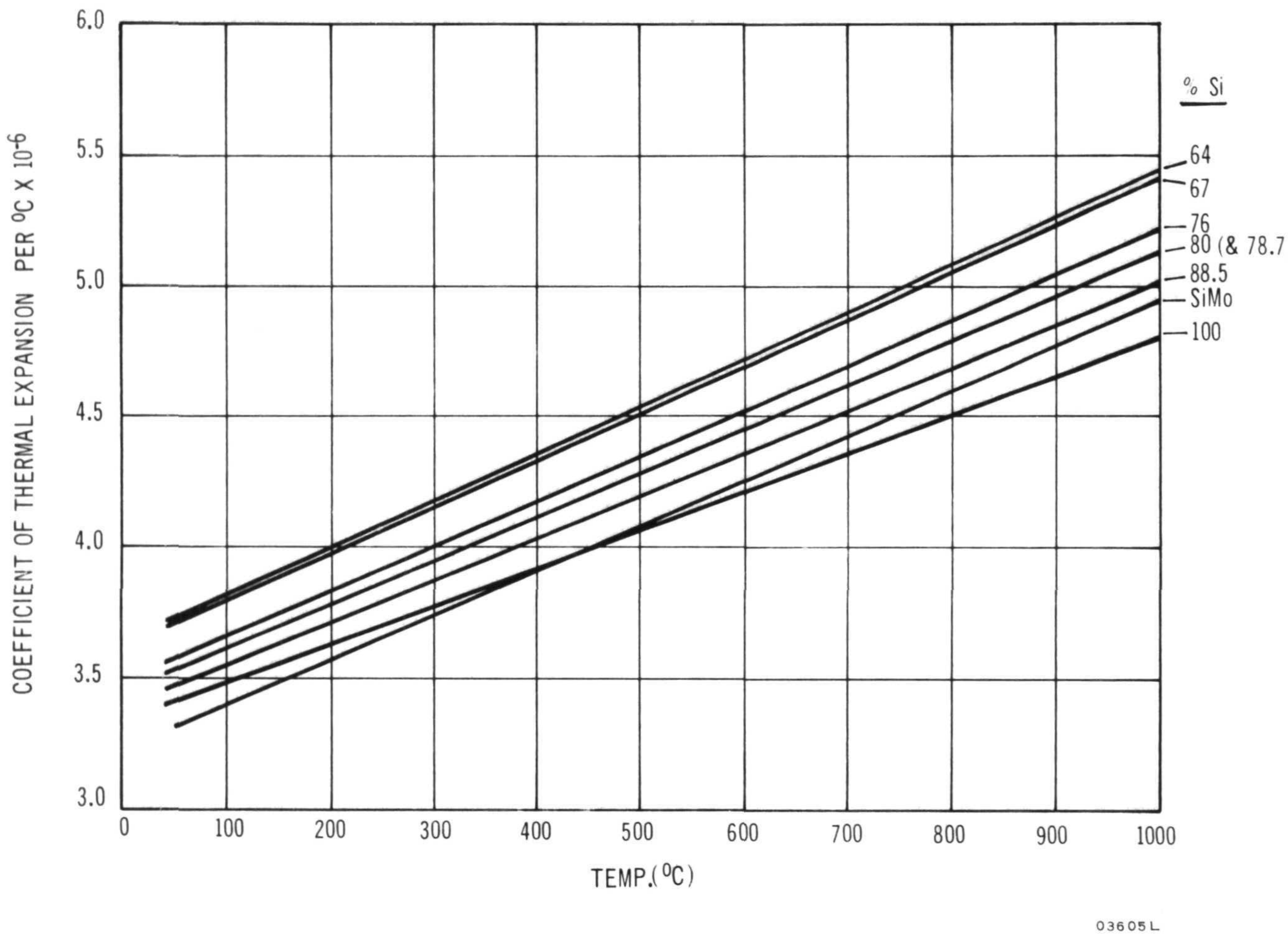

Figure 28. Coefficient of Thermal Expansion as Function of Temperature for SiGe and SiMo Alloys

The bonding of the tungsten cold shoe ring to the p-SiGe (63.5 at.% Si) cylinder initially involved a direct eutectic-type diffusion bond, which forms a WSi_2 intermediate layer. Tests conducted with this system did not result in hermetic seals; therefore, development of an alternate attachment technique was undertaken. A low temperature braze technique was developed in which a nickel coating was applied to the SiGe surface via an electroless plating technique. This braze system produced hermetic seals at the p-SiGe element cold shoe interface.

Thermal cycling of subcomponents with the tungsten shoe brazed at the cold end resulted in leak-tight seals after ten cycles from 316°C (600°F) to 93°C (200°F).

In subsequent development of the p-SiGe--p-SiMo subcomponent, the SiGe alloy was changed from 63.5 at.% Si to 80 at.% Si. In order to obtain improved strength, a return to the eutectic-type diffusion bond (WSi_2) at the cold end was made. The resultant bonds were metallurgically sound and formed hermetic seals (see Figure 29), both as-fabricated and after thermal cycling tests. The tensile strength of the as-fabricated and life-tested specimens, 316°C (600°F) for 4032 hours, averaged 2300 psi with the break occurring in the bulk SiGe. The cold shoe bond was tested for 6200 hours at 316°C (600°F) with no observable change in bond resistance. This type bond had been previously used in the SNAP 10 thermoelectric modules and has been tested in excess of five years at 500°C (938°F) with stable electrical characteristics.

As a result of these subcomponent tests, the composition and bonds for this segment of the Hybrid couple were selected as follows: an 85 wt.% p-SiMo heat receptor bonded directly to an 80 at.% p-SiGe cylinder leg which is simultaneously bonded at the cold end to a tungsten shoe.

2. <u>n-SiGe Element</u>

The n-SiGe element consists of a n-SiGe pellet metallurgically bonded to a n-SiMo hot shoe on one end and a tungsten cold shoe on the other end; see Figures 30a and 30b. These metallurgical bonds have been used extensively in the past and have exhibited good stability and life capability at the Hybrid couple design operating temperatures.

A limited number of subcomponents were fabricated and subjected to various screening tests. Life tests at 982°C (1800°F) for 300 hours and 1090°C (2000°F) for four hours showed no change in electrical or physical properties. The tungsten-n-SiGe bond was not included in these test samples due to the temperature limitation of the WSi_2 bond. Metallographic examination indicated normal n-SiGe--n-SiMo bonds with no discernible change from initial bonds (see Figures 30a and 30b).

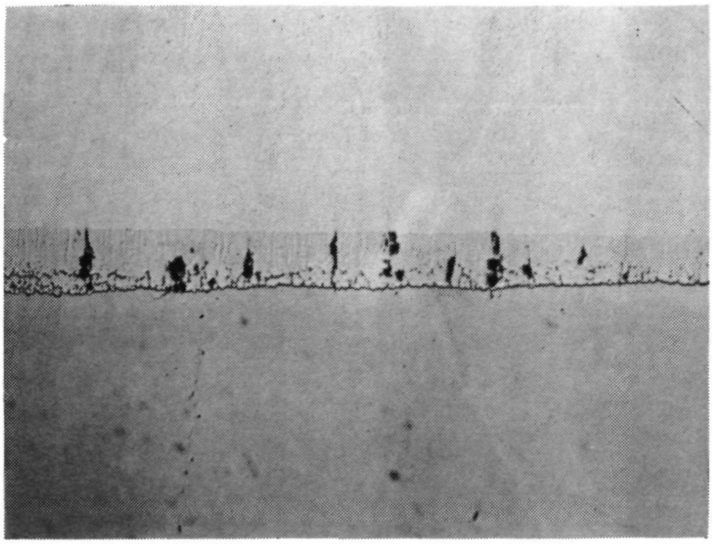

Figure 29. p-SiGe (80.0 at. % Si) Bonded to Tungsten Cold Shoe

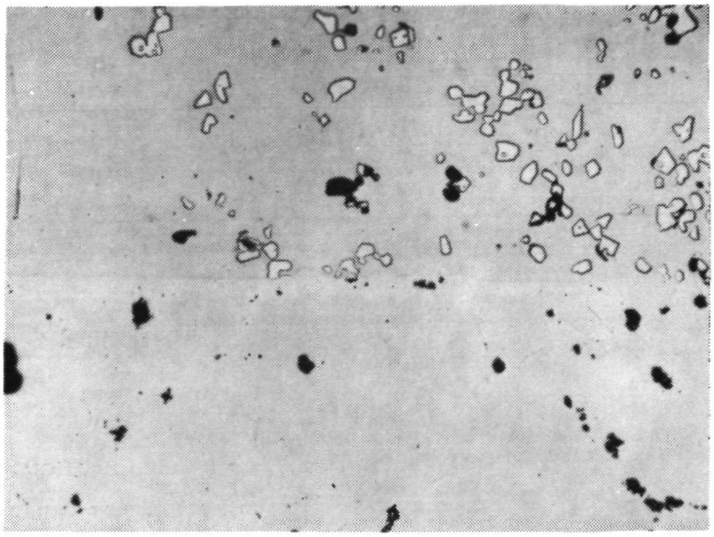

Figure 30a. Hot Shoe Bond n - SiGe Leg to n - SiMo Hot Shoe

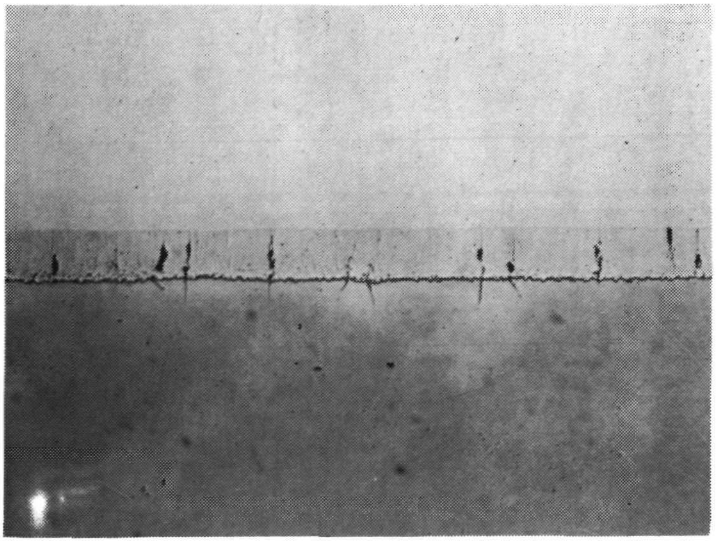

Figure 30b. Cold Shoe Bond n - SiGe Leg to Tungsten Cold Shoe

A summary of the tensile and shear strength tests made on as-fabricated and life-tested specimens is given in Table XI. These strength values are normal for SiGe with the fractures occurring in the bulk SiGe material.

TABLE XI

TENSILE AND SHEAR STRENGTH OF n-SiGe ELEMENTS

		Tensile Strength*, psi			Shear Strength*, psi	
Design	Number of Specimens	As-bonded	After 300 hours @ 982°C (1800°F)	After 4 hours @ 1090°C (2000°F)	As-bonded	After 300 hours @ 982°C (1800°F)
A	15	3600-4000	3500-3800	3500-3800	2000-2500	2000-2500
B	15	3600-4000	3700-4000	3700-4000	2300-2500	2000-2500
C	15	3600-4000	3700-4000	3700-4000	2300-2600	2000-2500

* Measured at room temperature

3. n-PbTe Element

The n-PbTe element consists of a 3N PbTe pellet metallurgically bonded to 303 stainless steel shoes, which have been treated with a tungsten diffusion barrier layer and a minimum of bonding medium layer.

The shoe is an electrical contact which is chosen for its thermal expansion match with the PbTe element. In this application, it is supplemented with a chemically stable tungsten barrier. Therefore, the chemical purity of the PbTe is maintained to permit its normal life without the poisoning effects of foreign elements.

The tungsten is applied by chemical vapor deposition using commercial tungsten hexafluoride. A plating thickness of 0.1 to 0.5 mil is adopted for standard practice; Figure 31. These tolerances are maintained by sampling one of each batch of five shoes (Figure 32). The barrier is restricted to the actual shoe bond area by the die. This thin tungsten barrier should maintain good adherence and soundness throughout the life expectancy of the PbTe element.

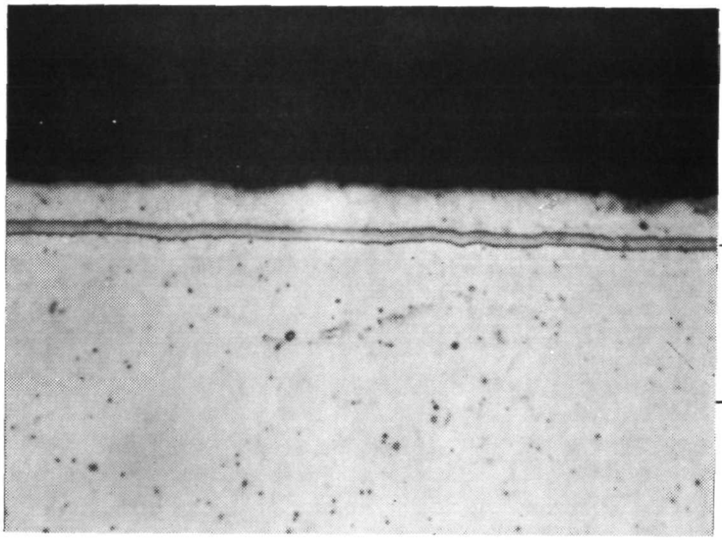

H603 - 7 561X

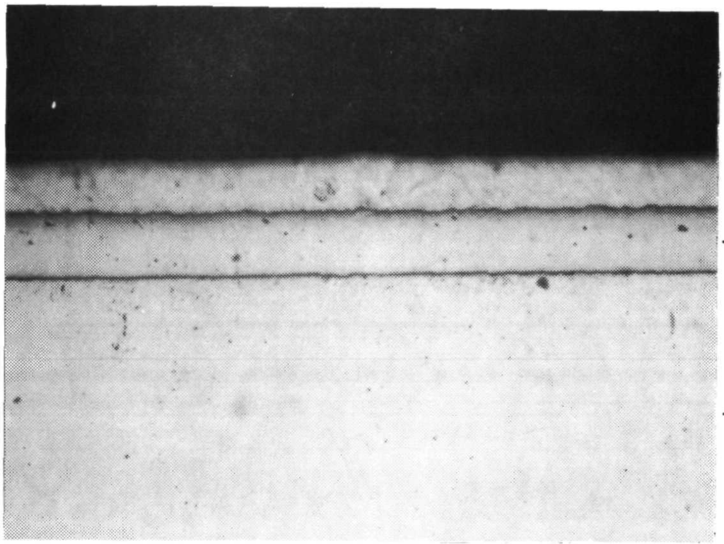

H626 561X

Figure 31. Thickness Limits of Chemical Vapor Plated Tungsten on 303 Stainless Steel Shoes

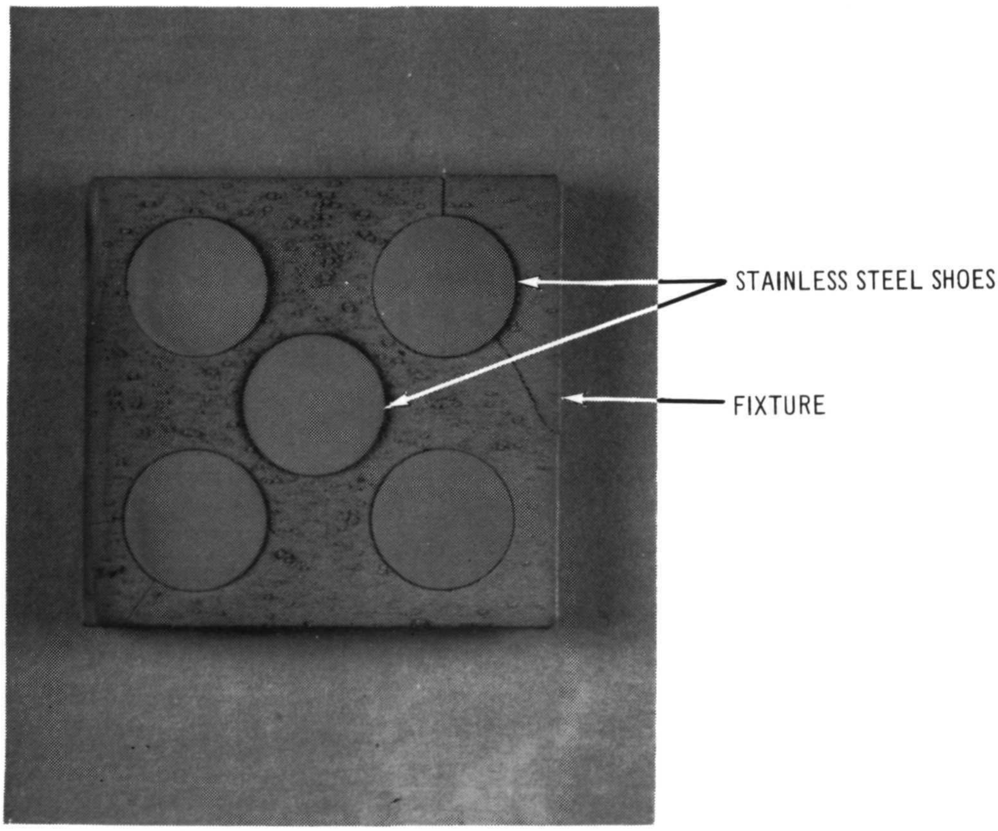

Figure 32. Tungsten Vapor Plated 303 SS Shoes One Run of Five Shoes .375D X .040

The shoe is bonded to the PbTe pellet with a procedure which forms a complete void-free interface and one free of surface oxides developed on the surface of the pellet. This solves many of the recognized problems with a W-PbTe bond which includes (1) poor wetting characteristics of the PbTe surface, (2) rapid surface oxide formation on a mechanically cleaned surface, and (3) negligible solubility of PbTe into tungsten for bonding purposes.

The procedure uses nickel as a bonding medium and a die to provide alignment and mechanical pressure (Figure 33). In the bonding cycle, with an inert atmosphere, the nickel diffuses into the tungsten and dissolves a thin surface layer of PbTe to form the bond. With the die and pressure rods fixing the position of the shoes relative to the pellet, additional pressure is applied to eject the excess melt and, along with it, any residual oxides and foreign matter. The bond overflow is contained in the immediate area of the bond, as shown in Figure 34, and discarded in the finishing operation. What is left is a perfectly sound, clean and void-free bond. Appropriate photomicrographs are presented in Figures 35 and 36.

The tensile and shear strength of as-fabricated PbTe elements of 0.635 cm (0.250 in.) and 0.951 cm (0.375 in.) OD are given in Table XII.

TABLE XII

TENSILE AND SHEAR STRENGTH OF n-PbTe ELEMENTS

Specimen OD cm (in.)	Specimen Number	Tensile Strength psi
	Pellet	1080
0.635 (0.25)	Element 1	712
	" 2	1570
	" 3	*
	" 4	361
0.951 (0.375)	" 5	*
	" 6	729
		Shear Strength psi
0.951 (0.375)	" 7	284
	" 8	203

* broke while attaching tensile fixtures

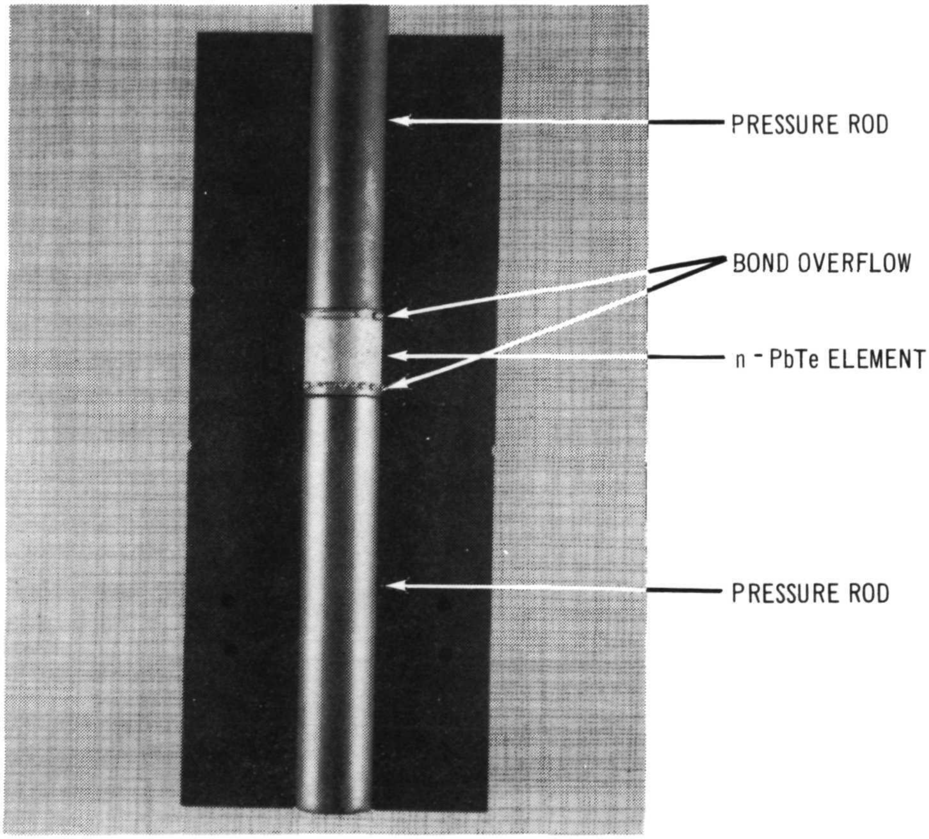

Figure 33. PbTe Element in Shoe Bonding Die

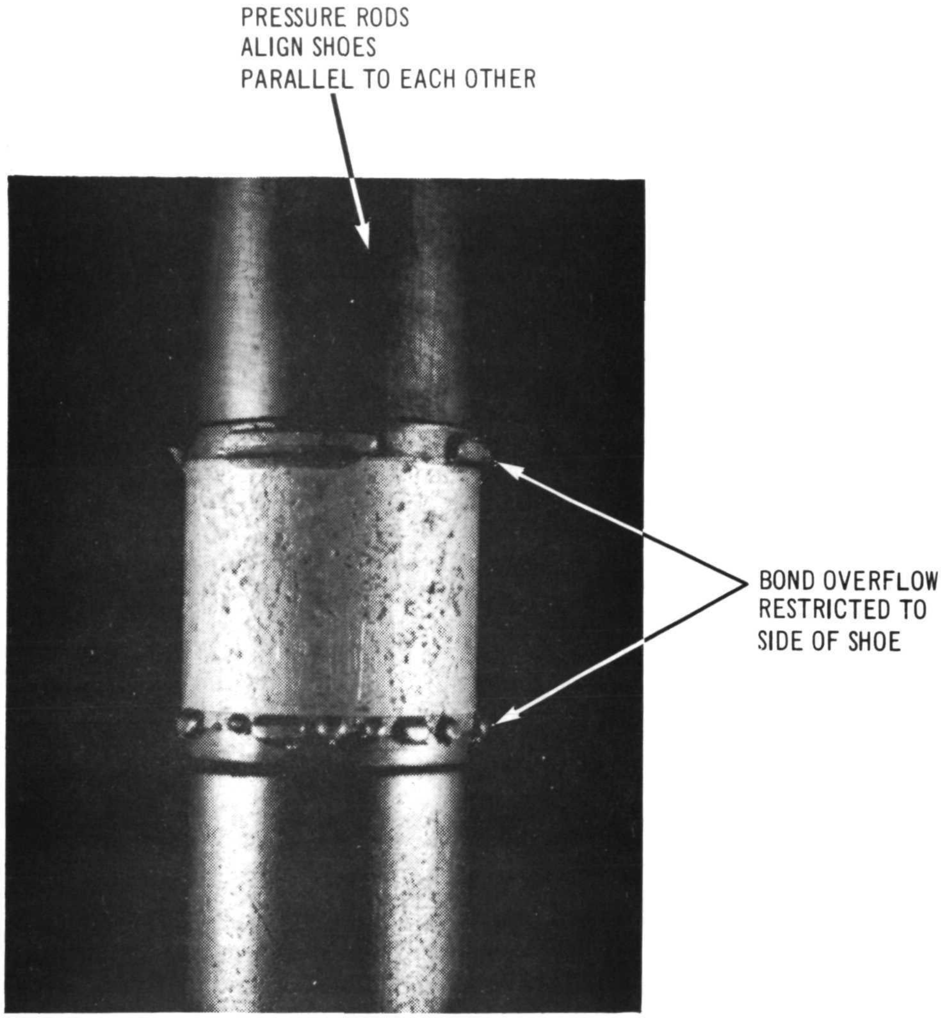

Figure 34. n - Type PbTe Element—Bond Overflow

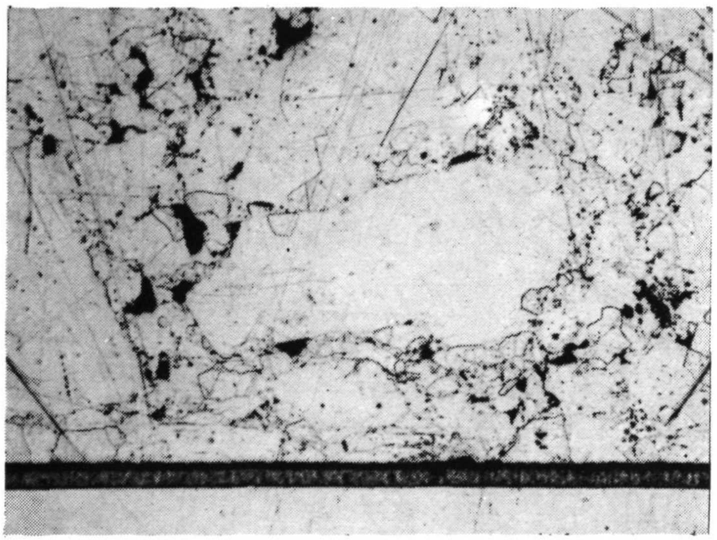

Figure 35. PbTe 3N Element Bond Structure

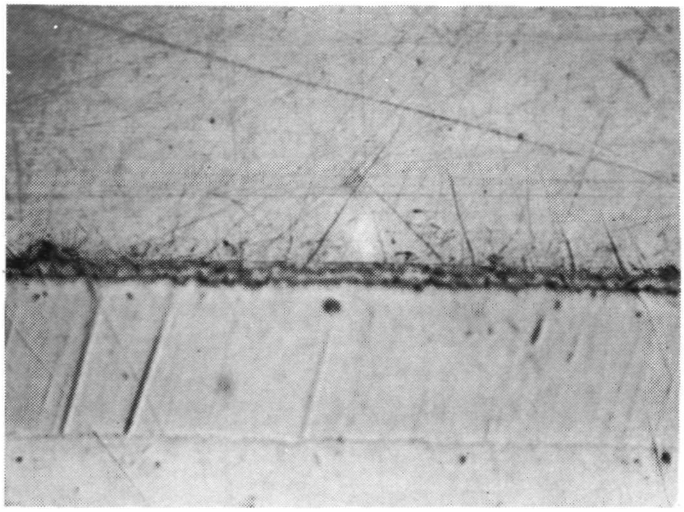

UNETCHED

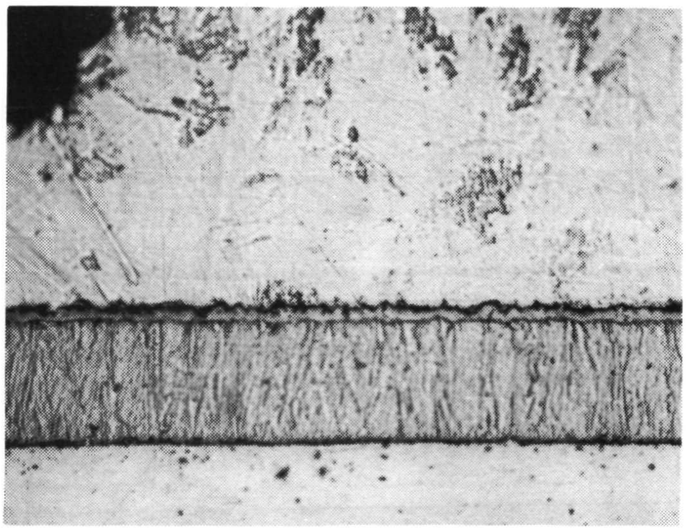

H627 ETCHED 580X

Figure 36. PbTe 3N Element Bond Structure

Note that the strength of the elements is lower than that of the pellets. The element strength, however, should be adequate for the stresses encountered in the device. The current technique of shear testing was not suitable for elements with 0.635 cm (0.250 in.) OD and no shear strength data were obtained for these elements. Resistance measurements made before and after isothermal life tests of the 0.635 cm (0.25 in.) OD and 0.951 cm (0.375 in.) OD PbTe elements are tabulated in Table XIII. Note that the sum of the PbTe bulk and contact resistances do not equal the total measured resistance since some of the bulk resistance is unavoidably included in the measurement of the contact resistance. Only minimum changes occurred in the electrical resistance and physical appearance of the elements subjected to isothermal life tests. Metallographic examination of the life-tested specimens showed sound structures with very little discernible change in the PbTe-W barrier nickel-303 stainless steel bond structure (Figures 37 and 38). In general, the n-PbTe elements subjected to life tests have shown good stability.

4. Cold Stack

The cold stack subcomponent consists of the n- and p-electrical connectors (copper), ceramic insulators (alumina (Al_2O_3)), mount stud (copper and steel), and copper exhaust tubulation brazed together into a single subassembly. Previous studies have shown that the use of a T-mount copper stud (Figure 39a) rather than a tapered mount steel stud (Figure 39b) results in an improved temperature drop (10°C versus 17°C). The T-mount stud also was found to minimize stresses which may be transmitted to the ceramic insulator when the stud is secured to the module mounting panel. These stresses could ultimately fracture the insulator and produce a separation in the cold stack. Shock and vibration measurements made on the T-mount design have also indicated the superiority of this design concept. Accordingly, this concept was pursued in the development of the cold stack for the Hybrid couple.

Two methods of fabricating the T-mount stud were investigated; (1) a single piece copper stud including the threaded section (Figure 39a), and (2) a multipiece stud, copper with a brazed steel threaded section (Figure 40). Strength tests of the "as fabricated" cold stacks, utilizing the single piece copper stud including the threaded section (Figure 41a) were made and compared with those of the multipiece T-mount copper stud employing brazed threaded steel section (Figure 41b). Force was applied to the nut with a torque wrench in increments of 10 inch-pounds, starting at 10 to 50 in.-lbs. Deformation of the one piece stud was noticeable in the lower half of the stud and the thread stripped at 45 in.-lbs on one sample. No distortion of the parts was detected in the multipiece stud with the brazed threaded steel section at 50 in.-lbs. The two-piece T-mount was therefore selected for the cold stack construction.

A total of nine cold stack structures of the multipiece stud design were fabricated and subjected to the following tests:

TABLE XIII

RESISTANCE OF PbTe ELEMENTS
SUBJECTED TO ISOTHERMAL LIFE TESTING IN ARGON

Test No.	Element OD cm (in.)	Soak Temperature °C (°F)	Time at Temperature hours	RT Resistance, milliohms Total	Contacts 1	Contacts 2	Bulk PbTe
1	0.951 (0.375)	RT	AB	0.313	0.030	0.020	0.30
		540 (1000)	330	0.341	0.020	0.020	0.32
2		RT	AB	0.32	0.025	0.025	0.30
		540 (1000)	330	0.335	0.025	0.020	0.30
3		RT	AB	0.34	0.020	0.020	-
		593 (1100)	138	0.385	0.025	0.020	0.345
		593 (1100)	252	0.365	0.025	0.030	0.330
4		RT	AB	0.32	0.015	0.020	-
		593 (1100)	138	0.343	0.015	0.020	-
5	0.635 (0.250)	RT	AB	0.92	0.015	0.025	0.910
		540 (1000)	475	0.99	0.030	0.040	0.960
6		RT	AB	0.92	0.022	0.035	0.905
		540 (1000)	475	0.98	0.020	0.030	0.950
7		RT	AB	0.93	0.020	0.025	0.890
		593 (1100)	159	0.935	0.025	0.030	0.900
8		RT	AB	0.94	0.020	0.030	0.915
		593 (1100)	159	0.97	0.030	0.040	0.935

RT Room Temperature

AB As Bonded

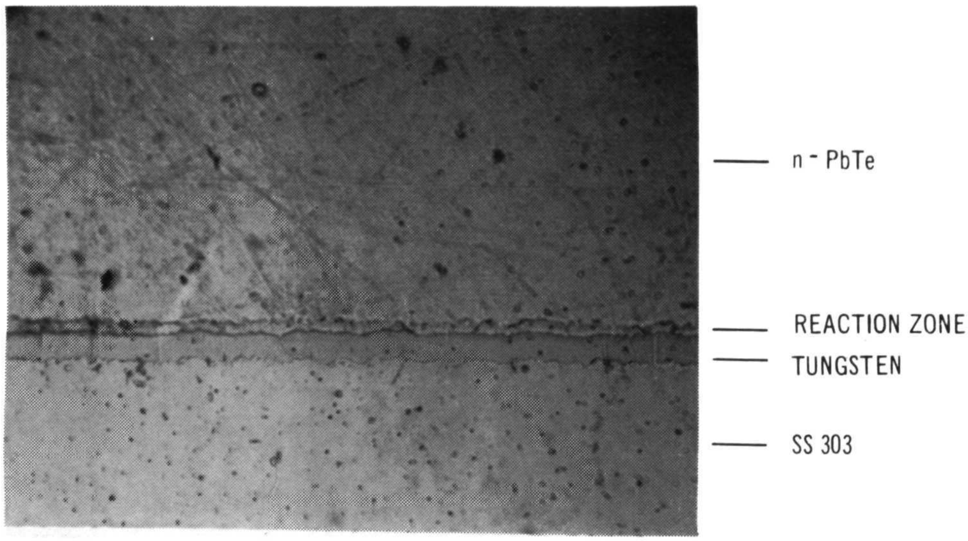

H682 580X

AS BONDED

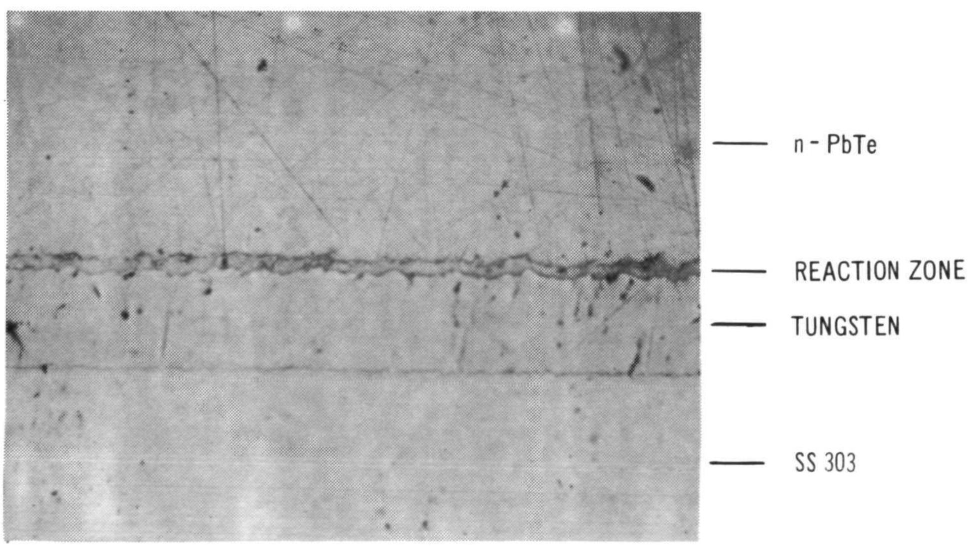

H688 580X

475 HOURS AT 1000°F

Figure 37. 3N PbTe Element Shoe Bond Structure

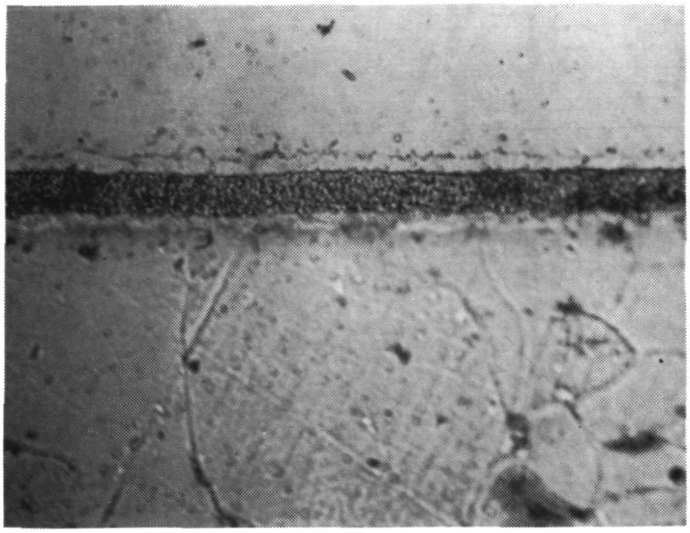

H630 - 27 580X

330 HOURS AT 1000°F

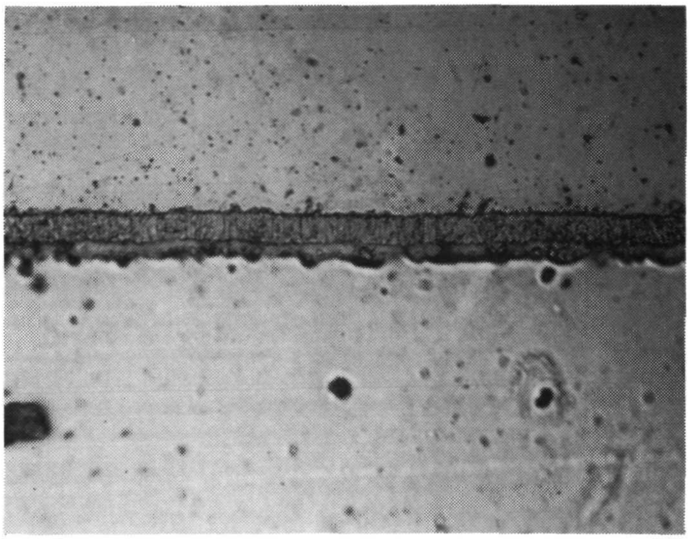

H630 - 29 580X

138 HOURS AT 1100°F

Figure 38. 3N PbTe Element Shoe Bond Structure

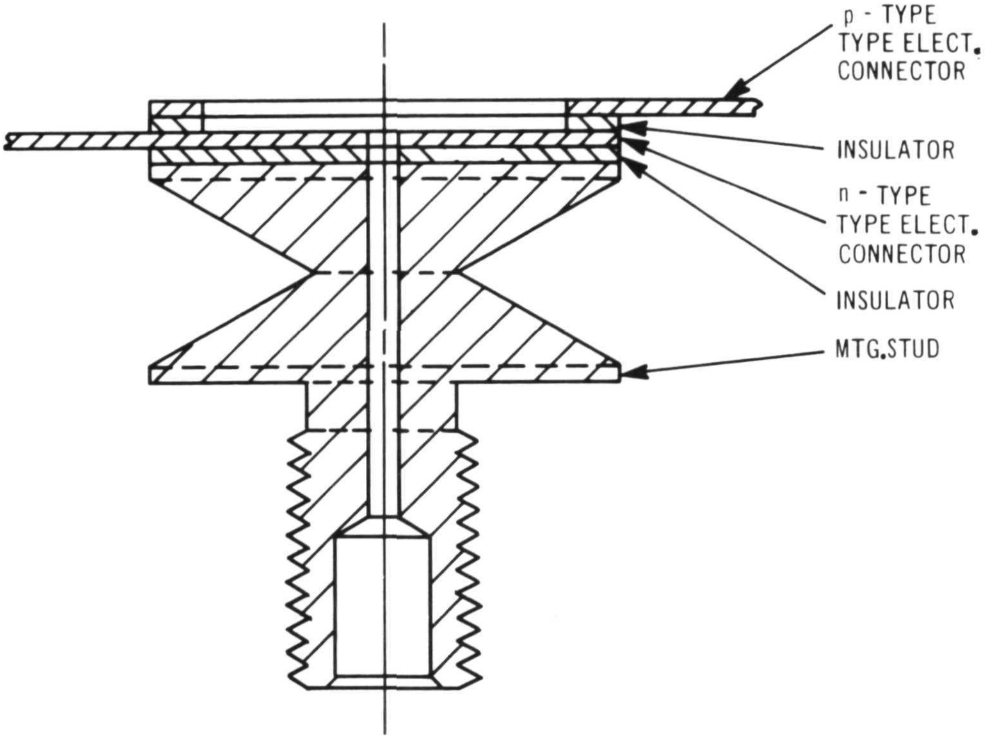

a. One Piece Copper T-Mount Stud–Cold Stack Design

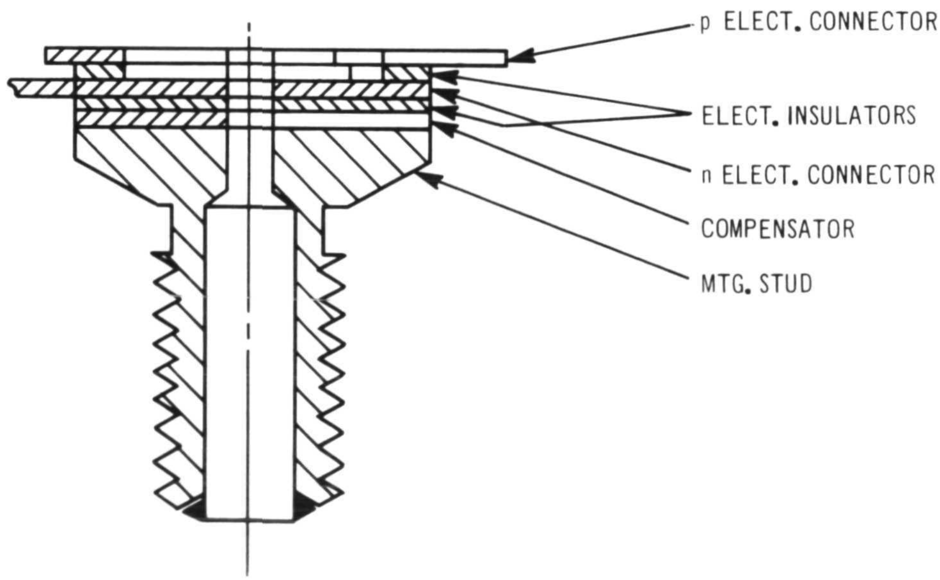

b. Tapered Mount Steel Stud Cold Stack Designs

Figure 39. Experimental Cold Stack Designs

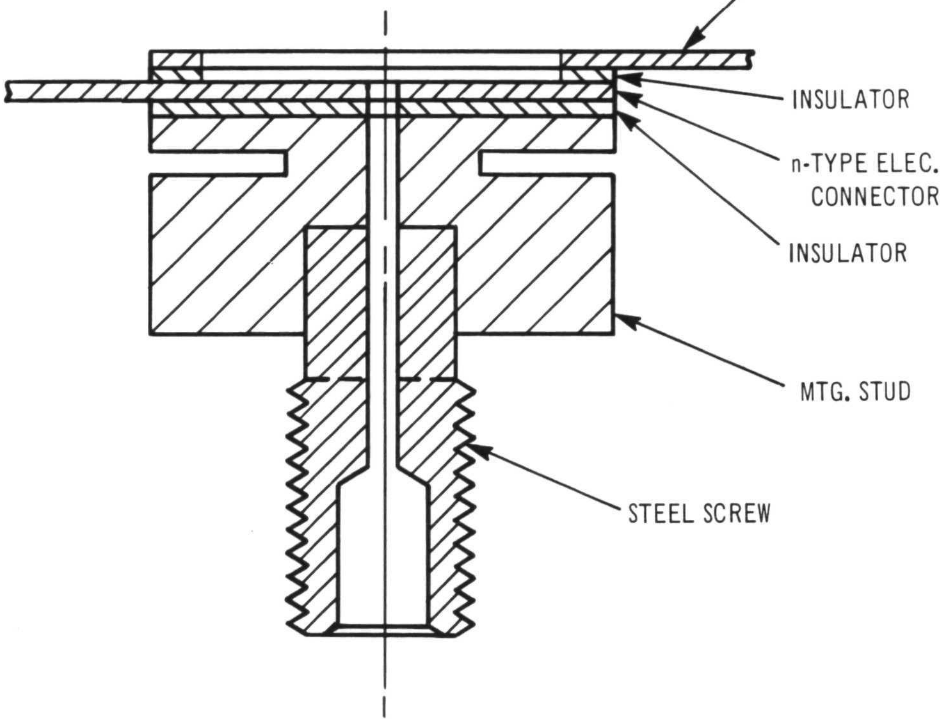

Figure 40. Two Piece T-Mount Stud – Cold Stack Design
(Copper T - Steel Screw)

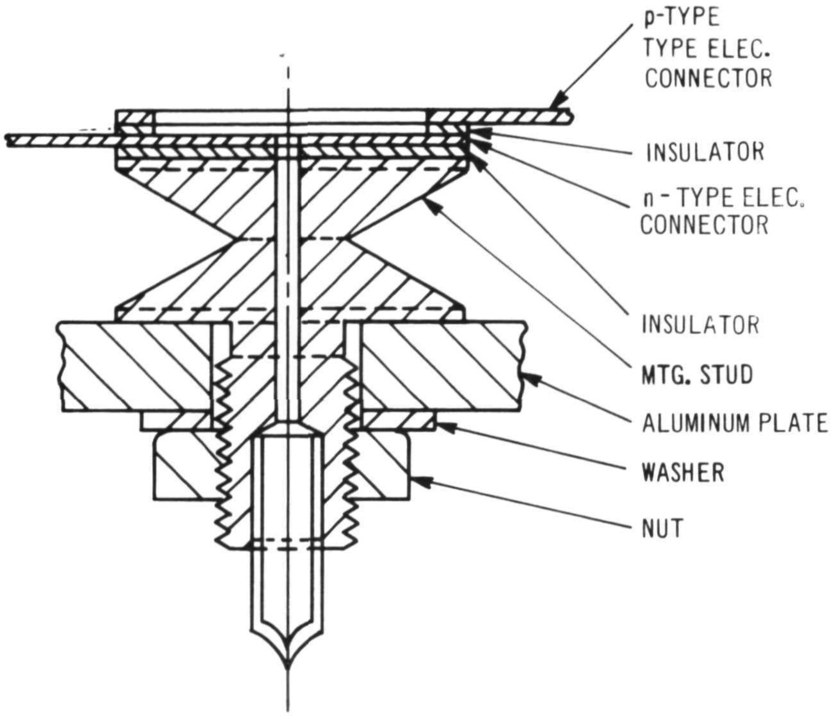

Figure 41a. One Piece Copper T- Mount Stud – Cold Stack Design – Aluminum Plate

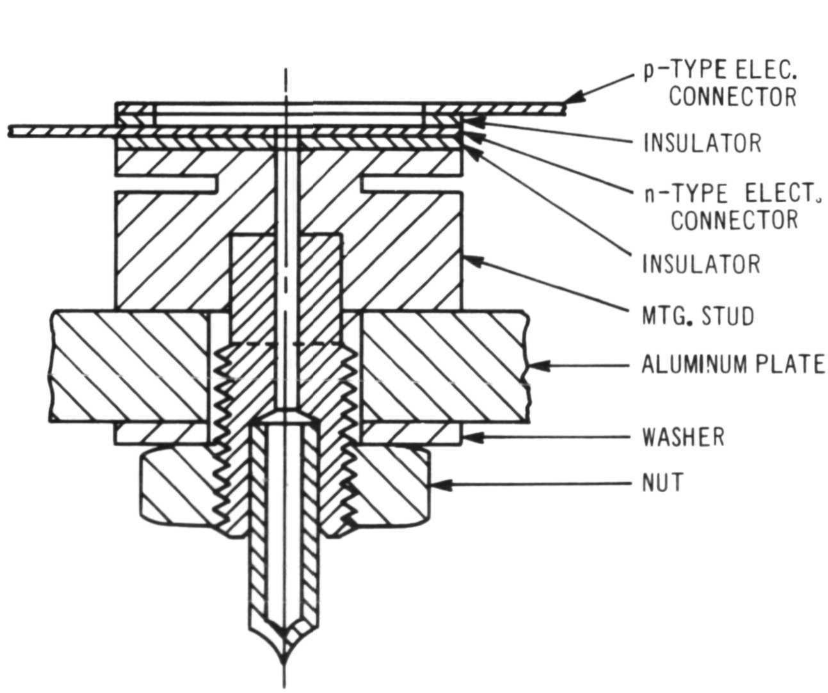

Figure 41b. Cold Stack Design (Copper T – Steel Screw) Aluminum Plate.

Number of Samples	Type of Test
1	Metallographic examination
2	Tensile test
2	Shear test
2	300 hours life test
2	Accelerated life test

Metallographic analysis of the structure showed excellent brazes between all component parts.

Tensile test: This test was performed by exerting a longitudinal force between a tungsten disc and screw (see Figure 42). The forces required to break the samples were 320 pounds (6400 psi) to 400 pounds (8000 psi). Both breaks occurred through the ceramic insulator ring, showing typical tensile cracks (Figure 43).

Shear test: This test was performed by exerting a force at right angles to the longitudinal plane of the structure (Figure 44). One sample was lost when tightened into the Instron fixture. The other sample failed at 355 pounds (7100 psi). The mechanism of failure in both samples was through the ceramic insulator ring.

Life tests: Two samples completed 170 hours of testing at 200°C and another two samples 170 hours at 300°C, under isothermal conditions.

All the above samples were checked for hermeticity after life testing and were found to be leak-tight. Metallographic analyses of these samples showed sound, void-free structures.

5. Intermediate Bond System

The intermediate bond system includes (1) the top gold compensator bonded between the n-SiGe tungsten cold shoe and the n-PbTe 303 stainless steel hot shoe, and (2) the lower gold compensator bonded to the n-PbTe 303 stainless cold shoe. The intermediate bond subcomponent consists of a gold disc diffusion bonded between a nickel-plated 303 stainless steel disc and a nickel-plated tungsten disc (Figure 45). This bond system consists of a nickel-gold diffusion bond which has been used in a number of air-vac thermoelectric devices with excellent results. The intermediate bond test coupons were fabricated according to the process HTS-4 described in Section V-A. They were subjected to the following screening tests:

Tests	Number of Samples	Temperature °F	Time hours
Tensile	2	room temp.	-
Shear	2	room temp.	-
Isothermal life	2	1100	330
Isothermal life	2	1200	4
Metallographic evaluation	1	room temp.	

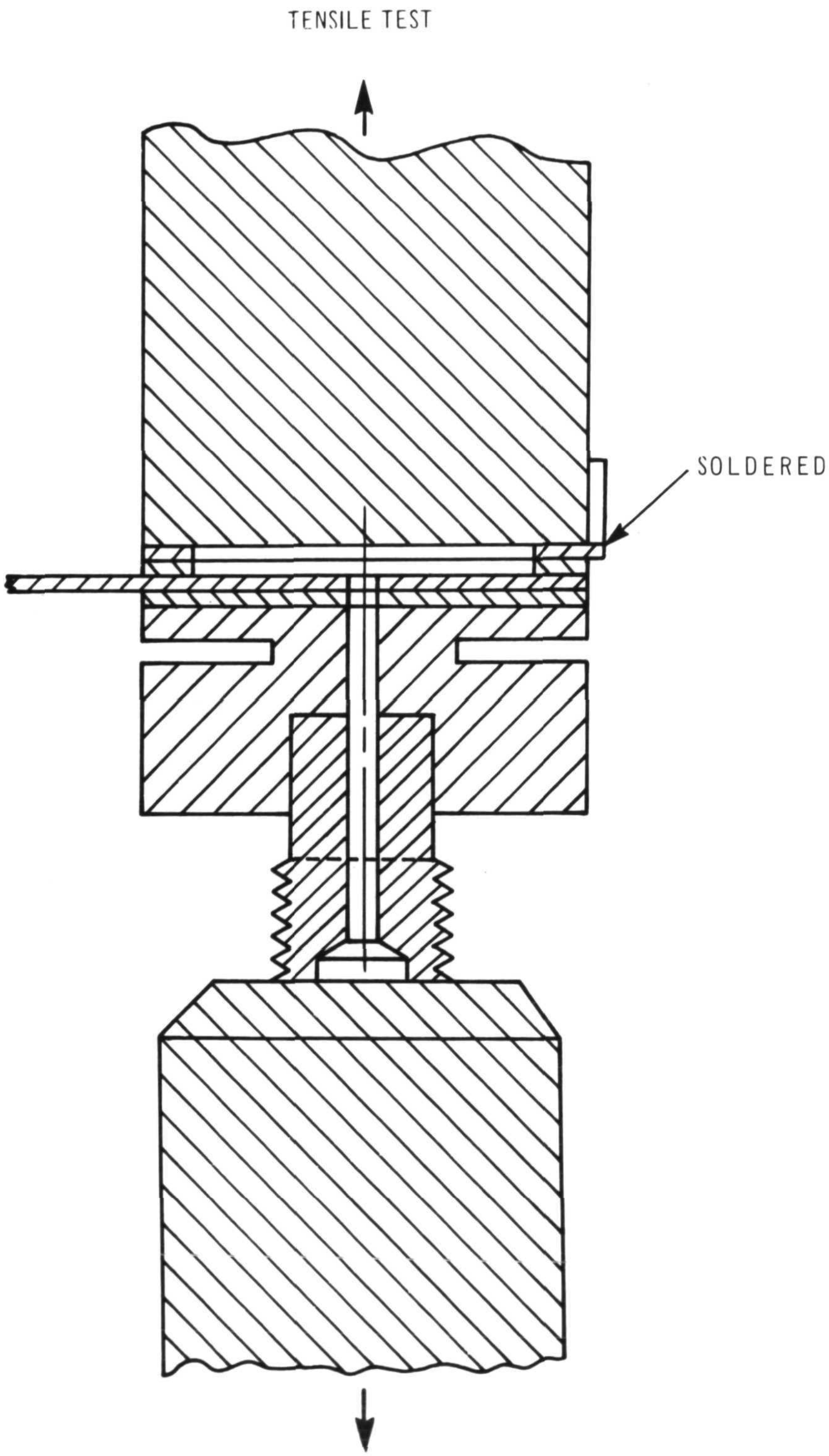

Figure 42. Two Piece T–Mount Stud – Cold Stack Design
(Copper T – Steel Screw)

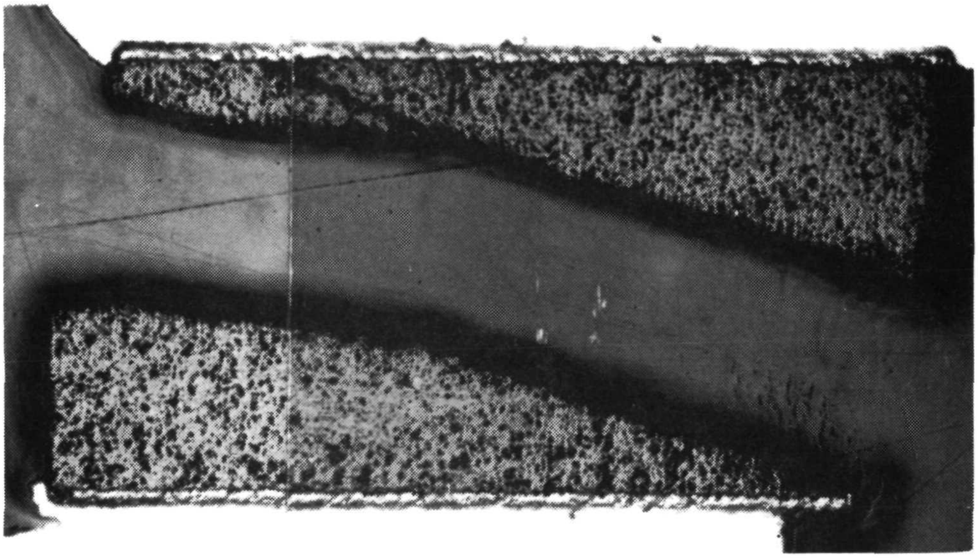

Figure 43. Tensile Tested at 320 lbs.(6400 psi)

SHEAR TEST

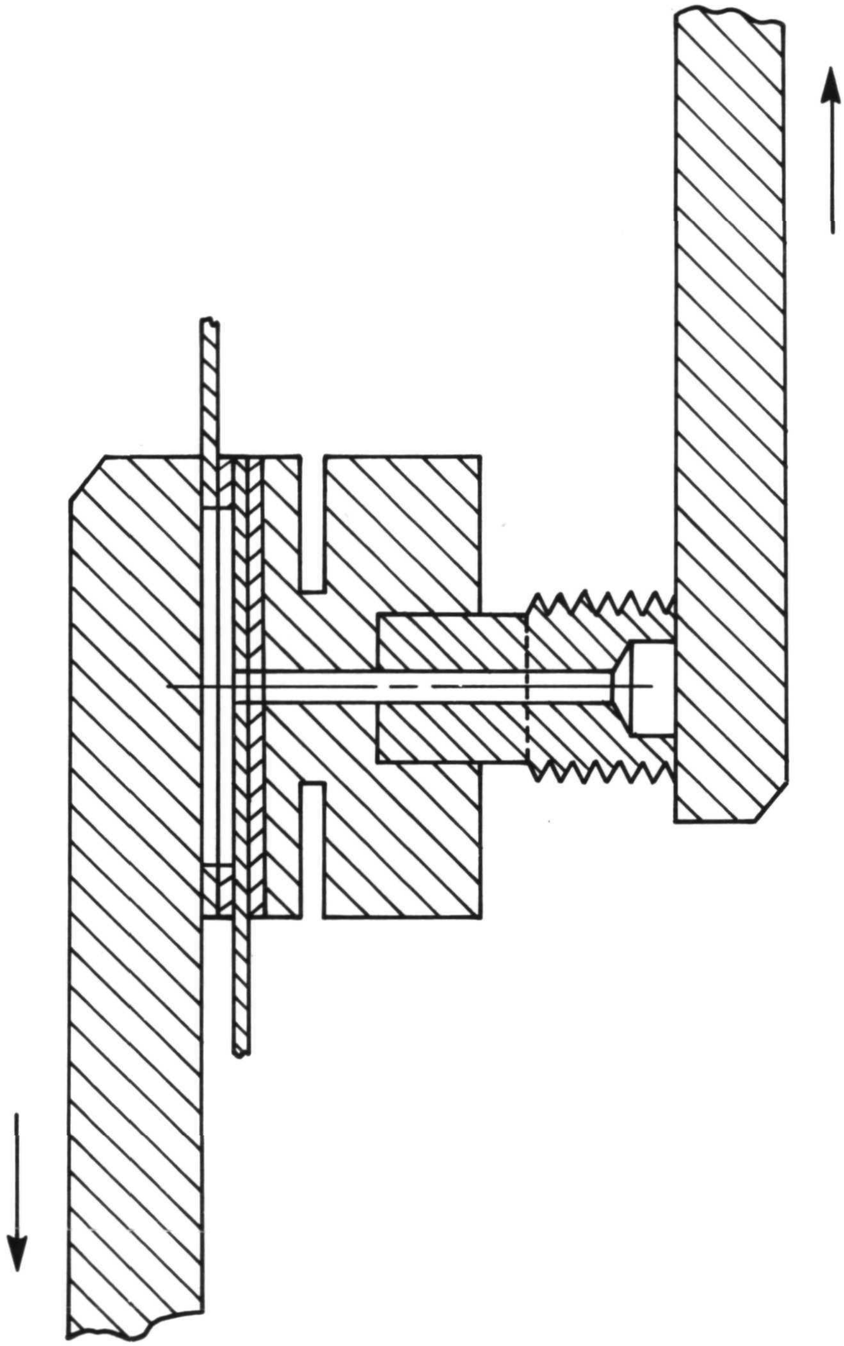

Figure 44. Two Piece T- Mount Stud – Cold Stack Design
(Copper T – Steel Screw)

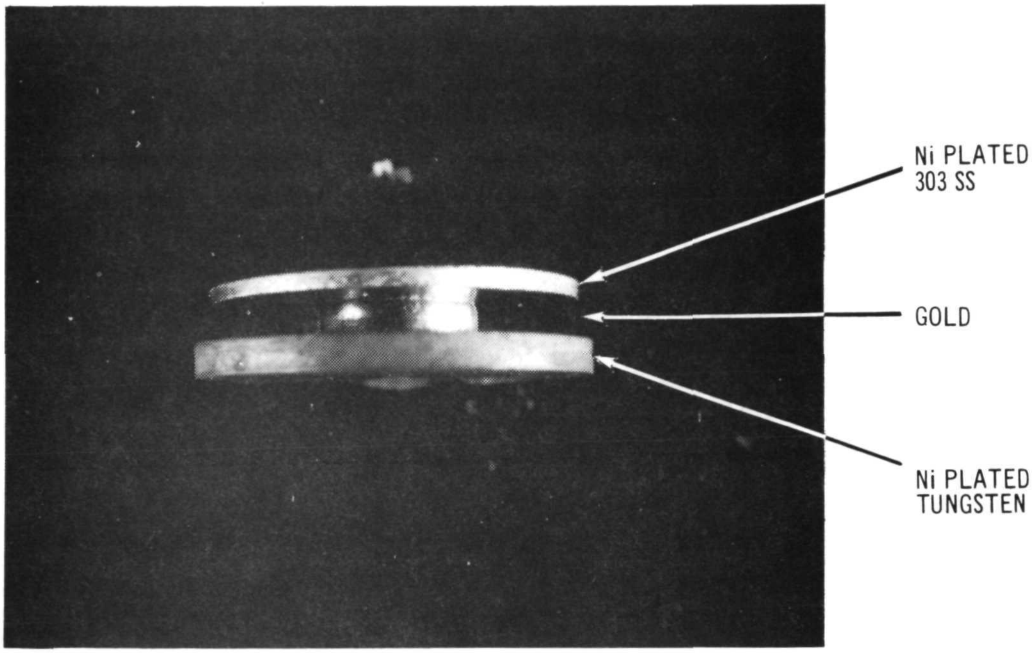

Figure 45. Intermediate Bond System Coupon

The tensile testing resulted in the separation of the specimens in the gold-nickel bond region, as expected. Specimens subjected to accelerated life testing had approximately the same strength as as-bonded specimens (i.e., 6200 and 11,900 psi as-bonded compared to 8600 and 6400 psi after life test). The tensile results are summarized in Table XIV.

TABLE XIV

TENSILE STRENGTH OF INTERMEDIATE BOND COUPONS

Specimen Number	Soak Temperature °C (°F)	Time at Temperature hours	RT Tensile Strength psi
1	RT	AB	6,200
2	RT	AB	11,900
3	593 (1100)	330	8,600
4	640 (1200)	4	6,400
5	593 (1100)	481	9,660
6	649 (1200)	4	11,890*

* attachment failure; coupon did not rupture

Shear strengths of two as-fabricated specimens were 11,500 and 13,800 psi. Metallographic examination showed that the bonds were sound, both before and after life test; see Figures 46 and 47. Overall integrity of this bond system was excellent.

B. Thermocouple Development

Hybrid thermocouple assembly sequences and material and part specifications are presented in detail in Section V-A. The preliminary thermocouple assembly sequences selected are described below (see Figure 48).

1. Heat Receptor Subassembly (A). This assembly consists of an n-SiMo disc, 0.320 in. OD, 0.040 in. thick, metallurgically bonded via a diffusion barrier to a 0.960 in. x 0.960 in. x 0.125 in. thick p-SiMo heat receptor plate.

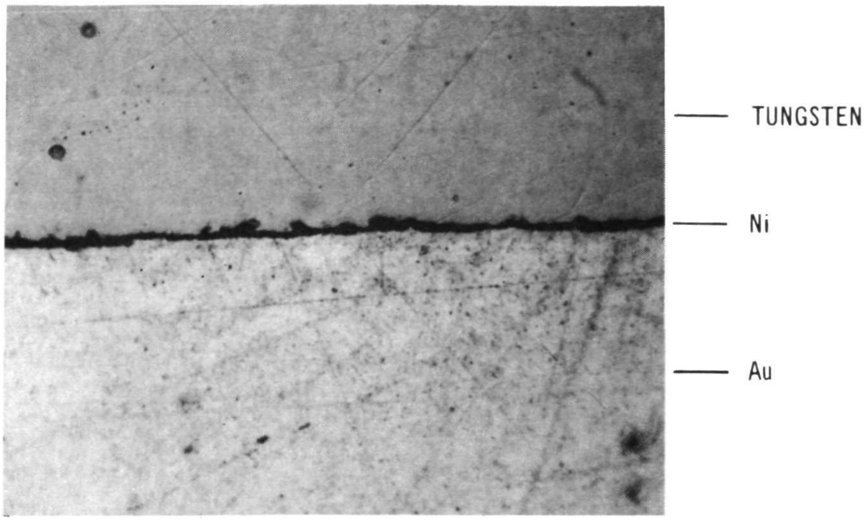

580X

A. AS BONDED (ETCHED)

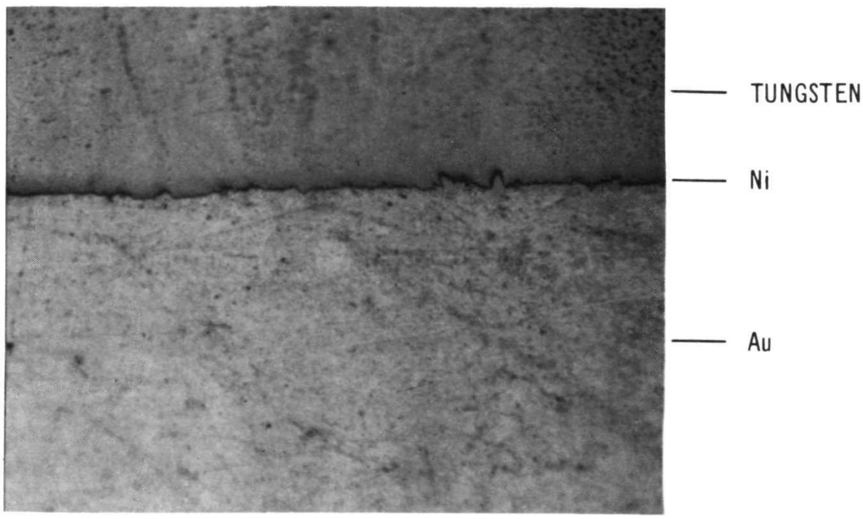

580X

B. UNETCHED, AFTER 300 HOURS AT 1100°F

Figure 46. Intermediate Bond Coupon, Tungsten - Gold Bond Structure

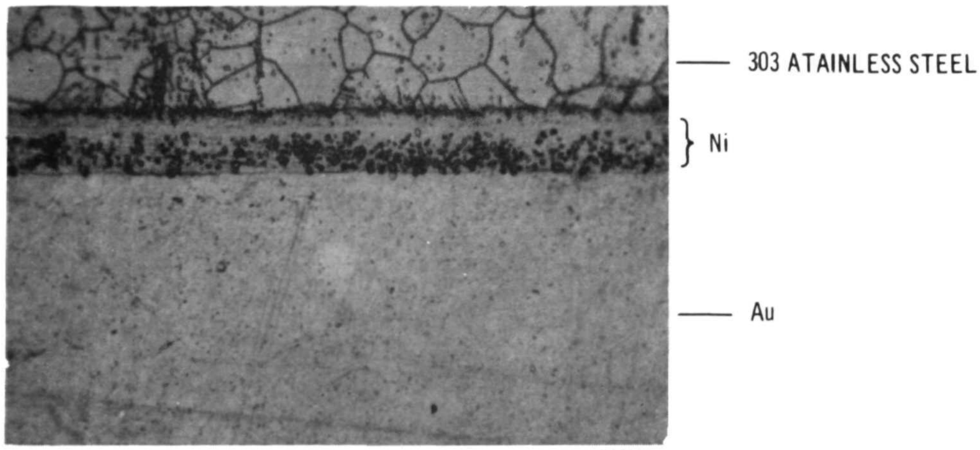

A. AS BONDED (ETCHED) 580X

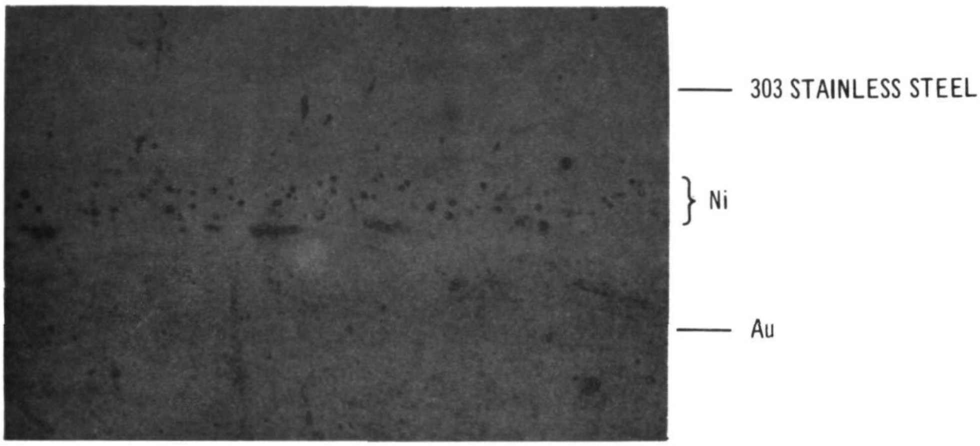

B. AFTER 4 HOURS AT 1200^{0}F 580X

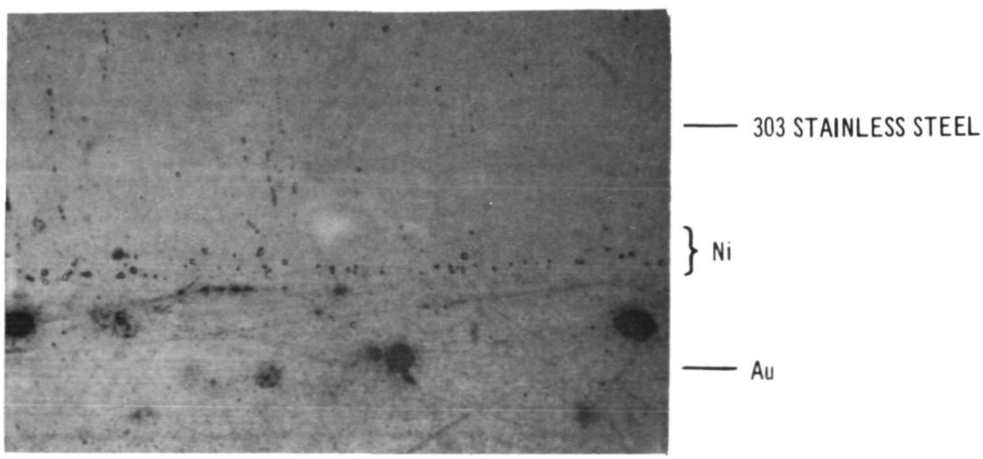

C. AFTER 300 HOURS AT 1100^{0}F 580X

Figure 47. Intermediate Bond Coupon, 303 Stainless Steel - Gold Bond Structure

2. SiGe Subassembly (B). The heat receptor assembly (A), p-type SiGe cylinder, n-type SiGe pellet, and n- and p-type SiGe tungsten cold shoes are simultaneously metallurgically bonded together.

3. n-type PbTe Subassembly (C). This subassembly is identical to subcomponent (C), n-PbTe element, discussed in Section IV-A-3.

4. Thermocouple Subassembly (D). The SiGe subassembly (B), n-PbTe subassembly (C) and the gold compensators are diffusion bonded together.

5. Cold Stack Subassembly (E). This subassembly is identical to subcomponent (D) discussed in Section IV-A-5.

6. Final Assembly (F). The thermocouple subassembly (D) and the cold stack subassembly (E) are brazed together to form the Hybrid thermocouple. Prior to this final assembly step, the gap between the n-segment and the wall of the p-SiGe cylinder is filled with 99.5% aluminum oxide powder and microquartz insulation to reduce heat transfer through this space. Following this final braze operation, the couples are evacuated and back-filled with argon, and the copper tubulation is pinched off.

Based on the results of the subcomponent screening tests described in Section IV and preliminary investigation of thermocouple assembly techniques, two preliminary Hybrid Couple Designs, B and B-1 (see Table V), were selected as the designs to be used in the development of the thermocouple fabrication techniques. These two designs are identical except B-1 has an increased p-SiGe cylinder wall thickness. As a result of the effort conducted in this study, couple design B was selected as the Hybrid Reference Design Couple.

The development effort conducted in arriving at a preferred method for fabricating the Hybrid Couple and selecting the Reference Design involved many variations of the initial assembly methods described above. A summary of the three principal fabrication methods employed throughout this development phase and the final method selected are presented in Table XV.

Assembly technique A (Figure 48) was the initial method; techniques B (Figure 49) and C (Figure 50) were intermediate techniques; and technique D (Figure 51) was the final method selected for fabrication of the Hybrid module panel sections.

A list of other important fabrication modifications made throughout the development program, in addition to those given in Table XV, are presented chronologically in Table XVI. A detailed discussion of the bonding processes and assembly techniques investigated in arriving at the final assembly technique D (Figure 51) is presented in the following.

TABLE XV

SUMMARY OF FABRICATION METHODS - HYBRID THERMOCOUPLE

	Assembly Method			
	A	B	C	D
	Fig. 48*	Fig. 49*	Fig. 50*	Fig. 51*
1. Heat Receptor Subassembly (A)	X	-	-	X
2. Heat Receptor Subassembly (B)	-	X	-	-
3. SiGe Subassembly (A)	X	-	-	-
4. SiGe Subassembly (B)	-	X	-	-
5. Heat Receptor-SiGe Subassembly	-	-	X	-
6. PbTe Element Subassembly	X	X	X	X
7. Thermocouple Subassembly	X	X	X	X
8. Cold Stack Subassembly	X	X	X	X
9. Final Assembly	X	X	X	X

* See Figures 48 through 51 for detailed description of assembly steps

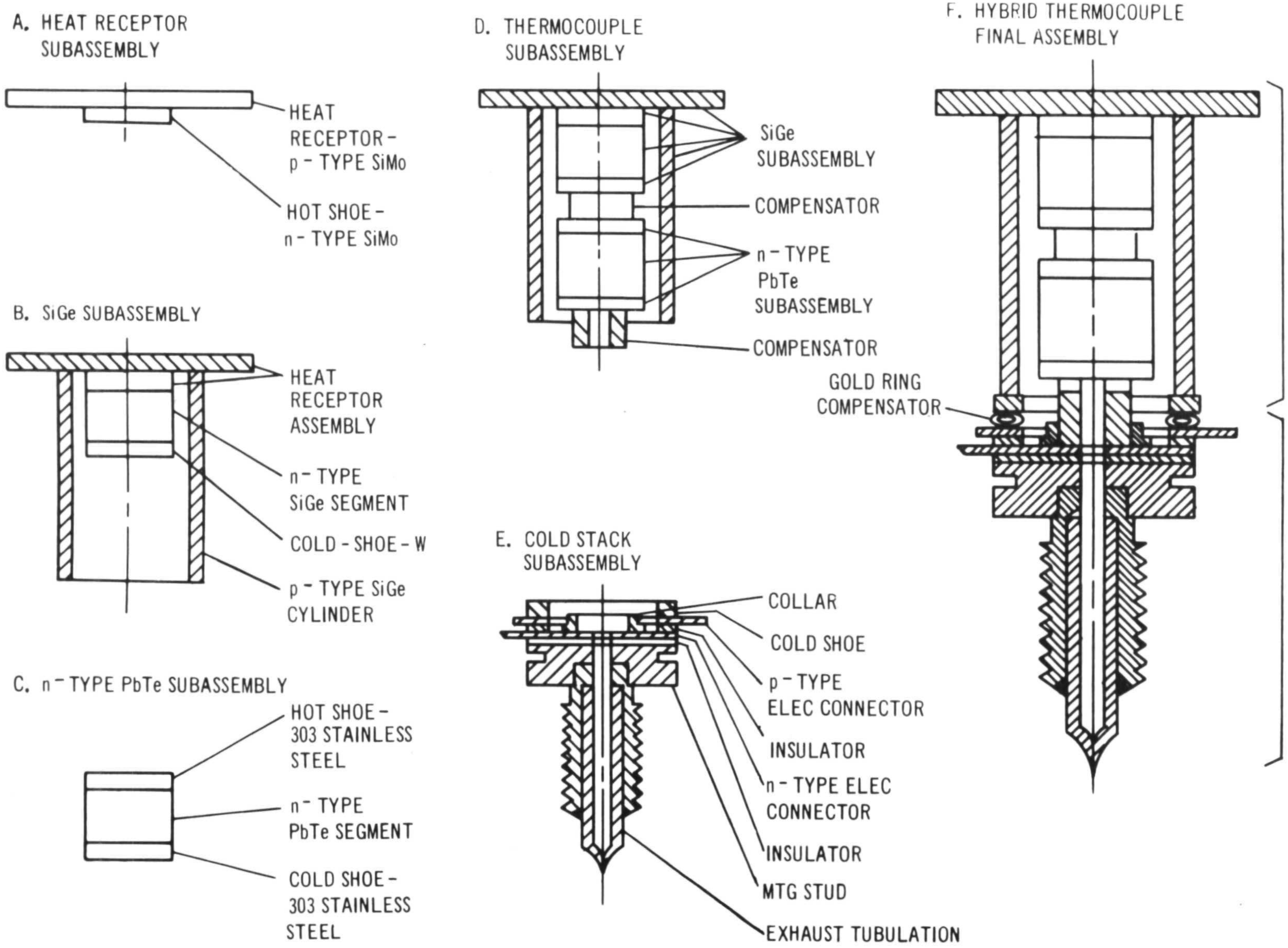

Figure 48. Hybrid Thermocouple Assembly Sequence - A

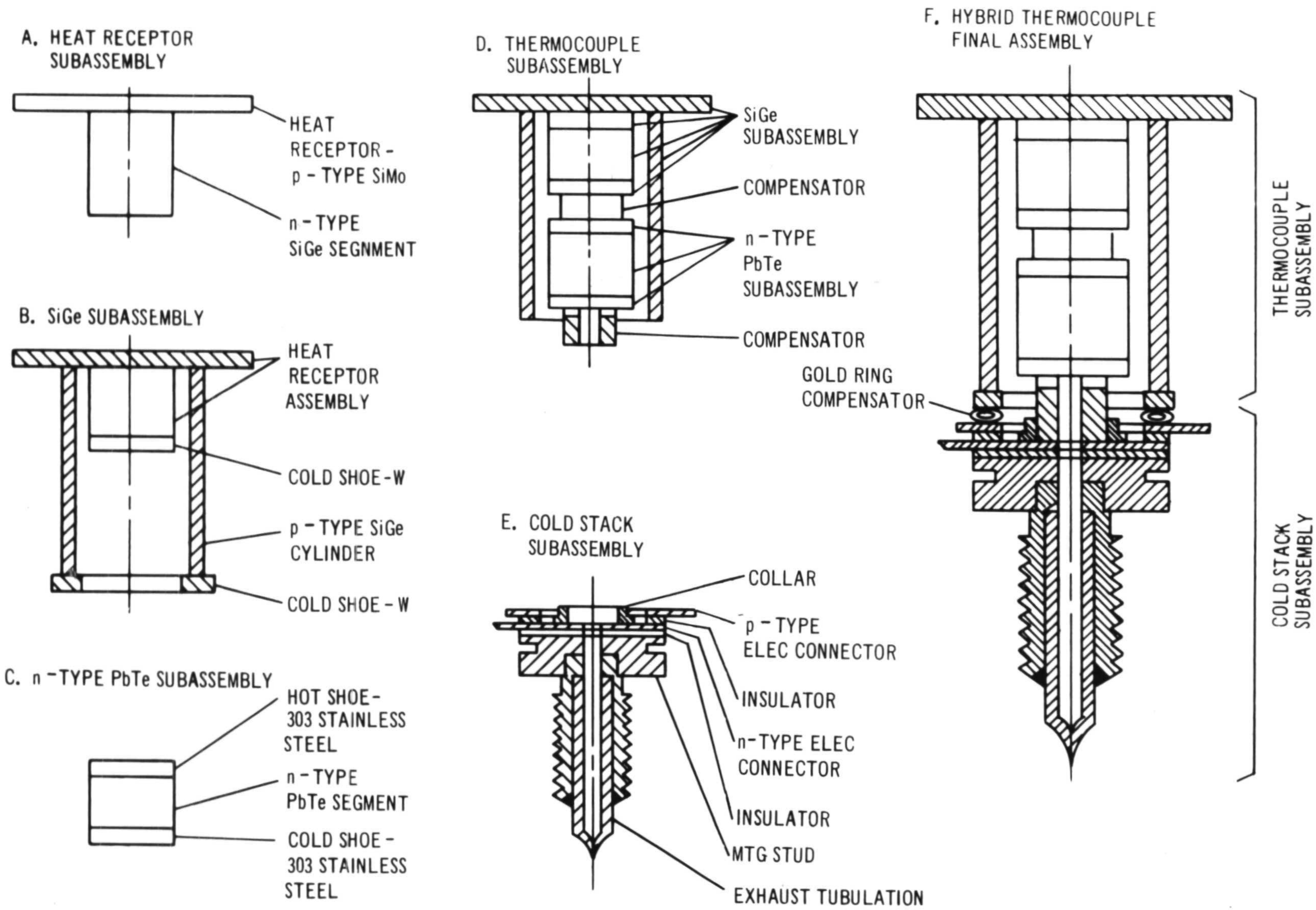

Figure 49. Hybrid Thermocouple Assembly Sequence - B

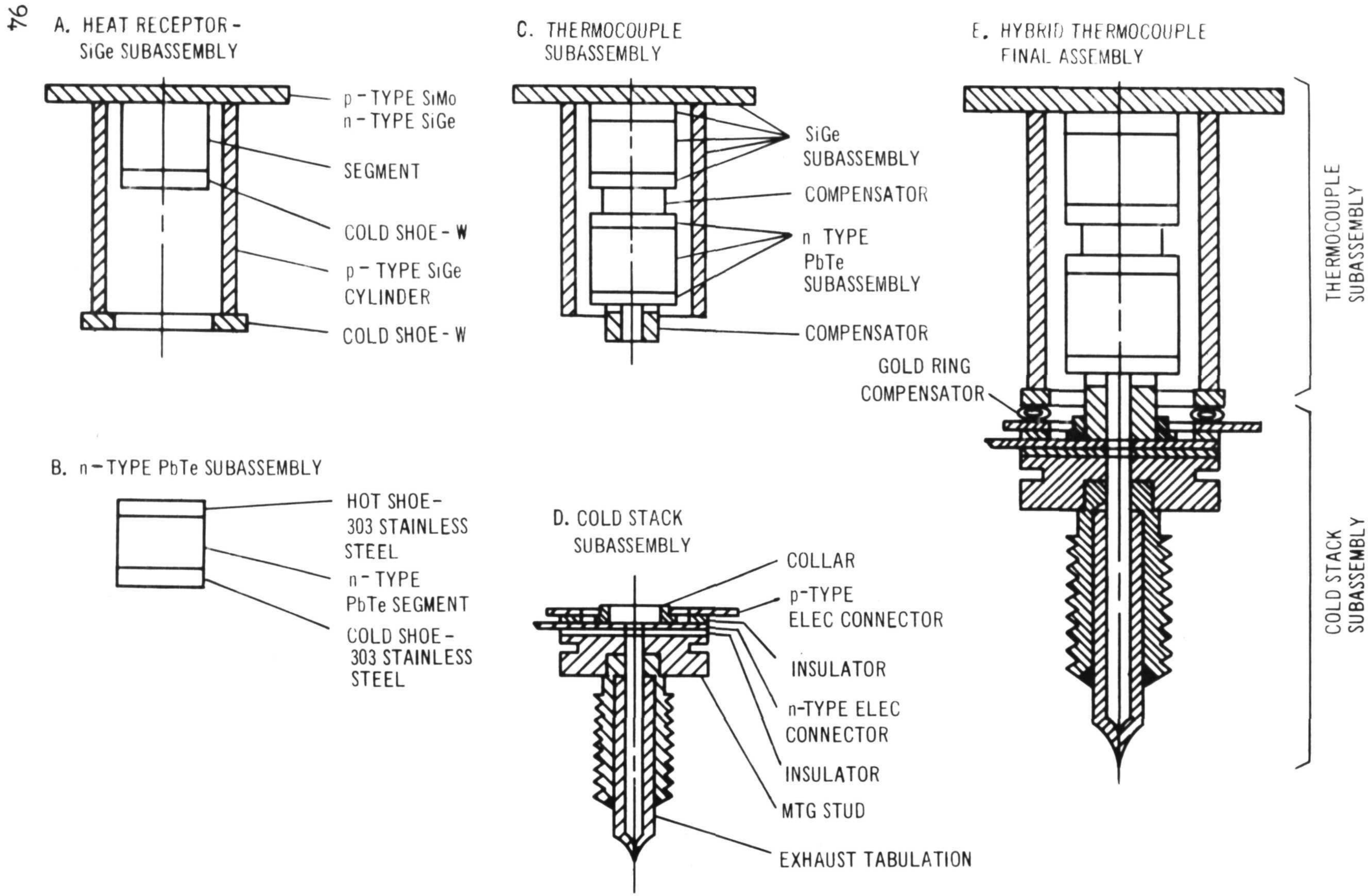

Figure 50. Hybrid Thermocouple Assembly Sequence - C

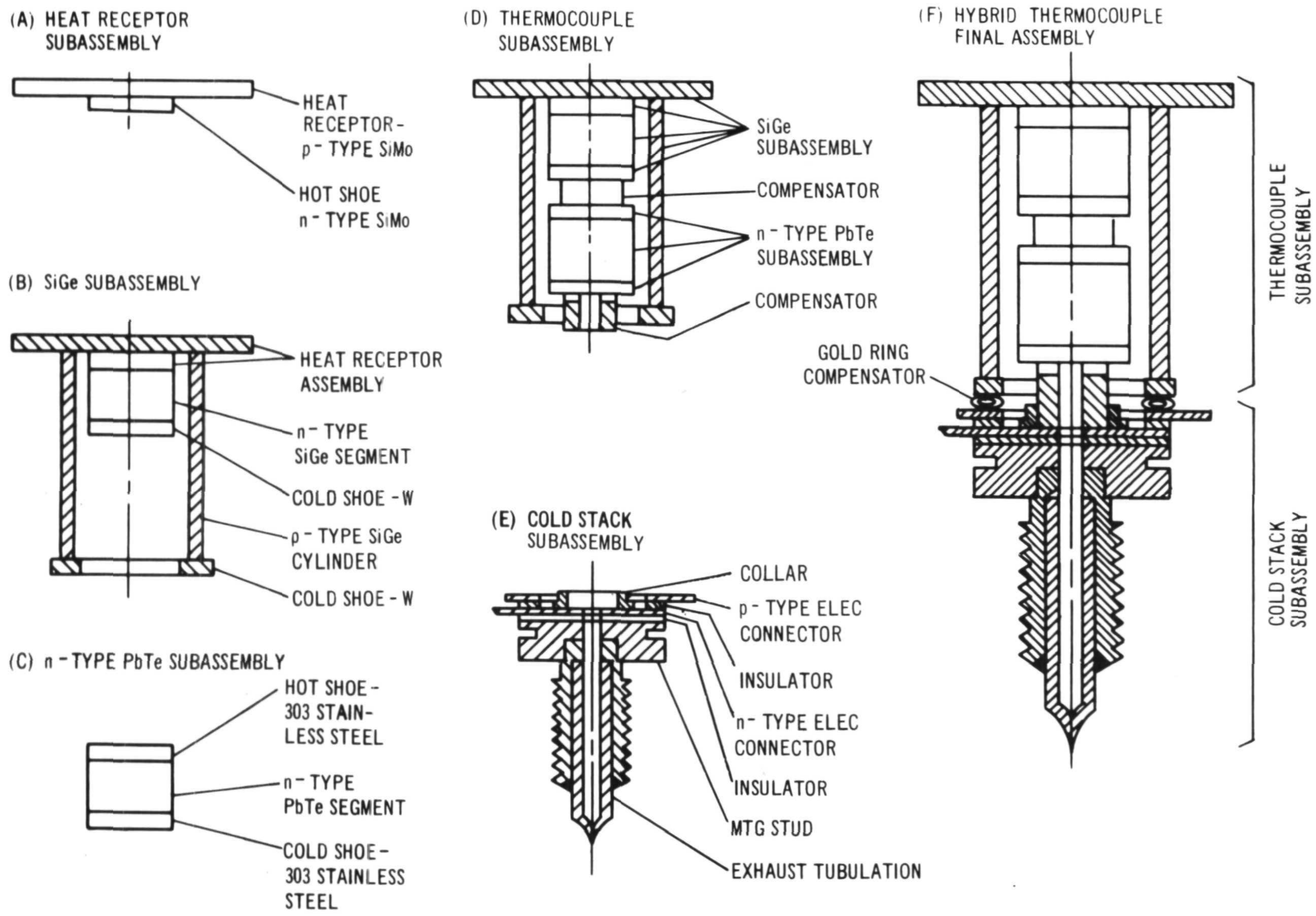

Figure 51. Hybrid Thermocouple Assembly Sequence - D

TABLE XVI

CHRONOLOGICAL FABRICATION MODIFICATIONS - HYBRID THERMOCOUPLE

Couple Number	Subassembly Operation	Fabrication Modification	Results
B-4	Thermocouple Subassembly	Changes from "one step" bonding of gold compensators (2) to "two step" bonding operation.	Both gold compensator bonds to (1) n-SiGe cold shoe and n-PbTe hot shoe and (2) n-PbTe cold shoe were excellent.
		Used bonding support "pad" same diameter as n-SiGe to replace large (p-SiMo) "hot shoe" area pad.	p-SiMo heat receptor leak-tight; eliminated small fissures.
B-8	Final Assembly	Introduced "gold ring" between p-SiGe-tungsten cold shoe and p-electrical connector.	p-SiGe-tungsten cold shoe bond leak-tight; eliminated small fissures.
B-10	Heat Receptor Subassembly	Bonded n-SiGe leg via titanium barrier directly to p-SiMo heat receptor.	Sound bond interface with good mechanical integrity.
B-18	Combined Heat Receptor and SiGe Subassemblies operations	Bonded n-SiGe, p-SiGe (including respective tungsten cold shoes) to p-SiMo heat receptor in one bonding operation.	Obtained excellent metallurgical bonds with variations in initial electrical resistances.
* P-1	Heat Receptor Subassembly	Increased p-SiMo thickness to 0.125 in. and n-SiMo thickness to 0.040 in.	Obtained excellent metallurgical bonds with low electrical resistances.

* Panel Couples

1. Heat Receptor Subassembly

Two different bonding methods were investigated during the development of the heat receptor subassembly. The first utilized the standard air-vac technology of hot pressing the p- and n-types SiMo heat receptors with a titanium diffusion barrier. The second method employed a high temperature diffusion bond again using titanium.

Initially the component dimensions used in both studies were: p-SiMo, 2.54 cm (1.00 in.) x 2.54 cm (1.00 in.) x 0.19 cm (0.075 in.) thick, and the n-SiMo hot shoe, 0.635 cm (0.250 in.) OD by 0.051 cm (0.020 in.) thick. Both of the materials were vacuum cast with a composition of 85 wt % Si, 15 wt % Mo.

Attempts to hot press the 0.051 cm (0.020 in.) thick n-SiMo disc to the p-SiMo heat receptor plate resulted in good metallurgical bonds; however, extensive cracking of the thin n-SiMo hot shoe occurred. The hot press pressure control was not sensitive enough to apply the required pressure to such a small area part and the excessive pressure caused the cracking. Because of equipment limitations and the fact that only one subassembly could be processed at one time, this approach was eliminated. Initial attempts at diffusion bonding the thin n-SiMo hot shoe to the p-SiMo heat receptor resulted in a sound metallurgical bond. However, due to the thinness of the n-SiMo, the diffusion barrier material diffused through to the outer surface which resulted in a poor bond in the subsequent subassembly operation (SiGe subassembly) at the n-SiMo/n-SiGe interface. In an attempt to eliminate this difficulty, a direct bond of n-SiGe-(diffusion barrier) to p-SiMo was made, thus eliminating the thin n-SiMo disc.

Two variations were investigated; (1) Assembly Sequence B, heat receptor subassembly (see Figure 49, part A); and (2) Assembly Sequence C, heat receptor-SiGe assembly (see Figure 50, part A). Both methods resulted in sound metallurgical bonds initially; however, some variations in initial electrical resistances were observed. During life testing of couples using these bonds, anomalies in the electrical resistance occurred. Because of the uncertainties regarding the n-SiGe/p-SiMo bond, it was decided to return to the conventional air-vac n-SiMo to p-SiMo bond system. In order to alleviate the cracking problems encountered earlier with this system, the thickness of n-SiGe disc was increased from 0.051 cm (0.020 in.) to 0.102 cm (0.040 in.), and that of the p-SiMo heat receptor plate from 0.19 cm (0.075 in.) to 0.318 cm (0.125 in.). Also, hot pressed n-SiMo was substituted for the vacuum case material (n-type only). These modifications resulted in sound metallurgical bonds in the Hybrid couple with low electrical resistances. A photomicrograph of this bond is shown in Figure 52. This bond system was employed in the fabrication of the Hybrid panel couples. Figure 51, part A, shows the final heat receptor assembly configuration.

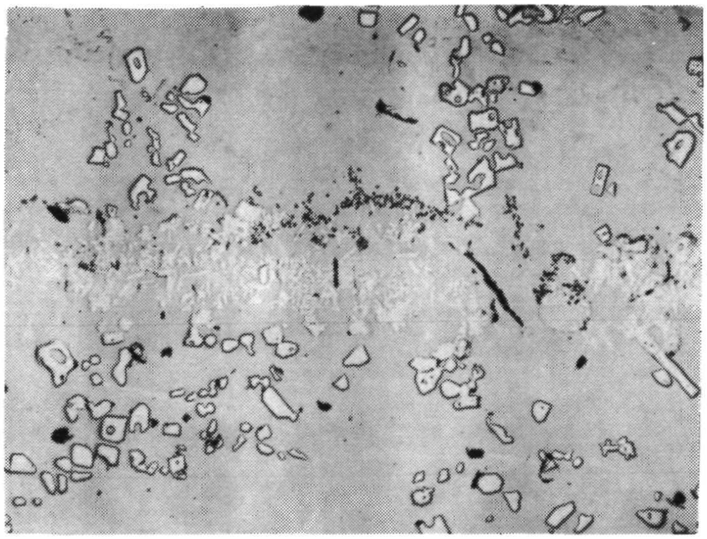

Figure 52. Heat Receptor Bond — p-SiMo — n-SiMo

2. <u>SiGe Subassembly</u>

The principal variations investigated in the fabrication of the SiGe subassembly were necessitated by difficulties in the heat receptor assembly, as discussed previously. The attempt to make this subassembly in one step as opposed to two (process C versus process B), showed this approach to be feasible, but the use of the air-vac heat receptor subassembly for the final assembly technique (Figure 51, part A) precluded the use of this approach.

A minor modification made in the SiGe subassembly was the inclusion of the tungsten cold shoe ring of the p-SiGe cylinder in the bonding operation, process D (Figure 51, part B).

3. <u>n-Type PbTe Subassembly</u>

No changes or modifications were made in the assembly technique developed for the n-type PbTe subassembly (subcomponent (C)). Details of this subassembly are presented in Section IV-A-3.

4. <u>Thermocouple Subassembly</u>

Two difficulties were experienced in the development of the assembly technique for this subassembly; (1) fissures developed in the p-SiMo heat receptor during the diffusion bonding operation, and (2) the bond of the upper gold compensator to the n-SiGe cold shoe and n-PbTe hot shoe was marginal. It was found that by using a support pad (under the p-SiMo heat receptor), having the diameter of the n-SiMo disc rather than the area of the heat receptor, the fissures were eliminated and the p-SiMo heat receptor was leak-tight; The upper and lower gold compensators have different diameters (different areas), the upper having the larger area, and it was found that in the bonding operation insufficient pressure was being transmitted to the upper compensator, thus resulting in a poor bond. The process was changed from a "one step" to a "two step" bonding operation. First, the upper compensator bond was made, then the lower compensator was bonded with the bonding pressure adjusted for each area. All resultant bonds were excellent.

5. <u>Cold Stack Subassembly</u>

Only a minor modification was made in the cold stack as developed in the subcomponent (D), Section IV-A-5: a "collar" or flange was introduced to mate with the lower gold compensator in the final assembly, thus providing the thermal and electrical path for the n-segment.

6. <u>Final Assembly</u>

The only modification made in the final assembly was the incorporation of a gold ring, made from hollow gold tubing, 0.050 in. OD with a 0.010-in. thick wall, between the p-SiGe tungsten cold shoe and the cold stack. This modification eliminated stresses which caused fissures in the p-SiGe--tungsten bond area. The resultant bond area was sound metallurgically and leak-tight.

A summary of the thermocouples fabricated in this task and their disposition is given in Table XVII. The test results of the couples are discussed in the following section IV-C. The final assembly technique developed, assembly sequence D, Figure 51, was used to fabricate the Hybrid couple for the module panels.

C. Thermocouple Testing

Testing of the developmental Hybrid couple structures was conducted simultaneously with the thermocouple structure development phase to provide rapid feedback so that modifications could be made to either the processing or components, as required. Both design and accelerated life testing and thermal cycling tests were employed in these evaluation.

The design test conditions for the Hybrid couple are hot junction temperature, T_{HJ} = 926°C (1700°F); interstage-n-PbTe hot shoe temperature, I_I = 538°C (1000°F); and cold junction temperature, T_{CJ} = 232°C (450°F).

The first Hybrid couple tested was couple B-1-1, which developed high resistance after 228 hours and three thermal cycles at design test conditions. Upon removing the couple from the test stand, a separation occurred in the brazed bond between the p-SiGe and the tungsten ring of the cold stack. This was the only couple tested of the B-1 design (i.e., having the thicker p-SiGe wall) as success in fabrication of the thinner wall p-SiGe cylinders allowed the selection of couple design B as the Hybrid Reference Design thermocouple.

A summary of the Reference Design couples tested (Design B) is given in Table XVIII comparing "initial" (20-hour) data, 1500-hour reference design point for SiGe, and longest data point for each individual couple.

Couples B-7 and B-9 experienced an abnormal increase in couple resistance after a relatively short time on test; 328 hours and 656 hours, respectively. Couple B-7 separated on demounting at the brazed joint between the p-SiGe and gold compensator ring similar to the failure exhibited in couple B-1-1. This obviously weak bond, gold compensator brazed directly to SiGe, was eliminated starting with couple B-8. The tungsten ring (p-SiGe cold shoe) was first bonded directly to p-SiGe and the gold compensator ring was subsequently brazed between the tungsten ring and the p-electrical copper connector of the cold stack.

Couple B-9 had been operated at an accelerated hot shoe temperature, 960°C (1760°F) versus 941°C (1725°F). The couple was demounted and an X-ray radiograph taken in order to examine the internal couple structure. It showed that a separation had occurred in the n-leg between the n-PbTe and its hot shoe. Upon further examination, a ring of material was noted on

TABLE XVII

SUMMARY OF HYBRID COUPLES FABRICATED

Design	No.	Process	Disposition	Remarks
B-1	1	A	Life tested	- - -
	2			p-SiMo--p-SiGe brazed bond leaked
	3		Completed TC subassy	p-SiMo--p-SiGe brazed bond leaked
	4		Completed TC subassy	p-SiMo--p-SiGe bond leaked
	5		Completed TC subassy	p-SiMo--p-SiGe bond leaked
	6		Completed TC subassy	Metallographic examination
	7		Life test	- - -
	8		Completed TC subassy	n-SiMo--p-SiMo separation
	9		Completed TC subassy	n-SiMo--p-SiMo separation
	10		Metallographic exam.	Fissures braze p-SiGe--W
	11		Metallographic exam.	Bonds OK
B	1	A	Completed TC subassy	Met. exam; poor bond upper Au comp.
	2		Not tested	Leaked brazed bond p-SiGe--W
	3		Completed TC subassy	PbTe hot shoe separation
	4		Not tested	High res. n-leg (n-SiGe to p-SiMo)
	5		Metallographic exam.	PbTe hot shoe bond poor
	6		Life test	- - -
	7		Life test	- - -
	8		Life test	- - -
	9		Life test	- - -
	10	B	Met. Lab.	Bonds OK
	11		Completed TC subassy	n-SiGe--p-SiMo bond separation
	12		Life test	- - -
	13		Completed TC subassy	n-SiGe--p-SiMo bond separation
	14		Life test	- - -
	15		Completed TC subassy	n-SiGe--p-SiMo bond separation
	16		Life test	- - -
	17		Life test	- - -
	18	C	Life test	- - -
G	1		Met. Lab.	Bonds OK
	2		Met. Lab.	Bonds OK
	3		Shipped to NASA Lewis	for test and evaluation
	4		Shipped to NASA Lewis	for test and evaluation
	5		Life test	- - -
	6		Life test	- - -
BX(1)	1		Life test	
	2		Life test	
	3		Life test	
	4		Life test	
P(2)	1-25	D	Used to fabricate two 9-couple Hybrid Module Panels. Delivered to NASA Lewis for their test and evaluation.	

NOTES: (1) Special resistance test couples
(2) Couples fabricated for Hybrid Module Panels.

TABLE XVIII

HYBRID COUPLE PERFORMANCE SUMMARY

	Nominal 20 Hr.					Nominal 1500 Hr.						Test Completed					
Couple No.	No. of Thermal Cycles	T_s °C	T_c °C	Res. mohm	P_{ML} watt	No. of Thermal Cycles	Test Time, Hrs.	T_s °C	T_c °C	Res. mohm	P_{ML} watt	No. of Thermal Cycles	Test Time, Hrs.	T_s °C	T_c °C	Res. mohm	P_{ML} watt
B-6	0	935	229	30.8	0.70	0	1506	915	230	33.6	0.65	2	4842	921	228	39.1	0.52
B-7	0	910	233	30.3	0.61		-	-	-	-	-	1	328	897	237	32.8	0.58
B-8	0	947	233	26.6	0.81	0	1553	938	235	32.4	0.69	3	2868	932	229	37.0	0.62
B-9	0	960	231	27.0	0.83		-	-	-	-	-	11	656	951	229	30.6	0.76
B-12[1]	1	938	216	32.54	0.71	2	1482	937	216	37.0	0.67	5	6284	941	220	38.4	0.67
B-14[1]	5	904	223	39.12	0.49	6	1834	908	228	43.7	0.45	10	5888	907	231	43.4	0.44
B-16[1]	5	863	219	31.56	0.59	7	1494	872	226	37.3	0.55	10	6396	869	226	36.6	0.54
B-17[1]	5	940	225	36.10	0.66	6	1382	934	230	39.3	0.63	9	5550	939	234	40.8	0.60
B-18[1]	0	901	200	28.4	0.73	2	1171	903	231	32.5	0.62						

Note 1: These data have been normalized to the design test conditions via the ΔT^2 relationship as described below:

$$\text{Normalized } P_{Norm} = P_{ML} \times \frac{(\Delta T_N)^2}{(\Delta T_X)^2}$$

T_N - Design Temperature
T_X - Actual Temperature

the inside surface of the p-SiGe cylinder wall adjacent to the n-PbTe hot shoe bond. A chemical analysis of this deposit showed the composition to be Pb and Te. No effect on the microstructure or the integrity of p-SiGe cylinder was noted. It would appear that the PbTe hot shoe bond was operated above the 538°C design temperature and PbTe sublimation occurred.

Couples B-6 and B-8 completed 4842 and 2868 hours of life testing at nominal design operating temperatures. Couple B-6 developed high resistance after a severe thermal cycle due to a power failure. Separation occurred in the brazed bond region between the p-SiGe and gold compensating ring and at the PbTe hot shoe bond. Both of these areas were modified in later couples, initiating with couples B-8 and B-10, respectively. Further inspection indicated that the PbTe shoe bond separated first, while contact was sustained by the p-leg until separation ultimately occurred there also. The life test station in which couple B-8 was being tested slowly developed a leak which degraded both the heater and the instrumentation attached to the couple. This couple was not initially vacuum-tight due to a problem in brazing the gold ring to the tungsten cold shoe at the time of fabrication; therefore, the inside of the couple was exposed to oxygen. The life test station was cycled down following the last measurement. When cold, the couple showed an abnormally high resistance, in ohms, in the n-leg. Subsequent X-ray examination of this couple showed that PbTe material from the hot shoe bond area had deposited on the inside of p-cylinder wall. Various X-ray views of this bond, however, did not show physical separation as was apparent in B-9, reported above. The high resistance was evidently a result of the loss of PbTe material from the hot shoe bond area and probably oxygen contamination of the PbTe element.

A program test goal was to operate a number of thermocouples for a 5000-hour life test, prior to building the final Hybrid module test panels, to assure that the couple structure and performance were satisfactory. The next four couples tested, viz., B-12, -14, -16 and -17, were all fabricated using process B. Although the initial resistances of these couples were somewhat high, ranging from 31 to 39 mohms, reasonable stability was exhibited during the 5000-hour test. Subsequent p-series Hybrid couples, fabricated for the 9-couple panels using process D, exhibited much lower initial resistance, ranging from 25 to 28 mohms, and also exhibited improved stability after about 700 hours of testing. The resistance of 7 of the 9 p-couples ranged from 28 to 30 mohms at 700 hours. (The P-Hybrid couple data is based on NASA-LeRC test results, to date, on panel #1.) The increase in resistance of the individual couples as a function of test time is presented in Figure 53. Note the high resistances exhibited by the B couples compared to that of the P couples. The sharp increase in the resistance of couples B-6 and B-8 indicates the onset of the bond separation described above.

The original design data obtained early in the program predicted a power output of 0.87 watts/couple. Since that time, data gathered in both the Silicon-Germanium Thermoelectric Material and Module Development Program, Contract AT(29-2)-2510, and the Multi-Hundred Watt RTG Program, Contract

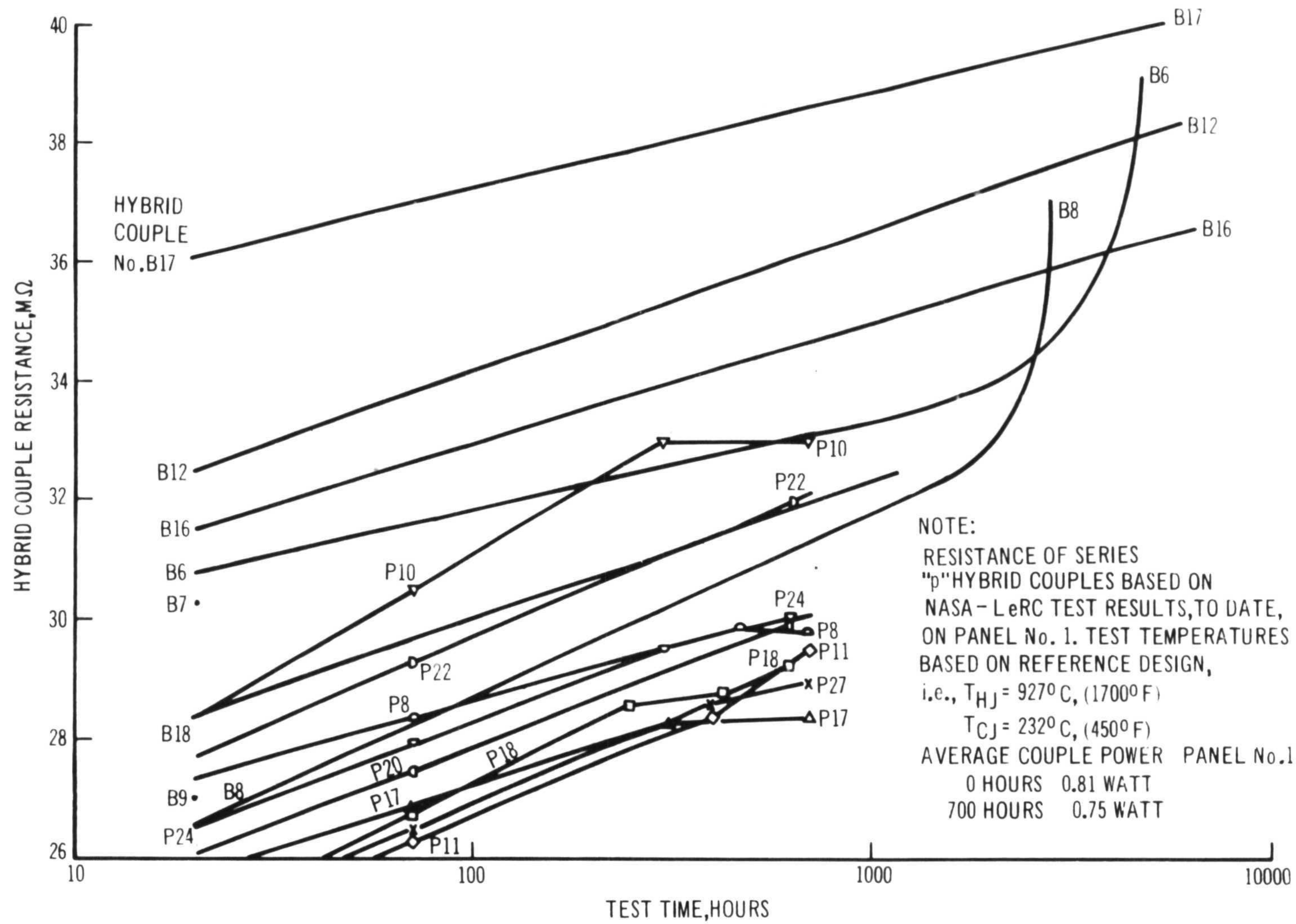

Figure 53. Hybrid Couple Resistance Plotted Against Test Time

AT(29-2)-2831, have established the "contact" resistances of air-vac couples at 20% of the SiGe material resistance. This compares with approximately 5% assumed at the start of the Hybrid Program and reduces the predicted design value at the 1500-hour stabilization point from 0.87 watts to 0.77 watts per couple. Measured power of the four B couples is approximately 0.63 watt at 1500 hours while the P couples average 0.75 watt at 700 hours compared to the predicted (1500 hour) design of 0.77 watts per couple.

Couples B-12, B-16 and B-17, with 6284, 6396 and 5550 hours of life testing, respectively, were examined by taking radiographs to determine their condition. Couple B-14 with 5888 hours of life testing was damaged upon removing it from the test stand and was not submitted for examination. The radiograph of couple B-12 showed no cracks or separations in the cylinder wall or bond areas.

The radiograph of B-16 also showed no separations in any of the bonds. However, the start of deterioration of the bond between the stainless steel hot shoe and the lead telluride is evident. This deterioration is manifest by the erosion of the lead telluride at the edges of the pellet at the interface of the hot shoe and the telluride. Also evident in the radiograph is a misalignment of the gold compensator between the cold shoes of the n-SiGe and the hot shoe of the n-lead telluride. The radiograph of couple B-17 shows a definite separation between the stainless steel hot shoe and the n-lead telluride with evidence of some telluride material deposited on the inner wall of the cylinder in the vicinity of the separation. This deposit is evident in most couples; however, it appears to be heavier in the case of couple B-17. This heavy deposit of material on the cylinder wall seems to indicate the loss of hermeticity in the couple and a higher than normal operating temperature.

Based on the radiographs, couple B-12 was selected for metallurgical examination. The examination of B-12 revealed no cracks in the p-SiGe cylinder wall or p-SiMo hot shoe. No separation was found at any of the bonds including the braze joints of the cold stack. Figures 54a, 54b and 55 are photomicrographs of bond areas of p-SiMo--n-SiGe, n-SiGe to tungsten, and stainless steel hot shoe n-lead telluride, respectively. Each shows sound bonds with no evidence of deterioration. The barrier layer in p-SiMo to n-SiGe and stainless steel hot or cold shoe to lead telluride bonds is clearly evident and is continuous for the entire length of the bond.

Concurrent with the testing period of the above four couples, it was decided to fabricate and specially instrument a Hybrid thermocouple so that individual resistances and temperature measurements could be monitored for the following: (1) n-leg, individual SiGe and PbTe segments; (2) n-SiGe--p-SiMo segment; (3) p-SiGe--p-SiMo segment; and (4) overall couple resistance. Accordingly, couple B-18 was instrumented and placed on test. Figure 56 shows the location of the attached wires for both resistance and temperature measurements. All wires except that at location

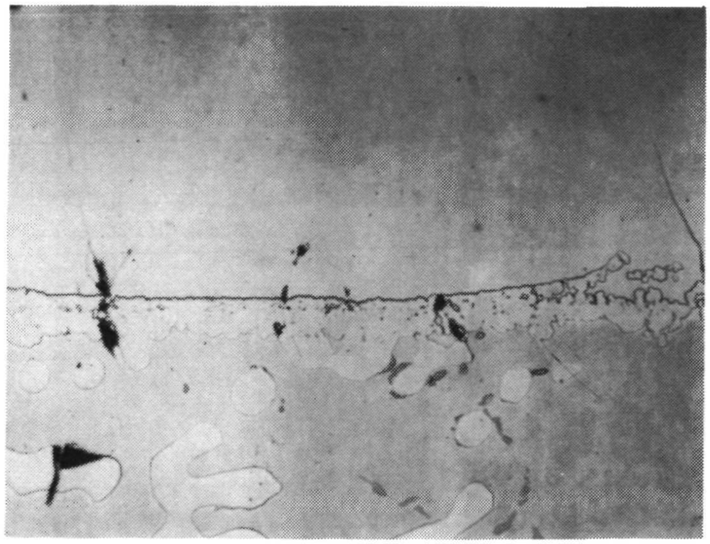

A. p - SiMo -- n - SiGe BOND

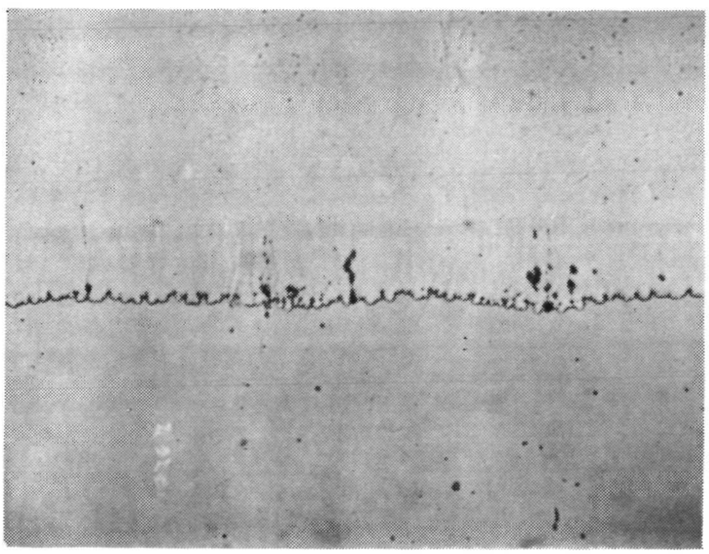

B. n - SiGe -- TUNGSTEN BOND

Figure 54. Couple B-12, 6284 Hours — T_S 938°C (1720°F)–T_C 216°C (418°F)

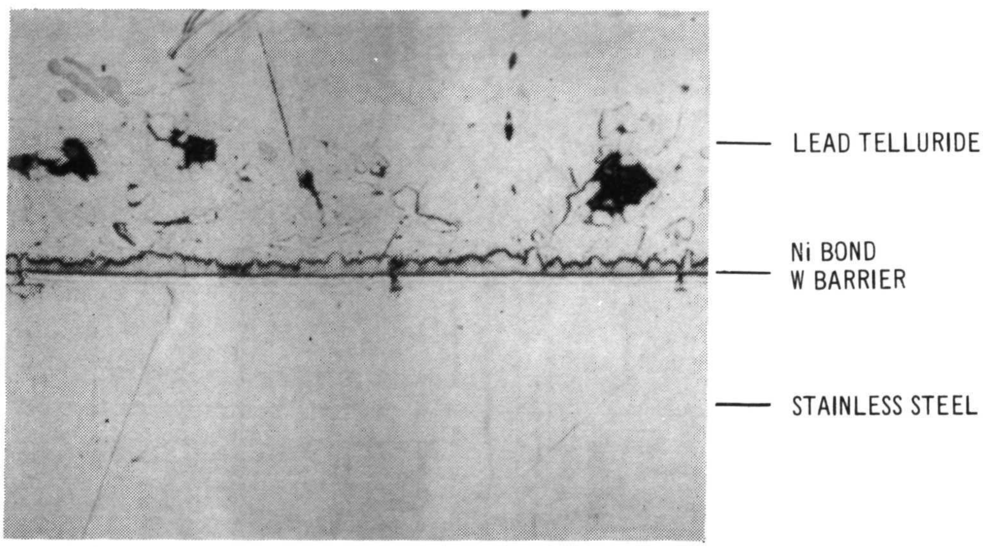

STAINLESS STEEL HOT SHOE-TELLURIDE BOND

Figure 55. Couple B - 12, 6284 Hours—T_S 938°C (1720°F), T_C 216°C (418°F)

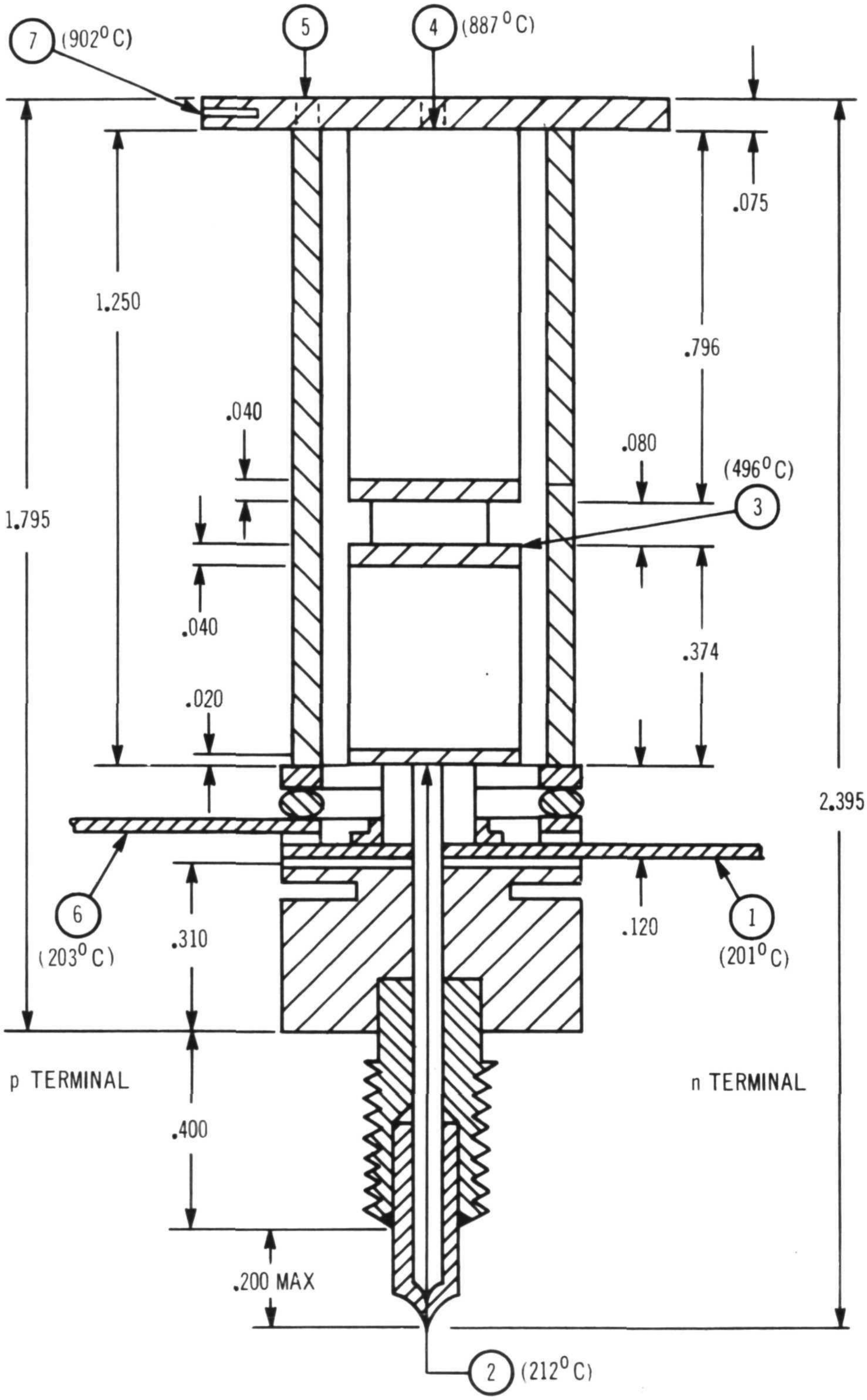

Figure 56. Thermocouple Attachments Couple No. B-18

#5 denote coincident temperature and resistance measurement locations. Location #5 was for resistance measurements only. All resistance measurements were made using a milliohmeter after the couple temperatures had stabilized at open circuit conditions. Comparison of resistance design data to actual measured resistances shows that the greatest deviation occurs in the segment between n-PbTe hot shoe and the p-SiMo hot shoe (location 3-5). Comparable resistances between locations (see Figure 56) are shown in Table XIX.

TABLE XIX

SPECIALLY INSTRUMENTED THERMOCOUPLE B-18

Segment	Location	Resistance Measurement (mohms)					
		Design	20 hours	226[3] hours	514 hours	835 hours	1172 hours
n-PbTe	1-3	2.10	2.08	2.40	2.73	2.48	2.56
n-SiGe	3-4	9.05	9.42	14.70	15.03	15.34	17.94
n-SiGe--p-SiMo	3-5	9.85	10.78	16.75	17.19	17.20	20.08
p-SiGe--p-SiMo	5-6	15.94	9.19[2]	9.66	10.09	10.87	13.08
Total Couple							
a. at temp.	1-6	28.3[1]	26.82[2]		30.01	30.56	31.86
b. room temp.	1-6	-	11.27		-	-	16.95

Note 1 assumes 5% contact resistance; based on 1500 hour SiGe material properties

2 p-SiGe material used had a lower resistivity than the value in the computer data table

3 severe thermal shock due to power failure

The reason for the high resistance of the n-SiGe--p-SiMo segment was not apparent. The initial "as bonded" room temperature resistance of this segment was 5.7 mohms, and the initial resistance at temperature was 10.78 mohms which was in good agreement with the design data. A resistance increase from 10.78 mohms to 16.75 mohms occurred after a severe thermal cycle caused by a power failure at 226 hours. The total resistance increase for this segment was 9.3 mohms, from 10.78 mohms to 20.08 mohms, while the total couple resistance increase was 5.04 mohms, from 26.82 mohms to 31.86 mohms. It is felt that the discrepancy in the ΔR of the couple compared to that of the n-segment is due to instrumentation.

Of further note is the temperature profile. (See temperatures indicated in brackets of Figure 56.) Although the test operates at a hot shoe "edge" temperature of 902°C (1656°F), the PbTe hot shoe temperature of 496°C (925°F) when extrapolated to design operating condition would be 526°C (979°F) as compared to 538°C (1000°F) design. Further, the 15°C (27°F) drop from hot shoe corner to hot junction also compares favorably with analysis. Thermally, therefore, the measured data shows good agreement with the design analysis.

Based on the test results of couple B-18, it was decided to further investigate the n-SiGe to p-SiMo segment. These tests were planned to provide some information as to (1) possible changes in the hot junction region, n-SiGe--p-SiMo; (2) possible sublimation effects of PbTe element upon the structure; and (3) a possible reaction of the alumina insulating material with SiGe resulting in the resistance increase observed in life-tested couples.

Accordingly, four specially constructed Hybrid couples, BX-1, -2, -3 and -4, were fabricated and placed on test. The construction details of these four couples are shown in Figures 57 through 60, and a description is given below:

1. Couple BX-1 (Figure 57) has a 70 at.% p-SiGe pellet substituted for the SiGe-PbTe n-segment. The insulating alumina (Al_2O_3) material has been eliminated from the inside of the structure.

2. Couple BX-2 (Figure 58) has a 70 at.% n-SiGe pellet in the inside. The PbTe n-pellet has been eliminated as well as the insulating Al_2O_3.

3. Couple BX-3 (Figure 59) is similar to BX-2 except that insulating alumina (Al_2O_3) powder has been included.

4. Couple BX-4 (Figure 60) is identical to the standard Reference Design B structure except that the insulating alumina (Al_2O_3) powder has been omitted.

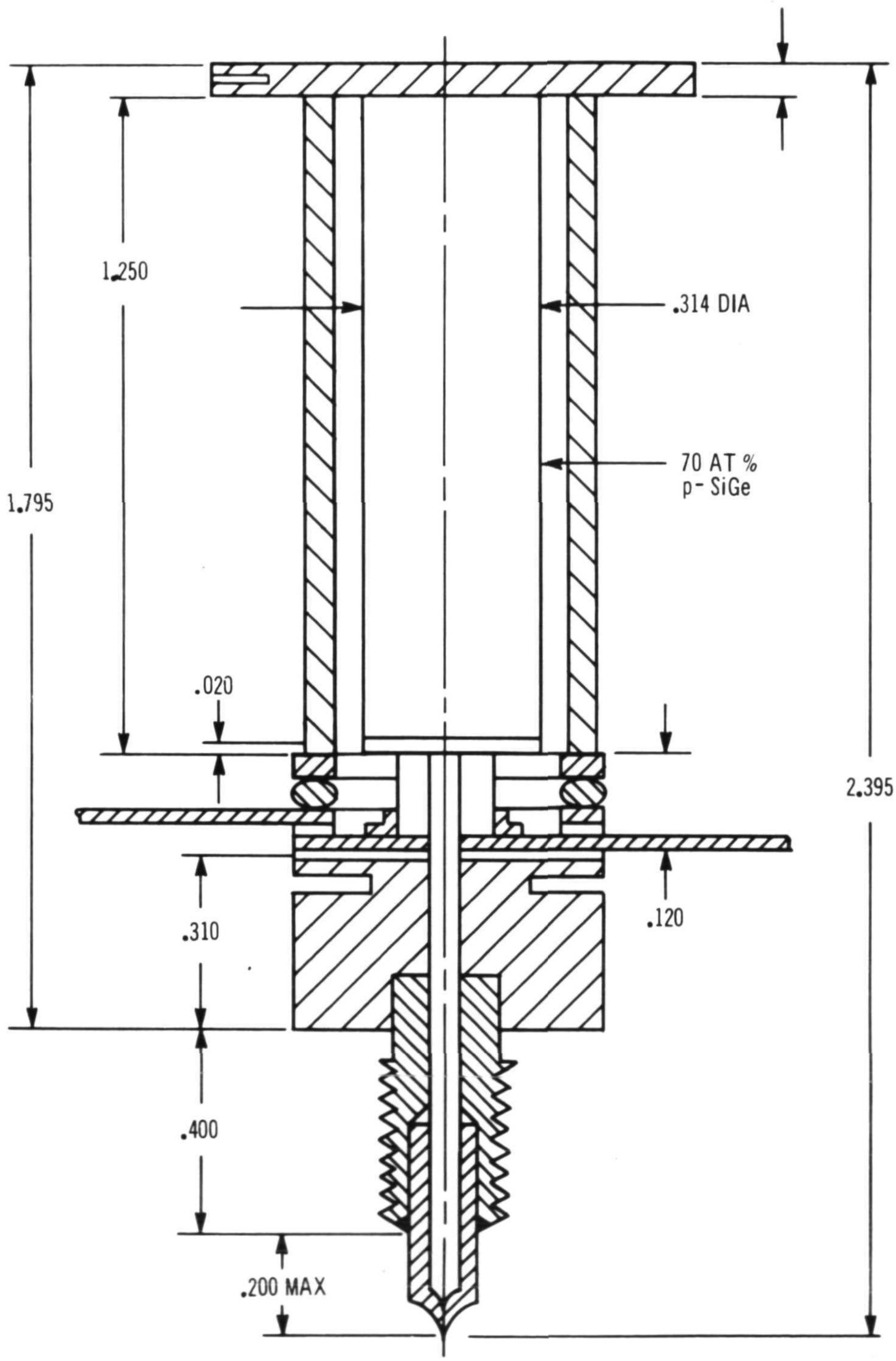

Figure 57. Hybrid Thermocouple Assembly - Design BX-1

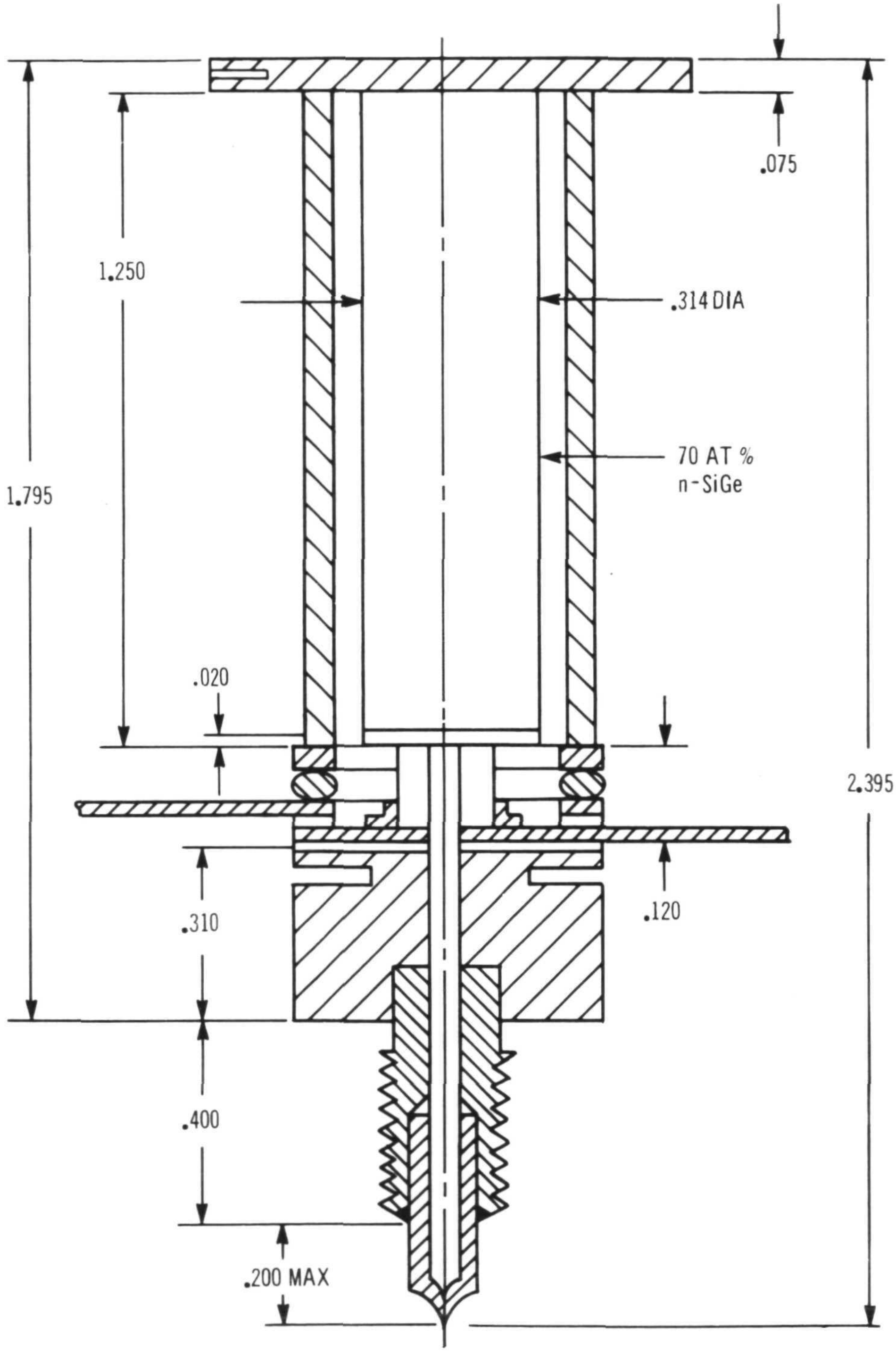

NOTE: DO NOT FILL INSIDE OF STRUCTURE WITH Al_2O_3

Figure 58. Hybrid Thermocouple Assembly - Design BX – 2

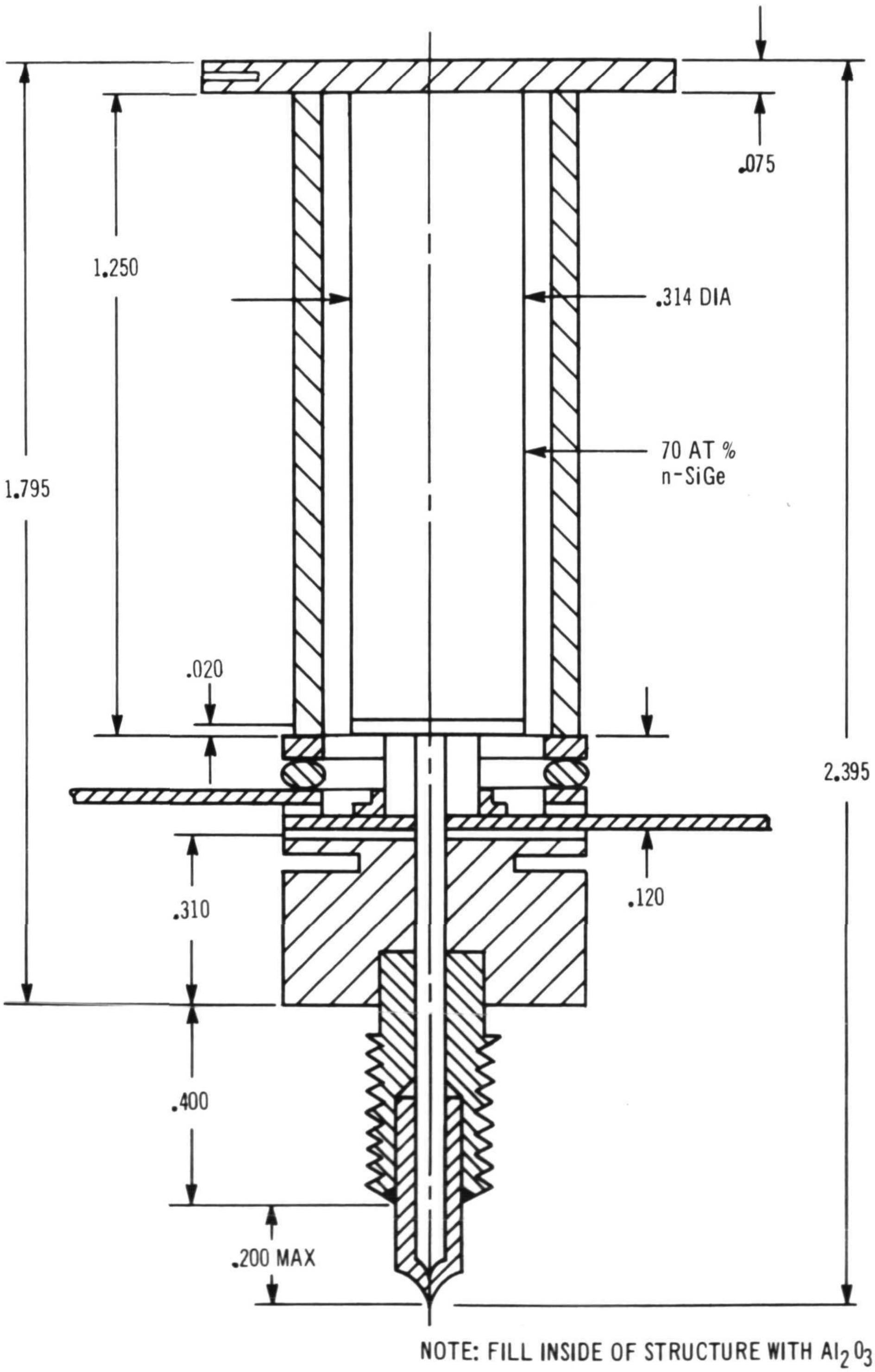

Figure 59. Hybrid Thermocouple Assembly - Design BX - 3

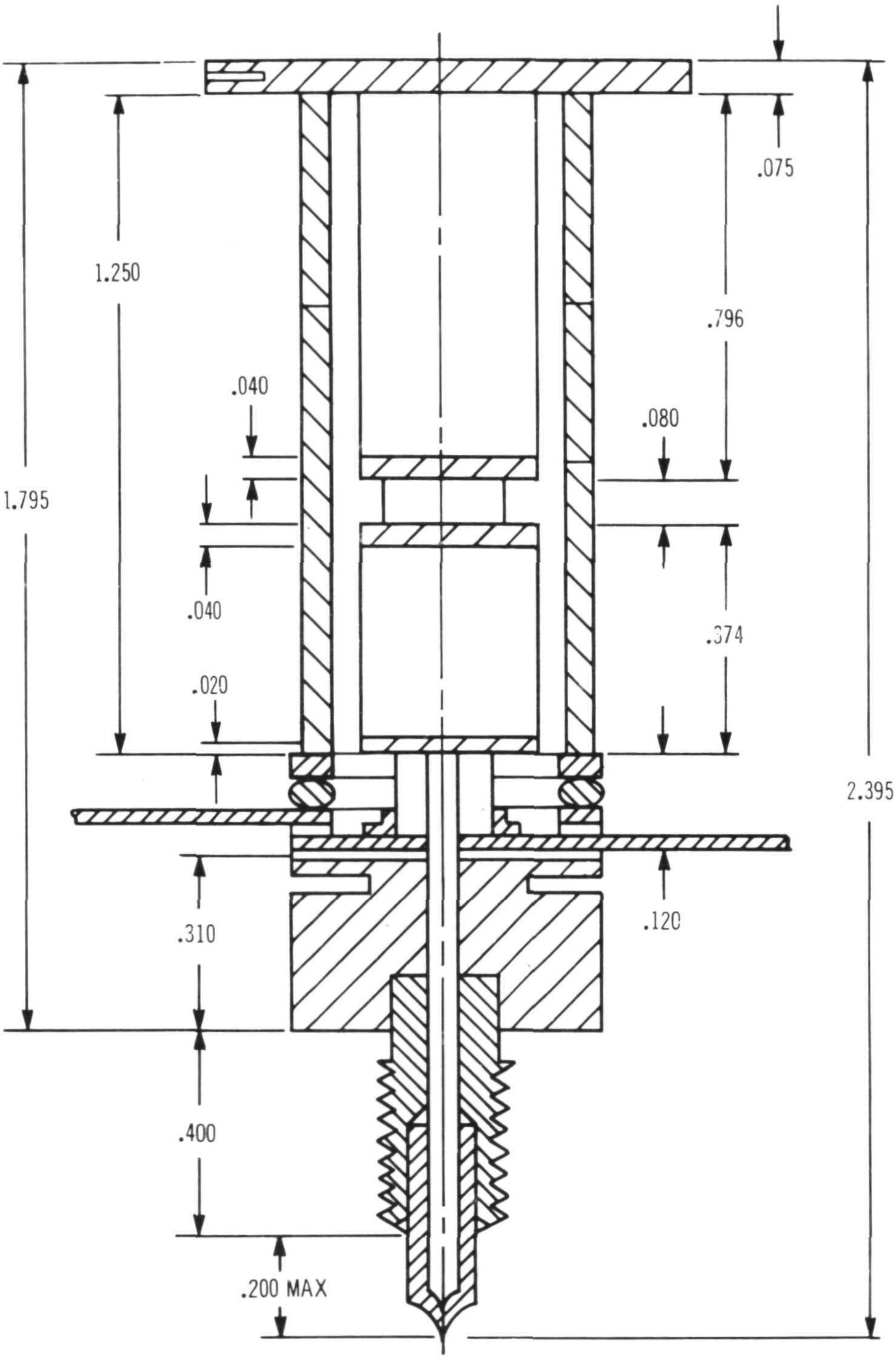

Figure 60. Hybrid Thermocouple Assembly – Design BX– 4

These couples were tested for a total of 2328 hours at design test conditions. Couple BX-4, a standard Hybrid couple without alumina powder insulation fill (see Figure 60) exhibited a resistance pattern similar to previously tested Hybrid couples, 29.46 mohms at zero hours increasing to 33.94 mohms after 2805 hours. Examination of the data of couples BX-1, -2 and -3 after 2328 hours showed that the resistance of the p-SiGe leg remained essentially constant with time and that the increase in resistance was primarily due to the n-SiGe segment, as noted in couples BX-2 and -3.

Based on these test results, it was decided to stop fabrication of the Hybrid couples, Series G, for the Hybrid panels, and return to the conventional air-vac hot shoe bond, p-SiMo--Ti-barrier layer--n-SiMo--n-SiGe (process D, Figure 51) rather than the modified air-vac bond, p-SiMo--Ti-barrier layer--n-SiGe (process C, Figure 50) in the fabrication of the Hybrid couples. This is fully discussed in Section IV-B-1 and involves an increase in thickness of both the p-SiMo heat receptor plate (from 0.19 cm, 0.075 in., to 0.318 cm, 0.125 in.), and the n-SiMo disc (from 0.051 cm, 0.020 in., to 0.102 cm, 0.040 in.). A number of special test samples were fabricated, employing the conventional air-vac bond system but with the thicker p-SiMo and n-SiMo heat receptor. Also, hot pressed versus vacuum cast n-SiMo was investigated.

In order to perform ingradient testing of these special test specimens, it was necessary to attach a cold stack to the specimen as shown in Figures 61a and b. A description of the specimens is given below.

No. of Test Samples		Fabrication Procedure	Room Temperature Bond Resistance
4	Step 1:	p-SiMo, 0.125 in. thickness (vacuum cast material) - barrier - n-SiMo, 0.040 in. thickness (vacuum cast material)	Avg. 0.10 mohms
	Step 2:	Subassembly 1 + n-SiGe and tungsten cold shoe	Avg. 0.08 mohms
4	Step 1:	p-SiMo, 0.125 in. thickness (vacuum cast material) - barrier - n-SiMo, 0.040 in. thickness (hot pressed material)	Avg. 0.10 mohms
	Step 2:	Subassembly 1 - n-SiGe and tungsten cold shoe	Avg. 0.08 mohms

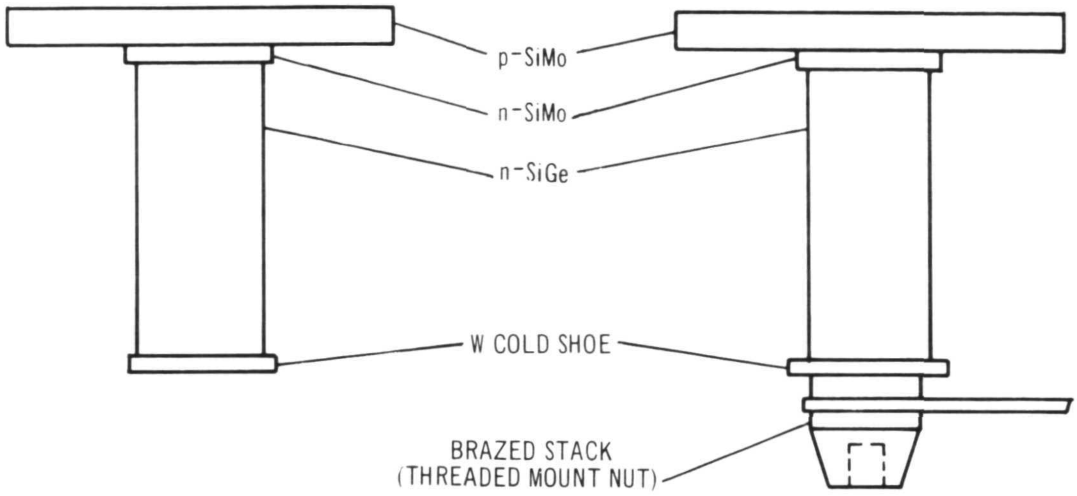

A. As Fabricated

B. Brazed Lower Cold Stack

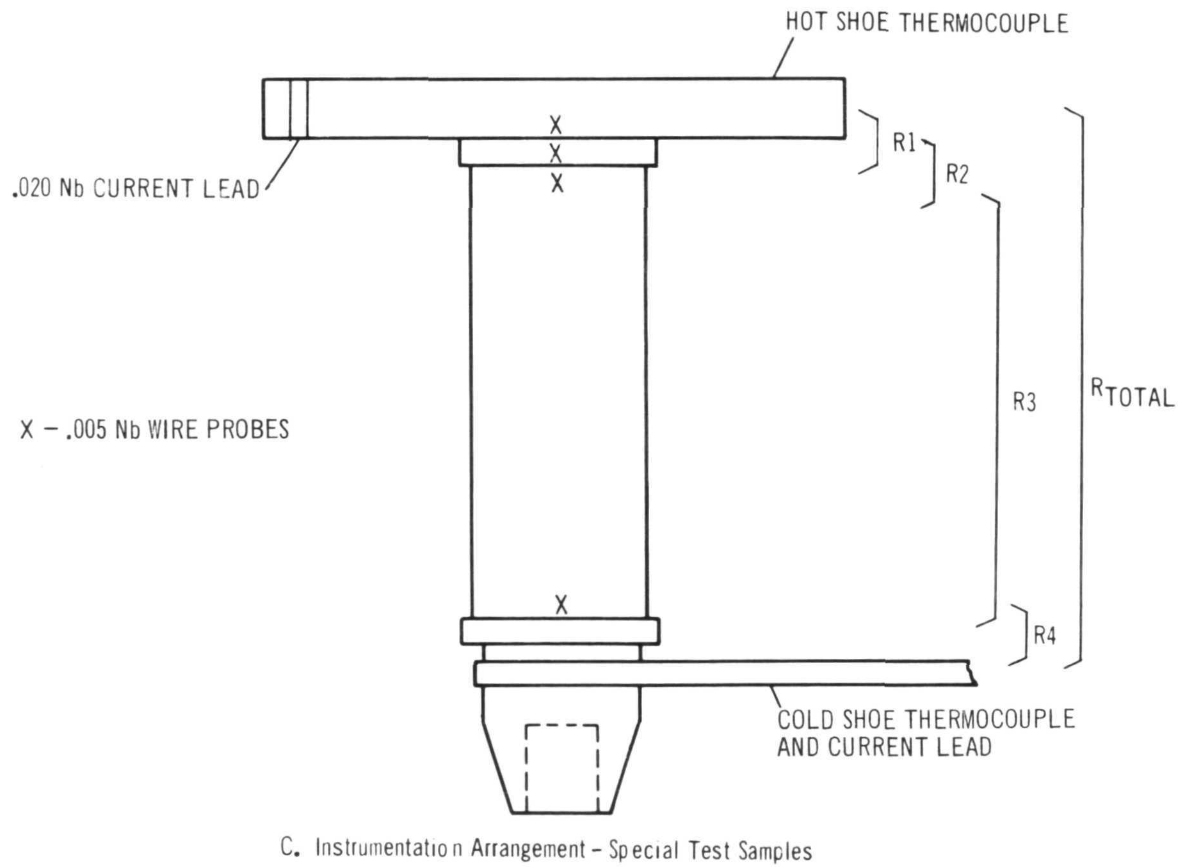

C. Instrumentation Arrangement - Special Test Samples

Figure 61. Special Test Samples

The bond resistances of the special test samples "as fabricated" and after being brazed with the lower stack structure are presented in Table XX. No significant changes occurred in any of the bond resistances as a result of this bonding operation.

TABLE XX

BOND RESISTANCES OF SPECIAL TEST SAMPLES

Sample No.		After Bonding					After Brazing Lower Stack				
		R_1	R_2	R_3	R_4	R_{total}	R_1	R_2	R_3	R_4	R_{total}
				(mohms)					(mohms)		
1	(a)	0.20	0.15	3.7	0.75	5.1	0.20	0.23	4.1	0.26	5.0
3	(a)	0.20	0.18	4.1	0.18	5.7	0.24	0.23	4.2	0.27	5.1
4A	(b)	0.20	0.20	4.3	0.15	5.2	0.30	0.25	4.4	0.24	5.3
4B	(b)	0.25	0.28	5.7	0.15	6.3	0.30	0.47	5.21	0.20	6.3

R_1 = p-SiMo--n-SiMo

R_2 = n-SiMo--n-SiGe

R_3 = n-SiGe

R_4 = n-SiGe--tungsten cold shoe

R_{total} = p-SiMo--tungsten cold shoe

Notes:

(a) vacuum-cast n-SiMo
(b) hot pressed n-SiMo

Photomicrographs of the bonds for the special test samples made with (a) vacuum-cast n-SiMo and (b) hot pressed n-SiMo, are shown, respectively, in Figures 62 and 63. All bonds were sound and are representative of typical air-vac bonds.

The instrumentation and wiring arrangement of the special test samples are given in Figure 64.

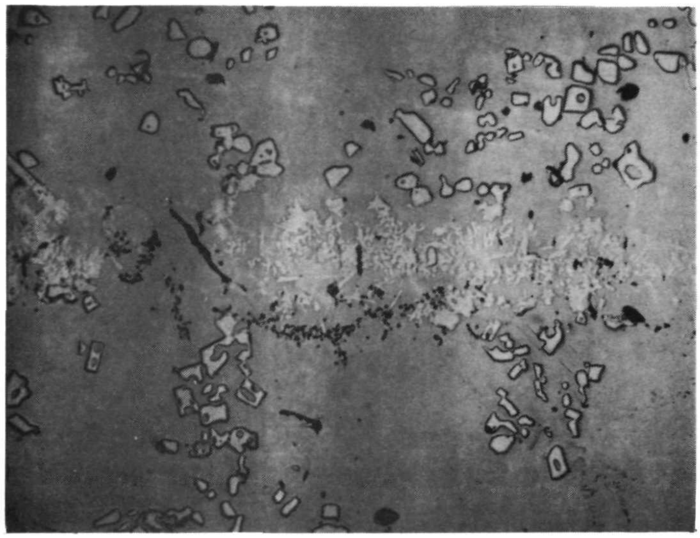

H826 - 2 72X

HOT SHOE BOND SYSTEM

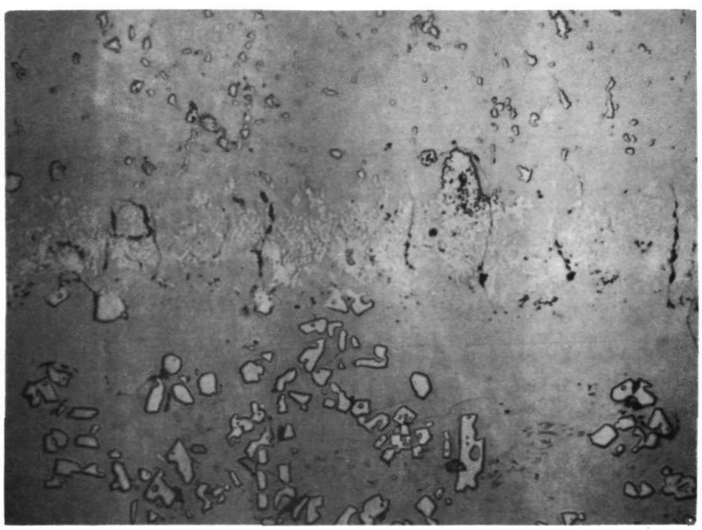

H826 - 5 72X

HOT SHOE BOND SYSTEM

Figure 62. Test Coupon Bond Systems

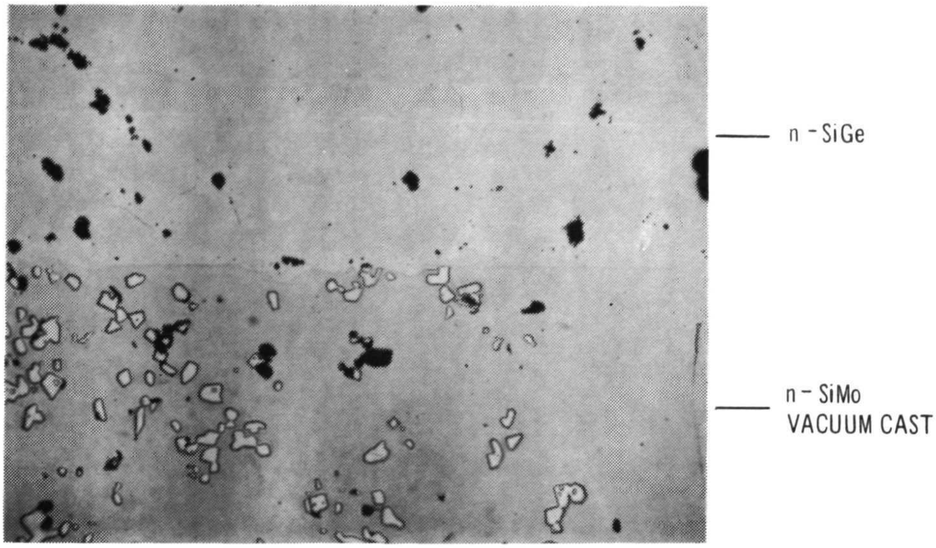

H826 - 2 HOT SHOE BOND SYSTEM 72X

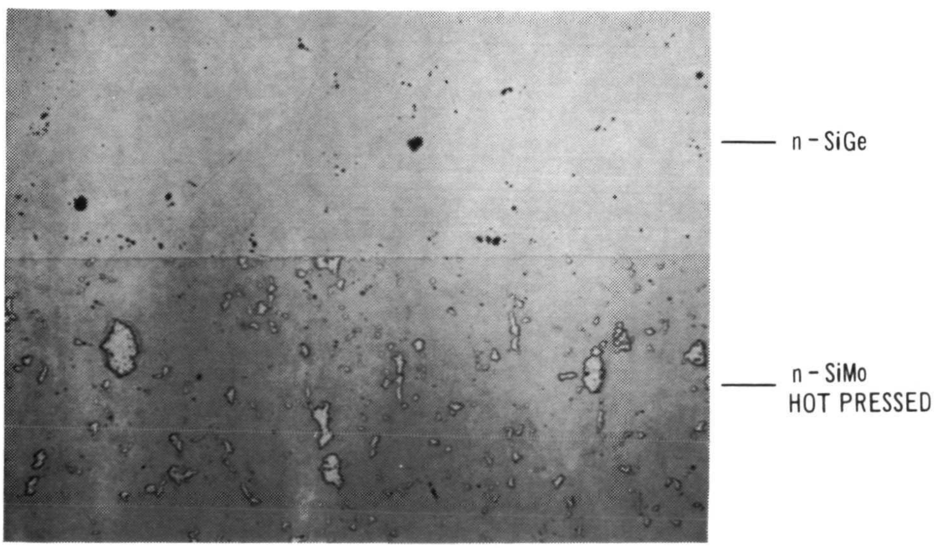

H826 - 5 HOT SHOE BOND SYSTEM 72X

Figure 63. Test Coupon Bond Systems

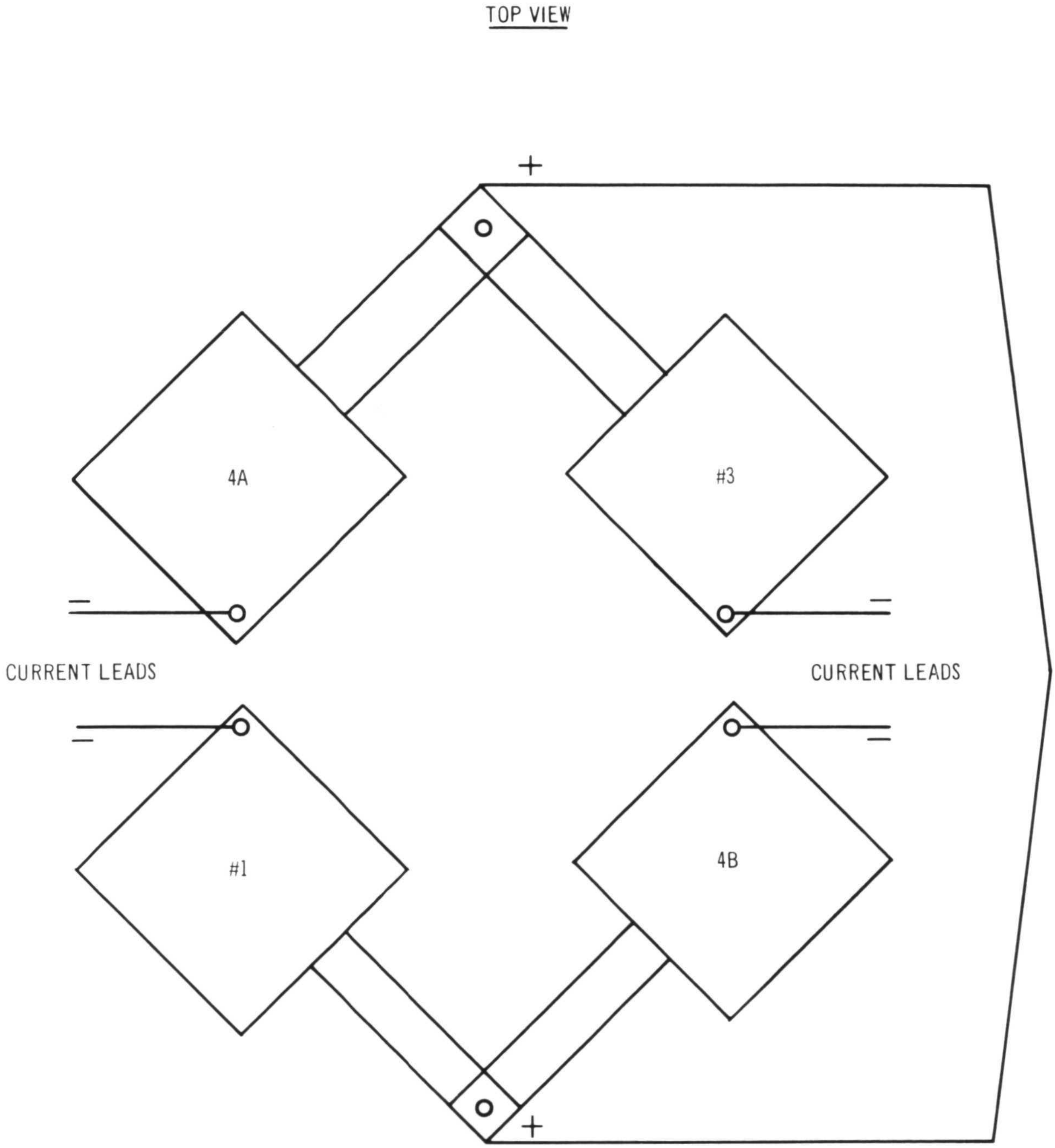

Figure 64. Wiring Arrangement – Special Test Samples

The room temperature and the high temperature bond resistances of the four special test samples, as measured in the life test station up to 381 hours, are given in Table XXI. The various bond resistances appear normal for air-vac couples; no abnormal increase in the resistance of either the n-SiGe or various bonds has occurred.

A leak occurred in the life test station in which these samples were being tested, and it was necessary to transfer them to another life test station. Room temperature resistance readings, taken in the test station after cycling to room temperature and in the new station prior to high temperature operation, were normal. The increase in the n-SiGe resistance with time is normal and is due to a temperature dependence of the solid solubility of the dopant. The higher the silicon content of the alloy and the higher the temperature of operation, the faster equilibrium is attained. Generally, the majority of the change occurs below 600°C. The contact resistance values always contain a small amount of the bulk resistance of the SiMo or SiGe as the attachment of the wires cannot be made closer than 0.010-0.015 in. to the joint. The contact resistances appear normal and show only minimal changes after test times in excess of 700 hours.

The testing of the four special test samples was interrupted due to a plant-wide power failure. With the loss of vacuum, the instrumentation leads were severely oxidized, necessitating their removal from the life test station. Visual inspection of the samples showed no damage or bond separation resulted after this thermal shock. Room temperature resistance readings of the bonds and bulk material were normal.

Prior to the power failure, the four test samples had completed 700 hours at design temperature conditions and various bond resistances were normal (see Table XXI). The data in Table XXI show the hot and cold shoe bonds to be quite stable. These values are listed under R_1, R_2 (hot end) and R_3 (cold end) and show only minimal changes to date. Two of the four samples, No. 1 and 4A, were reinstrumented and placed back on test and completed 3971 hours with stable performance.

As a result of all the testing conducted in the development of the thermocouple structure and more specifically the testing of the special test samples above, the conventional air-vac bond - p-SiMo--Ti-barrier--n-SiMo--n-SiGe - was selected as the bond system for the n-SiGe segment of the Hybrid couples that were fabricated for the two flat plate module test panels. Assembly process D, Figure 51, was the fabrication procedure used to produce the Hybrid thermocouple for the test panels.

TABLE XXI

BOND RESISTANCES OF SPECIAL TEST SAMPLES ON LIFE TEST

Sample No. 1

Hours		-	0	50	212	381	548	700	726
Hot Shoe Temp.	(°C)	25	936	926	930	934	933	930	
Cold Shoe Temp.	(°C)	-	419	420	420	419	418	418	
R_1	(mohms)	.22	.37	.84	1.01	1.00	1.01	.98	
R_2	"	.25	.35	.66	.53	.51	.54	.50	
R_3	"	4.29	6.40	12.46	13.05	13.12	13.32	13.27	Power Failure 7/1/71
R_4	"	.26	.28	.61	.65	.65	.68	.67	
R_{total}	"	5.01	7.38	14.60	15.22	15.32	15.53	15.42	

Sample No. 3

Hours		-	0	50	212	381	548	700	726
Hot Shoe Temp.	(°C)	25	939	930	934	937	939	935	
Cold Shoe Temp.	(°C)	-	419	417	416	416	415	414	
R_1	(mohms)	.25	.48	.66	.72	.72	.75	.72	
R_2	"	.24	.34	.66	.64	.63	.64	.63	
R_3	"	4.32	7.48	12.66	13.08	13.10	13.34	13.27	Power Failure 7/1/71
R_4	"	.27	.24	.61	.65	.64	.68	.66	
R_{total}	"	5.08	8.67	14.58	15.06	15.14	15.41	15.33	

Sample No. 4A

Hours		-	0	50	212	381	548	700	726
Hot Shoe Temp.	(°C)	25	928	918	922	925	927	923	
Cold Shoe Temp.	(°C)	-	419	424	424	424	415	422	
R_1	(mohms)	.22	.70	.84	.90	.94	.95	.94	
R_2	"	.27	.65	.53	.53	.48	.49	.48	
R_3	"	4.49	12.28	13.23	13.58	13.63	13.83	13.78	Power Failure 7/1/71
R_4	"	.25	.56	.46	.50	.50	.52	.52	
R_{total}	"	5.33	14.3	15.06	15.49	15.58	15.79	15.72	

Sample No. 4B

Hours		-	0	50	212	381	548	700	726
Hot Shoe Temp.	(°C)	25	934	925	928	932	933	930	
Cold Shoe Temp.	(°C)	-	415	419	419	414	413	412	
R_1	(mohms)	.32	.38	.70	.77	.77	.81	.78	
R_2	"	.50	.52	.91	.82	.70	.71	.71	
R_3	"	5.46	8.38	15.18	15.59	15.70	15.90	15.80	Power Failure 7/1/71
R_4	"	.22	.22	.44	.49	.47	.51	.48	
R_{total}	"	6.48	9.35	17.23	17.66	17.68	17.90	17.83	

Section V

FABRICATION OF MODULE PANELS

Two 9-couple panel sections of the Reference Design Hybrid module were fabricated and delivered to NASA Lewis for their testing and evaluation. This section describes the fabrication procedures used in making the panels. Detailed specifications for materials, parts and assembly processes were furnished to NASA Lewis and a list of these specifications is given in Tables XXII and XXIII. The assembly procedures developed in the thermocouple development task, Section IV-B, Sequence D, Fig. 51, were used to fabricate all couples for the panels. A detailed description of these assembly procedures is given at the end of this section.

The Hybrid couple components and a couple are illustrated in Figures 65 and 66, respectively. The Hybrid panel construction details are shown in Figures 67 and 68.

Photographs of the assembly sequences to fabricate the Hybrid panel are shown in Figures 69, 70 and 71. The heat receptor thermocouple location and power leads location are shown in Figure 72. The cold junction thermocouples, voltage taps and current leads location are shown in Figure 73. The couple location and individual couple room temperature resistance are presented in Figures 74 and 75 for Hybrid panels number 1 and 2, respectively. In both panels, the sum of the individual couple resistances were well within the required specification of 5% of the total couple resistance. The sum of the individual resistances versus the total for the two panels is given below.

Panel Number	Sum of Resistances	Total Couple Resistance
1	96.7	96.2
2	95.5	96.5

The couple leak rates for the couples used in the panel are given below.

Panel Number 1		Panel Number 2	
Couple Number	Leak Rate Std. cc Helium/sec	Couple Number	Leak Rate Std. cc Helium/sec
8	4.0×10^{-8}	5	4.0×10^{-8}
10	4.0×10^{-8}	13	$>1.0 \times 10^{-5}$
11	4.2×10^{-8}	21	1.0×10^{-6}
17	4.4×10^{-8}	25	$>1.0 \times 10^{-5}$
18	4.0×10^{-8}	26	1.3×10^{-7}
20	2.0×10^{-8}	28	1.0×10^{-8}
22	4.2×10^{-8}	30	1.0×10^{-6}
24	2.0×10^{-8}	36	1.0×10^{-6}
27	6.0×10^{-8}	37	1.0×10^{-8}

TABLE XXII

HYBRID THERMOCOUPLE MATERIAL AND PART SPECIFICATIONS

	Title	Material	Specification Number
1.	Heat Receptor	p-Type SiMo	HTP 171-A5A
2.	Hot Shoe	n-Type SiMo	HTP 10-J15D
3.	Cylindrical Leg	p-Type SiGe	HTP 170-B3A
4.	Segment (SiGe)	n-Type SiGe	HTP 10-I16D
5.	Cold Shoe	Tungsten	HTP 8-B17F
6.	Hot Shoe	303 Stainless Steel	HTP 4-D22K
7.	Segment (PbTe)	PbTe	HTP 10-H13D
8.	Cold Shoe	303 Stainless Steel	HTP 4-D22K
9.	Compensator Top	Gold	HTP 9-A23C
10.	Compensator Bottom	Gold	HTP 172-A4A
11.	Cold Shoe Ring	Tungsten	HTP 78-C5E
12.	Collar	Copper	HTP 148-A3A
13.	p-Type Elec. Connector	Copper	HTP 99-B42L
14.	n-Type Elec. Connector	Copper	HTP 99-B41L
15.	Insulator	Al_2O_3	HTP 78-B3D
16.	Insulator	Al_2O_3	HTP 78-B4D
17.	Mount Stud Pad	Copper	HTP 140-P20G
18.	Mount Stud Screw	C.R.S.	HTP 154-D9E
19.	Exhaust Tubulation	Copper	HTP 169-A2A
20.	Standard 1/4" Washer	C.R.S.	-
21.	Standard 1/4" x 28" Nut	C.R.S.	-
22.	Braze Shims		HTP 100-B5B
23.	Braze Shims		HTP 100-B6B
24.	Braze Shims		HTP 100-E6B
25.	Braze Shims		HTP 55-D9C
26.	Brazing Ring		HTP 46-D10B
27.	Brazing Ring		HTP 46-D8B
28.	Brazing Disc (Compensator)		HTP 100-E7B
29.	Compensating Ring	Gold	HTP 175-A1A
30.	Insulation Block	Min-K 2020	HTP 152-B44A
31.	Mounting Plate	Aluminum	HTP 159-B3A
32.	Heat Transfer Plate	Aluminum	HTP 159-B4A
33.	Shoulder Screw	303 Stainless Steel	HTP 178-A1A
34.	Cooling Plate	Aluminum	HTP 159-B5A
35.	Connector Screw	C.R.S.	HTP 154-G25C

TABLE XXIII

HYBRID THERMOCOUPLE ASSEMBLY SPECIFICATIONS

	Title	Specification Number
1.	Heat Receptor Assembly	HTS-1
2.	SiGe Assembly	HTS-2
3.	PbTe Element Assembly	HTS-3
4.	Thermocouple Assembly	HTS-4
5.	Cold Stack Assembly	HTS-5
6.	Hybrid Thermocouple Final Assembly	HTS-6
7.	Module Panel Assembly	HTS-7

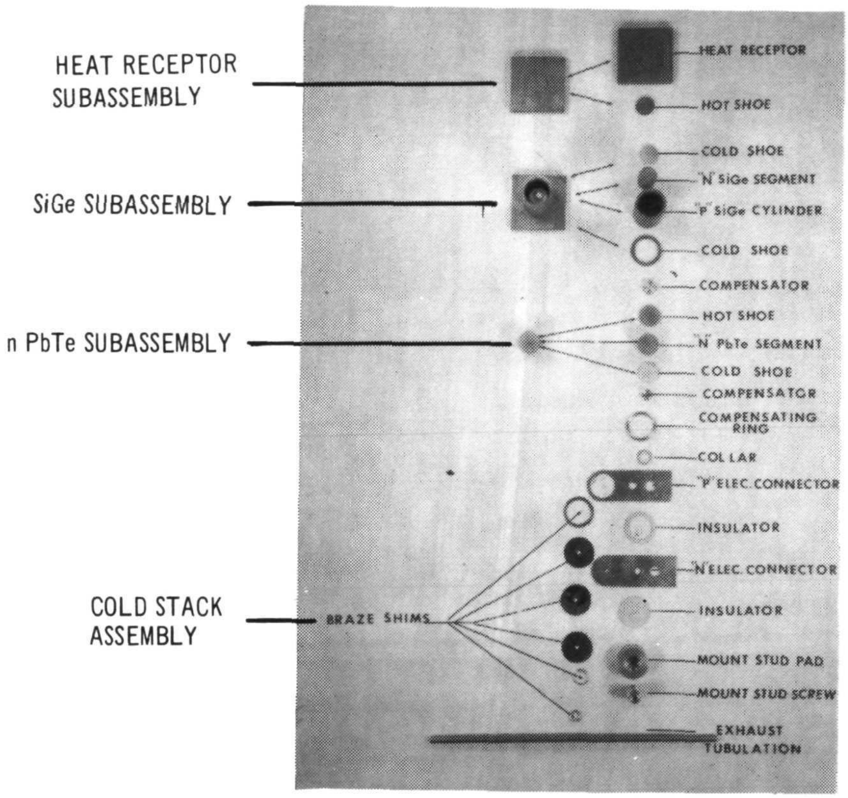

Figure 65. Hybrid Thermocouple Components

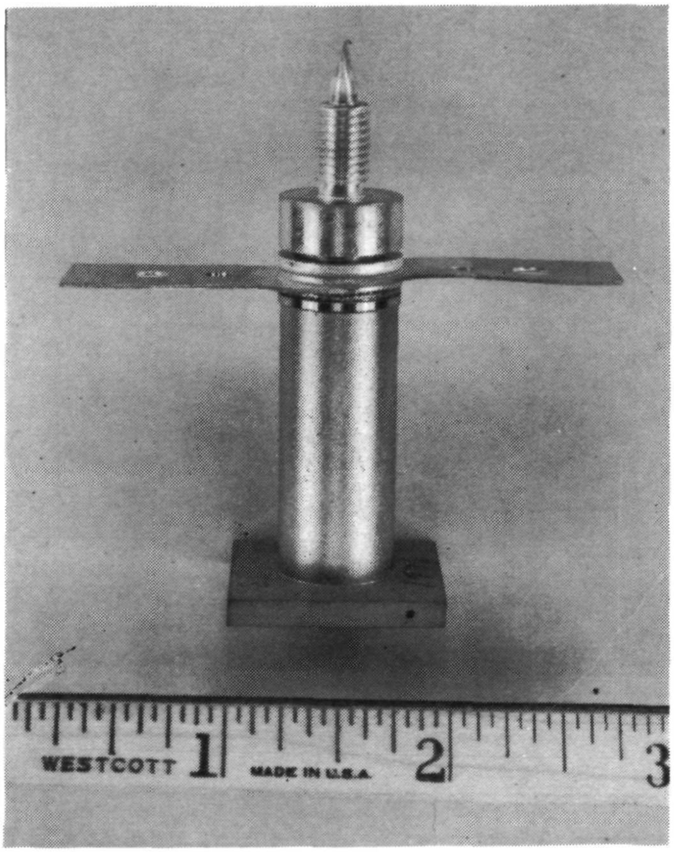

Figure 66. Reference Design Hybrid Couple

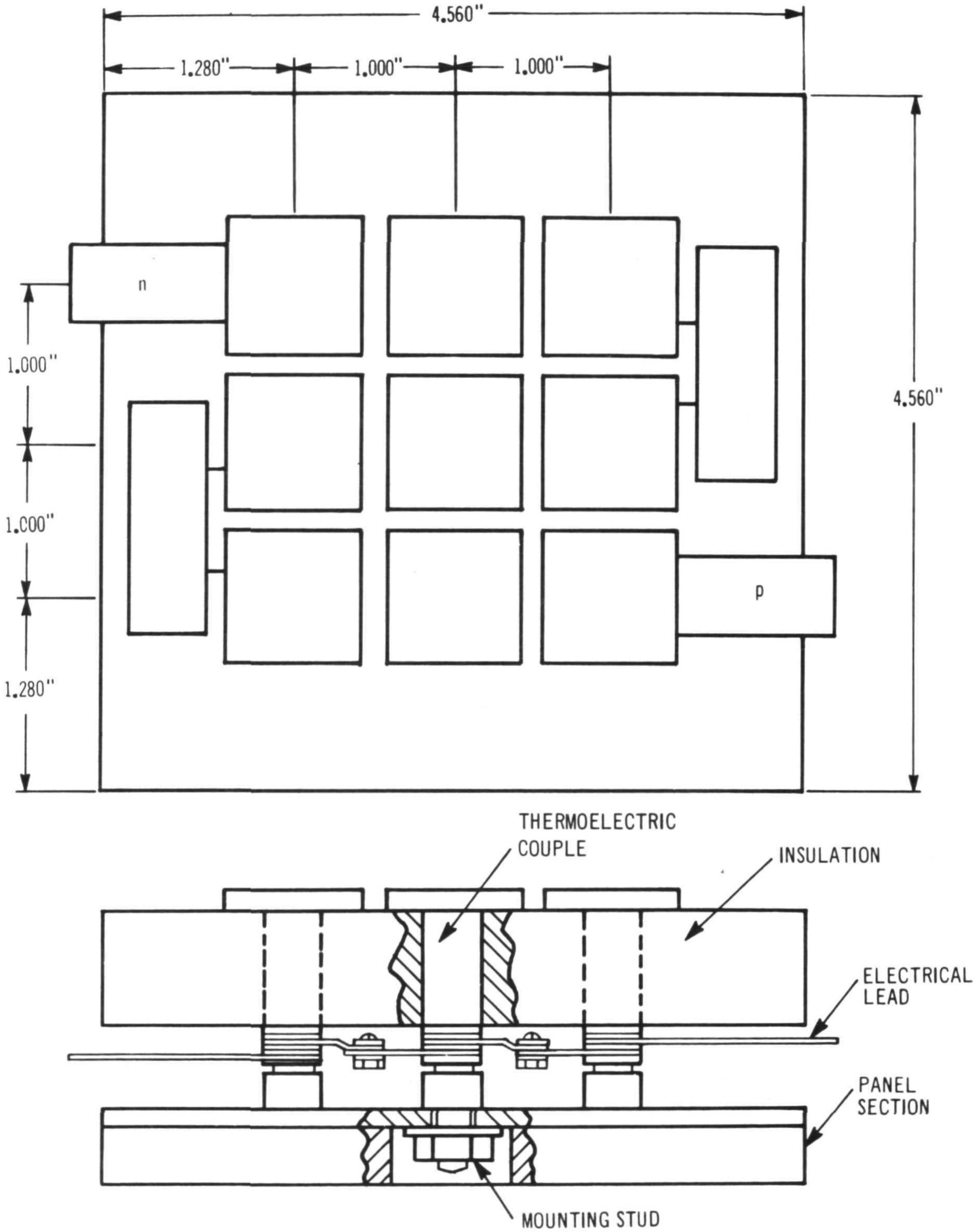

Figure 67. Hybrid Module Panel

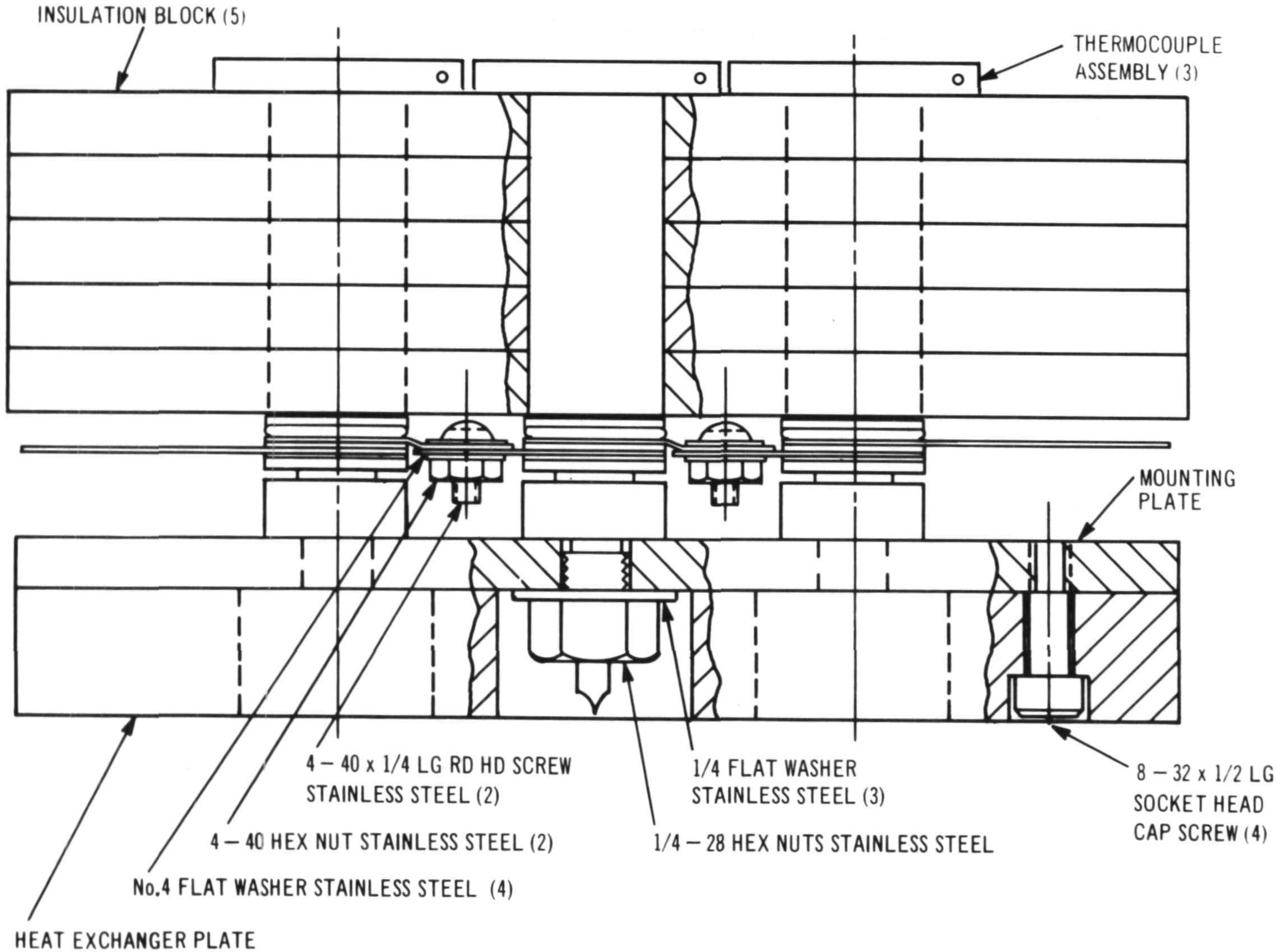

Figure 68. Hybrid Structure Module Panel Assembly

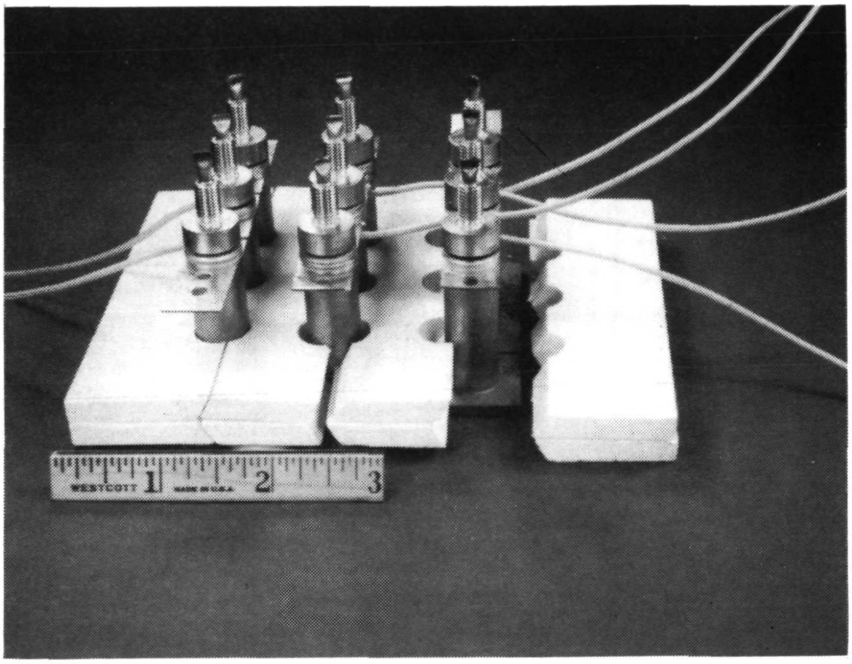

Figure 69. Hybrid Module Panel Strips

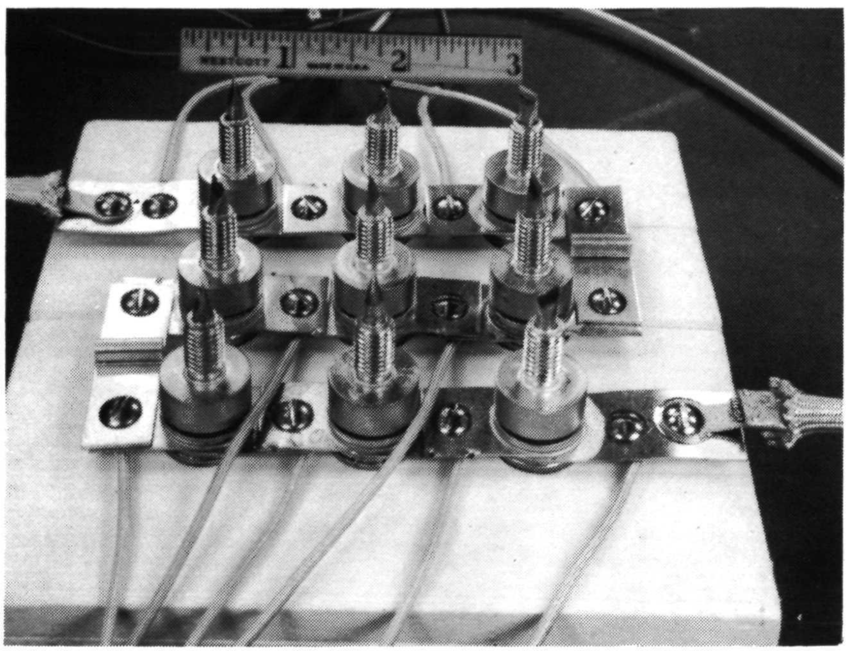

Figure 70. Hybrid Module Strips Instrumented – Cold Shoe Thermocouples

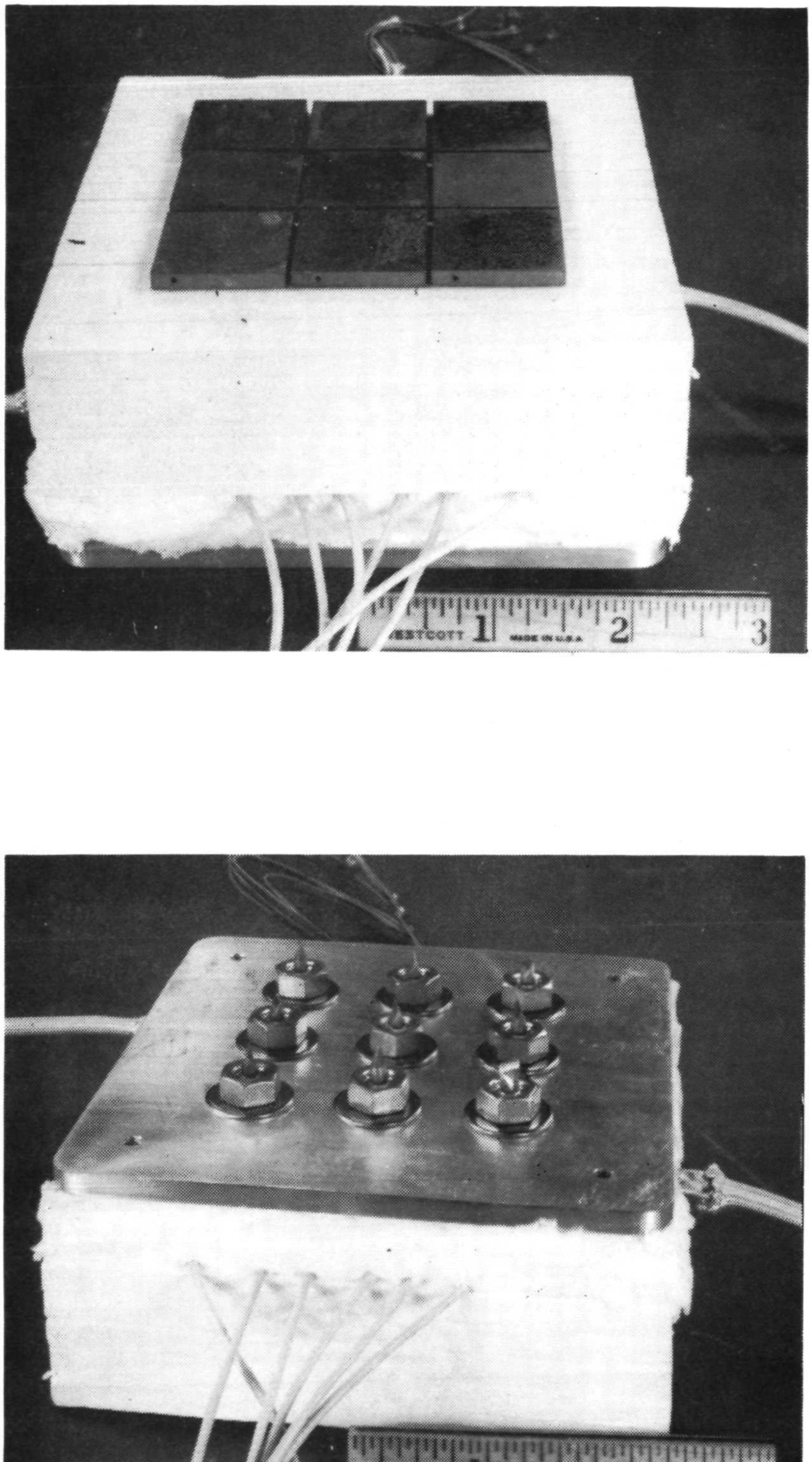

Figure 71. Completed Hybrid Flat Plate Panel Section

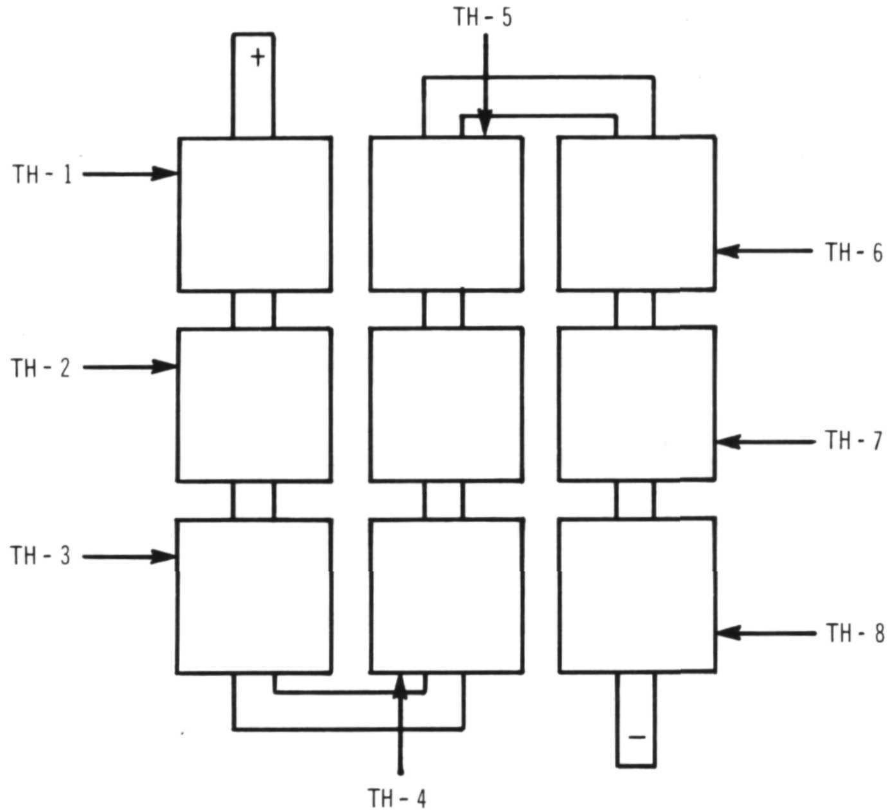

Figure 72. Heat Receptor Thermocouple Locations and Power Leads Locations, (W3Re/W25Re Thermocouples used)

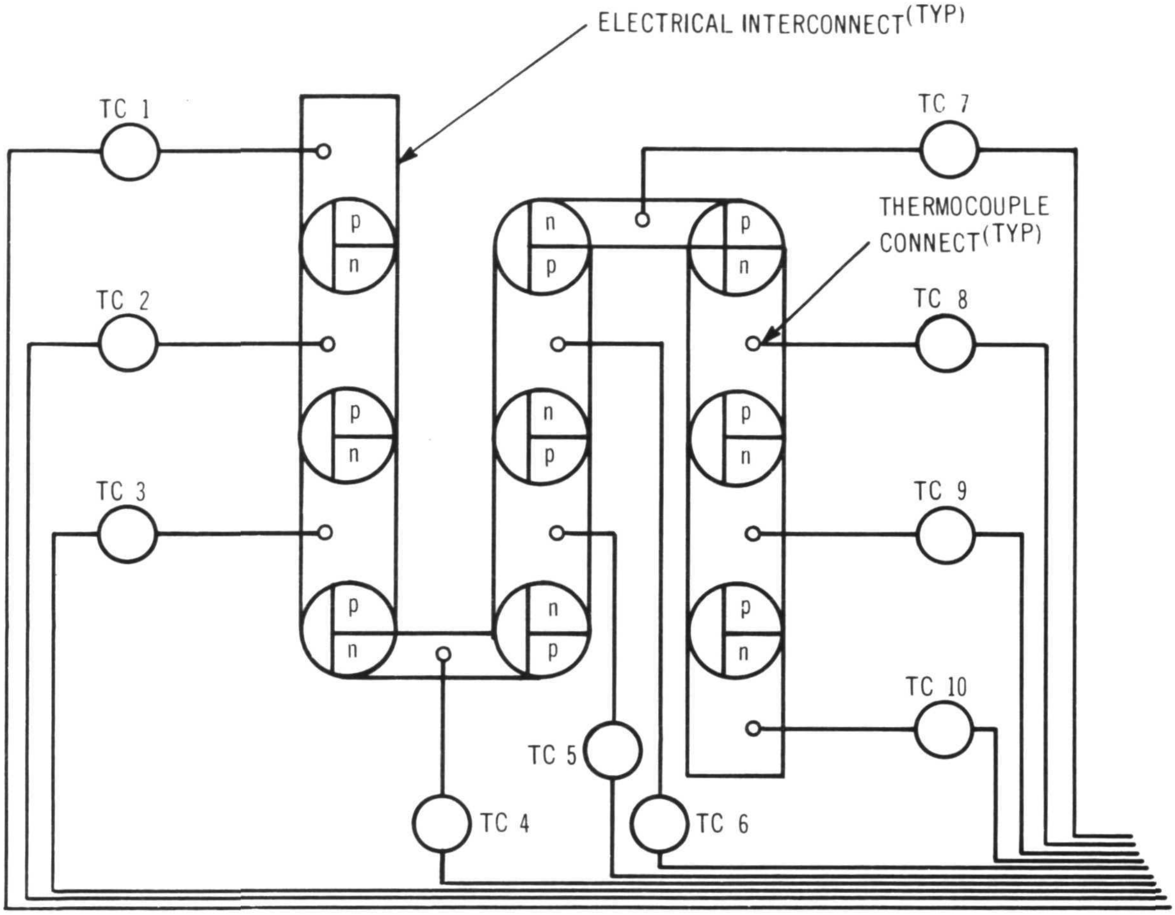

Figure 73. C/A Cold Junction T/C, Voltage Taps and Current Lead Location

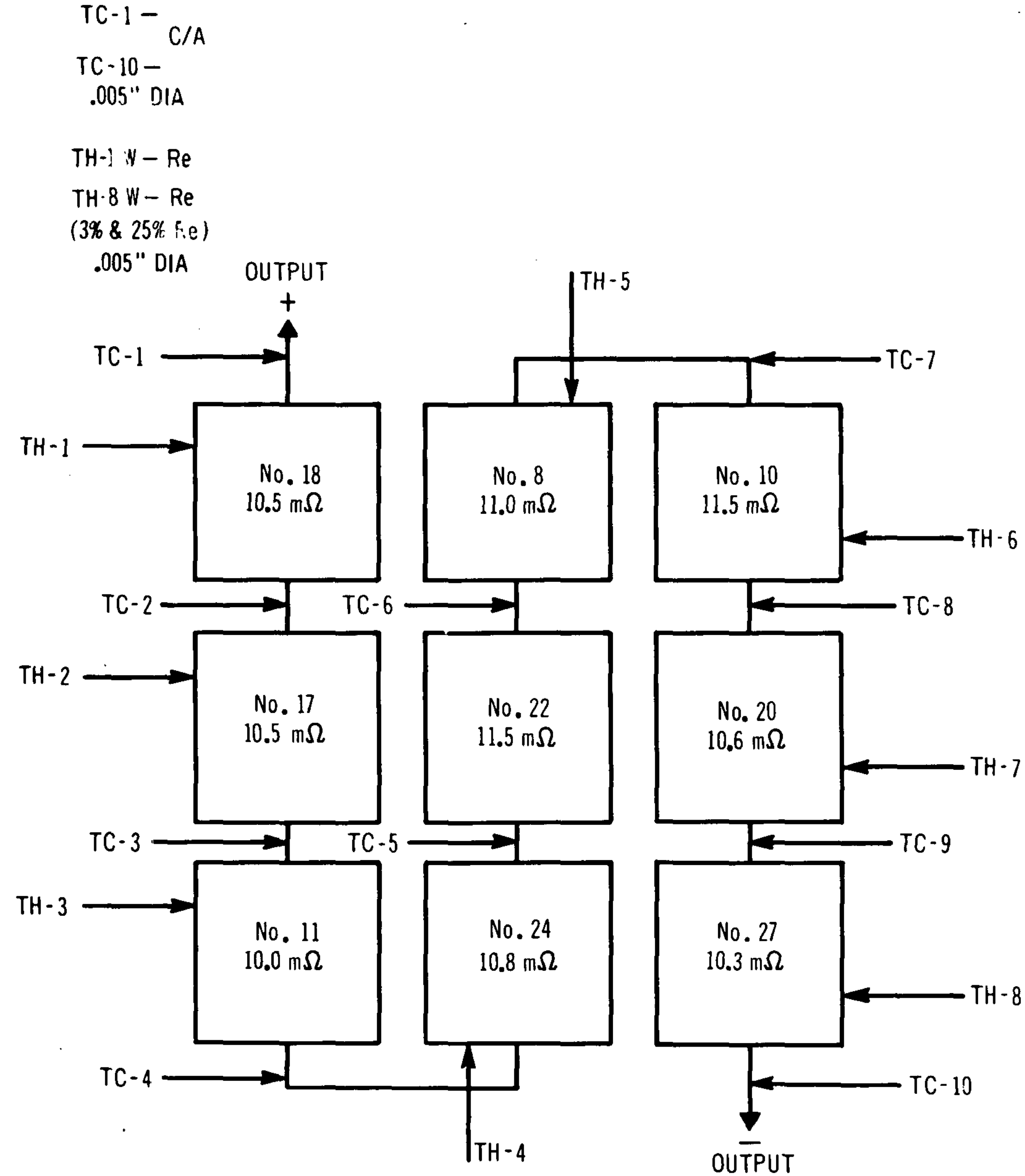

RESISTANCE TO GROUND ∞
(MODULE RESISTANCE AT 78° F 96.2 MILLIOHMS) VIEW: HOT SHOE SIDE OF MODULE

Figure 74. No.1 Panel Resistance Data

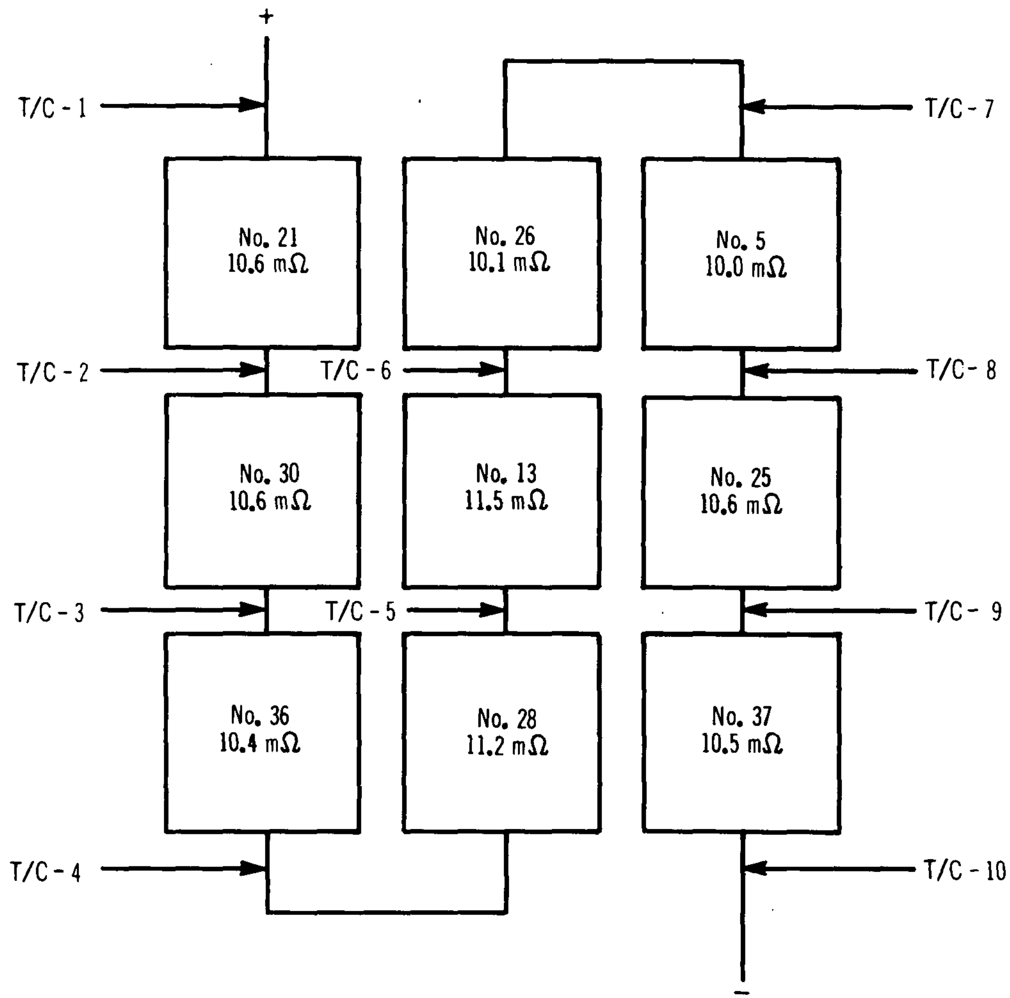

TOTAL MODULE RESISTANCE AT ROOM TEMPERATURE (25°C) 96.5 MILLIOHMS

MODULE RESISTANCE TO BASE PLATE ∞

8 HOT SIDE W/Re – W/Re (3% AND 25% Re) THERMOCOUPLES .005" (NOT SHOWN)

10 COLD SIDE C/A THERMOCOUPLES .005" DIA WIRE
VIEW:HOT SHOE SIDE OF MODULE

Figure 75. No. 2 Panel Resistance Data

A. Hybrid Couple and Panel Assembly Processes

1. HEAT RECEPTOR ASSEMBLY - HTS-1A1A

1.0.0 Heat Receptor Parts Assembly

1.1.0 Material

Polarity Type	Composition	Dopant	Fabrication Method
n	85 wt.% Si; 15 wt.% Mo	½% Phosphorus	Hot pressed
p	85 wt.% Si; 15 wt.% Mo	1% Boron	Vacuum cast

1.2.0 Equipment

1.2.1 Element alignment fixture HST-4

1.2.2 Small tools: tweezers, dropper, tungsten weight

1.3.0 Procedure

1.3.1 Slice 4.45 cm (1.75 in.) diameter p-SiMo casting to 2.44 cm (0.960 in.) x 2.44 cm (0.960 in.) x 0.318 cm (0.125 in.) thick heat receptor plates and the 5.08 cm (2.0 in.) diameter n-SiMo hot pressed disc to 0.813 cm (0.320 in.) diameter using Micromesh slicing equipment and metal bonded diameter wheels.

1.3.2 Measure and record the individual slice density using the water immersion technique. The material immersed in water is buoyed up with a force equal to the weight of the fluid displaced. Because the density of water at room temperature is one gram per cubic centimeter, the difference between the weight of the slice in air and in water represents its volume in cubic centimeters. Therefore:

$$\text{Density } (g/cm^3) = \frac{\text{Wt (gms) in air}}{\text{Wt (gms) in air} - \text{Wt (gms) in water}}$$

Match n-type and p-type slices according to density.

Polish one surface of each slice on a Brinkman metallurgical polishing table using silk cloth with Linde "A" abrasive followed by Rayvel synthetic velvet cloth with Linde "A" abrasive. Wash in methanol; dry with an air blower.

1.3.3 Place the p-SiMo heat receptor on a ceramic plate with the smooth or ground side of the heat receptor facing up. Then place the alignment fixture over the heat receptor making sure that the heat receptor fits snugly into the recess of the fixture. Apply one small drop of lucite cement onto the surface of the heat receptor at the hole in the boron nitride fixture, then immediately insert a titanium bonding shim into the hole and press firmly onto the heat receptor with tweezers. After a moment apply another drop of lucite to the surface of the bonding shim and apply an n-SiMo hot shoe and press the complete assembly with tweezers.

1.3.4 With pressure applied to the heat receptor assembly (tweezers or pick), remove alignment fixture.

1.3.5 Place the assembly into an air oven (approximate temperature 100°C) for drying for 3-5 minutes.

1.3.6 Inspect alignment. Titanium shim and n-SiMo must be located centrally on the p-SiMo heat receptor.

2.0.0 Heat Receptor Bonding

2.1.0 Equipment

2.1.1 Brew Furnace, Model 300MC or equivalent

2.1.2 Furnace rack

2.1.3 Ceramic spacers, tungsten weight (300 gms total)

2.2.0 Procedure

2.2.1 Determine temperature profile of furnace unit.

2.2.2 Load work onto the rack. Place a dummy n-SiMo hot shoe on the hot shoe being bonded, then position tungsten weight onto the dummy hot shoe. The tungsten weight must be supported to prevent shifting of the assembly.

2.2.3 Insert the work rack into the furnace, being certain that it is fully seated. Replace the furnace cover.

2.2.4 Evacuate the furnace to a pressure not to exceed 1 x 10^{-4} Torr.

2.2.5 Metallurgically bond assembly.

3.0.0 Inspection and Measurement

3.1.0 Lightly sandblast the bonded assembly after removing from the furnace. The bond is inspected under 30X magnification.

3.1.1 Bond resistance is measured using a Keithly milliohmeter.

2. SiGe ASSEMBLY - HTS-2A1A

1.0.0 SiGe Stage Assembly

1.1.0 Material

1.1.1 SiGe Alloys

Polarity Type	Composition	Dopant	Fabrication Method
n	70 at.% Si; 30 at.% Ge	0.3 wt.% Phosphorus	Zone leveled
p	80 at.% Si; 20 at.% Ge	0.1 wt.% Boron	Zone leveled

1.1.2 Cold Shoes

Tungsten Bar Stock - density: 18.9 gm/cm^3

1.1.3 Heat Receptor Assembly HTS-1A1A

1.2.0 Equipment

1.2.1 Alignment Fixture HST-7

1.2.2 Small tools: tweezers, dropper, clips, etc.

1.3.0 Procedure

1.3.1 Slice the n-ingot on the Micromesh slicing equipment, using a metal-bonded diamond wheel. Cylindrically grind the n-type SiGe elements with the proper radius to 0.798 cm (0.314 in.) diameter, using an 80-grit silicon carbide resin bonded wheel. End grind the n-type SiGe element to 1.82 cm (0.716 in.) length on the Sanford surface grinder, using an 80-grit silicon carbide resin-bonded wheel. Microfinish is not critical to subsequent processing. Weigh and inspect. Wash in 50% methanl-50% acetone. Package and identify individual pellets as to ingot number and position.

1.3.2 Slice the p-ingot on the Micromesh slicing equipment,using a metal-bonded diamond wheel, into blanks 1.52 cm (0.600 in.) diameter x 3.81 cm (1.500 in.) length. Send blanks to vendor to be diamond core drilled to finished dimensions, 1.34 cm (0.527 in.) OD x 1.1 cm (0.435 in.) ID x 3.17 cm (1.250 in.) length. Each machined p-SiGe cylinder is then checked for hermeticity, using a Veeco MS-9 leak detector and a dye penetrant leak test. Weigh and perform visual inspection. Wash in 50% methanol-50% acetone. Package and identify individual cylinders as to ingot number and position.

1.3.3 Fabricate n-SiGe cold shoe to a disc, 0.81 cm (0.320 in.) diameter x 0.102 cm (0.040 in.) thick. Fabricate p-SiGe cold shoe ring, 1.4 cm (0.550 in.) OD x 1.08 cm (0.425 in.) ID x 0.102 cm (0.040 in.) thick via Elox drilling technique (shoe fabricated by outside vendor). All shoes for the n- and p-type SiGe legs are to be rigidly inspected for dimensions and flatness, then washed in hot Blacosolv, hot water, and methanol to ensure a clean surface for bonding. The tungsten cold shoes are to be stored in clean, properly identified envelopes.

1.3.4 Place a heat receptor assembly on a ceramic pad with the hot shoe facing up.

1.3.5 Assemble n-SiGe pellet to heat receptor assembly. Use one small drop of lucite cement. Assemble a tungsten cold shoe to end of n-SiGe pellet using one small drop of lucite cement. Dry assembly with hot air gun.

1.3.6 To the above assembly, place the alignment fixture over the heat receptor making sure the heat receptor fits snugly into the recess of the fixture; the n-SiGe pellet facing up.

1.3.7 Apply two drops of lucite cement on the heat receptor at the recess of the fixture. Immediately place a p-SiGe cylinder over the n-leg and into the recess of the alignment fixture. Press slightly to squeeze the lucite to thinnest possible layer.

1.3.8 Apply lucite cement to the upper edge of the p-SiGe cylinder; Then place a tungsten ring on the edge and align the ring while pressing down.

1.3.9 To speed drying, place under lamp or in oven (maximum temperature 100°C). Allow to dry for approximately 5 minutes.

1.4.0 Remove alignment fixture. Inspect alignment.

2.0.0 <u>SiGe Stage Bonding</u>

2.1.0 <u>Equipment</u>

2.1.1 Brew Furnace, Model 300 MC or equivalent

2.1.2 Work rack

2.1.3 Ceramic spacers, tungsten weights

2.2.0 <u>Procedure</u>

2.2.1 Determine temperature profile of furnace unit.

2.2.2 Place tungsten weight (cylindrical) onto the tungsten cold shoe ring of the p-leg. Insert tungsten rod into the cylinder weight so that it rests on the tungsten cold shoe of the n-leg.

2.2.3 Load the above assembly onto the rack so that no shifting occurs.

2.2.4 Insert the work rack into the furnace, being certain it is fully seated. Replace furnace cover.

2.2.5 Evacuate the furnace to a pressure not to exceed 1 x 10^{-4} Torr.

2.2.6 Metallurgically bond assembly.

3.0.0 Inspection and Measurement

3.1.0 After removing the bonded SiGe stage from the furnace, all bonds are inspected under 30X magnification.

3.1.1 Bond resistances are measured on a Keithley milliohmeter.

3. n-TYPE PbTe ASSEMBLY - HTS-3A1A

1.0.0 N-Type PbTe Parts Assembly

1.1.0 Material

3M Co. 3N PbTe pellet
303 stainless steel hot and cold shoes

1.2.0 Equipment

1.2.1 Commercial chemical vapor deposition equipment

1.2.2 Split bonding die

1.3.0 Procedure

1.3.1 The 303 stainless steel alloy hot shoe, 0.953 cm (0.375 in.) diameter x 0.102 cm (0.040 in.) thick, and cold shoes, 0.953 cm (0.375 in.) diameter x 0.051 cm (0.020 in.) thick, are fabricated by punching from stock strip. They are then coated with a tungsten diffusion barrier layer and bonding layer.

1.3.2 Coat n-PbTe segment TP10H13D on cylindrical surface with Aquadag.

1.3.3 Place hot and cold shoes TP4D22K and TP4D23K with W-plated surface toward PbTe segment TP10H13D.

1.3.4 Align unbonded element in split bonding die with bond interfaces in line with bond overflow relief channels.

2.0.0 n-Type PbTe Element Bonding

2.1.0 Equipment

2.1.1 Vacuum Furnace

2.2.0 Procedure

2.2.1 Insert loaded die assembly in bonding furnace. Evacuate chamber to 1 x 10^{-5} Torr. Admit 95 Ar-5 H gas. Maintain positive pressure.

2.2.2 Metallurgically bond.

2.2.3 Remove bonded element from die. Sandblast to remove Aquadag and bond overflow.

2.2.4 Record T_1, T_2, T_3 (hot, cold contact and total element resistance).

2.2.5 Measure and record length.

2.2.6 Surface grind both shoes.

2.2.7 Nickel plate both shoes 0.0001. Fire 575°C 30 minutes in dry H_2.

2.2.8 Surface polish both shoes to mirror finish with Linde "A" immediately prior to couple assembly.

4. THERMOCOUPLE ASSEMBLY - HTS-4A1A

1.0.0 Thermocouple Parts Preparation

1.1.0 Materials, Components

1.1.1 SiGe Assembly, HTS-2A1A

1.1.2 n-PbTe Assembly, HTS-3A1A

1.1.3 Upper and lower gold compensator

1.2.0 Procedure

1.2.1 Sandblast the face of the TP8B17E tungsten shoe and the edge of the p-cylinder of the SiGe subassembly.

1.2.2 Wash subassembly ultrasonically in 50% methanol-50% acetone for 5 minutes.

1.2.3 Nickel plate and sinter the surface of the tungsten cold shoe and edge of the p-tungsten cold shoe ring.

1.2.4 Ultrasonically wash upper and lower gold compensators in Blaco-solv for 5 minutes. Rinse in distilled water and then methanol.

2.0.0 Bonding Operation

2.1.0 Equipment

2.1.1 Diffusion bonding fixture (CST-40)
2.1.2 316 SS pressure pads
2.1.3 Molybdenum pad
2.1.4 303 SS shim
2.1.5 Nichrome shim
2.1.6 TC structure
2.1.7 316 SS shim

2.2.0 Bonding Procedure

2.2.1 Glue the top compensator gold disc to the nickel-plated hot shoe of the PbTe element with lucite cement. Center the two with respect to each other using the locating sleeve "A".

2.2.2 Drop the glued subassembly into the cylinder with the gold top compensator against the TP8B17E nickel-coated shoe and secure with lucite. Use sleeve "B" for centering. Load into diffusion bonding fixture.

2.2.3 Apply 30 psi - 0.05 mil deflection of pressure to the subassembly.

2.2.4 Metallurgically diffusion bond.

2.2.5 Remove from furnace and check for bond resistance.

2.2.6 Glue the slotted side of the bottom gold compensator (TP172A4A) to the cold shoe (TP4D22K) of the PbTe element with lucite cement. Center the two using locating sleeve "B".

2.2.7 Assemble into bonding clamp CST40 and repeat procedure 2.1.0 through 2.2.4.

3.0.0 Inspection and Measurement

3.1.0 Remove from furnace and check for n- and p-joint resistances and n- and p-element resistances after each bonding cycle.

5. COLD STACK ASSEMBLY - HTS-5A1A

1.0.0 Cold Stack Assembly (HTS-5)

1.1.0 Equipment

1.1.1 Fixture Assembly (HST-5)
1.1.2 Carbon block with boron nitride insert
1.1.3 Nichrome pin coated with boron nitride
1.1.4 Ceramic ring
1.1.5 Tungsten wire clips

1.2.0 Cold Stack Assembly Procedure

1.2.1 Load the following component parts in the prescribed order onto the boron nitride insert of the jig assembly:

TP148A3A	copper collar
TP99B42L	p-type electrical copper connector
TP100B6B	braze shim
TP78B4B	ceramic insulator
TP100B5B	braze shims

1.2.2 Load the following onto the nichrome pin set into the jig subassembly in the prescribed order:

TP99B41L	n-type electrical copper connector
TP100B5B	braze shims
TP78B3B	ceramic insulator
TP100B5B	braze shims
TP140D206	copper mount stud pad

1.2.3 Load the following into the TP140D20G mount stud pad:

TP46D10B	brazing ring
TP154D9E	CRS mount stud screw
TP46D8B	brazing ring
TP169A2A	copper exhaust tubulation

1.2.4 Slide the ceramic ring of the jig assembly over the mount stud screw onto the mount stud pad.

1.2.5 Use four tungsten wire clips to secure the assembly by clipping to the ceramic and carbon block.

2.0.0 Metallurgically braze assembly.

3.0.0 Inspection and Measurement

3.1.0 Check the assembly for continuity to determine that no short exists between the n- and the p-type electrical connectors.

3.1.1 Check assembly for leaks on the Veeco. Cap across the cold shoe ring and check for leaks from outside to the tubulated region. Make sure that tubulation is not blocked. If blocked, open with a drill.

6. FINAL ASSEMBLY - HTS-6A1A

1.0.0 Final Parts Assembly

1.1.0 Materials, Components

1.1.1 Thermocouple Assembly HTS-4A1A
1.1.2 Cold Stack Assembly HTS-5A1A
1.1.3 Gold Compensator Ring

1.2.0 Procedure

1.2.1 Fill the area between the inner wall of the p-cylinder and internal parts with powdered alumina (Al_2O_3) to the level of the p-tungsten cold ring. Pack Microquartz fibers on top of the alumina to secure it and prevent spillage.

1.2.2 Place brazing shims (TP100E7B) inside the collar (TP148A3A).

1.2.3 Place brazing shims (TP100E6B) onto the p-type electrical connector of the Cold Stack Assembly and secure with lucite cement.

1.2.4 Place the gold compensating ring (TP175A1A) on top of the brazing shims.

1.2.5 Place an additional brazing shim (TP100E6B) on top of the gold compensating ring and secure with lucite cement.

1.2.6 Assemble the Thermocouple Subassembly (HST-8) onto the Cold Stack Assembly (HTS-7) being careful that the bottom gold compensator fits into the collar brazed to the n-electrical connector. Align the brazing rings with the tungsten cold shoe ring.

1.2.7 Secure both assemblies with four tungsten wire clips.

1.2.8 Inspect the assembly for alignment of hot shoe, location of thermocouple holes with respect to the n- and p-electrical connectors.

2.0.0 Bonding Operation

2.1.0 Metallurgically braze the assembly in a vertical position with the cold stack on top.

3.0.0 Inspection and Measurement

3.1.0 Inspect for braze quality and leak test the assembly on the Veeco Leak Detector.

3.1.1 Check the assembly for shorts and bond resistance.

3.1.2 Back fill the assembly with argon at 1/3 atmosphere and pinch off tubulation close to the screw.

7. MODULE PANEL ASSEMBLY HTS-7A1A

1.0.0 Module Panel Assembly

1.1.0 Equipment

1.1.1 Fixture Assembly HTS-7

1.2.0 Procedure

1.2.1 Form the electrical connectors using jig assembly HST-7. Both n- and p-end connectors on TC #1 and #9 are to be left long.

1.2.2 Load thermocouples 1, 2 and 3 into holes 1, 3 and 5 of plate jig HST-7, respectively. Trim the ends of the connectors to the proper length, approximately 0.440 in. from the edge of the p-cold shoe ring.

1.2.3 Clamp the assemblies to the plate by securing the nut on the mount stud screw.

1.2.4 Clamp the electrical connectors between TC 1 and 2 and TC 2 and 3, using TP154G25C screw and nut.

1.2.5 Clamp a copper connector strap at right angles to the p-connector of TC #3.

1.2.6 Loosen the nuts from the mount stud screw and remove from plate.

1.2.7 Assemble the remaining two strips consisting of TC 4, 5 and 6 and TC 7, 8 and 9 in a similar manner. Care should be taken to maintain the proper orientation of the thermocouple holes in the heat receptor with respect to panel location.

1.2.8 Instrument all eight outer p-SiMo hot shoes with W-Re thermocouples. Instrument all cold shoes with Cr-Al thermocouples at the electrical connectors between couples.

2.0.0 <u>Insulating Module Panel Assembly</u>

2.1.0 Load module strip #1 into the outer insulation blocks (TP152B44A). Bring the cold shoe thermocouples outside the area of the mounting plate.

2.1.1 Load the mating segment of inner insulation blocks (TP152B44A) on the other side of module strip #1 and lock into outer insulation block.

2.1.2 Repeat this procedure for module strips 2 and 3. Use the other outside insulation blocks TP152B44A for securing module strip #3.

2.1.3 Bring the hot shoe instrumenting thermocouples along the outside of the insulating block in channels provided at this time.

2.1.4 Band the insulating material around the outside to secure the insulation in place.

Section VI

SUMMARY OF RESULTS

The results of the work performed under the Hybrid Thermocouple Development Program are as follows.

1. An analytical study was conducted to estimate Hybrid couple efficiency and define practical Hybrid couple geometries. The study indicated that the Hybrid couple efficiency would be 10 to 15 per cent better than that of all-SiGe (63 at.% Si alloy) couples.

2. A preliminary design of a planar generator using Hybrid thermocouples and a water heat pipe radiator was prepared. A specific power of 3.5 watts/kg (1.6 watts/lb) was estimated for a generator using current-design Hybrid couples operating at a hot shoe temperature of 941°C (1726°F) (hot junction temperature of 926°C (1700°F) and a cold junction temperature of 232°C (450°F)). A specific power of 5.3 watts/kg (2.4 watts/lb) is projected assuming the use of improved thermoelectric materials and operation at a hot junction temperature of 1000°C (1832°F).

3. A total of 64 Hybrid couples were built, using a number of different assembly techniques. Couples fabricated early in the program were, in general, characterized by high initial resistance (from 10 to 30 per cent higher than design), and, in some cases, bond separation after several thousand hours of testing. Couples made later in the program, using improved fabrication techniques, exhibited much lower initial resistance, closely approximating design values, and after limited testing, i.e., 700 hours, exhibit a resistance increase which is consistent with that expected as a result of phosphorus precipitation in the n-SiGe segment. Further testing and evaluation, presently being performed at NASA-LeRC, will be required to fully assess the performance of the Hybrid couple.

APPENDIX I

THERMOELECTRIC MATERIAL PROPERTIES

TABLE XXIV

PHYSICAL PROPERTIES - THERMOELECTRIC MATERIALS

(approximate values)

Property	SiGe	Si-Alloy Hot Shoe	PbTe
Thermal Expansion	4.8 to 5.0 x 10^{-6} °K	same as SiGe	19.5 to 20.5 x 10^{-9} °K
Tensile Strength			
p-type: 932°F (500°C)	3900 psi	--	1000 psi
n-type: 932°F (500°C)	4400 psi	--	1000 psi
Compressive Strength	150,000 psi	--	10,000 psi
Avg. Modulus of Rupture	3600 psi	--	2 x 10^6 psi
Vapor Pressure	3 x 10^{-9} at 1472°F (800°C)	--	5 x 10^{-5} at 932°F (500°C)
Density	3 to 3.5 g/cm^3	2.6 g/cm^3	8.15 g/cm^3

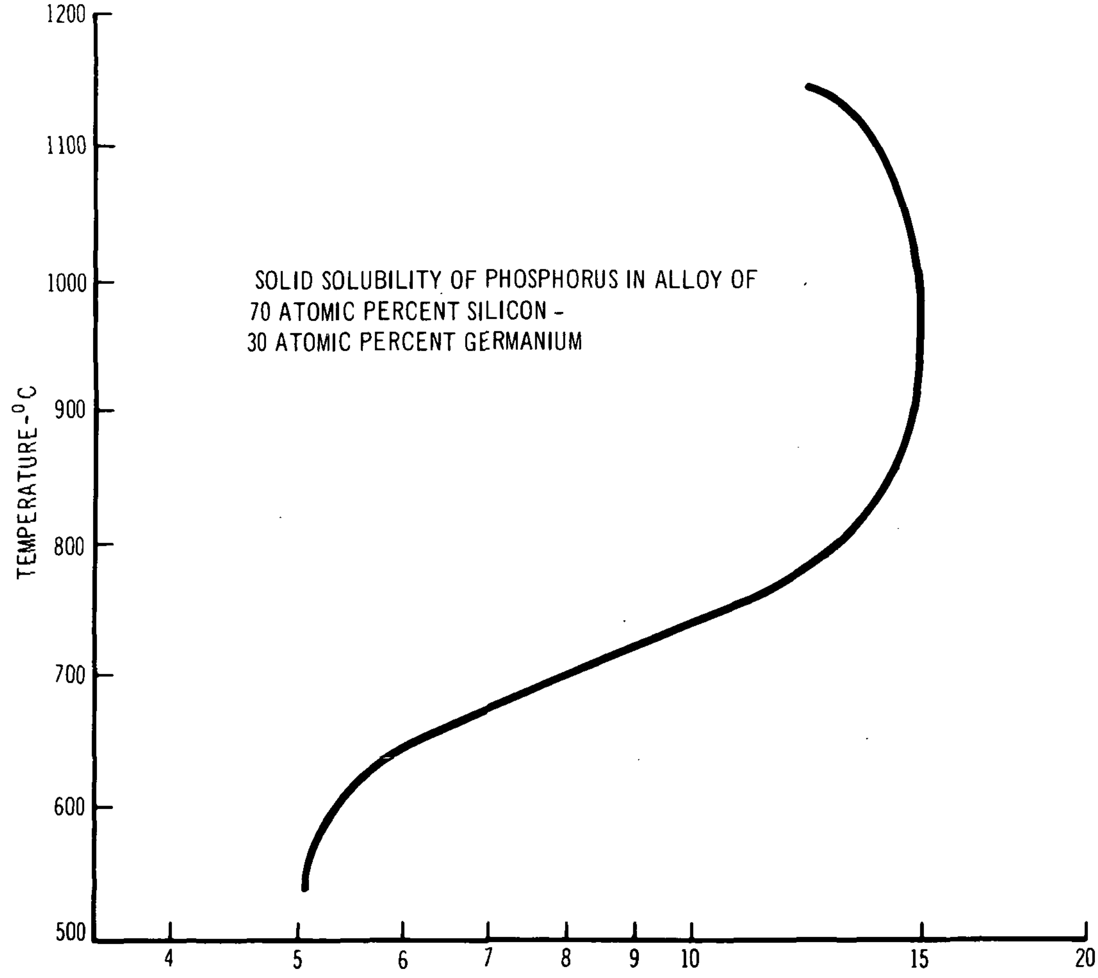

Figure 76. Carrier Concentrations (Atoms per Cubic Centimeter x 10^{19})

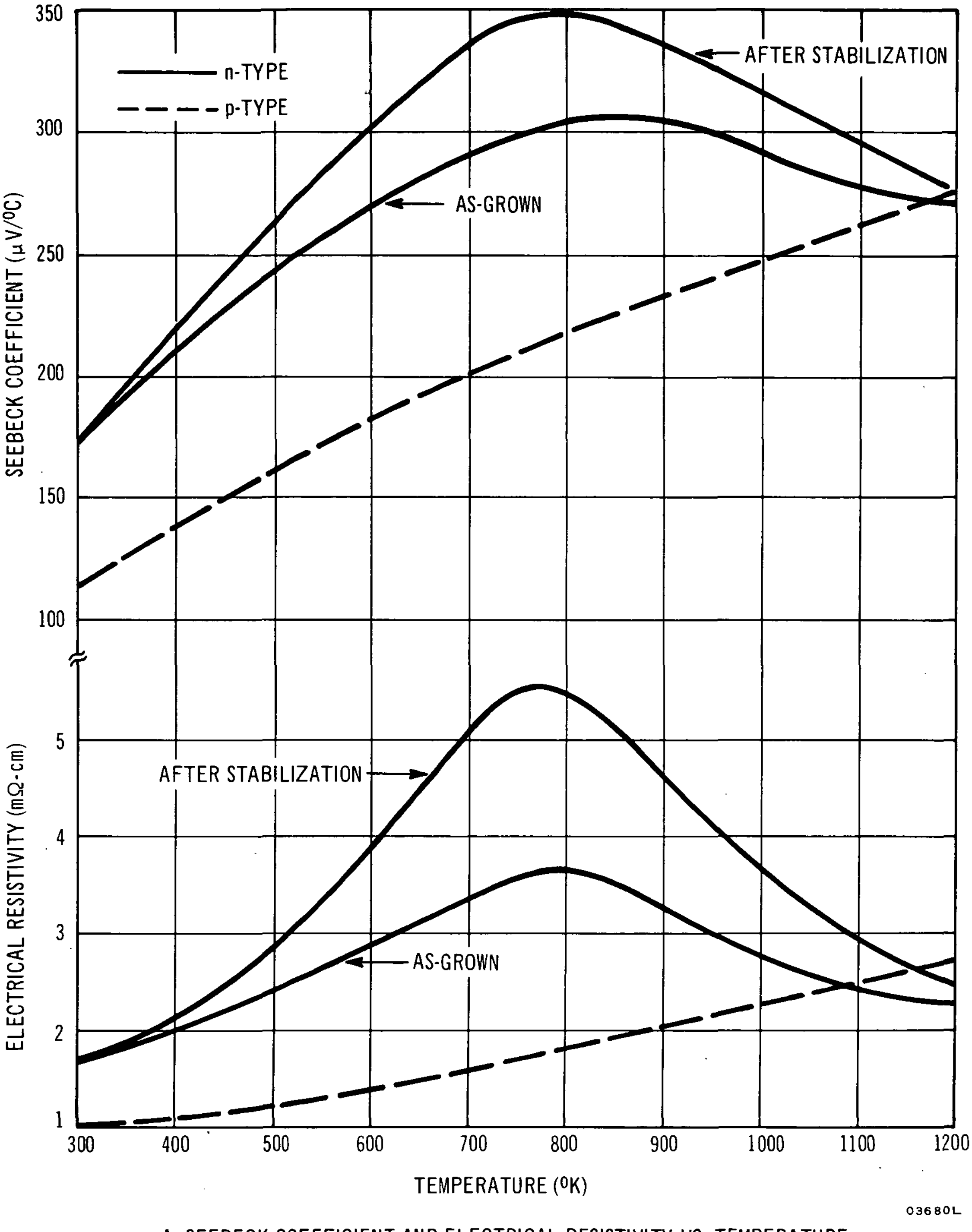

A. SEEBECK COEFFICIENT AND ELECTRICAL RESISTIVITY VS. TEMPERATURE

Figure 77. 63.5 At. % SiGe, Thermoelectric Properties (Sheet 1 of 2)

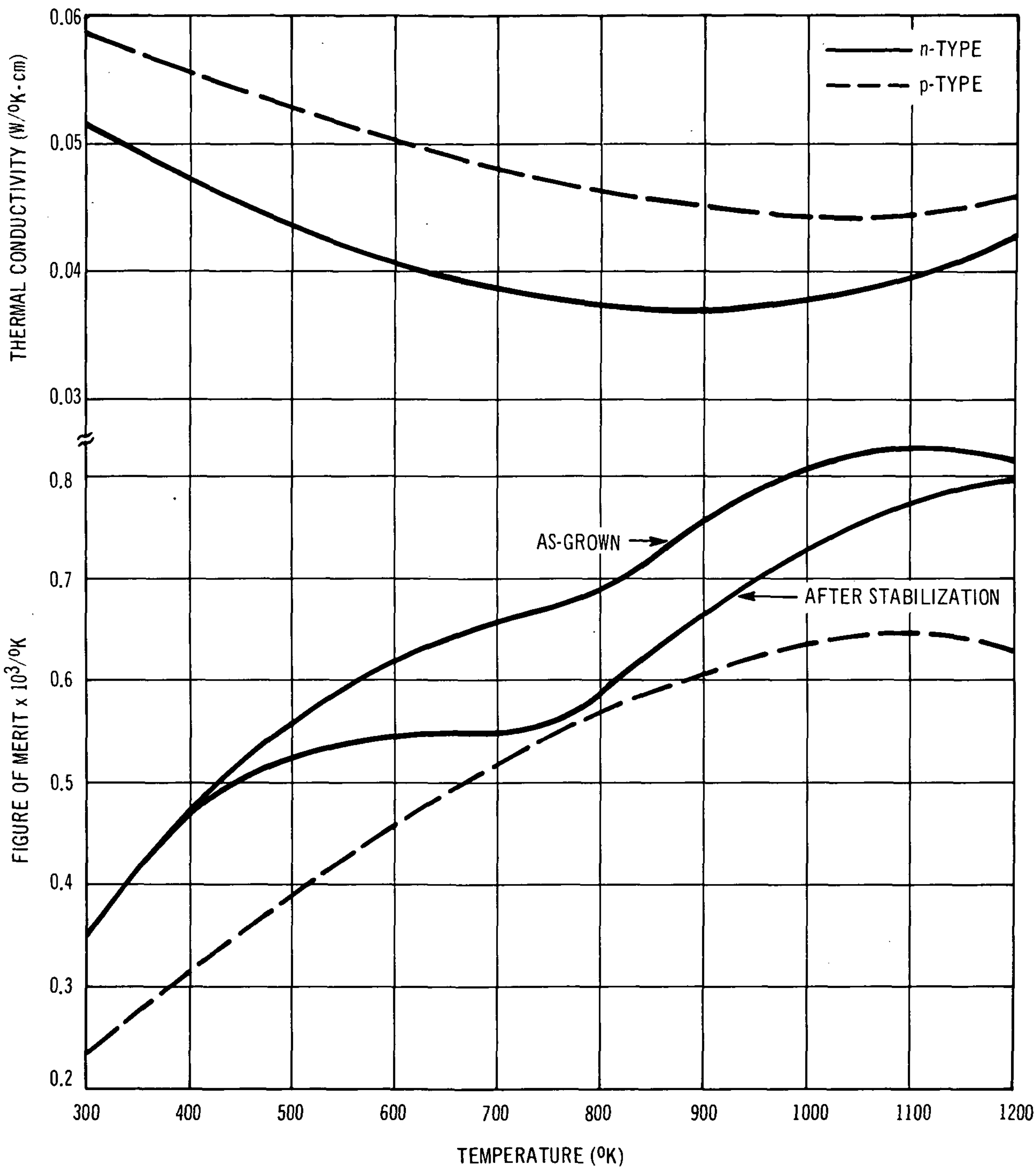

B. THERMAL CONDUCTIVITY AND FIGURE OF MERIT VS. TEMPERATURE

Figure 78. 63. 5 At. % SiGe, Thermoelectric Properties (Sheet 2 of 2)

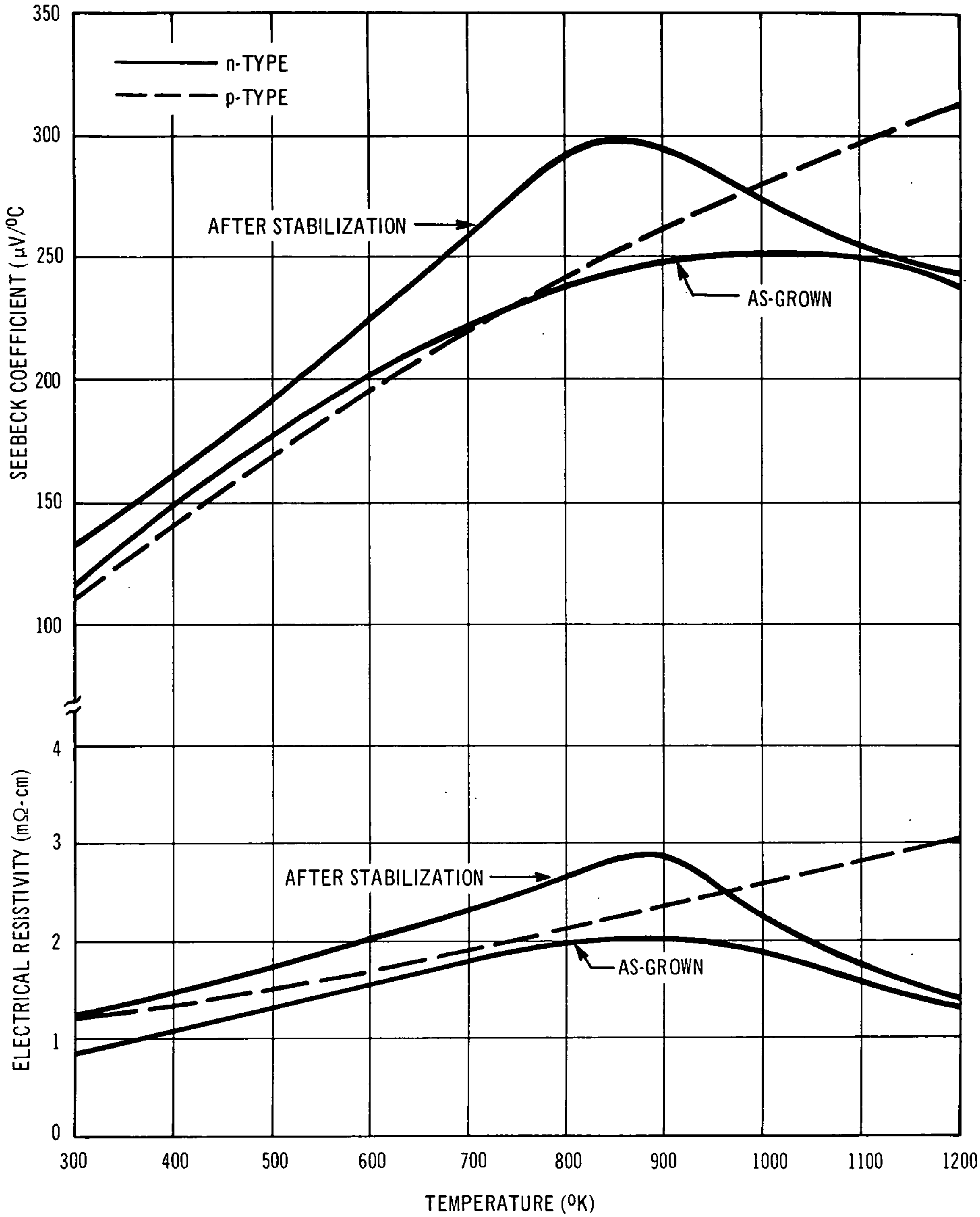

A. SEEBECK COEFFICIENT AND ELECTRICAL RESISTIVITY VS. TEMPERATURE

Figure 79. 80.0 At. % SiGe, Thermoelectric Properties (Sheet 1 of 2)

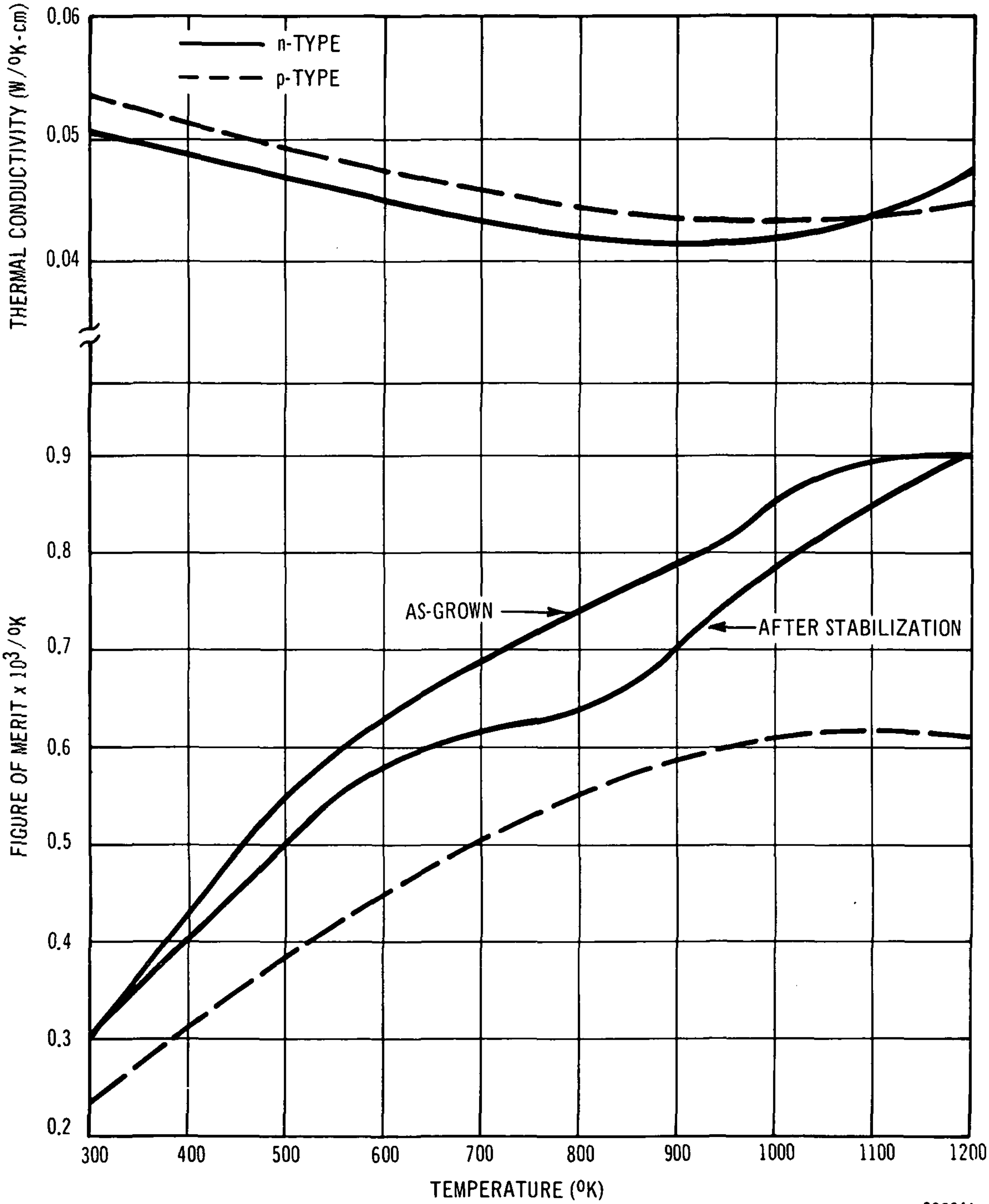

B. THERMAL CONDUCTIVITY AND FIGURE OF MERIT VS. TEMPERATURE

Figure 80. 80.0 At. % SiGe, Thermoelectric Properties (Sheet 2 of 2)

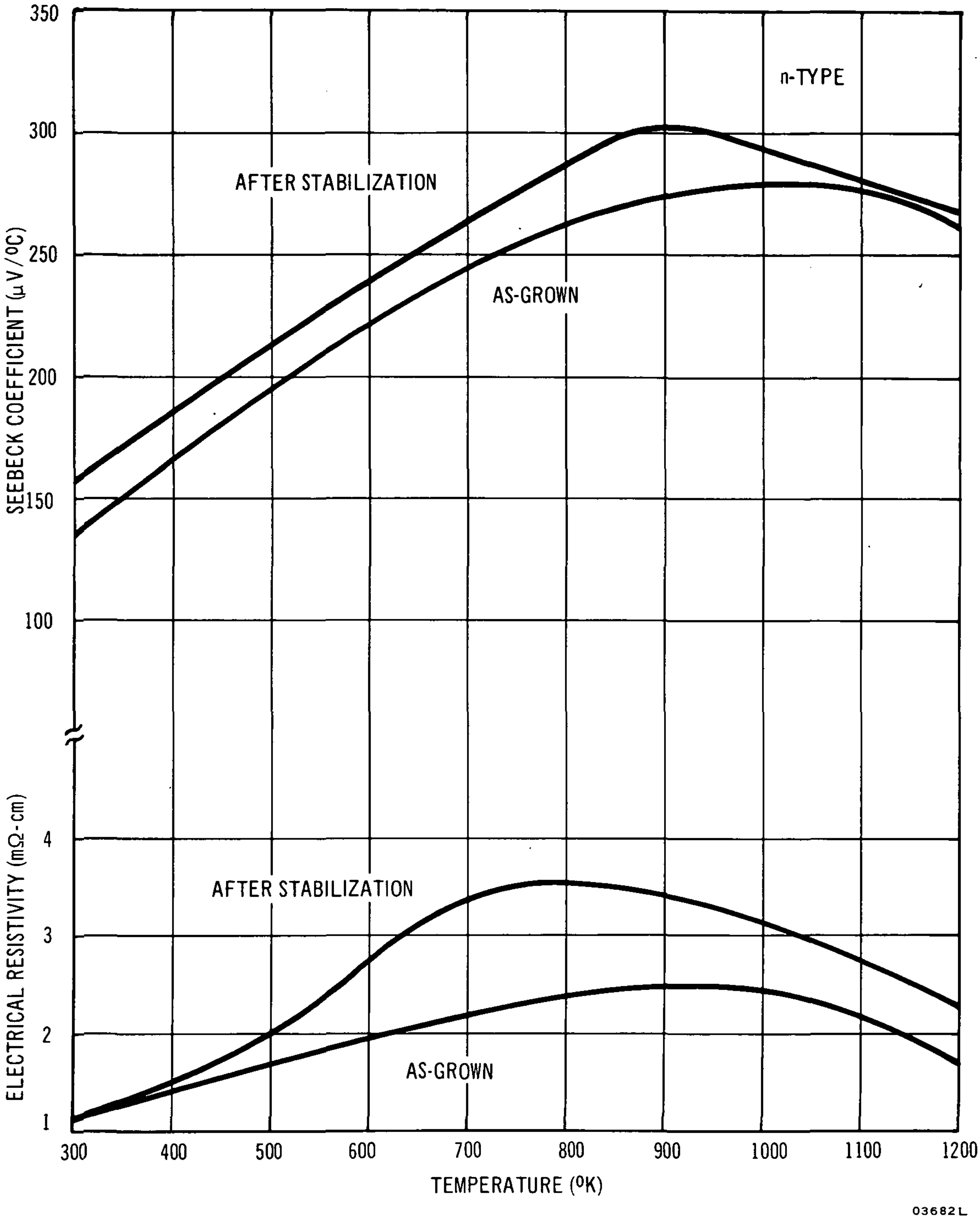

A. SEEBECK COEFFICIENT AND ELECTRICAL RESISTIVITY VS. TEMPERATURE

Figure 81. 70.0 At. % SiGe, Thermoelectric Properties (Sheet 1 of 2)

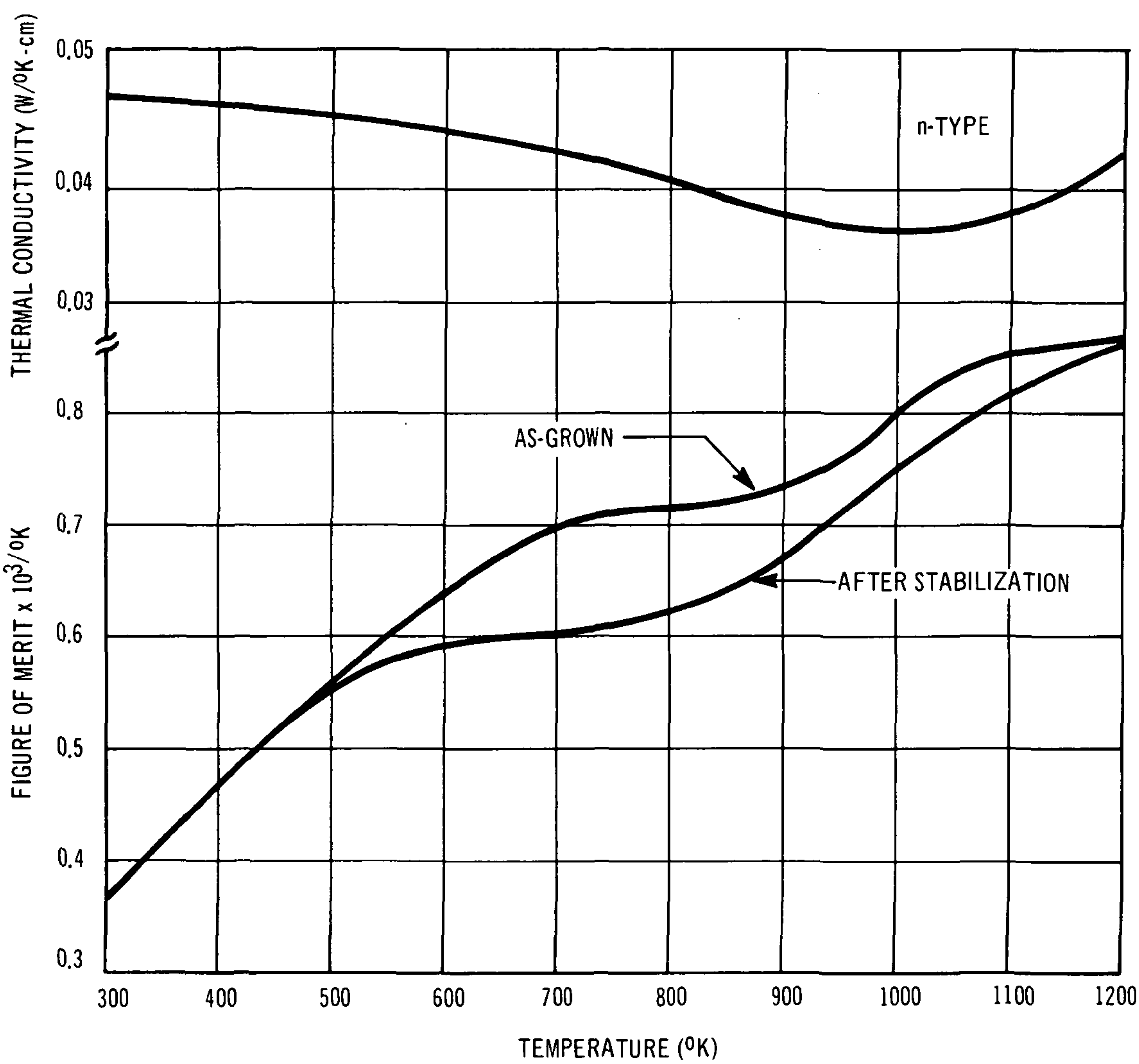

B. THERMAL CONDUCTIVITY AND FIGURE OF MERIT VS. TEMPERATURE

Figure 82. 70.0 AT. % SiGe, Thermoelectric Properties (Sheet 2 of 2)

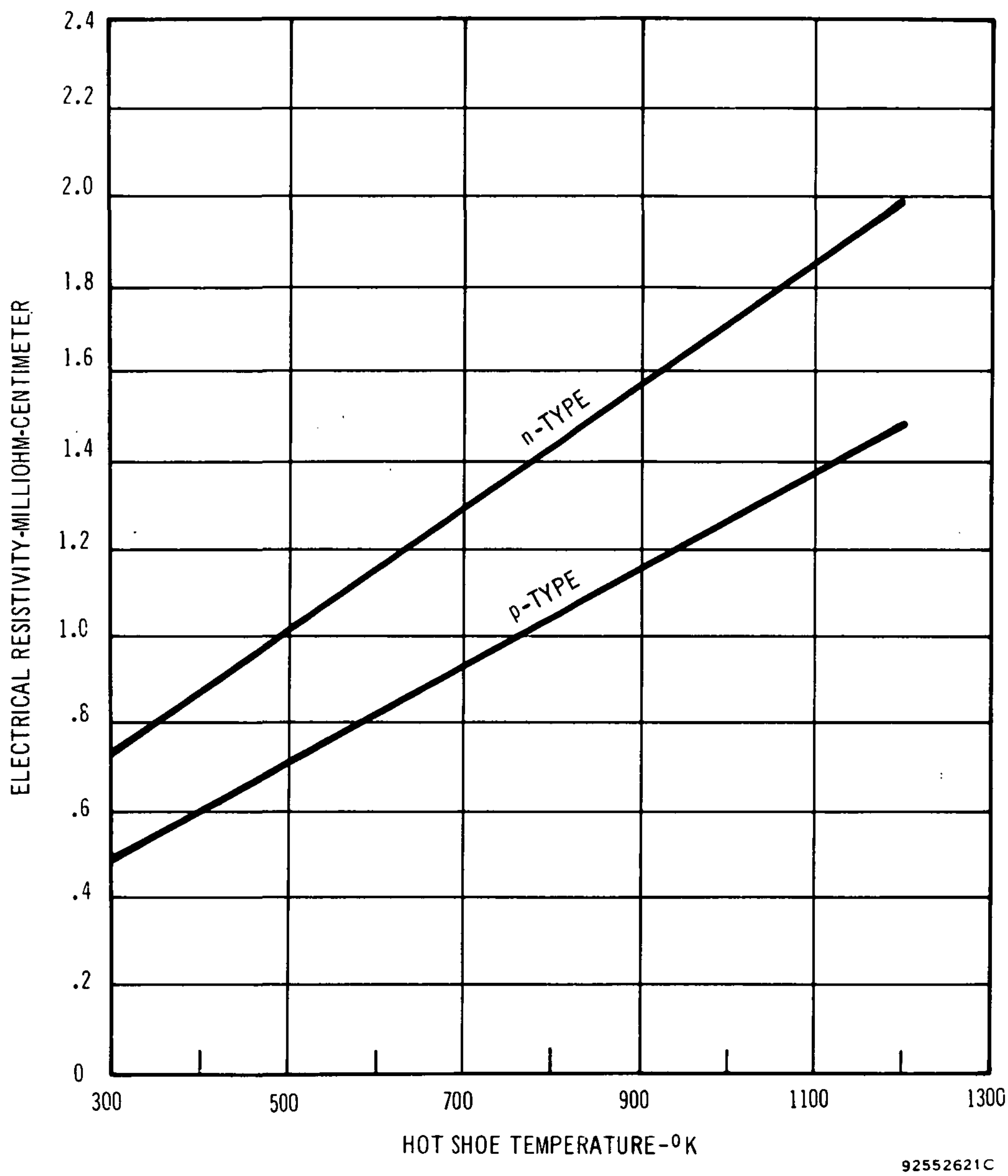

Figure 83. Electrical Resistivity N– Type and P–Type Silicon Molybdenum Alloy

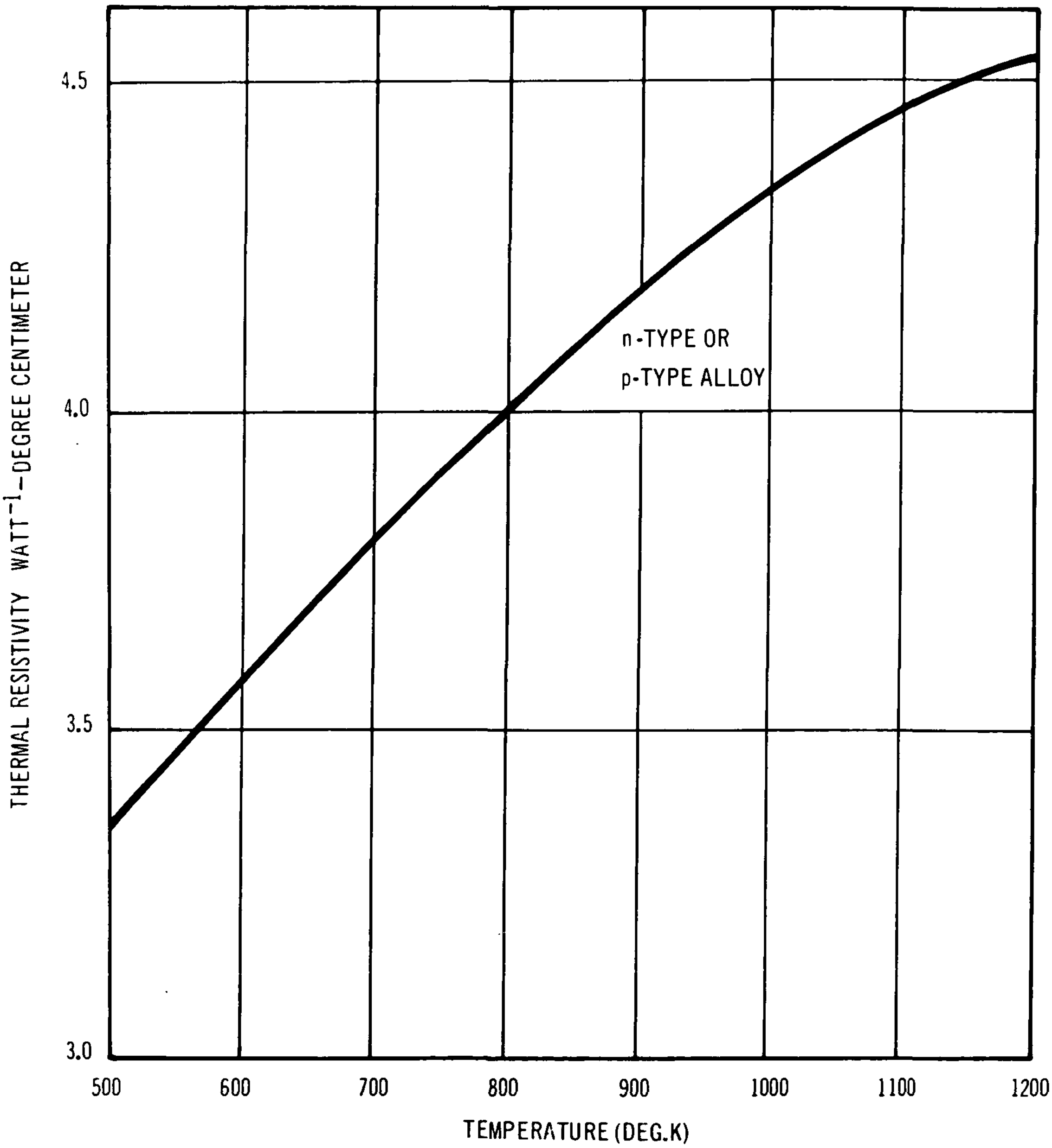

Figure 84. Thermal Resistivity of Silicon Molybdenum Alloy

APPENDIX II

COMPUTER DESIGN PROGRAMS

Page

A. Hybrid Couple Computer Program 161

B. HYGEN Converter Computer Program 167

C. Computer Program Data Tables 174

1. HYGEN Data Tables 174

a. 63.5 at.% Si - n- and p-SiGe 174

b. 3M - 3N PbTe 176

2. HDATA1 Data Tables 178

a. 80.0 at.% Si - n- and p-SiGe 178

b. RCA n-type PbTe 180

D. Input/Output Computer Program Symbols 182

1. Hybrid Couple Program Symbols 182

2. Converter Program Symbols 185

APPENDIX II-A
HYBRID COUPLE COMPUTER PROGRAM

```
/EDIT HYBRID
1-99999
ALLOCATE 9,13,1,6,3
  REAL TEMP(51),XSN(51),XPN(51),XRN(51),XSP(51),XPP(51),XRP(51)
  REAL TEMP2(31),XSN2(31),XPN2(31),XRN2(31),XSP2(31),XPP2(31),XRP
 2(31)
REAL FKI(11)
 REAL FUNCTION MAX1(A,B)
 MAX1=A
 IF(B.GT.A)MAX1=B
 RETURN
 END
 INTEGER FUNCTION XMAX1(A,B)
 XMAX1=A
 IF(B.GT.A)XMAX1=B
 RETURN
 END
 INTEGER FUNCTION XMIN1(A,B)
 XMIN1=A
 IF(B.LT.A)MIN1=B
 RETURN
 END
 REAL FUNCTION MIN1(A,B)
 MIN1=A
 IF(B.LT.A)MIN1=B
 RETURN
 END
C FORM ARRAY OF INPUT VARIABLES FOR SN AND SP
  DO 100 J=1,51
  READ 9002,TEMP(J),XSN(J),XRN(J),XPN(J),XSP(J),XRP(J),XPP(J)
9002  FORMAT(F10.0,6F10.6)
100  TEMP(J)=TEMP(J)+273.
  DO 110 J=1,31
  READ 9009,TEMP2(J),XSN2(J),XRN2(J),XPN2(J),XSP2(J),XRP2(J),XPP2
 (J)
9009  FORMAT(F10.0,6F10.6)
110  TEMP2(J)=TEMP2(J)+273.
DO 398 I=1,11
398 READ 9236,FKI(I)
9236 FORMAT(E12.5)
GKHP=.22
GKA=.22
GKB=.35
GKC=.43
GKD=.332
GKCP=2.37
TTA=2.54*.020
TTB=2.54*.120
TTC=2.54*.250
TTD=2.54*.190
TTCP=2.54*.125
TTHP=2.54*.075
RHOA=.0011
RHOB=.0000216
RHOC=.000039
RHOD=.0000057
RCN=.0002
RCN2=.00035
RCP=.0001
RSH=.001
J=10
PI=3.1415926
SIGP=.567E-11
```

P.1

```
610 ETC=.3
620 THP=273.+1010.
630 TCP=273.+190.
640 THN2=273.+550.
650 EM=1.2
660 GAP=2.54*.030
670 TCN2=TCP
680 THN=THP
690 TCN=THN2
700 QSO=0
710 QSI=0
720  QTA=3.
730 QTB=10.
740 QT=30.
750 FL2B=0.6
760 QH=20.
770 AHA=45.
780 K3=0
790 PRINT 8000
800 8000 FORMAT(//28X,'HYBRID-1F')
810 DO 1000 J4=14,14,2
820 ANP=J4/10.
830 PDUMP ANP
840 DO 1000 J1=10,10
850 ANR=J1/10.
860 PDUMP ANR
870 DO 1000 J3=125,125,25
880 FLP=2.54*J3/100.
890 PDUMP FLP
900 DO 1000 J2=6,6
910 DPHI=J2*1.
920 PDUMP DPHI
930 PHI=DPHI
940 DO 1000 J5=20,20,4
950 RRN=2.54*J5/100.
960 PDUMP RRN
970 K2=0
980 AN=PI*RRN**2
990 AN1=AN*ANR
1000 DTRR=(RRN+GAP)*((1.+1./ANP*(RRN/(RRN+GAP))**2)**.5-1.)
1010 AT=10.
1020 RROP=RRN+GAP+DTRR
1030 RRPO=RRN+GAP
1040 ARROP=.5*(RROP+RRPO)
1050 AP=2.*PI*ARROP*DTRR
1060 AD=AP*2.
1070 FII=5.0*(THN-TCN)/(THN2-TCN2)
1080 FL2=(FLP+TTD-TTA-TTB-TTC)/(FII+1)
1090 FL1=FLP-FL2-TTA-TTB-TTC-TTD
1100   101 XN=(1273.0-THP)/20.0+1.0
1110   XM=(1273.0-TCP)/20.0+1.0
1120   XY=XM-XN+1
1130  YM=MAX1(0.,XM-51.)
1140  XM=MIN1(XM+0.,51.)
1150   YN=MAX1(0.,(1.-XN))
1160  XN=MAX1(XN+0.,1.)
1170 M=XM
1180 RM=XM-M
1190 N=XN
1200 RN=XN-N
1210 SHP=XSP(N)
1220 SCP=XSP(M)
1230   SSN=XSN(1)*YN+XSN(51)*YM+XSN(M)*RM-XSN(N)*RN
1240   SPN=XPN(1)*YN+XPN(51)*YM+XPN(M)*RM-XPN(N)*RN
1250   SRN=XRN(1)*YN+XRN(51)*YM+XRN(M)*RM-XRN(N)*RN
```

P.2

```
      SSP=XSP(1)*YN+XSP(51)*YM+XSP(M)*RM-XSP(N)*RN
      SPP=XPP(1)*YN+XPP(51)*YM+XPP(M)*RM-XPP(N)*RN
      SRP=XRP(1)*YN+XRP(51)*YM+XRP(M)*RM-XRP(N)*RN
      DO 200 II=N,M
      SSN=SSN+XSN(II)
      SPN=SPN+XPN(II)
      SRN=SRN+XRN(II)
      SSP=SSP+XSP(II)
      SPP=SPP+XPP(II)
      200 SRP=SRP+XRP(II)
      SP=SSP/XX
      PP=SPP/XX
      RHOP=SRP/XX
 UP=0
 DO 320 I=N,M-1
 320 UP=UP+((TEMP(I)+TEMP(I+1))/2)*(XSP(I)-XSP(I+1))/20.
 UP=UP/(XX-1.)
 XM=(1273.-TCB)/100.+1.
 XN=(1273.-THP)/100.+1.
 XX=XM-XN+1.
 YN=MAX1(0.,1-XN)
 XN=MAX1(XN,1.)
 YM=MAX1(0.,XM-11)
 XM=MIN1(XM,11.)
 M=XM
 N=XN
 RM=XM-M
 RN=XN-N
 G=FKI(M)*RM-FKI(N)*RN+FKI(1)*YN+FKI(11)*YM
 DO 311 I=N,M
 311 G=G+FKI(I)
 FKI=G/XX
       XN=(1273.0-THN)/20.0+1.0
      XM=(1273.0-TCN)/20.0+1.0
      XX=XM-XN+1
   YM=MAX1(0.,XM-51.)
   XM=MIN1(XM+0.,51.)
      YN=MAX1(0.,(1.-XN))
   XN=MAX1(XN+0.,1.)
 M=XM
 RM=XM-M
 N=XN
 RN=XN-N
 SHN=XSN(N)
 SCN=XSN(M)
     SSN=XSN(1)*YN+XSN(51)*YM+XSN(M)*RM-XSN(N)*RN
     SPN=XPN(1)*YN+XPN(51)*YM+XPN(M)*RM-XPN(N)*RN
     SRN=XRN(1)*YN+XRN(51)*YM+XRN(M)*RM-XRN(N)*RN
     SSP=XSP(1)*YN+XSP(51)*YM+XSP(M)*RM-XSP(N)*RN
     SPP=XPP(1)*YN+XPP(51)*YM+XPP(M)*RM-XPP(N)*RN
     SRP=XRP(1)*YN+XRP(51)*YM+XRP(M)*RM-XRP(N)*RN
      DO 275 II=N,M
     SSN=SSN+XSN(II)
     SPN=SPN+XPN(II)
     SRN=SRN+XRN(II)
     SSP=SSP+XSP(II)
     SPP=SPP+XPP(II)
     275 SRP=SRP+XRP(II)
     SN=SSN/XX
     PN=SPN/XX
     RHON=SRN/XX
 UN=0
 DO 321 I=N,M-1
 321 UN=UN+((TEMP(I)+TEMP(I+1))/2)*(XSN(I)-XSN(I+1))/20.
 UN=UN/(XX-1.)
F3     XN=(373.0-THN2)/20.0+1.0
```

```
1920   XM=(373-TCN2)/20.0+1.0
1930   XX=XM-XN+1
1940 YM=MAX1(0.,XM-31.)
1950  XM=MIN1(XM+0.,31.)
1960   YN=MAX1(0.,(1.-XN))
1970  XN=MAX1(XN+0.,1.)
1980 M=XM
1990 RM=XM-M
2000 N=XN
2010 RN=XN-N
2020 SHN2=XSN2(N)
2030 SCN2=XSN2(M)
2040   SSN2=XSN2(1)*YN+XSN2(31)*YM+XSN2(M)*RM-XSN2(N)*RN
2050   SPN2=XPN2(1)*YN+XPN2(31)*YM+XPN2(M)*RM-XPN2(N)*RN
2060   SRN2=XRN2(1)*YN+XRN2(31)*YM+XRN2(M)*RM-XRN2(N)*RN
2070   SSP2=XSP2(1)*YN+XSP2(31)*YM+XSP2(M)*RM-XSP2(N)*RN
2080   SPP2=XPP2(1)*YN+XPP2(31)*YM+XPP2(M)*RM-XPP2(N)*RN
2090   SRP2=XRP2(1)*YN+XRP2(31)*YM+XRP2(M)*RM-XRP2(N)*RN
2100   DO 210 II=N,M
2110   SSN2=SSN2+XSN2(II)
2120   SPN2=SPN2+XPN2(II)
2130   SRN2=SRN2+XRN2(II)
2140   SSP2=SSP2+XSP2(II)
2150   SPP2=SPP2+XPP2(II)
2160   210 SRP2=SRP2+XRP2(II)
2170   SN2=SSN2/XX
2180   PN2=SPN2/XX
2190   RHON2=SRN2/XX
2200 UN2=0
2210 DO 322 I=N,M-1
2220 322 UN2=UN2+((TEMP2(I)+TEMP2(I+1))/2)*(XSN2(I)-XSN2(I+1))/20.
2230 UN2=UN2/(XX-1.)
2240 HKA=GKA*AN1/TTA
2250 HKB=GKB*AN/TTB
2260 HKC=GKC*AN/TTC
2270 HKD=GKD*AD/TTD
2280 RA=TTA/AN1*RHOA
2290 RB=TTB/AN*RHOB
2300 RC=TTC/AN*RHOC
2310  RD=TTD/AD*RHOD
2320 EOC=SP*(THP-TCP)+SN*(THN-TCN)+SN2*(THN2-TCN2)
2330 RN=FL1/AN1*RHON+2.*RCN/AN1+FL2/AN*RHON2+2.*RCN2/AN+RA+RB+RC
2340 RP=FLP/AP*RHOP+2.*RCP/AP+RD
2350 R=RN+RP+RSH
2360 CUR=EOC/((1+EM)*R)
2370 RL=EM*R
2380 PO=CUR**2*RL
2390 DTP=THP-TCP
2400 DTN=THN-TCN
2410 DTN2=THN2-TCN2
2420 QOC=PP*AP/FLP*DTP+CUR*SCP*TCP+.5*CUR**2*RP+.5*CUR*UP*DTP
2430 DT=DTP+QOC/HKD
2440 QI2C=PN2*AN/FL2*DTN2+CUR*SCN2*TCN2+.5*CUR**2*RN+.5*CUR*(UN*DTN+UN
     2*DTN2)
2450 TCN2=TCP-QOC/HKD+QI2C/HKC
2460 TCB=TCP-QOC/HKD
2470 QI1H=PN*AN1/FL1*DTN+CUR*SHN*THN-.5*CUR**2*RN-.5*CUR*(UN*DTN+UN2*D
     TN2)
2480 THN=THP-QI1H/HKA
2490 QI1C=PN*AN1/FL1*DTN+CUR*SCN*TCN+.5*CUR**2*RN+.5*CUR*(UN*DTN+UN2*D
     TN2)
2500 QI2H=PN2*AN/FL2*DTN2+CUR*SHN2*THN2-.5*CUR**2*RN-.5*CUR*(UN*DTN+UN
     2*DTN2)
2510 TCN=THN2+QI1C/HKB
2520 FL2A=FL2
2530 FL2=(PN2*AN*DTN2)/(PN*AN1/FL1*DTN+CUR*(SCN*TCN-SHN2*THN2)+1.0*CUR
```

```
     **2*RØ+CUR*(UØ*DIN+UN2*DIN2))
FL2B=FL2
FL1=FLP+TTD-FL2-TTA-TTB-TTC
HKP=PP*AP/FLP
HKN=PN*AN1/FL1
HKN2=PN2*AN/FL2
HKT=(HKP*HKD)/(HKP+HKD)+((HKN*HKN2*HKA*HKB*HKC)/((HKN*HKN2*HKA*HK
B)+(HKN*HKN2*HKA*HKC)+(HKN*HKN2*HKB*HKC)+(HKN*HKA*HKB*HKC)+(HKN2*
HKA*HKB*HKC)))
QHA=QH
QH=HKT*DT+CUR*(SHP*THP+SHN*THN)-.5*CUR**2*R-.5*CUR*(UP*DTP+UN*DTN
+UN2*DTN2)
QHB=QH
 715 IF (ABS(QHA-QH)/QHA .LE. (.ØØ1))IF(ABS(FL2A-FL2B)/FL2A.LE.(.
ØØ1))GO TO 7Ø3
K2=K2+1
IF(K2.GT.9Ø) PDUMP K2,FL2,QS,QH,QI2C,QI1H,QI1C,QI2H,QSO,QT,QSI
IF(K2.GE.15Ø)GO TO 9ØØØ
GO TO 1Ø1
AT=((SQRT(AH))+2.54*.Ø2Ø)**2.
7Ø3AH=QH/PHI
73Ø CONTINUE
AHH=((SQRT(AT))-2.54*.Ø2Ø)**2.
RH=((QT*(1-(PI*RROP**2)/AH)-QSO)/(AH-PI*RROP**2))/TTHP
IF(AH.LE.(.1))AH=PI*RROP**2+.2
RRTO=SQRT(AH/PI)
QK=Ø
DO 8Ø2 NNN=1,1Ø
RR=RROP+((NNN-.5)*(RRTO-RROP))/1Ø.
THR=RH/(2.*GKHP)*(RRTO**2*LOG(RR/RROP)-.5*(RR**2-RROP**2))+THP
RIC=-((QT-PO)*(1.-(PI*RROP**2)/AH)-QSO/(AH-PI*RROP**2))/TTCP
TCR=RIC/(2.*GKCP)*(RRTO**2*LOG(RR/RROP)-.5*(RR**2-RROP**2))+TCB
IF(TCR.LE.5Ø.)TCR=5Ø.
DR=(RRTO-RROP)/1Ø.
802 QK=QK+(THR-TCR)*RR*DR
QSO=(2.*PI*FKI)/(FLP+TTD)*QK
EI=1./(1./EHP+1./ETC-1.)
QSI=PI*(RRPO**2.-RRN**2)*EI*SIGP*(THP**4.-TCB**4.)
QS=QSO+QSI
QT=QH+QS
PHIA=PHI
PHI=QT/AH
AHB=AHA
AHA=AH
AH=AHA+(DPHI-PHI)*(AHA-AHB)/(PHI-PHIA)
 IF(ABS(AHA-AH)/AHA .LE. (.ØØ1))IF(ABS(DPHI-PHI)/DPHI .LE.(.ØØ1))
GO TO 7Ø5
K3=K3+1
IF(K3.EQ.99)IF(AH.LT.(PI*RROP**2))GO TO 9112
IF(K3.GE.1ØØ)GO TO 9112
GO TO 73Ø
7Ø5EL=PO/CUR
PDUMP AH
ETA=PO/QT
THPC=THP-273.Ø
TCPC=TCP-273.Ø
TCBC=TCB-273.Ø
THN2C=THN2-273.Ø
TCN2C=TCN2-273.Ø
TCNC=TCN-273.Ø
THNC=THN-273.Ø
PRINT 91ØØ,THPC,AN,FL1,ETA
91ØØ FORMAT('     THPC='F7.1,7X,'AN='F7.4,6X,'FL1='F7.4,6X,'ETA='F
7.5)
PRINT 91Ø1,TCPC,AP,FL2,PO
91Ø1 FORMAT('     TCPC='F7.1,7X,'AP='F7.4,6X,'FL2='F7.4,7X,'PO='F7
```

```
PRINT 9102,TCBC,DTRR,QT,EL
9102 FORMAT('      TCBC='F7.1,5X,'DTRR='F7.4,7X,'QT='F7.3,5X,'VOLT=
'F7.4)
PRINT 9103,THNC,THN2C,QS,R
9103 FORMAT('      THNC='F7.1,4X,'THN2C='F7.2,7X,'QS='F7.3,8X,'R='F
7.5)
PRINT 9104,TCNC,TCN2C,QSO,PHI
9104 FORMAT('      TCNC='F7.1,4X,'TCN2C='F7.2,6X,'QSO='F7.3,6X,'PHI
='F7.4//)
1000 CONTINUE
STOP
9000 PRINT 9001
9001 FORMAT(' TOO MANY SEARCHES FOR QH')
GO TO 1000
9110 PRINT 9111
9111 FORMAT('  TOO MANY SEARCHES FOR AH')
GO TO 1000
9112 PRINT 9113
9113 FORMAT ('  AH.LT.COUPLE AREA')
GO TO 1000
```

APPENDIX II-B
HYGEN CONVERTER COMPUTER PROGRAM

```
/RESEQ HYGEN1
READY
/EDIT
1-500
C T 01/08/70
 ALLOCATE 7,10,1,11,3
   REAL TEMP(51),XSN(51),XPN(51),XRN(51),XSP(51),XPP(51),XRP(51)
    REAL TEMP2(31),XSN2(31),XPN2(31),XRN2(31),XSP2(31),XPP2(31),XR
 P2(31)
  REAL FUNCTION MAX1(A,B)
  MAX1=A
  IF(B.GT.A)MAX1=B
  RETURN
  END
  INTEGER FUNCTION XMAX1(A,B)
  XMAX1=A
  IF(B.GT.A)XMAX1=B
  RETURN
  END
  INTEGER FUNCTION XMIN1(A,B)
  XMIN1=A
  IF(B.LT.A)MIN1=B
  RETURN
  END
  REAL FUNCTION MIN1(A,B)
  MIN1=A
  IF(B.LT.A)MIN1=B
  RETURN
  END
C  FORM ARRAY OF INPUT VARIABLES FOR SN AND SP
   DO 100 J=1,51
   READ 9002,TEMP(J),XSN(J),XRN(J),XPN(J),XSP(J),XRP(J),XPP(J)
 9002  FORMAT(F10.0,6F10.6)
 100  TEMP(J)=TEMP(J)+273.
   DO 110 J=1,31
   READ 9009,TEMP2(J),XSN2(J),XRN2(J),XPN2(J),XSP2(J),XRP2(J),XPP
 2(J)
 9009  FORMAT(F10.0,6F10.6)
 110  TEMP2(J)=TEMP2(J)+273.
 GKHP=.22
 GKA=.22
 GKB=.86
 GKC=.43
 GKD=.332
 GKE=.465
 GKCPBE=1.3
 TTA=2.54*.020
 TTB=2.54*.120
 TTC=2.54*.250
 TTD=2.54*.190
 TTCP=2.54*.250
 TTHP=2.54*.075
 TTCASE=2.54*.200
 RHOA=.0011
 RHOB=.0000216
 RHOC=.000009
```

```
510-1020
  510  RHOD=.0000057
  520  RCN=.0002
  530  RCN2=.00005
  540  RCP=.0001
  550  RSH=.001
  560  J=10
  570  PI=3.1415926
  580  SIGP=.567E-11
  590 ER=.85
  600  EHP=.6
  610  ETC=.3
  620  EFC=.85
  630  THP=273.+926.
  640  DO 1000 I1=500,538,38
  650 THN2=I1+273.
  660 THN2C=THN2-273.
  670 PDUMP THN2C
  680  DO 1000 I2=122,232,55
  690  TCP=I2+273.
  700  TCPC=TCP-273.
  710  PDUMP TCPC
  720  TCV=273.+25.
  730  TCA=73.
  740  ANR=.7
  750  EM=1.2
  760  DTRR=2.54*.055
  770  FAS=2.54*.040
  780  GAP=2.54*.030
  790  FLP=2.54*1.250
  800  RHCU=.65E-8*TCP-.35E-6
  810  RRN=2.54*.1875
  820  AN=PI*RRN**2.
  830  ANI=ANR*AN
  840  RROP=RRN+GAP+DTRR
  850  RRPO=RRN+GAP
  860  ARROP=.5*(RROP+RRPO)
  870  AP=2.*PI*ARROP*DTRR
  875 ANP=AN/AP
  880  AD=2.*AP
  890  FKIE=.00016
  900  FKIC=.001
  910  CAPFL=2.54*6.75
  920  CAPW=2.54*3.50/.866
  930  CAPH=2.54*3.50
  940  ACAP=CAPFL*CAPW
  950  CWFUEL=2.5
  960  PZ=635.
  970  D=(GKHP*TTHP)/(EHP*SIGP*THP**3.*PI*RROP**2.)
  980  FLG=FLP+TTD+TTHP+2.54*0.5+CAPH
  990  FLINS=FLP
 1000  FH=2.54*1.01
 1010  AH=FH**2.
 1020  AT=(FH+FAS)**2.
```

```
1030-1250
 1030 ASTUD=2.*PI*(.550**2-.200**2)*6.45
 1040 QH=5.0
 1050 C  INITIALIZED CONDITIONS
 1060 (THR=THP+30;THN=TCP;THF=THR+50.;TCN=THN2;TCN2=TCP;FI=5.*(THN-TCN)
       /(THN2-TCN2);FL2=(FLP+TTD-TTA-TTB-TTC)/(FI+1.0);FL1=FLP-FL2-TTA-T
       TB-TTC+TTD;ETAN=0.5;ETAF=.5;GQT=4000.;GPO=250.;GEL=28.;)
 1070 K1=0
 1080 K3=0
 1090 K5=0
 1100 101 XN=(1273.0-THP)/20.+1.0
 1110 (XM=(1273.0-TCP)/20.0+1.0;XX=XM-XN+1;YM=MAX1(0.,XM-51.);XM=MIN1(X
       M+0.,51.);YN=MAX1(0.,(1.-XN));XN=MAX1(XN+0.,1.);M=XM;RM=XM-M;N=XN
       ;RN=XN-N;SHP=XSP(N);SCP=XSP(M);SSN=XSN(1)*YN+XSN(51)*YM+XSN(M)*RM
       -XSN(N)*RN;SPN=XPN(1)*YN+XPN(51)*YM+XPN(M)*RM-XPN(N)*RN;)
 1120 (SRN=XRN(1)*YN+XRN(51)*YM+XRN(M)*RM-XRN(N)*RN;SSP=XSP(1)*YN+XSP(5
      1)*YM+XSP(M)*RM-XSP(N)*RN;SPP=XPP(1)*YN+XPP(51)*YM+XPP(M)*RM-XPP(
      N)*RN;SRP=XRP(1)*YN+XRP(51)*YM+XRP(M)*RM-XRP(N)*RN;DO200II=N,M;SS
      N=SSN+XSN(II);SPN=SPN+XPN(II);SRN=SRN+XRN(II);)
 1130 (SSP=SSP+XSP(II);SPP=SPP+XPP(II);200SRP=SRP+XRP(II);SP=SSP/XX;PP=
      SPP/XX;RHOP=SRP/XX;UP=0;DO320I=N,M-1;320UP=UP+((TEMP(I)+TEMP(I+1)
      )/2)*(XSP(I)-XSP(I+1))/20.;UP=UP/(XX-1.);XN=(1273.0-THN)/20.0+1.0
      ;XM=(1273.0-TCN)/20.0+1.0;XX=XM-XN+1;YM=MAX1(0.,XM-51.);)
 1140 (XM=MIN1(XM+0.,51.);YN=MAX1(0.,(1.-XN));XN=MAX1(XN+0.,1.);M=XM;RM
      =XM-M;N=XN;RN=XN-N;SHN=XSN(N);SCN=XSN(M);SSN=XSN(1)*YN+XSN(51)*YM
      +XSN(M)*RM-XSN(N)*RN;SPN=XPN(1)*YN+XPN(51)*YM+XPN(M)*RM-XPN(N)*RN
      ;SRN=XRN(1)*YN+XRN(51)*YM+XRN(M)*RM-XRN(N)*RN;)
 1150 (SSP=XSP(1)*YN+XSP(51)*YM+XSP(M)*RM-XSP(N)*RN;SPP=XPP(1)*YN+XPP(5
      1)*YM+XPP(M)*RM-XPP(N)*RN;SRP=XRP(1)*YN+XRP(51)*YM+XRP(M)*RM-XRP(
      N)*RN;DO205II=N,M;SSN=SSN+XSN(II);SPN=SPN+XPN(II);SRN=SRN+XRN(II)
      ;SSP=SSP+XSP(II);SPP=SPP+XPP(II);205SRP=SRP+XRP(II);)
 1160 (SN=SSN/XX;PN=SPN/XX;RHON=SRN/XX;UN=0;DO321I=N,M-1;321UN=UN+((TEM
      P(I)+TEMP(I+1))/2)*(XSN(I)-XSN(I+1))/20.;UN=UN/(XX-1.);XN=(873.0-
      THN2)/20.0+1.0;XM=(873-TCN2)/20.0+1.0;XX=XM-XN+1;YM=MAX1(0.,XM-31
      .);XM=MIN1(XM+0.,31.);IF(XM.LE.1.0)XM=1.0;)
 1170 (YN=MAX1(0.,(1.-XN));XN=MAX1(XN+0.,1.);M=XM;RM=XM-M;N=XN;RN=XN-N;
      SHN2=XSN2(N);SCN2=XSN2(M);SSN2=XSN2(1)*YN+XSN2(31)*YM+XSN2(M)*RM-
      XSN2(N)*RN;SPN2=XPN2(1)*YN+XPN2(31)*YM+XPN2(M)*RM-XPN2(N)*RN;SRN2
      =XRN2(1)*YN+XRN2(31)*YM+XRN2(M)*RM-XRN2(N)*RN;)
 1180 (SSP2=XSP2(1)*YN+XSP2(31)*YM+XSP2(M)*RM-XSP2(N)*RN;SPP2=XPP2(1)*Y
      N+XPP2(31)*YM+XPP2(M)*RM-XPP2(N)*RN;SRP2=XRP2(1)*YN+XRP2(31)*YM+X
      RP2(M)*RM-XRP2(N)*RN;DO210II=N,M;SSN2=SSN2+XSN2(II);SPN2=SPN2+XPN
      2(II);SRN2=SRN2+XRN2(II);SSP2=SSP2+XSP2(II);)
 1190 (SPP2=SPP2+XPP2(II);210SRP2=SRP2+XRP2(II);SN2=SSN2/XX;PN2=SPN2/XX
      ;RHON2=SRN2/XX;UN2=0;DO322I=N,M-1;322UN2=UN2+((TEMP2(I)+TEMP2(I+1
      ))/2)*(XSN2(I)-XSN2(I+1))/20.;UN2=UN2/(XX-1.);)
 1200 (HKA=GKA*AN1/TTA;HKB=GKB*AN/TTB;HKC=GKC*AN/TTC;HKD=GKD*AD/TTD;RA=
      TTA/AN1*RHOA;RB=TTB/AN*RHOB;RC=TTC/AN*RHOC;RD=TTD/AD*RHOD;)
 1210  EOC=SP*(THP-TCP)+SN*(THN-TCN)+SN2*(THN2-TCN2)
 1220  RN=FL1/AN1*RHON+2.*RCN/AN1+FL2/AN*RHON2+2.*RCN2/AN+RA+RB+RC
 1230  RP=FLP/AP*RHOP+2.*RCP/AP+RD
 1240  RCONN=RHCU*SQRT(AT)/(RROP*2.54*.020)
 1250  RSH=2*PI*RHOA*TTHP/ALOG(RROP/(RRN*ANR))
```

```
1260-1680
 1260  R=RN+RP+RSH+RCONN
 1270  CUR=EOC/((1+EM)*R)
 1280  RL=EM*R
 1290 EL=CUR*RL
 1300  PO=CUR**2*RL
 1310  DTP=THP-TCP
 1320  DTN=THN-TCN
 1330  DTN2=THN2-TCN2
 1340  QOC=PP*AP/FLP*DTP+CUR*SCP*TCP+.5*CUR**2*RP+.5*CUR*UP*DTP
 1350  DT=DTP+QOC/HKD
 1360  QI2C=PN2*AN/FL2*DTN2+CUR*SCN2*TCN2+.5*CUR**2*RN+.5*CUR*(UN*DTN+U
      N2*DTN2)
 1370  TCN2=TCP-QOC/HKD+QI2C/HKC
 1380 TCB=TCP-QOC/HKD
 1390  QI1H=PN*AN1/FL1*DTN+CUR*SHN*THN-.5*CUR**2*RN-.5*CUR*(UN*DTN+UN2*
      DTN2)
 1400  THN=THP-QI1H/HKA
 1410  QI1C=PN*AN1/FL1*DTN+CUR*SCN*TCN+.5*CUR**2*RN+.5*CUR*(UN*DTN+UN2*
      DTN2)
 1420  QI2H=PN2*AN/FL2*DTN2+CUR*SHN2*THN2-.5*CUR**2*RN-.5*CUR*(UN*DTN+U
      N2*DTN2)
 1430  TCN=THN2+QI1C/HKB
 1440  FL2=(PN2*AN*DTN2)/(PN*AN1/FL1*DTN+CUR*(SCN*TCN-SHN2*THN2)+1.0*CU
      R**2*RN+CUR*(UN*DTN+UN2*DTN2))
 1450  FL1A=FL1
 1460  FL1=FLP+TTD-FL2-TTA-TTB-TTC
 1470   FL1B=FL1
 1480   FL1=(FL1A+FL1B)/2.
 1490  HKP=PP*AP/FLP
 1500  HKN=PN*AN1/FL1
 1510  HKN2=PN2*AN/FL2
 1520  HKT=(HKP*HKD)/(HKP+HKD)+((HKN*HKN2*HKA*HKB*HKC)/((HKN*HKN2*HKA*H
      KB)+(HKN*HKN2*HKA*HKC)+(HKN*HKN2*HKB*HKC)+(HKN*HKA*HKB*HKC)+(HKN2
      *HKA*HKB*HKC)))
 1530  QHA=QH
 1540  QH=HKT*DT+CUR*(SHP*THP+SHN*THN)-.5*CUR**2*R-.5*CUR*(UP*DTP+UN*DT
      N+UN2*DTN2)
 1550  QHB=QH
 1560    IF (ABS(QHA-QH)/QHA .LE. (.001))IF(ABS(FL1A-FL1B)/FL1A.LE.(.00
      1))GO TO 703
 1570  K1=K1+1
 1580   IF(K1.GT.180) PDUMP K1,QH,QHA,QHB,FL1,FL2,FL1A,FL1B
 1590  IF(K1.GE.200)GO TO 9000
 1600  GO TO 101
 1610 703  QSI=PI*(RRPO**2.-RRN**2.)*(THP-TCB)*FKIC/(FLP+TTD-TTA)
 1620  IGCPL=GEL/EL
 1630  GPO1=2.*IGCPL*PO
 1640  GCPL=2.*IGCPL
 1650 505 IGCPL=SQRT(GCPL+1)+K3
 1660 GCPL=IGCPL**2.
 1670  GPO1=PO*GCPL
 1680  GEL1=EL*GCPL/2.
```

1690-2170

```
IF(GEL1.GE.GEL)IF(GPO1.GE.GPO) GO TO 500
K3=K3+1
IF(K3.GE.100)GO TO 9005
GO TO 505
500 GPO=GPO1
GEL=GEL1
GAT=GCPL*AT
GQSO=(GAT-GCPL*AH)*FKIE*(THF-TCP)/FLP+(GCPL*AH-GCPL*PI*RROP**2.)*
FKIE*(THR-TCP)/FLP
GQH=GCPL*QH
GAC=GAT
ACASE=(SQRT(GAC)+2.*FLP)**2.+4.*FLG*(SQRT(GAC)+FLP)
GQCASE=ACASE*FKIE*1.25*(THF-TCV)/FLINS
GQSI=GCPL*QSI
GQT=(GQH+GQSO+GQSI+GQCASE)*1.05
B=RROP**2.*PI/AH
Z=D**.1*B**.125
IF(Z.LE.(0.9))GO TO 525
ETAN=-14.971+42.821*Z-43.221*Z**2.+19.457*Z**3.-3.295*Z**4.
GO TO 530
525 ETAN=0.1126*Z+.6579*Z**2.-1.365**Z**3.+1.4342*Z**4.
530 IF(ETAN.GE.1.0)ETAN=1.0
EN=1./(1./EFC+1./(EHP*ETAN)-1.)
TFC=((GQH+GQSO+GQSI)/(SIGP*EN*GAC)+THP**4.)**.25
THR=THP+420.*(1.-ETAN)/1.8
535 TCRR=TCB-QH/(GKE*ASTUD)-(GQH+GQSO+GQSI-GPO)*TTCP/(GKCPBE*GAC)
AFIN=(GQH-GPO+GQSO+GQSI)/(SIGP*ETAF*ER*(TCRR**4.-TCA**4.))
IF(ETAF.GE.1.0)ETAF=1.0
IF(ETAF.LE.(.01))ETAF=.01
540 IF(ETAF.LT.(0.58))GO TO 545
ZF=360.516-1846.222*ETAF+3502.456*ETAF**2.-2916.253*ETAF**3.+901
.006*ETAF**4.
GO TO 550
545 ZF=0.002+5.504*ETAF-17.629*ETAF**2.+29.950*ETAF**3.-19.505*ET
AF**4.
550 BF=GAC/AFIN
DF=(ZF/BF**.125)**10.
TTFIN=ER*SIGP*TCRR**3.*GAC*DF/GKCPBE
IF(ABS(TTCP-TTFIN).LE.(.01*TTCP))GO TO 555
ETAF1=ETAF
ETAF=ETAF1-ETAF1*(TTFIN-TTCP)/TTFIN
ETAF=(7*ETAF1+ETAF)/8.
IF(ETAF.GE.1.0)ETAF=1.0
IF(ETAF.LE.(.01))ETAF=.01
IF(K5.GE.98)GO TO 9114
K5=K5+1
GO TO 535
C WEIGHT CALCULATIONS FOLLOW;W PREFIX=WEIGHT,D PREFIX=DENSITY
555 DSIMO=2.80
DSIGE=3.535
DPBTE=8.15
DNI=8.20
```

2180-2610

```
2180 DAL2O3=3.85
2190 DALMN=2.82
2200 DSS=8.02
2210 DBRYL=1.85
2220 DCU=8.95
2230 DMINK=.32
2240 DASTRO=.838
2250 DMOLY=10.2
2260 DPLAT=21.5
2270 DZRO2=.485
2280 DSIO2=.056
2290 DQURTZ=.16
2300 DZCAR=.225
2310 DAU=19.6
2320 DW=19.3
2330 C ASSUME FOR TH=1000 DEGREES C,30% MOLY,60% NI,AND 10% AL.  FOR
      TH=1100 DEGREES C USE 30% MOLY-,ZRO2,15% MOLY-ASTRO AND 10%
      AL-SIO2
2340 C FOR TH=1100 DEGREES C,35% PLATINUM WITH DZRO2,45% PLATINUM WITH
       DASTRO,AND 20% DNI WITH DASTRO.
2350 C DFOIL=.35*(.5*DZRO2*9.75+DPLAT*.25)/10.+.45*(.5*DASTRO*9.75+DPL
      AT*.25)/10.+.20*(.5*DASTRO*9.75+DNI*.25)10.
2360 DFOIL=.30*(.7*DZRO2*8.33+DMOLY*.25)/8.58+.15*(.5*DASTRO*10.+DMOLY
      *.25)/10.25+.48*(.5*DASTRO*10.+DNI*.25)/10.25+.07*(DSIO2*8.33+DAL
      MN*.25)/8.58
2370 WHP=DSIMO*TTHP*AH
2380 WSIGE=DPBTE*AN*FL2+DSIGE*ANI*FL1+DSIGE*AP*FLP
2390 C PARTS=AU PIECE+AU SPACER+S.S.SHOES+SIMO NSHOE+W COLD SHOE
2400 WPARTS=.573+DAU*.040*PI*.25**2.*16.38/4.+DSS*.060*2.54*AN+DSIMO*A
      NI*2.54*.020+DW*.020*ANI*2.54
2410 C WEIGHT OF NUT=WNUT=S.S.NUT AND WASHER+COLD STACK WITH W P.C.S.
2420 WNUT=5.71+18.846
2430 WCONN=DCU*(FH+FAS)*2.*RROP*2.54*.020
2440 WTOT=WHP+WSIGE+WPARTS+WNUT+WCONN
2450 WGCPL=WTOT*GCPL
2460 WFIN=DBRYL*AFIN*TTFIN
2470 WFOIL=DFOIL*FLP*((SQRT(GAC)+2.*FLP)**2.+4.*(SQRT(GAC)+FLP)*FLG+GA
      T-GCPL*PI*RROP**2.)
2480 WCASE=DBRYL*ACASE*TTCASE*1.3
2490 WGEN=(WGCPL+WFIN+WFOIL+WCASE)/453.59
2500 WGPO=GPO/WGEN
2510 GETA=GPO/GQT
2520 TFCC=TFC-273.
2530 THRC=THR-273.
2540 THPC=THP-273.0
2550 TCPC=TCP-273.0
2560 TCRRC=TCRR-273.
2570 TCBC=TCB-273.0
2580 THN2C=THN2-273.0
2590 TCN2C=TCN2-273.0
2600 TCNC=TCN-273.0
2610 THNC=THN-273.0
```

```
2620-99999
  2620 TCVC=TCV-273.0
  2630 TCAC=TCA-273.0
  2640 FL1=FL1/2.54
  2650 FL2=FL2/2.54
  2660  DTRR=DTRR/2.54
  2670 GAT=GAT/6.45
  2680 PHI=(GQH+GQSO+GQSI)/(GCPL*AH)
  2690 AH=AH/6.45
  2700 AFIN=AFIN/6.45
  2710 ETA=PO/(QH+QSI+GQSO/GCPL)
  2720 PDUMP WGPO,WGEN,GQSO,GQH,GQSI,GQCASE,GQT,GCPL,GAT,GPO,GEL,THRC,TF
       CC,ETAN,TTFIN,ETAF,AFIN,WGCPL,WTOT,WFIN,WFOIL,WCASE,ETA,TCRRC,DFO
        IL
  2730 PRINT 9100,THPC,AN,FL1,GETA
  2740 9100 FORMAT('     THPC='F7.1,7X,'AN='F7.4,6X,'FL1='F7.4,5X,'GETA='
        F7.5)
  2750 PRINT 9101,TCPC,AP,FL2,PO
  2760 9101 FORMAT('     TCPC='F7.1,7X,'AP='F7.4,6X,'FL2='F7.4,7X,'PO='F7
       .4)
  2770 PRINT 9102,TCBC,DTRR,GQT,EL
  2780 9102 FORMAT('     TCBC='F7.1,5X,'DTRR='F7.4,6X,'GQT='F7.0,7X,'EL='
       F7.4)
  2790 PRINT 9103,THNC,THN2C,WGPO,R
  2800 9103 FORMAT('     THNC='F7.1,4X,'THN2C='F7.2,5X,'WGPO='F7.3,8X,'R=
       'F7.5)
  2810 PRINT 9104,TCNC,TCN2C,WGEN,PHI
  2820 9104 FORMAT('     TCNC='F7.1,4X,'TCN2C='F7.2,5X,'WGEN='F7.2,6X,'PH
       I='F7.4//)
  2830 1000 CONTINUE
  2840 STOP
  2850 9000 PRINT 9001
  2860 9001 FORMAT(' TOO MANY SEARCHES FOR QH')
  2870 9005 PRINT 9006
  2880 9006 FORMAT('   TOO MANY SEARCHES FOR GCPL')
  2890 GO TO 1000
  2900 9110 PRINT 9111
  2910 9111 FORMAT('   FUEL CAPSULE EXCEEDS GAT')
  2920 GO TO 1000
  2930 GO TO 1000
  2940 9114 PRINT 9115
  2950 9115 FORMAT('    TOO MANY SEARCHES FOR ETAF')
  2960 GO TO 1000
```

APPENDIX II-C
COMPUTER PROGRAM DATA TABLES

1. HYGEN Data Tables

a. 63.5 at.% Si - n- and p-SiGe

Seq #	K_p	°C Temp	S_N	ρ_N	K_N	S_p	ρ_p
10	SIGE1	500					
20	.051500	1000	.000263	.001860	.047000	.000284	.002870
30	.049500	980	.000267	.001950	.045400	.000282	.002820
40	.048000	960	.000270	.002050	.044200	.000279	.002770
50	.046900	940	.000274	.002150	.043100	.000277	.002720
60	.045900	920	.000278	.002260	.042200	.000274	.002670
70	.045100	900	.000281	.002370	.041400	.000272	.002620
80	.044500	880	.000285	.002490	.040800	.000270	.002580
90	.044200	860	.000289	.002620	.040190	.000268	.002530
100	.043900	840	.000293	.002780	.039600	.000265	.002480
110	.043800	820	.000297	.002920	.039000	.000263	.002440
120	.043600	800	.000302	.003080	.038500	.000260	.002400
130	.043600	780	.000306	.003260	.038100	.000257	.002340
140	.043700	760	.000310	.003420	.037700	.000255	.002300
150	.043800	740	.000314	.003620	.037350	.000252	.002260
160	.044000	720	.000318	.003800	.037100	.000249	.002220
170	.044200	700	.000322	.003990	.036850	.000246	.002170
180	.044400	680	.000326	.004180	.036700	.000243	.002130
190	.044700	660	.000330	.004360	.036600	.000240	.002080
200	.044900	640	.000333	.004540	.036500	.000236	.002040
210	.045100	620	.000337	.004720	.036600	.000233	.002000
220	.045400	600	.000340	.004890	.036630	.000230	.001960
230	.045700	580	.000343	.005080	.036680	.000226	.001920
240	.045000	560	.000346	.005240	.036850	.000223	.001880
250	.046300	540	.000349	.005420	.037100	.000220	.001840
260	.046500	520	.000352	.005530	.037350	.000217	.001795

Seq #	K_p	°C Temp	S_N	ρ_N	K_N	S_p	ρ_p
270	.047000	500	.000349	.005590	.037650	.000213	.001700
280	.047300	480	.000348	.005570	.037950	.000209	.001710
290	.047700	460	.000345	.005440	.038300	.000206	.001670
300	.048100	440	.000339	.005240	.038600	.000202	.001635
310	.048500	420	.000333	.005020	.039050	.000199	.001590
320	.049000	400	.000326	.004790	.039500	.000195	.001550
330	.049400	380	.000320	.004520	.039950	.000191	.001510
340	.049800	360	.000312	.004260	.040400	.000187	.001480
350	.050200	340	.000305	.004000	.040900	.000183	.001440
360	.050700	320	.000297	.003740	.041400	.000179	.001400
370	.051200	300	.000289	.003510	.042000	.000175	.001370
380	.051700	280	.000280	.003290	.042550	.000171	.001340
390	.052200	260	.000272	.003100	.043100	.000167	.001300
400	.052600	240	.000264	.002920	.043700	.000162	.001260
410	.053200	220	.000256	.002760	.044400	.000158	.001240
420	.053700	200	.000247	.002600	.044900	.000154	.001200
430	.054200	180	.000239	.002450	.045650	.000149	.001170
440	.047000	160	.000230	.002320	.046400	.000145	.001140
450	.055200	140	.000221	.002190	.047000	.000140	.001110
460	.055700	120	.000213	.002080	.047750	.000136	.001080
470	.056200	100	.000205	.001980	.048500	.000130	.001055
480	.056800	80	.000195	.001880	.049300	.000126	.001030
490	.057200	60	.000186	.001790	.050000	.000122	.001000
500	.057800	40	.000177	.001710	.050800	.000117	.000980
510	.058400	20	.000169	.001650	.051600	.000113	.000960
520	.059000	0	.000161	.001590	.052400	.000109	.000940

b. 3M - 3N PbTe

530 C PBTE-3N DATA RICHARDS(AUG'68) P-TYPE SIMILAR TO 2P

Seq. #	K_p	°C Temp	S_N	ρ_N	K_N	S_p	ρ_p
550	.0144	600	.000226	.004640	.0208	.000224	.00454
560	.0135	580	.000231	.004420	.0197	.000226	.00440
570	.0127	560	.000234	.004160	.0188	.000227	.00433
580	.0121	540	.000235	.003890	.0180	.000228	.00427
590	.0117	520	.000234	.003640	.0174	.000227	.00418
600	.0112	500	.000233	.003400	.0170	.000225	.00406
610	.0109	480	.000231	.003150	.0167	.000223	.00393
620	.0106	460	.000227	.002910	.0164	.000220	.00379
630	.0104	440	.000223	.002680	.0163	.000216	.00364
640	.0106	420	.000219	.002460	.0162	.000211	.00348
650	.0105	400	.000214	.002240	.0162	.000205	.00331
660	.0106	380	.000208	.002030	.0162	.000199	.00313
670	.0108	360	.000203	.001830	.0163	.000192	.00297
680	.1111	340	.000197	.001670	.0164	.000184	.00280
690	.0115	320	.000190	.001520	.0165	.000176	.00264
700	.0119	300	.000184	.001380	.0168	.000168	.00248
710	.0124	280	.000178	.001270	.0171	.000160	.00234
720	.0130	260	.000172	.001160	.0175	.000151	.00220
730	.0136	240	.000166	.001040	.0179	.000144	.00206
740	.0142	220	.000160	.000930	.0184	.000136	.00193
750	.0149	200	.000154	.000840	.0190	.000129	.00182
760	.0156	180	.000147	.000750	.0196	.000121	.00170
770	.0163	160	.000141	.000660	.0203	.000114	.00159
780	.0171	140	.000134	.000580	.0211	.000107	.00149
790	.0178	120	.000128	.000520	.0222	.000101	.00140
800	.0186	100	.000121	.000470	.0230	.000094	.00131

b. 3M - 3N PbTe (contd.)

Seq #	K_p	°C Temp	S_N	ρ_N	K_N	S_p	ρ_p
810	.0194	80	.000114	.000420	.0243	.000088	.00124
820	.0203	60	.000106	.0003610	.0258	.000083	.00116
830	.0211	40	.000099	.000320	.0275	.000078	.00110
840	.0220	20	.000091	.000280	.0292	.000074	.00104
850	.0229	0	.000082	.000240	.0312	.000070	.00100

855 /ENDO
860 MK202469 MinK 2020 Fibrous Insulation
870 1.04E-3
880 0.83E-3
890 0.67E-3
900 0.54E-3
910 0.43E-3
920 0.34E-3
930 0.27E-3
940 0.20E-3
950 0.14E-3
960 0.10E-3
970 0.05E-3

2. HDATA1 Data Tables

a. 80.0 at.% Si - n- and p-SiGe

Seq #	K_p	°C Temp	S_N	ρ_N	K_N	S_p	ρ_p
10-270							
10	SIGE80						
20	.049527	1100	.000225	.001300	.046296	.000339	.003370
30	.048780	1080	.000224	.001320	.045977	.000336	.003340
40	.047915	1060	.000224	.001340	.045558	.000332	.003310
50	.047505	1040	.000224	.001350	.045248	.000329	.003280
60	.046838	1020	.000226	.001360	.044742	.000325	.003240
70	.045296	1000	.000228	.001380	.044444	.000321	.003190
80	.045755	980	.000229	.001420	.043917	.000318	.003150
90	.045248	960	.000231	.001450	.043764	.000314	.003110
100	.044843	940	.000234	.001490	.043478	.000311	.003070
110	.044444	920	.000236	.001480	.043196	.000308	.003030
120	.044052	900	.000239	.001520	.042918	.000304	.002970
130	.043763	880	.000242	.001580	.042553	.000301	.002930
140	.043383	860	.000246	.001650	.042372	.000298	.002880
150	.043290	840	.000248	.001720	.042105	.000296	.002840
160	.043177	820	.000251	.001800	.041841	.000293	.002790
170	.043103	800	.000254	.001850	.041666	.000290	.002750
180	.043173	780	.000257	.001960	.041580	.000286	.002690
190	.043103	760	.000263	.002050	.041322	.000283	.002640
200	.043103	740	.000266	.002160	.041237	.000279	.002600
210	.043140	720	.000271	.002250	.041152	.000276	.002560
220	.043233	700	.000276	.002420	.041152	.000272	.002510
230	.043290	680	.000282	.002560	.040816	.000269	.002470
240	.043290	660	.000286	.002710	.040816	.000265	.002420
250	.043535	640	.000290	.002860	.041152	.000262	.002380
260	.043706	620	.000294	.002980	.041322	.000258	.002340
270	.043378	600	.000293	.002930	.041493	.000255	.002290

Seq #	K_p	°C Temp	S_N	ρ_N	K_N	S_p	ρ_p
280-530							
280	.044052	580	.000291	.002920	.041701	.000251	.002250
290	.044247	560	.000288	.002810	.041963	.000248	.002210
300	.044444	540	.000285	.002720	.042194	.000244	.002160
310	.044722	520	.000281	.002620	.042462	.000241	.002120
320	.044964	500	.000275	.002560	.042698	.000237	.002080
330	.045207	480	.000271	.002500	.042918	.000233	.002040
340	.045454	460	.000266	.002430	.043196	.000230	.001990
350	.045632	440	.000261	.002360	.043478	.000226	.001950
360	.045993	420	.000255	.002300	.043763	.000222	.001910
370	.046296	400	.000249	.002240	.044052	.000218	.001870
380	.046533	380	.000243	.002170	.044365	.000214	.001830
390	.046882	360	.000237	.002110	.044642	.000210	.001790
400	.047169	340	.000231	.002050	.044984	.000206	.001750
410	.047169	320	.000225	.001990	.045310	.000202	.001710
420	.047846	300	.000219	.001930	.045662	.000198	.001670
430	.048216	280	.000214	.001880	.045977	.000193	.001630
440	.048543	260	.000207	.001820	.046446	.000188	.001590
450	.048971	240	.000201	.001760	.046728	.000184	.001560
460	.049285	220	.000195	.001710	.047058	.000179	.001520
470	.049751	200	.000188	.001660	.047393	.000174	.001490
480	.050250	180	.000182	.001610	.047801	.000168	.001460
490	.050479	160	.000175	.001560	.048169	.000162	.001430
500	.050890	140	.000169	.001520	.048543	.000156	.001400
510	.051282	120	.000162	.001470	.048947	.000149	.001370
520	.051733	100	.000156	.001430	.049309	.000142	.001350
530	.052113	80	.000149	.001400	.049751	.000135	.001320

a. 80 at.% Si - n- and p-SiGe (contd.)

Seq #	K_p	°C Temp	S_N	ρ_N	K_N	S_p	ρ_p
540-800							
540	.052575	60	.000142	.001360	.050175	.000125	.001300
550	.052966	40	.000135	.001330	.050556	.000116	.001280
560	.053475	20	.000128	.001290	.051020	.000106	.001260
570	.054054	0	.000121	.001270	.051493	.000095	.001240
580 b.RCA PBTE DATA TABLE n and p alloys							
590 PBTEO							
600	.012048	600	.000253	.005600	.013240	.000288	.007850
610	.010416	580	.000257	.005150	.012650	.000295	.007400
620	.009661	560	.000260	.004950	.012040	.000300	.007100
630	.009259	540	.000264	.004790	.011620	.000302	.006600
640	.009000	520	.000266	.004620	.011290	.000302	.006200
650	.008849	500	.000268	.004430	.010980	.000300	.005850
660	.008771	480	.000268	.004260	.010750	.000297	.005500
670	.008710	460	.000266	.004070	.010630	.000293	.005150
680	.008733	440	.000263	.003800	.010540	.000287	.004850
690	.008849	420	.000259	.003590	.010430	.000280	.004500
700	.008968	400	.000254	.003350	.010520	.000272	.004150
710	.009132	380	.000248	.003100	.010700	.000262	.003840
720	.009389	360	.000242	.002830	.010920	.000254	.003480
730	.009708	340	.000235	.002570	.011230	.000243	.003140
740	.010000	320	.000229	.002350	.011590	.000231	.002830
750	.010449	300	.000221	.002100	.012190	.000217	.002550
760	.010928	280	.000214	.001930	.012730	.000202	.002340
770	.011627	260	.000206	.001720	.013150	.000187	.001920
780	.012422	240	.000198	.001560	.013790	.000173	.001750
790	.013227	220	.000191	.001420	.014490	.000161	.001550
800	.014285	200	.000183	.001250	.015150	.000148	.001350

.. RCA PbTe Data Table - n- and p-Alloys (contd.)

Seq #	K_p	Temp	S_N	ρ_N	K_N	S_p	ρ_p
810-900							
810	.015197	180	.000175	.001100	.015870	.000135	.001180
820	.016393	160	.000166	.000970	.016660	.000121	.001040
830	.017543	140	.000159	.000860	.017540	.000108	.000920
840	.018796	120	.000150	.000775	.018510	.000097	.000798
850	.020000	100	.000142	.000695	.019600	.000085	.000695
860	.021413	80	.000133	.000605	.020700	.000075	.000605
870	.022727	60	.000124	.000540	.021880	.000066	.000525
880	.024096	40	.000117	.000475	.023250	.000058	.000450
890	.025316	20	.000108	.000440	.024690	.000050	.000380
900	.026315	0	.000100	.000370	.025310	.000042	.000350

APPENDIX II-D
INPUT/OUTPUT COMPUTER PROGRAM SYMBOLS

1. Hybrid Couple Program Symbols

AH	Area of Heat-Reception Plate
AN	Cross-Sectional Area of n-type SiGe Thermoelement
ANP	Cross-Sectional Area Ratio of n-Type PbTe Thermoelement/p-Type SiGe Thermoelement
ANR	Cross-Sectional Area of n-Type SiGe Element/ n-Type PbTe Element
AP	Cross-Sectional Area of p-Type Thermoelement
CUR	Current Flowing Through The Thermocouple
DTRR	Wall Thickness of p-type Element
EHP	Emissivity of Inner Surfaces of Heat-Reception Plates
EL	Load Voltage
EM	Ratio of Load to Internal Electrical Resistance
ETA	Efficiency of Thermocouple
ETC	Emissivity of Inner Surfaces of Heat-Rejection Plates.
FLP	Length of SiGe p-type Element
FL1	Length of SiGe n-type Element
FL2	Length of PbTe n-type Element
GAP	Distance Between Surface of n-type PbTe Inner Segment and Inner Wall Surface of p-type Cylinder
GKA	Thermal Conductivity of n-type SiMo Hot Shoe
GKB	Effective Thermal Conductivity of Interface Materials Between n-type Segment
GKC	Effective Thermal Conductivity of n-type Cold Stack
GKCP	Thermal Conductivity of Heat-Rejection Plate
GKD	Effective Thermal Conductivity of p-type Cold Stack
GKHP	Thermal Conductivity of p-SiMo Heat-Reception Plate
PHI	Heat Flux Incident on Heat-Reception Plate

PO Electrical Power Output per Couple

QT Total Heat Incident on Heat-Reception Plate

QSI Total Amount of Shunt Heat Loss Between Heat Reception and Rejection Plates Which Flows in the Gap Between these Two Surfaces.

QSO Amount of Shunt Heat - Flowing thru Insulation and External to the p-type Element

QH Heat Absorbed by the Thermocouple Materials

R Total Electrical Resistance of Couple

RCN Contact Resistivity of SiGe n-type Thermoelement per contact

RCNZ Contact Resistivity of PbTe n-type Thermoelement per contact

RCP Contact Resistivity of SiGe p-type Thermoelement per contact

RHOA Electrical Resistivity of n-type SiMo Hot Shoe

RHOB Effective Electrical Resistivity of Metallic Interface Material

RHOD Effective Electrical Resistivity of n-type Cold Stack to End of Electrical Connector

RHOC Effective Electrical Resistivity of p-type Cold Stack to End of Electrical Connector

RSH Assummed Resistance Value of SiMo n-type to p-type Junction in Heat Receptor

RRN Radius of n-type PbTe Element

SIGP Stefan-Boltzmann Constant

TCBC Heat Rejection Base Plate Temperature, °C

TCNC Heat Rejection SiGe N-Type Plate Temperature, °C

TCN2C PbTe n-type Cold Junction Temperature, °C

TCPC SiGe p-type Element Cold Junction Temperature, °C

THNC SiGe n-type Hot Junction Temperature, °C

THNZC-PbTe n-type Hot Junction Temperature, °C

THPC SiGe p-type Hot Junction Temperature, °C

THRC SiMo p-type Hot Shoe Edge Temperature, °C

TTA	Thickness of n-type Si-Mo Hot Shoe
TTB	Composite Thickness of n-type Interface Materials
TTC	Composite Thickness of n-type Cold Stack
TTCP	Thickness of Heat Rejection Plate
TTD	Composite Thickness of p-type Cold Stack
TTHP	Thickness of p-SiMo Heat Reception Plate

2. Converter Program Symbols

A STUD	Surface Contact Area Of Couple Cold Stack Incontact With Mounting Plate
AH	Area of Heat-Reception Plate
AN	Cross-Sectional Area of n-Type SiGe Thermoelement
ANP	Cross-Sectional Area Ratio of n-Type PbTe Thermoelement/p-Type SiGe Thermoelement
ANR	Cross-Sectional Area Ratio of n-Type SiGe Element/n-Type PbTe Element
AP	Cross-Sectional Area of p-Type Thermoelement
CUR	Current Flowing Through The Thermocouple
D	Dimensionless Quantity
D FOIL	Density of Multi-Layered Foil
DTRR	Wall Thickness of p-Type Element
EHP	Emissivity of Inner Surfaces of Heat-Reception Plates
EL	Load Voltage
EM	Ratio of Load to Internal Electrical Resistance
ETA	Efficiency of Thermocouple
ETC	Emissivity of Inner Surfaces of Heat-Rejection Plates
FAS	Distance Between Adjacent Heat Receptors
FKIC	Effective Thermal Conductivity of Dynaquartz Insulation
FKIE	Effective Thermal Conductivity of Composite Foil Insulation
FLG	Total Case Height Above Fin Mounting Plate
FLP	Length of SiGe p-Type Element
FL1	Length of SiGe n-Type Element
FL2	Length of PbTe n-Type Element

GAP	Distance Between Surface of n-Type PbTe Inner Segment and Inner Wall Surface of p-Type Cylinder
GAT	Planar Area Occupied By Couples Facing Heat Source
GCPL	Number Of Couples
GEL	Converter Output Voltage Delivered to Load
GETA	Converter Efficiency
GKA	Thermal Conductivity of n-Type SiMo Hot Shoe
GKB	Effective Thermal Conductivity of Interface Materials Between n-Type Segments
GKC	Effective Thermal Conductivity of n-Type Cold Stack
GKCP	Thermal Conductivity of Heat-Rejection Plate
GKD	Effective Thermal Conductivity of p-Type Cold Stack
GKHP	Thermal Conductivity of Heat-Reception Plate
GPO	Converter Output Power
PHI	Heat Flux Incident on Heat-Reception Plate
PO	Electrical Power Output per Couple
QT	Total Heat Incident on Heat-Reception Plate
QSI	Total Amount of Shunt Heat Loss Between Heat Reception and Rejection Plates Which Flows in the Gap Between These Two Surfaces
QSO	Amount of Shunt Heat Flowing Through Insulation and External to the p-Type Element
QH	Heat Absorbed by the Thermocouple Materials
R	Total Electrical Resistance of Couple
RCN	Contact Resistivity of SiGe n-Type Thermoelement
RCNZ	Contact Resistivity of PbTe n-Type Thermoelement

RCP	Contact Resistivity of SiGe p-Type Thermoelement
RHOA	Electrical Resistivity of n-Type SiMo Hot Shoe
RHOB	Effective Electrical Resistivity of Metallic Interface Material
RHOD	Effective Electrical Resistivity of n-Type Cold Stack to End of Electrical Connector
RHOC	Effective Electrical Resistivity of p-Type Cold Stack to End of Electrical Connector
RSH	Assumed Resistance Value of SiMo n-Type to p-Type Junction in Heat Receptor
RRN	Radius of n-Type PbTe Element
SIGP	Stefan-Boltzmann Constant
TCBE	Heat Rejection Base Plate Temperature,°C
TCNC	SiGe n-Type Element Cold Junction Temperature, °C
TCN2C	PbTe n-Type Cold Junction Temperature,°C
TCPC	SiGe p-Type Element Cold Junction Temperature,°C
TFCC	Fuel Source Surface Temperature,°C
THNC	SiGe n-Type Hot Junction Temperature,°C
THNZC	PbTe n-Type Hot Junction Temperature,°C
THPC	SiGe p-Type Hot Junction Temperature,°C
TT CASE	Thickness of Case Protecting Insulation Around Heat Source
TTA	Thickness of n-Type Si-Mo Hot Shoe
TTB	Composite Thickness of n-Type Interface Materials
TTC	Composite Thickness of n-Type Cold Stack
TTCP	Thickness of Heat Rejection Plate
TTD	Composite Thickness of p-Type Cold Stack
TTHP	Thickness of Heat Reception Plate
W CASE	Weight of Case
THRC	SiMo p-Type Hot Shoe Edge Temperature, °C

W FIN	Weight of Fin
W FOIL	Weight of Foil
WGCPL	Weight of Couples
WGPO	Specific Power - Watts/lb.

DISTRIBUTION LIST FOR CONTRACT NAS 3-11843

Aerojet-General Corporation
P.O. Box 296
Azusa, California 91702
Attn: Myra T. Grenier, Corp. Librarian

Aerojet-General Corporation
P.O. Box 15847
Sacremento, California 95813
Attn: M.S. Nylin, Tech. Library

Aero-jet-General Corporation
San Ramon Plant
P.O. Box 86
San Ramon, California 94583
Attn: Sandra L. Johnson, Doc. Cust.

Headquarters
U.S. Air Force (AFRSTG)
Washington, D.C. 20330
Attn: Chief, Nuclear Div.

Air Force Weapons Laboratory (WLXL)
Kirtland Air Force Base
New Mexico 87117
Attn: M.F. Canova

Air University Library
Maxwell Air Force Base
Alabama 36112
Attn: Mrs. E.C. Pittman, AUL3T-7143

Allison Division - GMC
P.O. Box 24013
Indianapolis, Indiana 46224
Attn: R.R. Blackwell, Security Coord.

Argonne National Laboratory
9700 South Cass Ave.
Argonne, Illinois 60439
Attn: E.N. Pettitt

Headquarters
U.S. Army Ballistic Research Labs.
Aberdeen Proving Ground, Md. 21004
Attn: Security Officer

Chief of Research & Development
Headquarters
Department of the Army
Washington, D.C. 20310
Attn: Chief, Nuclear, Chemical-
Biological Div.

Commanding Officer
U.S. Army Materials Research Agency
Watertown, Massachusetts 02172
Attn: AMXMR-ATL

Redstone Scientific Information Ctr.
U.S. Army Missile Command
Redstone Arsenal, Alabama 35809
Attn: Chief, Document Section

Nuclear Power Field Office
U.S. Army Engineer Reactors Group (USAERDL)
Fort Belvoir, Virginia 22060
Attn: Security Officer

U.S. Atomic Energy Commission
Albuquerque Operations Office
P.O. Box 5400
Albuquerque, New Mexico 87115
Attn: L. P. Gise

U.S. Atomic Energy Commission
Isotope Power Systems Branch
Div. of Space Nuclear Systems
Washington, D.C. 20545
Attn: Leonard Topper

U.S. Atomic Energy Commission
Isotope Power Systems Branch
Div. of Space Nuclear Systems
Washington, D.C. 20545
Attn: Mr. R.B. Morrow F-309

U.S. Atomic Energy Commission
Isotope Power Systems Branch
Division of Space Nuclear Systems
Washington, D.C. 20545
Attn: Mr. P. O'Riordan

U.S. Atomic Energy Commission
Canoga Park Area Office
P.O. Box 591
Canoga Park, California 91305

U.S. Atomic Energy Commission
Chicago Operations Office
9800 South Cass Avenue
Argonne, Illinois 60439
Attn: George H. Lee

U.S. Atomic Energy Commission
Cincinnati Area Office
P.O. Box 39188
Cincinnati, Ohio 45239
Attn: Document Accountability

U.S. Atomic Energy Commission
Div. of Technical Information Extension
P.O. Box 62
Oak Ridge, Tennessee 37830

U.S. Atomic Energy Commission
AEC Library
Mail Station G-017
Washington, D.C. 20545

U.S. Atomic Energy Commission
New York Operations Office
376 Hudson St.
New York, New York 10014
Attn: Reports Librarian

U.S. Atomic Energy Commission
Oak Ridge Operations Office
Mail & Doc. Accountability Section
P.O. Box E
Oak Ridge, Tennessee 37830
Attn: Document Library

U.S. Atomic Energy Commission
Office of Asst. Genl. Counsel for Patents
Washington, D.C. 20545
Attn: Roland A. Anderson

Atomics International
A Div. of North American Aviation, Inc.
P.O. Box 309
Canoga Park, California 91304
Attn: Technical Library

Battelle Memorial Institute
Columbus Laboratories
505 King Avenue
Columbus, Ohio 43201
Attn: Dr. S.J. Paprocki

Battelle Memorial Institute
Pacific Northwest Laboratory
P.O. Box 999
Richland, Washington 99352
Attn: Tech. Info. Section

Brookhaven National Laboratory
Technical Information Division
Upton, L.I., New York 11973
Attn: Classified Documents Group

Office of the Director of Defense
Research and Engineering
Room 3E-1071, Pentagon
Washington, D.C. 20301
Attn: Frank J. Thomas, Asst. Dir.
Nuclear Programs

E.I. duPont de Nemours & Co.
Savannah River Laboratory
Document Transfer Station 703-A
Aiken, South Carolina 29801

General Dynamics
Fort Worth Division
P.O. Box 748
Fort Worth, Texas 76101
Attn: Keith G. Brown or B.S. Fain

General Electric Company
FPD Technical Information Center
Building 700 N-32
Cincinnati, Ohio
Attn: James J. Brady, Mgr.

General Electric Company
Missile & Space Division
P.O. Box 8555
Philadelphia, Pennsylvania 19101
Attn: C. Nemec, ANSO Library

General Electric Company
Atomic Power Equipment Dept.
P.O. Box 1131
San Jose, California 95108
Attn: Alleen Thompson

Gulf General Atomics, Inc.
P.O. Box 608
San Diego, California 92212
Attn: N. Elsner

Institute for Defense Analyses
400 Army-Navy Drive
Arlington, Virginia 22202
Attn: Patricia W. Andrews

Jet Propulsion Laboratory
4800 Oak Grove Drive
Pasadena, California 91103
Attn: Louis Canter, Mgr.
Library Section

Jet Propulsion Laboratory
4800 Oak Grove Drive
Pasadena, California 91103
Attn: Robert G. Ivanoff

Jet Propulsion Laboratory
4800 Oak Grove Drive
Pasadena, California 91103
Attn: Dr. Vince Truscello

The Johns Hopkins University
Applied Physics Laboratory
8621 Georgia Avenue
Silver Spring, Maryland 20910
Attn: Boris W. Kuvshinoff

Los Alamos Scientific Laboratory
P.O. Box 1663
Los Alamos, New Mexico 87544
Attn: Report Librarian

Martin Company
Div. of Martin Marietta Corp.
Nuclear Products
P.O. Box 5042
Middle River, Maryland 21220
Attn: AEC Document Custodian

Minnesota Mining & Manufacturing Co.
P.O. Box 7565
St. Paul, Minnesota 55119
Attn: H.C. Zeman, Security 235

Monsanto Research Corporation
Mound Laboratory
P.O. Box 32
Miamisburg, Ohio 45342
Attn: Records Management Section

National Aeronautics & Space Admin.
Washington, D.C. 20546
Attn: Dr. F. Schulman (Code RNP)
Arvin H. Smith (Code RNP)
S.V. Manson (NS-1)

NASA-Ames Research Center
Moffeet Field, California 94035
Attn: Library
A.C. Wilbur, M.S. N244-6

National Aeronautics & Space Admin.
Goddard Space Flight Center
Glenn Dale Road
Greenbelt, Maryland 20771
Attn: Librarian
Joseph Epstein
Dale Harris

National Aeronautics & Space Admin.
Langley Research Center
Langley Station
Hampton, Virginia 23365
Attn: Associate Director

National Aeronautics & Space Admin.
Lewis Research Center
21000 Brookpark Road
Cleveland, Ohio 44135
Attn: Dr. L. Rosenblum, 302-1
R. Breitwieser, 302-1
James Ward, MS 302-1
W.J. Bifano, MS 302-1
Tech. Util. Office, MS 3-19
Power Procurement Sect. 500-206
Library, MS 60-3

National Aeronautics & Space Admin.
Manned Spacecraft Center
Houston, Texas 77058
Attn: Asst. Chief for Tech. Info. Prgms.
T.E. Redding, Code EP-5
C.W. Robinson, Code EP-5
C.W. Glassburn, Code EP-5
J.L. Cioni, Code EP-5

National Aeronautics & Space Admin.
George C. Marshall Space Flight Center
Huntsville, Alabama 35812
Attn: Lois M. Robertson, MS-IL
Mr. Gene Young

National Aeronautics & Space Admin.
Scientific & Tech. Information Facility
P.O. Box 33
College Park, Maryland 20740
Attn: NASA Representative) (2 copies)

National Aeronautics & Space Admin.
Washington, D.C. 20546
Attn: Document Control Officer, USS-10

National Reactor Testing Station (INC)
P.O. Box 2869
NRTS Technical Library
Idaho Falls, Idaho 83401
Attn: Document Control

Naval Facilities Engineering Command Hdqt.
Department of the Navy
Washington, D.C. 20390
Attn: Code 042, Director, Nuclear Pwr. Div.

Director, Atomic Energy Division
Office of the Chief of Naval Operations
Department of the Navy
Washington, D.C. 20350

Director
U.S. Naval Research Laboratory
Washington, D.C. 20390
Attn: Classified Matl. Control Branch

Naval Ship Systems Command Hdqt.
Navships 08
Navy Department
Washington, D.C. 20360
Attn: Irene P. White

Naval Ship R & D Center
Annapolis Division
Annapolis, Maryland 21402
Attn: Mr. A. Bayne Neild

Nuclear Materials & Equipment Corp.
P.O. Box 354
Lewiston, New York 14092
Attn: R. Placentino, Security Officer

Pratt & Whitney Aircraft Division
United Aircraft Corporation
400 Main Street
East Hartford, Connecticut 06108
Attn: William H. Podolny

RCA Corporation
Astro Electronics Division
P.O. Box 11
Cranbury, New Jersey 08512
Attn: Joseph E. Hanlon

Director, USAF Project Rand
Via: Air Force Liaison Office
The Rand Corporation
1700 Main Street
Santa Monica, California 90406
Attn: Frank R. Collbohn

Power Conversion Department
Republic Aviation Division
Fairchild Hiller Corporation
Farmingdale, New York 11735
Attn: A.E. Kunen or A. Schock

Thermo Electron Engineering Corp.
Post Office Box 482
Waltham, Massachusetts 02154
Attn: J.H. Weinstein/J. Dunlay

Union Carbide Corporation
Nuclear Division
X-10 Laboratory Records Dept.
P.O. Box X
Oak Ridge, Tennessee 37830

University of California
Lawrence Radiation Laboratory
P.O. Box 308
Livermore, California 94551
Attn: Technical Information Div.

Westinghouse Electric Corporation
Aerospace Electrical Division
P.O. Box 7
Lima, Ohio 45802
Attn: George L. Arensman

Westinghouse Electric Corporation
Astronuclear Laboratory
P.O. Box 10864
Pittsburgh, Pennsylvania 15236
Attn: Florence McKenna, Librarian

Westinghouse Electric Corporation
Astronuclear Laboratory
P.O. Box 10864
Pittsburgh, Pennsylvania 15236
Attn: AEC Document Custodian
Dr. R. Novak